EXTENDED PERFORMANCE SOLAR ELECTRIC PROPULSION THRUST SYSTEM STUDY

(NASA-CR-135281) EXTENDED PERFORMANCE SOLAR ELECTRIC PROPULSION THRUST SYSTEM STUDY. VOLUME 2: BASELINE THRUST SYSTEM Final Report, 14 Feb. 1977 - 29 Aug. 1977 (Hughes Research Labs.) 260 p HC A12/MF A01 G3/20

N78-28167

Unclas 15130

Final Report

September 1977

Volume II

Baseline Thrust System

By

Ion Physics Department Staff

Hughes Research Laboratories

and

Technology Division Staff

Space and Communications Group

of

Hughes Aircraft Company

Prepared For

NATIONAL AERONAUTICS AND SPACE ADMINISTRATION

NASA Lewis Research Center

Contract NAS 3–20395

TECHNICAL REPORT STANDARD TITLE PAGE

1 Report No	2 Government Accession No	3 Recipient's Catalog No
CR-135281		

4 Title and Subtitle	5. Report Date
EXTENDED PERFORMANCE SOLAR ELECTRIC PROPULSION THRUST SYSTEM STUDY VOLUME II – BASELINE THRUST SYSTEM	September 1977
	6 Performing Organization Code

7 Author(s)	8 Performing Organization Report No
R L Poeschel and E I. Hawthorne, et al	

9 Performing Organization Name and Address	10 Work Unit No
Hughes Aircraft Company Hughes Research Laboratories 3011 Malibu Canyon Road Malibu, California 90265 Hughes Space & Com Group P.O. Box 92919 Los Angeles, CA 90009	11 Contract or Grant No NAS 3-20395
	13 Type of Report and Period Covered 14 Feb 1977-29 Aug 1977

12 Sponsoring Agency Name and Address	14 Sponsoring Agency Code
National Aeronautics and Space Administration Lewis Research Center 21000 Brookpark Road Cleveland, Ohio 44135	

15 Supplementary Notes

Project Manager: James Cake, NASA-Lewis Research Center, Cleveland, Ohio

16 Abstract

Ion-thruster technology has progressed during the past decade to the point that it is considered ready for application During this study, several thrust system design concepts were evaluated and compared using the specifications of the most advanced 30-cm engineering model thruster as the technology base Emphasis was placed on relatively high-power missions (60 to 100 kW) such as a Halley's comet rendezvous. The extensions in thruster performance required for the Halley's comet mission were defined and alternative thrust system concepts were designed in sufficient detail for comparing mass, efficiency, reliability, structure, and thermal characteristics Confirmation testing and analysis of thruster and power-processing components were performed, and the feasibility of satisfying extended performance requirements was verified A baseline design was selected from the alternatives considered, and the design analysis and documentation were refined The baseline thrust system design features modular construction, "conventional" power processing, and a "concentrator" solar array concept and is designed to interface with the Space Shuttle. A program development plan was formulated that outlines the work structure considered necessary for developing, qualifying, and fabricating the flight hardware for the baseline thrust system within the time frame of a project to rendezvous with Halley's comet during December 1985 An assessment was made of the costs and risks associated with a baseline thrust system as provided to the mission project under this plan. Critical procurements and interfaces were identified and defined. The results of this study are presented in the five volumes of this report

17 Key Words (Selected by Author(s))	18 Distribution Statement
Solar Electric Propulsion Thrust System Ion Propulsion Ion Thruster	Unclassified-Unlimited

19 Security Classif (of this report)	20 Security Classif (of this page)	21 No of Pages	22 Price*
UNCLASSIFIED	UNCLASSIFIED	261	

*For sale by the Clearinghouse for Federal Scientific and Technical Information, Springfield, Virginia 22151

FOREWORD

The work described herein was performed by the coordinated efforts of personnel within two divisions of the Hughes Aircraft Company. Responsibility for the study resided in the Ion Physics Department of Hughes Research Laboratories. This department is managed by Mr. J.H. Molitor. A major portion of the thrust system design activity was performed by a team of individuals assembled from the Technology Division of the Space and Communications Group and coordinated and directed by Dr E I. Hawthorne. The work was funded under contract NAS3-20395 and monitored by Mr. James E. Cake of the NASA Lewis Research Center. The key technical contributors were

R L. Poeschel	- Study manager for the final phases of the study and project engineer for the approach confirmation task
E.I. Hawthorne	- Manager of all thrust system design and program development activities
Y.C. Weisman	- Project engineer for structural design
M. Frisman	- Project engineer for structural design
G.C. Benson	- Project engineer for power management and control design
R.J McGrath	- Project engineer for thermal control design
R M. Martinelli	- Project engineer for capacitor diode voltage multiplier development and evaluation
T.L Linsenbardt	- Thermal analysis
J R. Beattie	- Thruster evaluation

SUMMARY

The primary objective of this study was to provide a data base for a program plan for the development of the ion-propulsion thrust system for the Halley's comet mission spacecraft. This data base was to include the definition of a design concept, selected from among alternate candidate configurations; the identification of required supporting technology, including the definition of critical areas and potential technical risks, the definition of a program development plan, including a development schedule and an assessment of potential schedule risks; and a preliminary estimate of yearly and total program costs.

A concurrent objective of the study was to conduct a hardware "approach confirmation" technology effort to evaluate the ion thruster's performance and lifetime at the power level required for the Halley's comet mission, to design and evaluate the thruster isolator required for operation at the higher power level, and to evaluate the design of a capacitor-diode voltage multiplier.

A thrust system baseline configuration was identified for the 30-cm extended-performance mercury ion thruster than can perform the Halley's comet rendezvous mission. The configuration is comprised of 10 thrusters configured with a power management and control system and a structure and thermal control system in a modular thrust system design The power management and control system uses conventional power processing. Power is provided to the thrust system with an 85 kW concentrating solar array. The thrust system mass is 1010 kg (including 15% contingency), the average system efficiency is 70%, and the estimated reliability upper bound is 72%

Adaptability of the 900-series 30-cm thruster design to the 6 to 7 kW range required for the Halley's comet mission was demonstrated with only minor design modification required, and an acceptable high-voltage isolator design was validated by laboratory tests. The design and performance of an alternate power management and control system design approach utilizing the capacitor-diode voltage multiplier was successfully demonstrated by laboratory model tests in excess of 1 kW.

The technology efforts mentioned above assisted in the identification of the level of technical risks associated with the thrust system design These risks have been found amenable to resolution through normal engineering development and, therefore, judged to be acceptable for mission application.

The program plan, which includes the procurement plan generated for the baseline configuration is a viable plan that provides for delivery in May 1981 of the flight thrust system to be integrated with the mission module and solar array. The cost of the thrust system development program is projected to be 54 million dollars (in fiscal year 1977 dollars) excluding contractor fee, of which approximately 13.5 million dollars will be required in fiscal year 1978.

In contrast to the low technical risk, the schedule risk for initiating this program development is of particular concern. Timely approval of the authorization of 13.5 million dollars for fiscal year 1978 must be granted so that the pre-project, or advanced development, activities can be initiated.

TABLE OF CONTENTS

LIST OF ILLUSTRATIONS

SECTION 1

INTRODUCTION

This volume is the second of a five-volume report that presents the results of a six-month study to define the design, program plan, and costs of an ion-propulsion thrust system for the Halley's comet mission spacecraft. The modular characteristics of the design developed during this study also make it applicable as the prime space propulsion system for other potential missions

This study, which is based on an initial system characterization (completed 7 February 1977) performed by the National Aeronautics and Space Administration's Lewis Research Center (NASA LeRC) was performed in three parts:

- Design tradeoff studies (14 February to 15 April 1977) to define and compare alternate design approaches.
- Conceptual design definition, program plan, and costs of a selected design approach (15 April to 15 June 1977).
- Approach confirmation of supporting technology in selected areas.

The results of this study are presented in five volumes Volume I summarizes the results of the entire program This volume, Volume II, discusses the conceptual design, program development plan, and cost estimates for the selected baseline thrust system design. Volume III describes the design tradeoff studies performed to compare alternate design approaches Volume IV presents the thruster technology evaluation for extended performance applications Volume V presents the details of the capacitor diode voltage multiplier (CDVM) circuit analysis and experimental evaluation. The results reported in these volumes have also been presented in briefings at NASA LeRC.

A. BACKGROUND

In the fall of 1976, the Office of Aeronautics and Space Technology (OAST) was given the responsibility of assessing the capability of the electric propulsion technology under development at NASA LeRC and of the solar array technology under development at Marshall Space Flight Center (MSFC) and the Jet Propulsion Laboratory (JPL) to perform the Halley's comet rendezvous mission proposed by JPL OAST established an "August Project" team from members of the three organizations to develop a preliminary program plan to support a fiscal year (FY) 1979 new start.

The August Project consisted of parallel efforts by JPL, LeRC, and MSFC to define the design approach, program plan, costs, and risks of the Halley's comet mission. Three areas were considered: the spacecraft (including the science payload), the ion propulsion subsystem (referred to as the thrust system in this report), and the solar array. The NASA LeRC program was conducted in two phases. First, initialization studies (completed 15 February 1977) were conducted to define requirements and to identify preliminary design characteristics. Second, during the 15 February to 15 July period, the design of the thrust system was defined, the program plan and projected costs were generated, and risk assessment was made. The results of the second phase of the program are reported in this volume. The design selection process included tradeoff studies among alternate design approaches, followed by a refinement of the conceptual design that had been selected. Iteration with design data available from the parallel activities at JPL and MSFC, and concurrent approach confirmation tests and analyses included in this study, serve to strengthen the conclusions of the thrust system study

NASA directed us to begin the study by identifying two candidate solar array configurations (flat or concentrator), three candidate power management and control (PMaC) approaches (conventional, direct drive, or voltage multiplier), and two structural design approaches (modular or integrated). A comparative assessment of the various configurations possible from combinations of these design choices was desired in terms of performance, mass, efficiency, reliability, and technical and schedule risks.

The thrust systems being considered are based on the electric propulsion technology which NASA LeRC has been developing for over a decade. The technical baseline for this application is the most recent operational engineering model thruster (EMT), the 900-series 30-cm mercury ion EMT. This thruster is a scaled-up version of the 15-cm thruster developed and flight tested during the 1960-1969 period for the SERT II program. The EMT operates at a 3-kW power level with a specific impulse of 3,000 sec By making minor modifications in the existing thruster design, extended performance at approximately 6 kW power level, 4,800 sec specific impulse, and 15,000 hr pre-wearout life (as required for a Halley's comet mission) was believed to be achievable at a low technical risk. This supposition was evaluated as part of this study.

In addition to the extended performance thruster, the key elements of the thrust system for this extended performance application are the PMaC subsystem, gimbal system, propellant storage and distribution system, thermal control system, and supporting structure. The background of extensive development in power-processing technology for mercury ion thrusters and technology developments in the other areas were the basis for the high level of confidence that the required extended performance levels could be achieved.

B. SCOPE

The scope of this study included the development of conceptual designs for various candidate systems, the selection, definition, and evaluation of a baseline design concept and its critical interfaces, an evaluation of the sensitivity of the baseline design to critical data base and design parameters; the generation of a development program plan for the baseline concept; estimation of costs and fiscal year funding requirements, fabrication of a demonstration scale model; and the conduct of supporting technology studies (including fabrication and testing of critical hardware components) to estimate the physical and electrical performance and to provide a baseline for subsequent work

The design characteristics, program plan, and costs of the baseline system were defined in parallel with the supporting technology effort Design definition was carried out in two consecutive phases:

- Phase 1· Definition and comparison of alternate configurations, leading to baseline selection.
- Phase 2· Design definition and evaluation of the baseline configuration, culminating in the generation of a program plan and cost estimates.

The concurrent technology effort comprised thruster performance and lifetime evaluation, thruster isolator design and evaluation, and the design and evaluation of a capacitor-diode voltage multiplier (CDVM) breadboard

The design study was necessarily limited to the conceptual definition of the key design features and characteristics However, sufficient understanding was achieved in all important areas to provide realistic estimates of masses; power requirements, which led to efficiency calculations; complexity and parts count, which led to reliability estimates; development, procurement, fabrication, and test requirements, which led to schedule definition, potential areas of uncertainty and concern, which led to an assessment of the technical and schedule risks; the scope and nature of system interactions, which led to the definition of principal interfaces, and requirements and phasing for hardware and manpower, which led to a cost estimate.

This volume presents the details of a design study for the thrust system configuration that was selected as the baseline. The analyses and descriptions of the baseline thrust system's principal elements and components are presented in Section 2. Section 3 summarizes the parameters that characterize the projected performance of the thrust system. Section 4 presents a program development plan and cost estimates for development and procurement of a thrust system to perform a Halley's comet rendezvous mission

SECTION 2

THE BASELINE THRUST SYSTEM· DESIGN AND ANALYSIS

The thrust system design for this study consists of ten thrusters, a conventional PMaC system, a modular structure, and a concentrator solar array. The baseline thrust system evolved from a tradeoff analysis (see Volume III) of seven alternative conceptual configurations. The components and the design approaches used in the baseline thrust system were specified by NASA LeRC either as elements of an initial data base or as selections from the configuration study. The key elements of the thrust system and the principal interfaces with the other elements of the spacecraft for the Halley's comet mission are shown in Figure 1. This section summarizes the principal characteristics of the thrust subsystems. The rationale for a particular design choice is discussed in those cases in which several options were possible. In the final subsection, the sensitivity of design characteristics to changes in design parameters is analyzed.

A. SOLAR ARRAY AND MISSION MODULE

Table 1 summarizes the key design data provided by NASA LeRC for the solar array and for the mission module. Supporting data is presented in Figures 2, 3, and 4. This data was used in defining the electrical, structural, and thermal designs and in evaluating system performance. The key input to the thrust system design is the postulated power profile shown in Figure 2. The solar array is shown in both the stowed and deployed configurations in Figure 4. The dimensions of the solar array in the stowed configuration played a major role in defining and sizing the thrust system structure. The length of the baseline structure is, in fact, wholly determined by the length of the stowed array

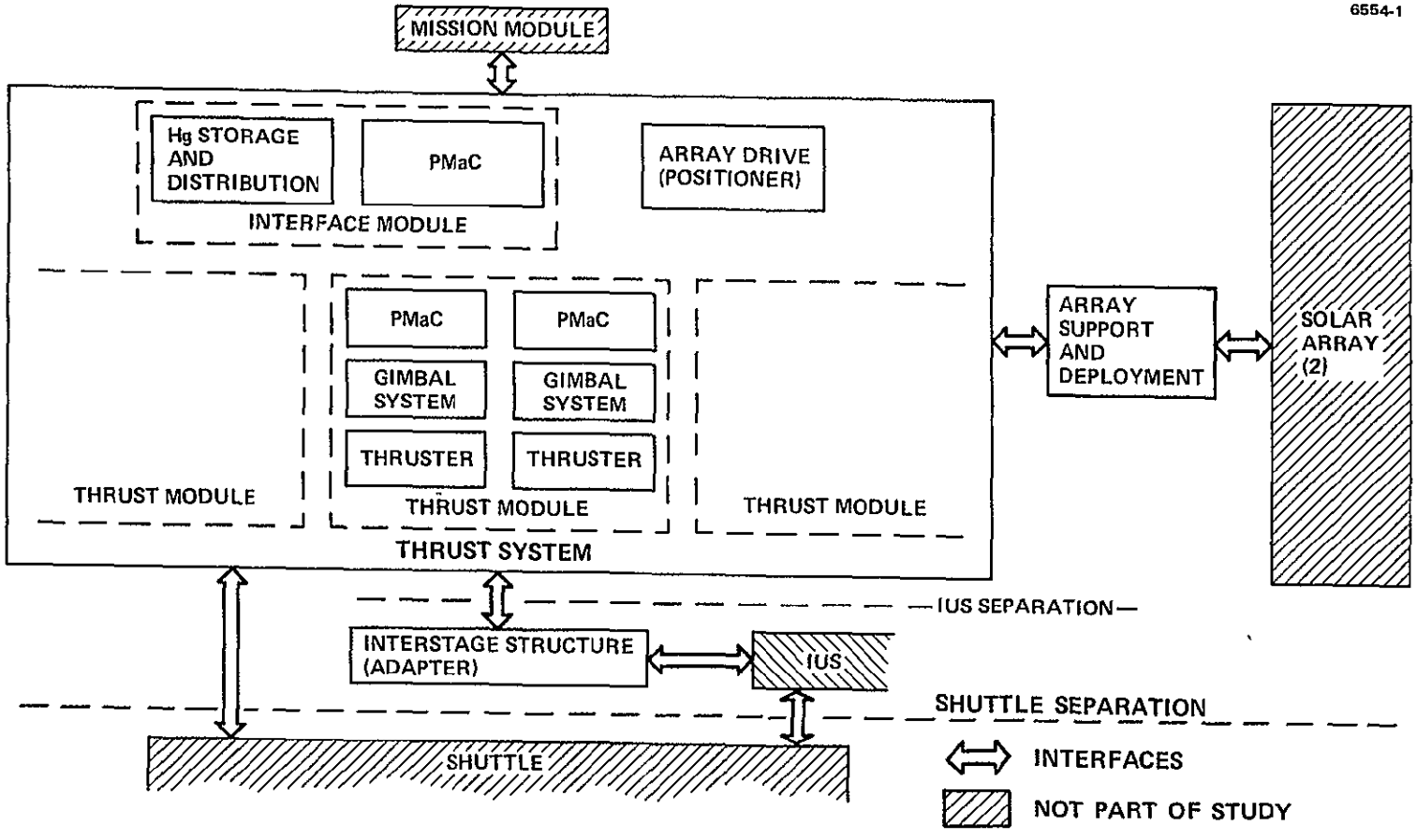

Figure 1. Thrust system block diagram showing principal interfaces.

Table 1. Data Base Summary

Solar Array Data
85 kW concentrator array
3·1 concentration ratio (max)
Conventional solar cells
Power profile· 48 kW max to thrusters (1.0 to 1.8 AU), see Figure 2
Voltage/current profiles provided (not shown in Figure 2) max voltage swing over trajectory: 2.6 to 1 (without reconfiguration)
Thermal characteristics (see Figure 3)
Deployed configuration (see Figure 4(a))
Side reflector angle· 45^{o} and 60^{o} (adjustable during mission)
Separation distance from thrust system sufficient to ensure Hg impingement angle of 50^{o} min at 0^{o} gimbal angle
$\pm 5^{o}$ about the axis perpendicular to the solar array axis
$\pm 35^{o}$ about the axis parallel to the solar array axis
Natural frequency at root of drive structure· 0.015 Hz
Stowed configuration (see Figure 4(b))
Mission Module
Weight: 450 kg
Height: 2.5 m (1.5 m above thrust-system interface plane)
Lowest lateral frequency: 30 Hz
Internal temperature: 5 to 50^{o}C
Conductance to interface truss: 0.01 $W/^{o}C$
Emittance of multilayer insulation blanket: 0.025
Thrust system interface area: 1.13 m^{2}
Power requirement
Thrust phase 400 W (max)
Rendezvous phase: 650 W (max)

5903

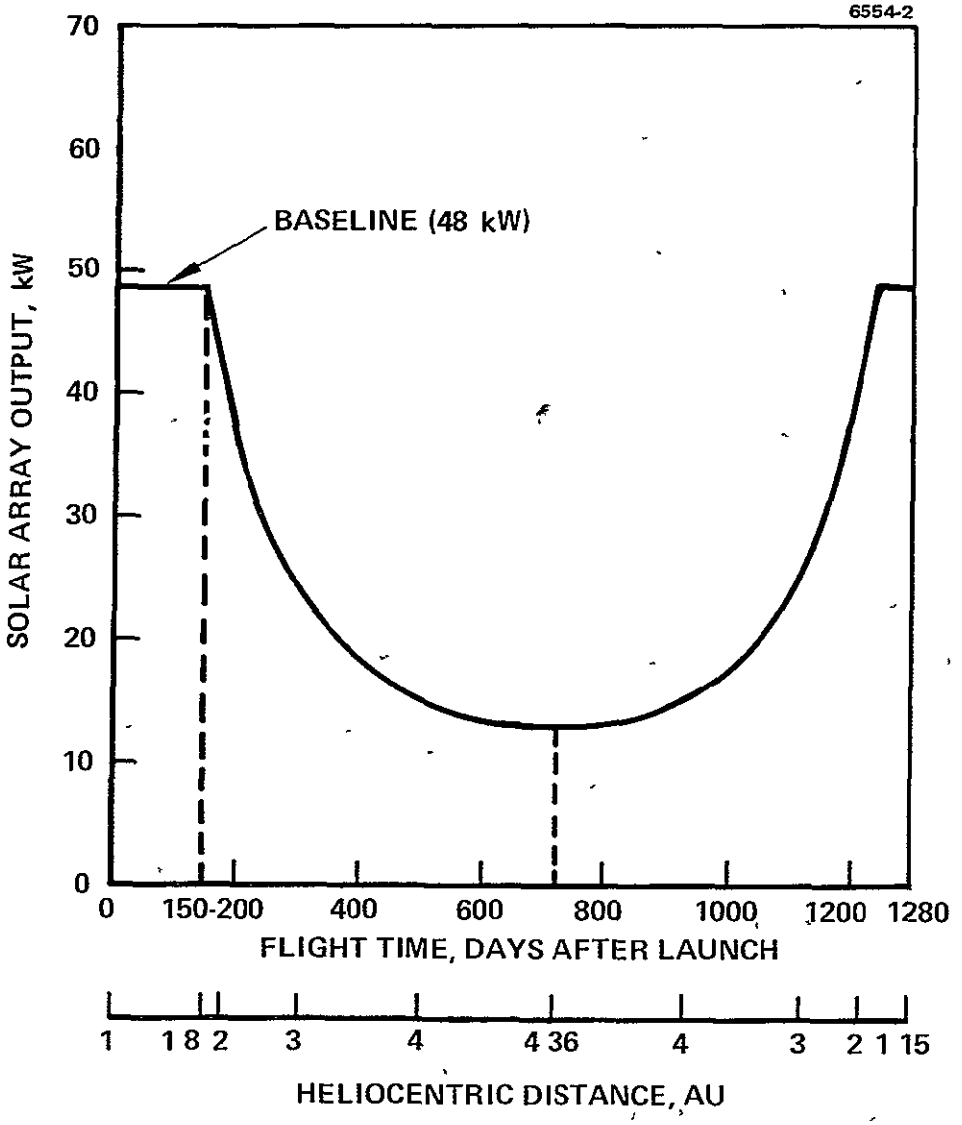

Figure 2. Power profile of the main solar array.

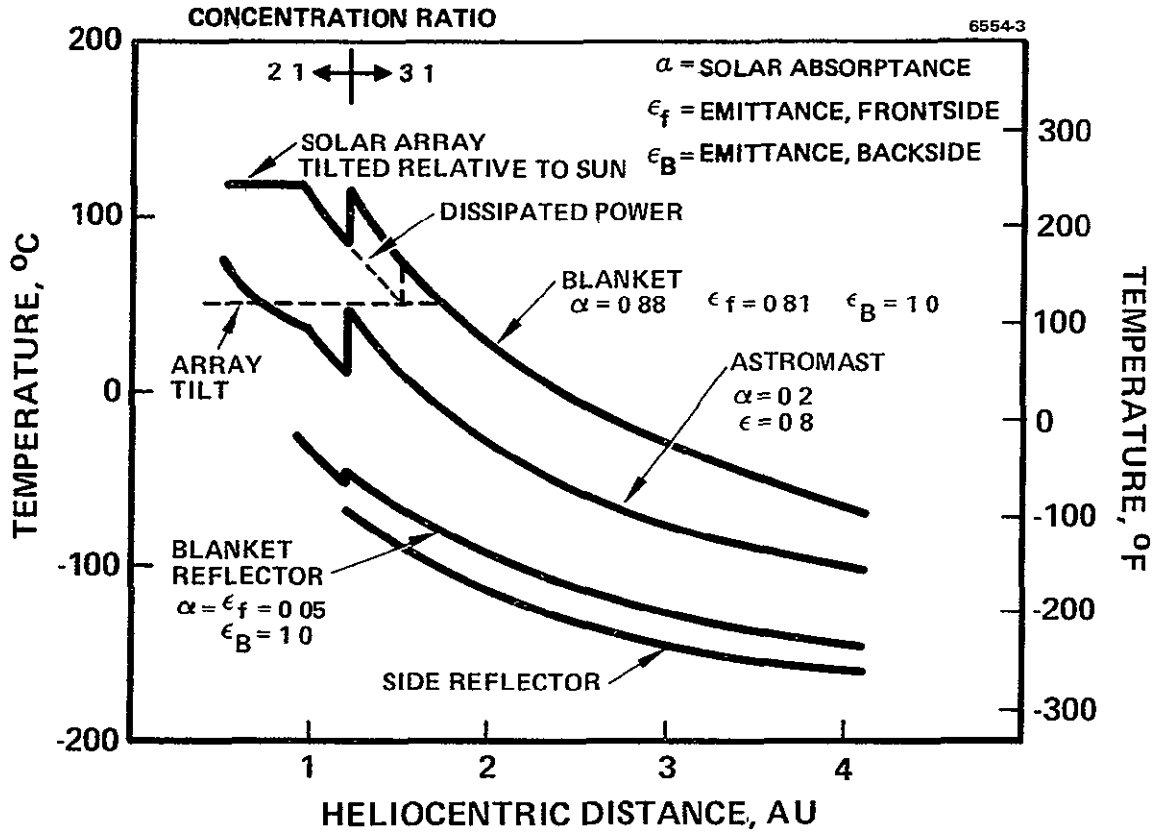

Figure 3. Thermal characteristics of the solar array.

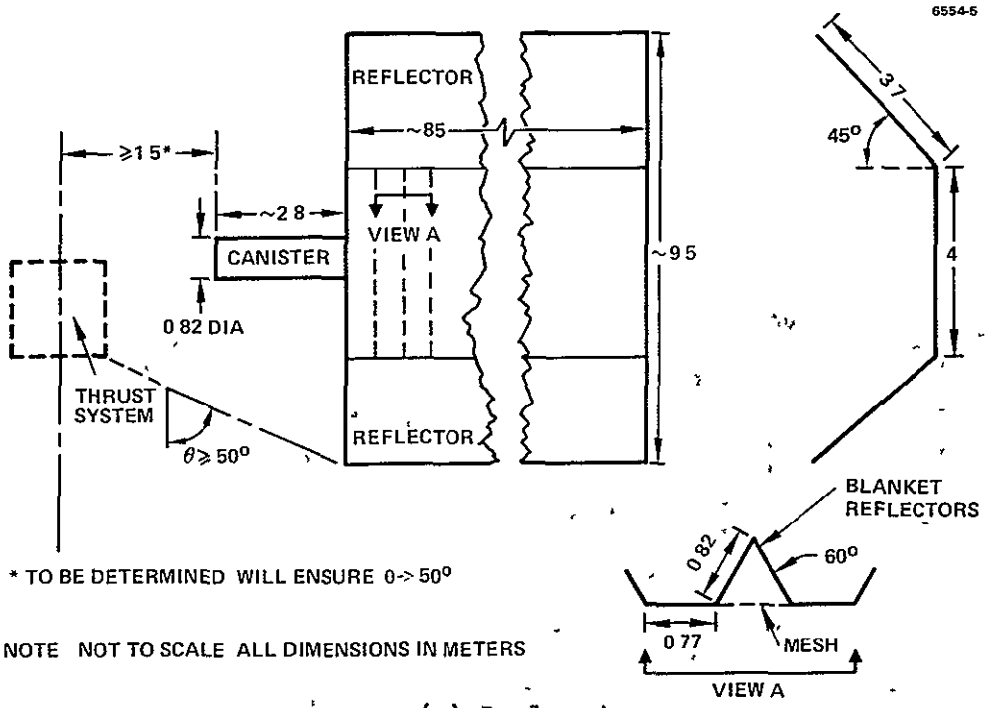

(a) Deployed

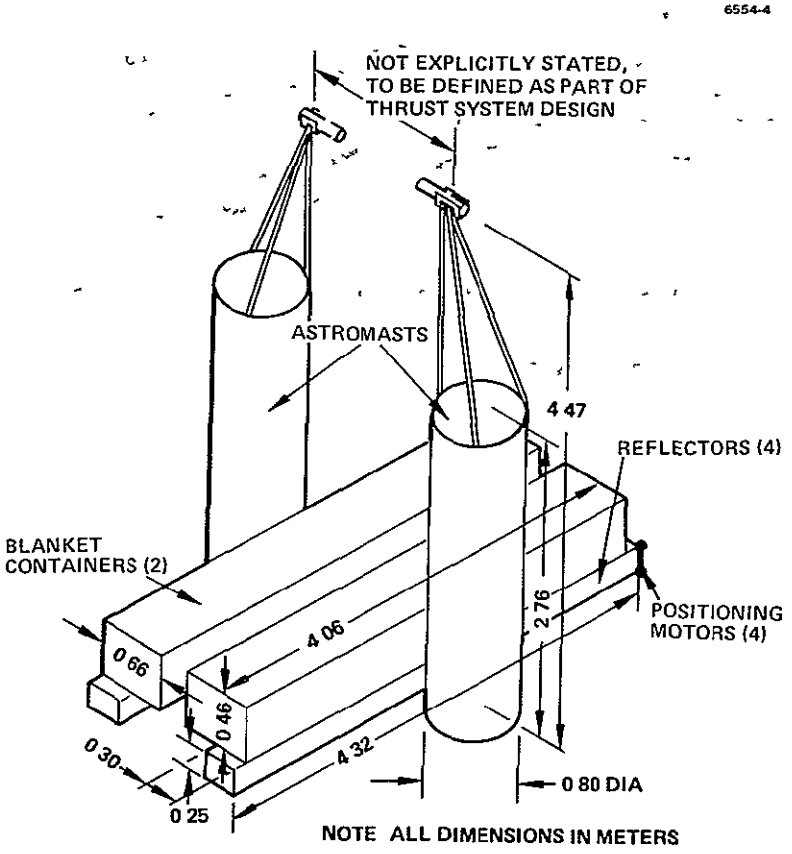

(b) Stowed

Figure 4. Configuration of the solar array.

Design assumptions and data base values assumed for the interim upper stage (IUS) and for the shuttle, particularly with regard to load conditions, are treated as part of the definition of the structural configuration in Section 2.D.

B. THRUSTERS AND GIMBALS

The 900-series EMT, which was the ion thruster used as the basis for the extended-performance thruster and the thrust systems evaluated under this study, produces a 30-cm-diameter beam of electrostatically accelerated mercury ions. The technology for this 30-cm EMT evolved from an earlier 15-cm mercury ion thruster that had been developed and flight tested under the direction of NASA LeRC in the SERT II program. (This development effort is discussed in Refs. 1, 2, and 3.) The EMT technology and design base is the result of nearly a decade of component development, performance assessment, and endurance testing. The essential features of the 30-cm EMT, are discussed in Section 1.

The design for the gimbal mechanisms used in this study is also based on technology developed by NASA LeRC. Since this is discussed in detail in Ref. 4, only a brief description of the gimbal mechanism is included here. The specific thruster and gimbal operating characteristics for the Halley's comet mission are then discussed. The impact of these characteristics on the thruster design base are identified in Section 4.

1. The 900-Series 30-cm EMT: Technology and Design Base

A schematic showing the essential components of a typical mercury ion thruster is shown in Figure 5. The thruster assembly vaporizes the liquid mercury propellant, ionizes the mercury vapor, and accelerates and expels the mercury ions in a neutralized, well-collimated beam. The major components of the thruster can be grouped by function:

- Propellant vaporizers and electrical isolators
- Ionization or discharge chamber
- Ion beam forming elements.

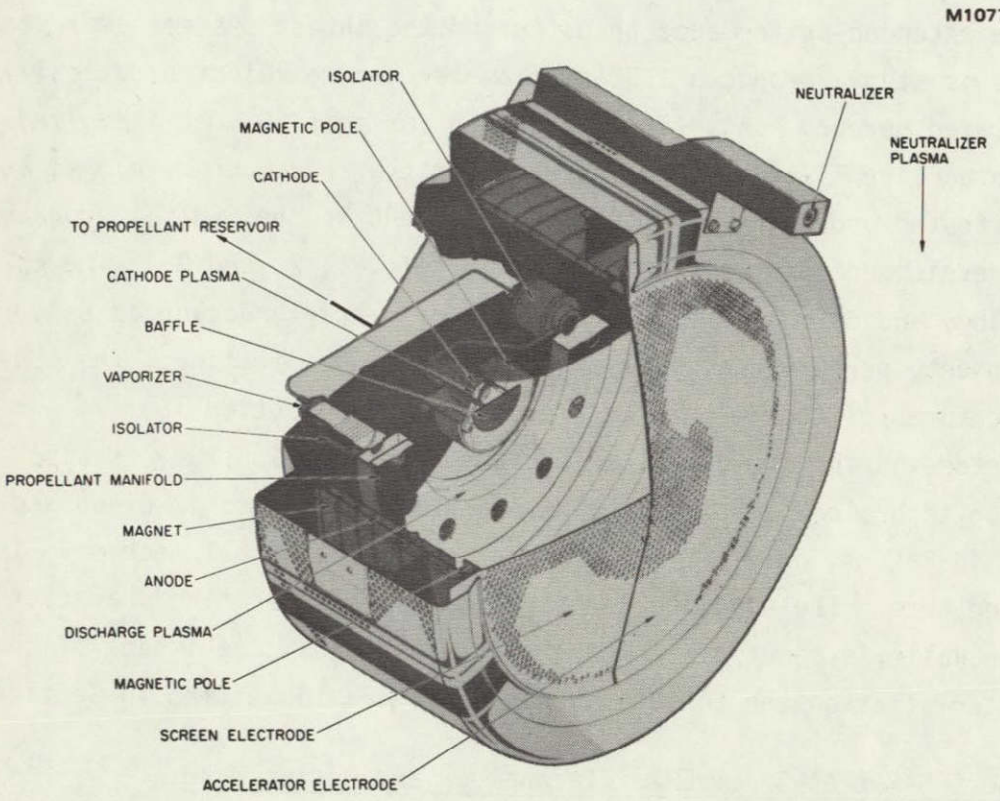

Figure 5. Cut-away illustration of a typical mercury ion thruster.

The operational principles and critical parameters of the components within each of these groupings will be discussed in more detail later. First we consider the structural and thermal properties of the overall thruster assembly shown in Figure 6. The thruster assembly is designed for mounting at two points to facilitate gimbaling. Mounting pads precisely aligned to the thruster axis are provided (in the photographs, one of these pads can be seen at the top of the thruster). The titanium structural elements that provide the support and rigidity necessary to withstand launch vibrations can also be seen in the figure. This structure is designed to withstand the test conditions listed in Table 2. Empirically determined structural properties of the thruster assembly are given in Ref. 5; these were used in this program in designing the thrust system structure. The mechanical interfaces are defined by Hughes drawings number 1095023 and 1026510.

The thermal properties of the thruster assembly have been measured under varying operating power and ambient conditions,[6] and a thermal analytic model of the thruster has been developed.[7] We used these results to design the thermal control subsystem for the thrust system. The thermal properties of the thruster assembly are more or less decoupled from the thrust assembly since heat produced in the thruster is rejected primarily in the direction of the ion beam. Therefore, thermal properties of the thruster had only a minimal impact on the design of the thermal control subsystem.

a. Propellant Vaporizers and Isolators

The propellant vaporizers supply mercury vapor to the thruster. This is done by inserting a porous tungsten disc in the feed line and heating this region to a temperature high enough that the mercury vapor pressure is adequate to cause it to flow through the pores of the tungsten (see Figure 7). To provide the vaporizer function, several porous-tungsten vaporizer configurations were tried during the evolution of the present designs. The thermal requirements of the thruster specifications for propellant reservoir pressure were the dominant factors determining the ultimate vaporizer designs.

M10535

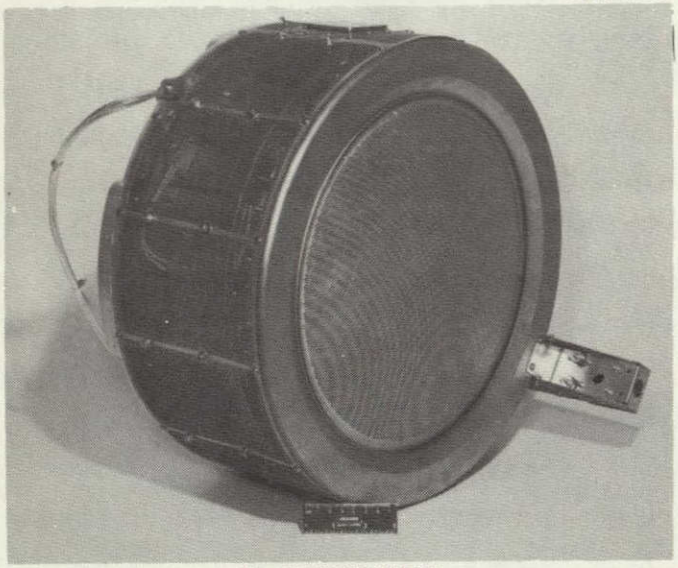

(a) FRONT VIEW

M10536

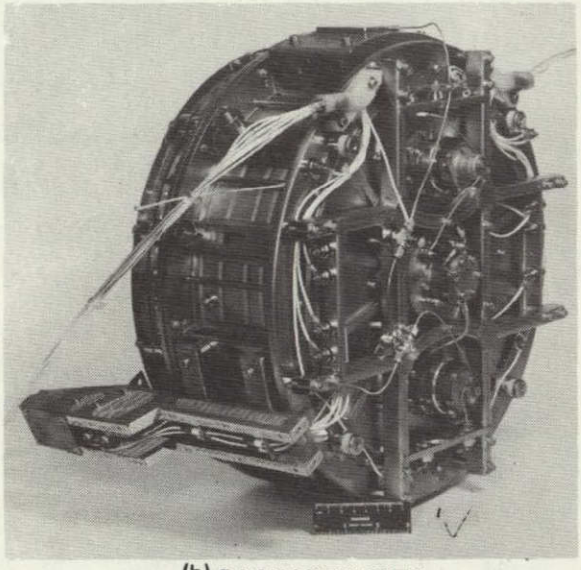

(b) BACK VIEW WITH COVER REMOVED

Figure 6. 900-series 30-cm EMT.

Table 2. Structural Integrity Test Conditions

Sinusoidal vibration (5 to 2000 Hz)
Low-level resonance search
In x direction[a] (1.0 g)
In y direction (1.0 g)
In z direction (1.0 g)
High-level resonance search
In x direction (11.0 g)
In y direction (11.0 g)
In z direction (11.0 g)
Half sine shock: 30 g peak
In x direction (3 each)
In y direction (3 each)
In z direction (3 each)
Random vibration: 19.8 g rms for 4.5 min (each axis)

[a]Axis orientation:

x axis – direction of thrust

z axis – direction of neutralizer

y axis – orthogonal to neutralizer.

5903

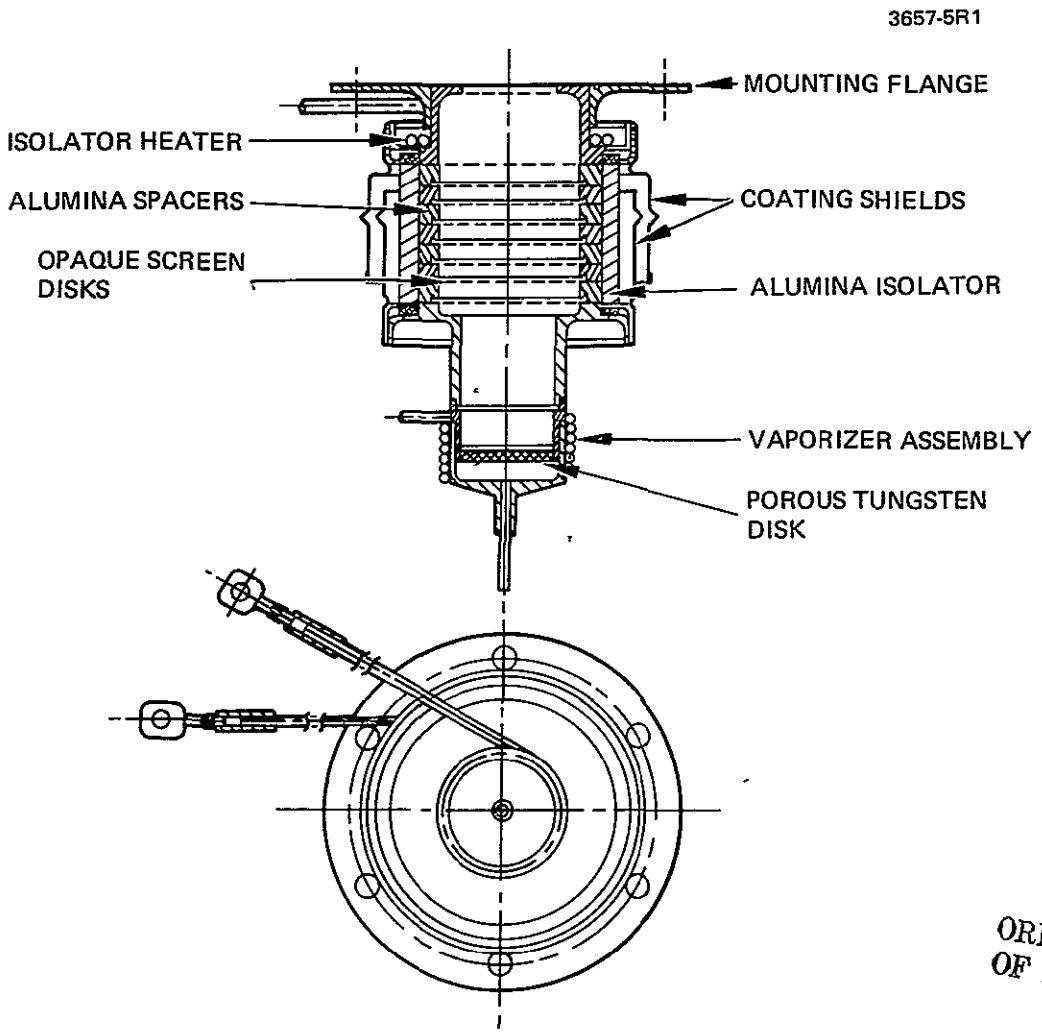

Figure 7. Isolator-vaporizer configuration for the 30-cm thruster.

Pore size must be small enough so that capillary forces prevent intrusion of liquid mercury, and there must be enough pores to allow the required vapor flow at feasible temperatures. Flow rates and temperatures are presently specified as shown in Figure 8. The porous tungsten must withstand liquid mercury pressure of 828 kPa (8.2 atm or 120 psig) without intrusion and must operate with a reservoir pressure of 345 kPa (3.4 atm or 50 psig).

Propellant electrical isolators allow the mercury vaporizer to operate at system common potential while the hollow cathodes and the discharge chamber are operating at substantially different potentials The propellant isolators for the 30-cm thruster require the propellant vapor to flow through a series of "chambers." In each chamber the voltage drop is below the Paschen minimum for mercury. These chambers are formed by spacing optically dense metallic screens in a ceramic tube that forms the isolator. Two isolator-vaporizer assemblies, the main isolator-vaporizer (MIV) and the cathode isolator-vaporizer (CIV), are needed to isolate the beam voltage (1100 V). Both assemblies are constructed with seven chambers An MIV is shown in Figure 7.

b. Discharge Chamber

The discharge chambers of the 30-cm EMT and of the SERT II thruster have essentially the same configuration. Figure 9 shows schematically the more important components of the discharge chamber. Ionization of the mercury vapor supplied by the vaporizers is performed in the discharge chamber by electron-bombardment in a crossed-field, or "Penning-type," discharge. Electrons are supplied by the cathode and magnetically confined to an annular region bounded by the critical magnetic lines of force shown in Figure 9 Inelastic collisions between electrons and atoms or ions randomize the electron motion and establish transport of electrons to the anode Ions are unaffected by the magnetic field and only experience forces arising from plasma potential gradients Anode voltage is typically 36 V and the plasma potential has a local maximum of approximately 40 V near the geometric center of the cylindrical discharge chamber. Consequently, ions formed near the center of the discharge chamber are driven by the potential gradient

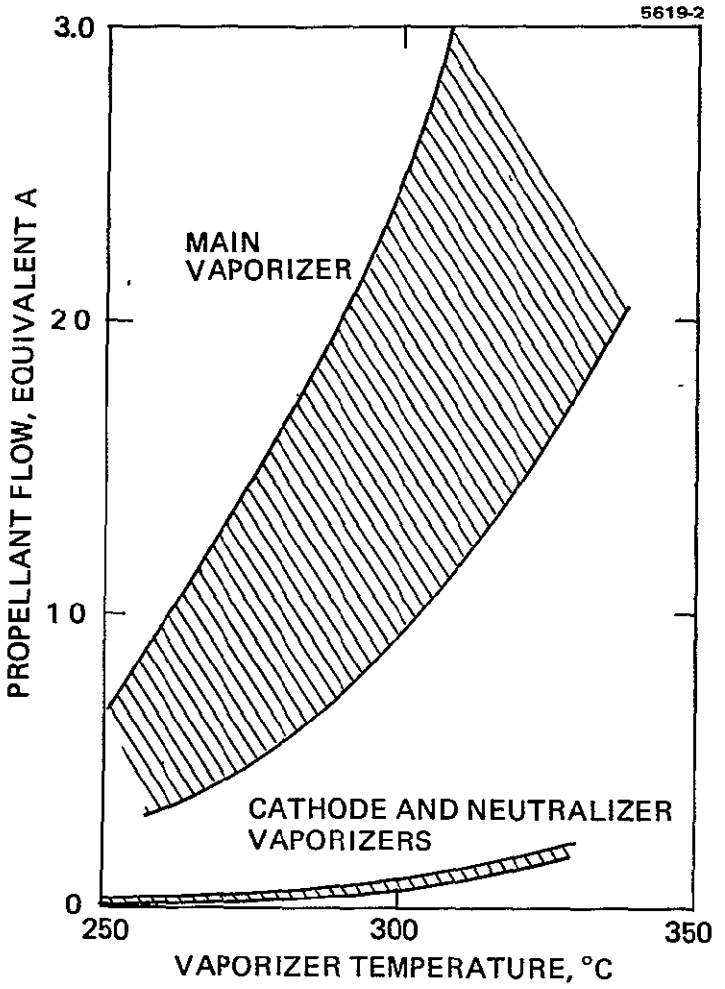

Figure 8. Propellant flow versus vaporizer temperature.

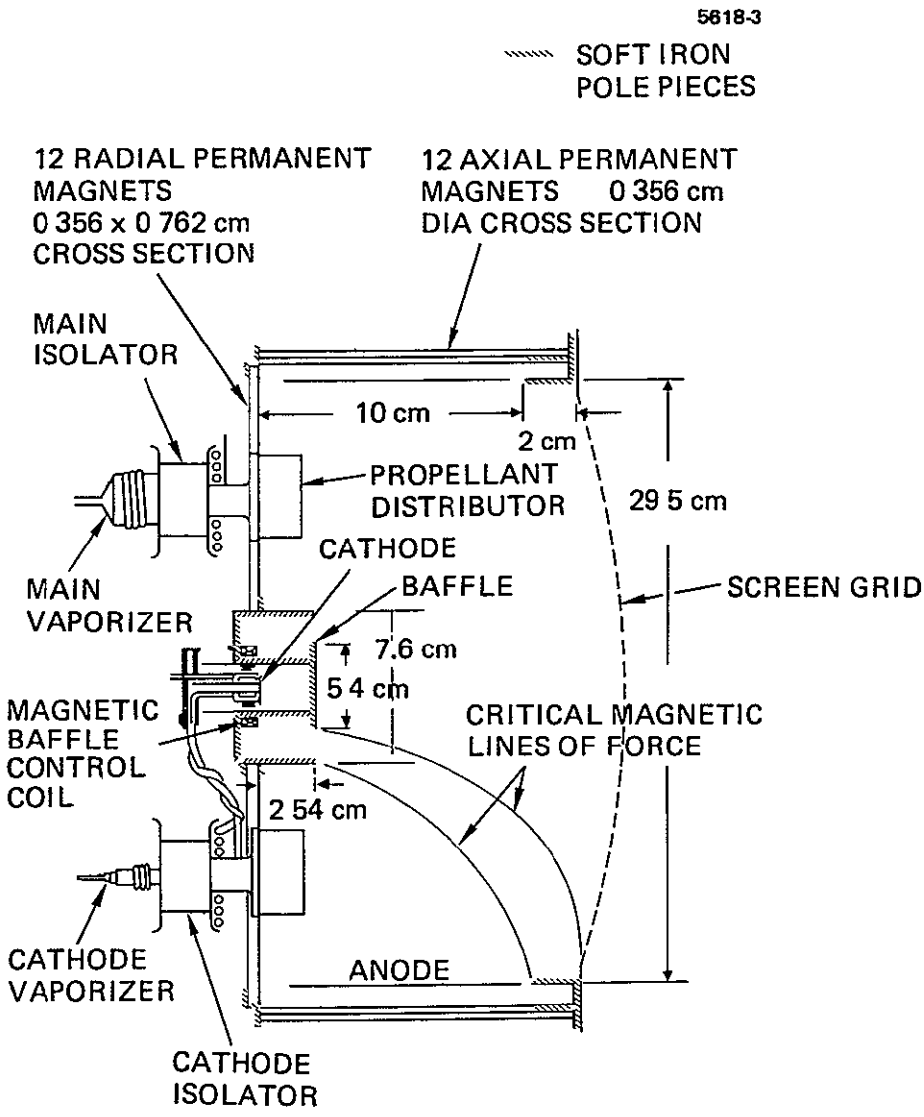

Figure 9. Schematic of the discharge chamber.

either to the baffle and cathode polepiece or to the screen electrode with sufficient energy to sputter away (erode) the surface This is the major source of discharge-chamber wear. To protect the magnetic circuit against this, the soft iron baffle and cathode polepiece are covered with tantalum, which has a low sputtering rate. We have not been able to protect the screen grid, which is also a critical component of the ion extraction and beam forming assembly (ion optics), in a similar manner without altering its function in the beam forming process. Consequently, the screen grid is at present the critical component in determining the wearout lifetime of the discharge chamber. The wear rate of the screen grid depends on several factors (discharge plasma density (beam current), discharge voltage, doubly charged ion fraction, etc). In this study, we assumed a wearout lifetime of 15,000 hr for operation at 2 A beam current.

The cathode that supplies electrons for the discharge process is a hollow cathode that in turn requires a discharge for operation The hollow cathode discharge is ignited initially between the cathode and an annular electrode called a "keeper " The keeper discharge thus acts as a plasma source of electrons for the main discharge volume Because the plasma potential in the keeper discharge plasma can be maintained at a voltage (4 to 10 V) that is well below the sputtering threshold, ion sputtering of the cathode is not a factor in lifetime consideration. Tests at NASA LeRC indicate that cathodes can perform under typical EMT operating conditions (1 1 A emission current) for more than 18,000 hr without degradation.

Erosion of the baffle, cathode polepiece, and screen grid generates a particle flux of molybdenum and tantalum within the discharge chamber. Because this material deposits on interior surfaces where ion impingement is low, a special surface treatment is required to prevent these deposits from spalling and forming large flakes Metallic flakes that are large enough to bridge the ion optics interelectrode gap or to partially obstruct one of the screen grid apertures can cause the thruster to fail prematurely. Several components of the 900-series EMT discharge chamber have received surface treatment for flake control.

Techniques developed for small thrusters[5] were used to cover the anode and propellant distributor with a fine wire mesh, and to grit blast the interior surfaces of the cathode polepiece. It has not yet been verified that these surface treatments can prevent large flakes from forming in 30-cm thrusters for the entire projected lifetime of the thruster

c. Ion Beam Forming Elements

The multi-aperture electrodes that accelerate and focus the ion beam (and are referred to as "ion optics") are the most critical subassembly of the thruster. The screen grid is one boundary of the discharge chamber. Those ions that pass into the screen grid apertures are accelerated and focused to form the ion beam Therefore, the effective transmission of incident ions through the screen grid is an important property of the ion optics. The assembly's current capacity, referred to as the "perveance," p, is a function of total beam current, I, and total extraction voltage, V.

$$p - \frac{I}{V^{3/2}}$$

The perveance depends on the self-consistent field (including the charge density of the ion current) in each aperture; the field is in turn determined by the effective interelectrode spacing (including electrode thicknesses) and by the aperture diameters. The EMT ion optics design has evolved from empirically optimizing the aperture diameter and the electrode spacing to obtain a high perveance, and a mechanically stable assembly. The electrodes are hydroformed to a 52-cm radius of curvature; the aperture specifications are given in Figure 10. The electrodes each have 15,173 apertures, these generate a beam envelope about 28 cm in diameter The measured average perveance per aperture is $2\ 6 \times 10^{-9}\ AV^{-3/2}$, which is about 40% of the calculated value for the dimensions given in Figure 10

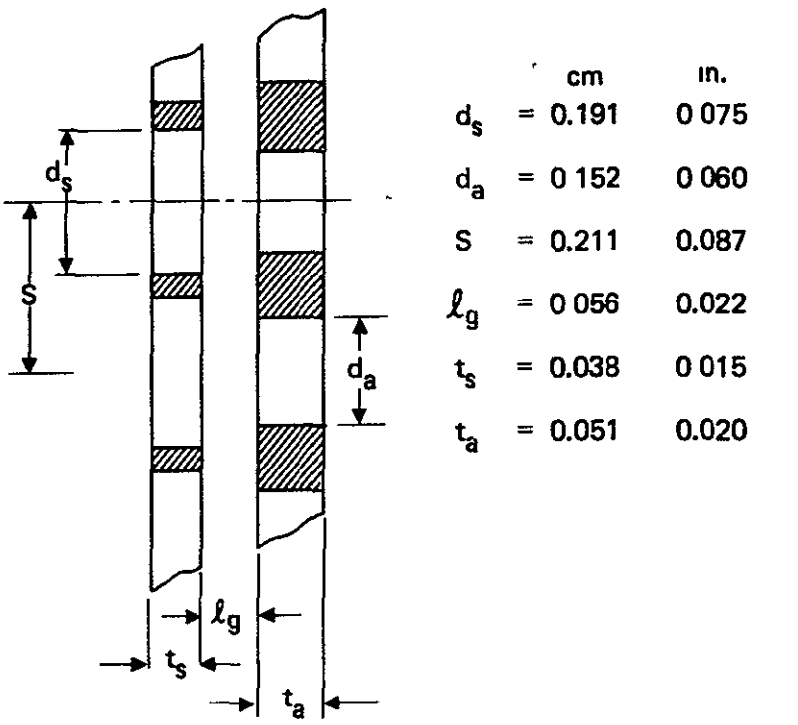

Figure 10. Aperture configuration used in 900-series 30-cm thruster ion optical assembly.

One fundamental limitation of the dished-electrode ion optical system is that the trajectories of the ions in the beam diverge because of the electrode curvature. If an individual pair of apertures on a spherical surface electrode set is aligned along the radius of curvature through the center of this aperture pair, then the beam produced by these apertures emerges along that radius. Hence the apertures near the edge of the beam produce "beamlets" that emerge at an appreciable angle with respect to the thruster axis and must be vectored to produce paraxial beamlets. Vectoring (i.e., "compensation") has been provided by displacing the screen-grid apertures with respect to the accelerator grid apertures by an amount proportional to the beam radius. This displacement is applied by contracting the screen grid aperture pattern.

Beamlet vectoring by aperture displacement is limited to approximately 15 to 18 deg, depending on beamlet current density, before direct interception of the focused ions occurs. Reduction of the screen hole pattern by 0.5% was found empirically to minimize beamlet divergence angle but evidence of some direct interception was noted on some of the outermost accelerator apertures (probably because the alignment tolerances permit vectoring to exceed the permissible limit). Reducing the screen hole pattern by 0.4% eliminated the direct interception; this has provided a slight margin for misalignment during assembly and introduced only a slight divergence in trajectories.

An important feature of the 30-cm ion optics system is that it can be removed from the thruster as a rigid subassembly. This is especially true for electrodes that have screen and accelerator electrode hole patterns that have been intentionally misaligned radially to provide divergence compensation. By using a structurally rigid mounting structure, the aperture alignment and interelectrode spacing can be carefully adjusted, measured, and secured. The EMT ion optics subassembly is shown in Figure 11. With the aperture parameters discussed earlier, this assembly has been operated at beam currents up to 4 A and total extraction voltages up to 2300 V.

M10403

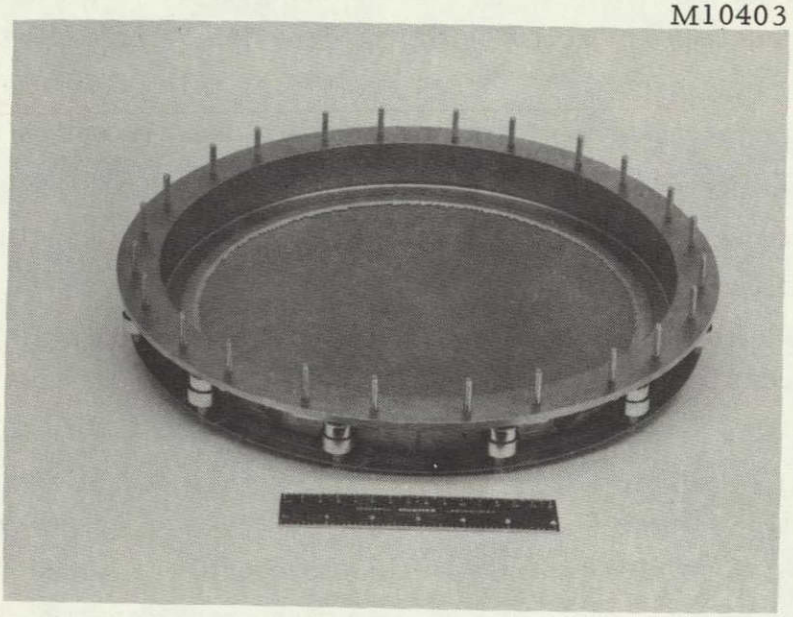

(a) Plasma side

M10404

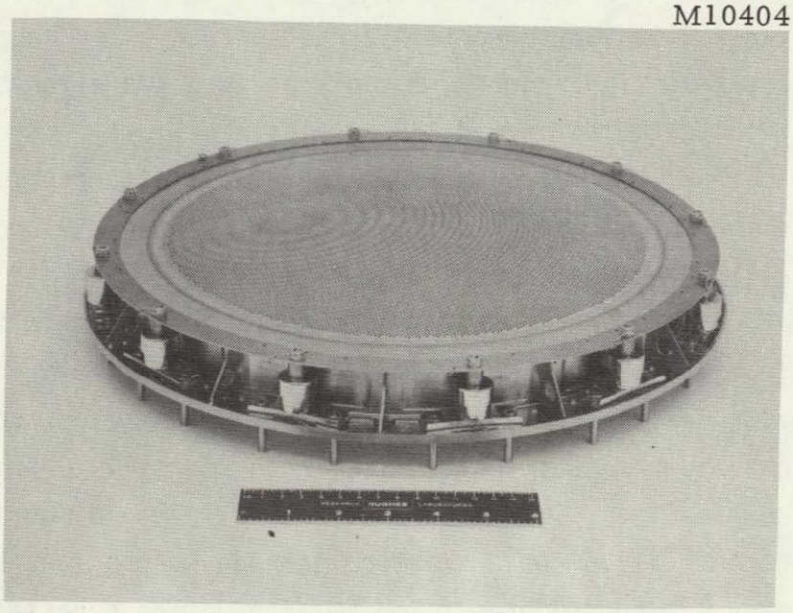

(b) Beam side

Figure 11. Ion optical system assembly with titanium support ring.

The neutralizer assembly, the remaining element required for ion beam formation, supplies electrons to establish space-charge neutrality within the ion beam This prevents differential charging of the thrust system with respect to the space plasma The electron source, as in the case of the discharge chamber, is a hollow-cathode discharge that supplies both the electrons and the "plasma bridge" to couple the electrons to the ion beam. Within the operating limits documented for the EMT, the properties of the neutralizer cathode are well documented and the neutralizer technology and wear mechanisms are completely understood [10,11]

2. The Thruster Gimbal Mechanism

The gimbal mechanism postulated for this study is one based on a gimbal system that was designed, fabricated, and tested with an 8-cm ion thruster at NASA LeRC. The description given here is quoted directly from Ref 4.

> Figure 12 shows the conceptual gimbal system interfacing with the 30 cm EMT
>
> The two linear actuators and a cross pin hinge or gimbal provide the thruster gimbal directions in two mutually orthogonal axes These components are mounted on a thruster mounting bracket which is attached to the mounting pads on the sides of the thruster and to standoffs at two of the four ground screen mounts on the back of the thruster. The two jackscrew type actuators are driven by a stepper-motor-gearhead assembly The actuators have a universal joint at both ends for compliance. A guide pin that is attached to the thruster mounting frame rides in the slot of a support bracket that is mounted to the lower truss of the module. One of the advantages of this system is that the arrangement of the actuators, cross pin hinge and guide pin provides stiffness in all directions thus eliminating the need for pin puller restraint during launch The static and dynamic launch loads are carried in the x direction by the two actuators and the cross pin hinge, in the y direction by the thrust washers in the cross pin hinge, and in the z direction by the cross pin hinge and the support bracket. The angle indicator system consists of two resolvers that are attached to the cross pins of the hinge and provide direct readout of the α and β gimbal angles. The flexible propellant feed line is a coiled spring tube
>
> A good thermal design is provided by the linear actuator gimbal system because the actuators are placed behind the thrusters. A thermal barrier could be placed between the

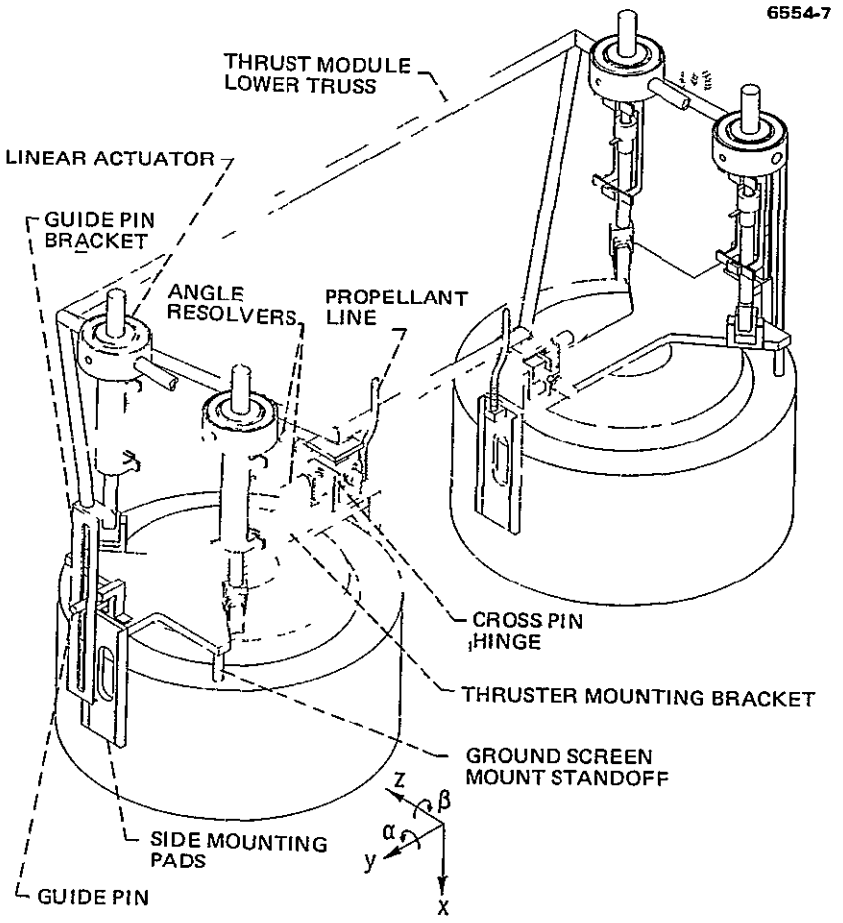

Figure 12. Interface between the gimbal system and the thruster.

thrusters and the lower truss of each module and thereby the gimbal actuators would be located within the controlled thermal environment

Specifications for the linear actuators are determined by the angles α and β required to direct the thrust vector of the outermost thruster through the center of mass of the spacecraft For the baseline thrust system design, α is $\pm 35^{o}$ and β is $\pm 5^{o}$.

3. Required Operating Characteristics of the Extended-Performance Thruster for the Halley's Comet Mission

The thruster operational characteristics of interest in the design of the thrust system are determined to a first approximation by the thrust required to perform the mission To evaluate parameter trades, it is desirable to have an analytic expression that characterizes the performance of the thruster assembly under different operational specifications. Quantities of interest are

$\eta_t \equiv$ the total thruster efficiency

$\eta_u \equiv$ the propellant utilization efficiency

$\eta_e \equiv$ the electrical efficiency

$I_{sp} \equiv$ the specific impulse

$T \equiv$ the thrust produced

$P \equiv$ the thruster power (total)

Independent control parameters for an ion thruster are beam current, I_B, and voltage, V_B. The quantities listed above can be derived either directly, in some instances, or empirically from these two beam parameters for any given thruster design

The operational characteristics listed above have been measured experimentally for several beam current values in the 0 5 to 2.5 A range at the EMT beam voltage (1100 V) The experimental data points can be

approximated quite well by substituting the appropriate values of I_B and V_B into the following set of analytic expressions:

$$P = I_B (V_B + 200) + 65 \text{ (in W)} \tag{1}$$

$$\eta_t = \gamma^2 \eta_u \eta_e \tag{2}$$

$$\eta_e = \frac{I_B V_B}{P} \tag{3}$$

$$\eta_u = \frac{1}{\beta} \left(\frac{I_B}{I_B + I_N} \right) \tag{4}$$

$$\beta = 1 - 0.08 \left[\frac{I_B + I_{Bx}^2}{2.2 + I_{Bx}^2} \right] \tag{5}$$

$$I_{Bx} = \begin{cases} I_B - 1 & \text{for } I_B \geq 1 \\ 0 & \text{for } I_B \leq 1 \end{cases}$$

$$I_N = 0\ 240 + 0.032\ I_B \text{ (in A)}$$

$$\gamma = 0.942 - 0.005\ I_B + \frac{0.025}{I_B + 0\ 6}$$

$$T = 2.039 \times 10^{-3}\ I_B\ \gamma\ V_B^{1/2} \text{ (in N)} \tag{6}$$

$$I_{sp} = 100\ \eta_u\ \gamma\ V_B^{1/2} \text{ (in sec)} \tag{7}$$

where I_N, β, and I_{Bx} are simply "dummy" variables. γ converts the measured beam current, which contains the contributions of doubly charged ions and of ions that have non-axial velocity components, to an equivalent current of singly charged ions that have paraxial velocities.

The equations listed above were used to analyze the thruster requirements for a Halley's comet mission using the solar array power input capability given in Figure 2 and the appropriate PMaC electronics efficiencies. In examining the thruster requirements, the following set of conditions were assumed:

- The thrust system uses the maximum power available from the solar array at any given time.

- Available power is utilized by operating the least number of thrusters at maximum available power (below the design maximum per thruster).

- Reduction in power during the mission (throttling) is achieved by reducing beam current only (as compared to reducing both beam voltage and current).

- Thrusters can be gimbaled to permit any combination of thrusters to be operated, the thrusters can therefore be turned on or off one at a time (although the minimum number of operating thrusters required for steering is two)

With these conditions, the goal was to determine the thruster parameters required to

- Maximize thruster efficiency

- Minimize the number of operating hours per thruster

For analyzing the baseline design, a restriction of 2 A maximum also was placed on the beam current. It was found that a maximum thruster power between 6 and 7 kW establishes these conditions. If we specify a maximum power below this value, it will be necessary to operate more than two thrusters for the long period of time when the vehicle is traveling at a large heliocentric distance Hence, the operating time for this period must be shared between the total number of thrusters, operating three at a time instead of two at a time This means that the operating time per thruster will be greater. Designing the thruster for higher maximum power (considering the total number of thrusters aboard to be constant) reduces the operating time per thruster, reduces the total propellant required, and increases the specific impulse (since J_B is not increased to more than 2 A, only V_B increases) It is more difficult to assess the higher power case If, for instance, the thruster is designed for a maximum power that is greater than the power available from the solar array at large heliocentric distances, then operating two thrusters will require deep throttling, to half power or less, over a long portion of the mission This would result in degrading average thruster efficiency Table 3 lists some of the variations in thruster parameters considered in evaluating the effects of increasing the maximum thruster

Table 3. Thruster Operational Parameters versus Design Options

Parameter	Option A	Option B	Option C	Option D
Maximum number of thrusters operating simultaneously	8	7	7	7
Beam voltage (constant during mission), kV	2.7	2.9	3.0	3 3
Average beam current, A	1.80	1.83	1.83	1 78
Maximum thruster power, kW	6.0	6.3	6 4	7.1
Average thruster power, kW	5.3	5.7	5.9	6 3
Specific impulse, sec	4520	4690	4770	4980
Average thruster efficiency, %	75.4	76.0	76 2	76.3
Total Hg propellant required, kg	2025	1830	1810	1660
Operating time per thruster, hr				
10 operational, no spares	13,870	12,360	12,200	11,475
9 operational, 1 spare	15,410	13,733	13,600	12,750
8 operational, 2 spares	17,340	15,450	15,250	14,343

Selected Baseline

Option C with 9 operational thrusters and 1 spare

Selection Criteria

Reliability, Hg weight, power/voltage, I_{sp}, efficiency

Selection Rationale

- Option A rejected: poor reliability, large Hg weight
- Option D rejected: high voltage, I_{sp} probably too high
- Option C preferred to option B: higher reliability and efficiency
- 9 operational and 1 spare preferred for better system reliability

5903

power; four options are shown. An increase from 6.4 kW to 7 kW would not only improve efficiency, but would also further decrease the propellant requirement and the operating time per thruster requirement. This comparison is based on the assumption that the solar array power output profile shown in Figure 2 does not change appreciably for the range of parameter variation indicated The trajectory for this power profile was analyzed and defined on the basis of operation at approximately 4700 sec specific impulse. Therefore, it is conceivable that a longer thrusting time would be required to travel the same trajectory at a specific impulse of 5000 sec, thus negating any real reduction in operating time or decrease in propellant use. Consequently, a value of 6.4 kW (Option C) was selected somewhat arbitrarily as the maximum power level for which the thruster would be designed. Since this power level represents a relatively small variation in specific impulse from that used for the trajectory analyzed, the parameters shown in Table 3 should have sufficient validity to realize a gain in system performance. However, to optimize the thruster power and parameter specifications would require analysing the trajectory changes that arise from modifying the thrust levels. Also, since the beam voltage (specific impulse) need not be held constant along the trajectory (as was assumed here), different thruster specifications could be generated For example, one of the options evaluated early in the study was to reduce the specific impulse at large values of heliocentric distance This increases the thrust at a more effective region of the trajectory, but requires an increase in the number of operating thrusters.

Table 3 shows that the thrust system for a Halley's comet mission will require 10 thrusters to obtain acceptable reliability (discussed in Section 3) and that the beam voltage required will be on the order of 3,000 V. Figure 13 shows the thruster operation plan proposed for Option C

4 Impact of the Halley's Comet Mission Requirements on the 900-Series 30-cm EMT Design

The impact of mission requirements on the 900-series EMT design are relatively minor. Operation of the thruster at higher beam voltage had

THRUSTER POWER		AVERAGE BEAM CURRENT	1 83 A
MAXIMUM	6 4 kW		
AVERAGE	5 9 kW	Hg PROPELLANT	1810 kg
CUMULATIVE HOURS OF OPERATION		PROPELLANT UTILIZATION	0 923 (AVG)
EACH THRUSTER	13,600 hr	SPECIFIC IMPULSE	4770 SEC (AVG)
TOTAL MISSION TIME	30,720 hr	THRUSTER EFFICIENCY	0.762 (AT AVG POWER)

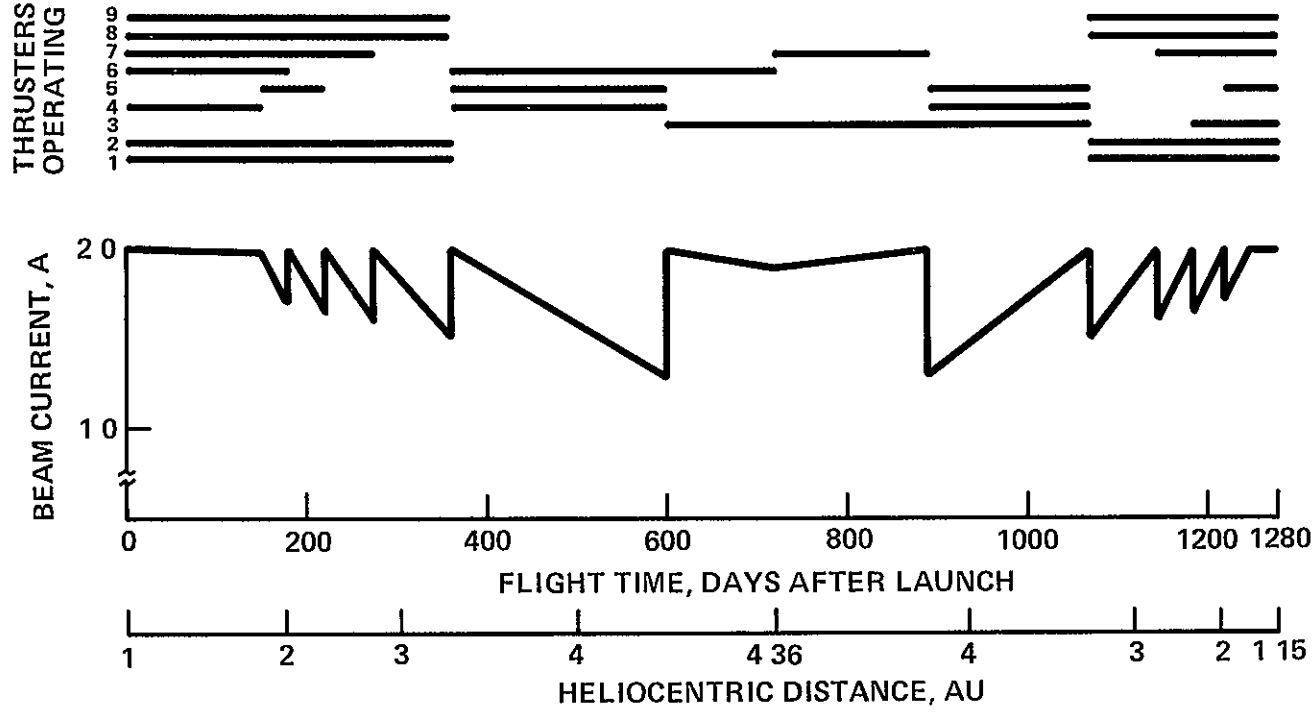

76282-15

Figure 13. Thruster operation plan.

been demonstrated before this study[12] and extensive testing at 3,000 V was also conducted under this program (see Volume IV). Thruster components directly affected are the ion optics assembly and the propellant electrical isolators The required modification in the ion optics assembly is an increase in the interelectrode spacing,[12] which can be achieved by simply replacing the support spacers with longer ones.

The propellant electrical isolators must be completely replaced by components with a high voltage rating (5,000 V). A high-voltage isolator suitable for installation on the 30-cm EMT had not been demonstrated before this study However, a straight forward scaling of the 900-series 30-cm EMT propellant isolator produced a component that is capable of operating at 6,000 V and is a direct replacement for the b aseline isolator (see Volume IV). Neither a review of the thruster design nor preliminary verification testing indicates that any other design modifications are necessary. Although it may ultimately be necessary to provide more margin in all high-voltage insulation (wiring, standoff length, part clearances, etc.), the initial examination did not reveal any significant problem areas

All other parameter specifications under Option C of Table 3 fall within the normal operating range for the 900-series 30-cm EMT Consequently, we assessed the lifetime and reliability characteristics of the modified extended-performance thruster by using the appropriate EMT parameters The useful lifetime (that is, the time before wearout mechanisms begin to cause performance to deteriorate) of the 900-series EMT has been projected to be 15,000 hr. Reliability of the thruster is assumed to be governed by a constant failure rate, λ, that is valid for the time period after initial failures (infant mortality) occur until the onset of wearout. The reliability, R, is computing using:

$$R = e^{-\lambda t} \quad ,$$

where t is time in hours. An accurate assessment of λ is traditionally based on the statistics generated in testing to failure. This type of data does not exist for ion thrusters, and the best estimate available was obtained by comparing thruster components and the anticipated failure modes to comparable aircraft or electronics components for which statistical data is available and then applying a rating factor to

account for differences in operating conditions. This technique produces a value of λ between 10^{-6} and 10^{-5} failures per hour Thus, we concluded that the 900-series 30-cm EMT, with the minor modifications listed above, could satisfy the requirements of a Halley's Comet mission (assuming that the specifications for the EMT are accurate)

C. POWER MANAGEMENT AND CONTROL

The PMaC subsystem consists of 10 sets of thrust module power supplies (one per thruster or two per module) and a set of electronic units on the interface module. It processes, conditions, and manages the power furnished by the solar array to provide the required voltages and currents for the operation of the thrusters, to furnish power for the thrust-system housekeeping and control functions, and to provide the required mission module power. Thrust module power units are comprised of beam, discharge, and low-voltage power supplies for the operation of individual thrusters. The interface module units perform power control, distribution, and conversion functions, and include a thrust system controller. The conventional PMaC electronics design selected for the baseline utilizes the low-voltage solar array power and accomplishes the required conversion within the thrust module power supplies by means of conventional solid-state circuitry. These power supplies use the current-controlled series-resonant power-inversion circuit approach currently under development for NASA LeRC for the 3 kW power level. The other PMaC approaches considered were the direct drive and voltage multiplier. The rationale for the selection of a conventional design are presented in Volume III. The following subsections present the design features of the baseline PMaC approach. The design requirements including the functional architecture are discussed in Section 2 C.1 Next, the principal trade-off studies for certain elements of the PMaC subsystem are presented. Section 2.C.3 describes the baseline PMaC subsystem architecture and elements. A description of the physical configuration of the PMaC subsystem is provided in Section 4.

1. Design Requirements

The design data base that defined the PMaC design requirements comprises. (1) the PMaC subsystem functional requirements furnished by NASA LeRC; (2) the specification of thruster power requirements, and (3) the definition of solar array output characteristics The original NASA LeRC PMaC subsystem block diagram, furnished as a study input from the earlier NASA LeRC initialization study, is shown in Figure 14 Thruster power requirements are listed in Table 4 The solar array output characteristics provided for the selected concentrator array baseline configuration were given in Section 2.A. Figure 15 further defines the solar array voltage and current variations (as a function of heliocentric distance) and the power profile.

An analysis of the functional architecture of the PMaC subsystem (for the initial configuration shown in Figure 14), of alternative means for partitioning PMaC functions, and of solar array power output characteristics led to several significant modifications. One of these stemmed from the requirement to maintain the PMaC subsystem input voltage ratio within the 2:1 limit required by the conventional power processor design. Figure 15(a) shows that a voltage swing of up to 2.6·1 exists at the solar array output over the range of heliocentric distances. This led to the incorporation of solar array control units. Input filters for the beam and discharge series resonant inverters were included in the power distribution units in the interface module rather than in the beam and discharge supplies in the thrust modules. Control functions common to all thrust modules were incorporated in the interface module PMaC units

For the beam and discharge supplies, we made use of the following design data provided by NASA LeRC. 94% beam supply efficiency, independent of thruster power level, 52 W discharge supply power dissipation, also independent of thruster power level; and mass of beam and discharge supplies of 20 kg and 5 kg, respectively, with the accelerator supply incorporated in the beam supply. Thrust module beam, discharge, and low-voltage supplies were packaged (using the "Z"-frame technique developed by NASA LeRC) within overall dimensions per module of 0 76 m x 1.02 m x 0.15 m (20 in x 40 in. x 6 in.), specified by NASA LeRC A

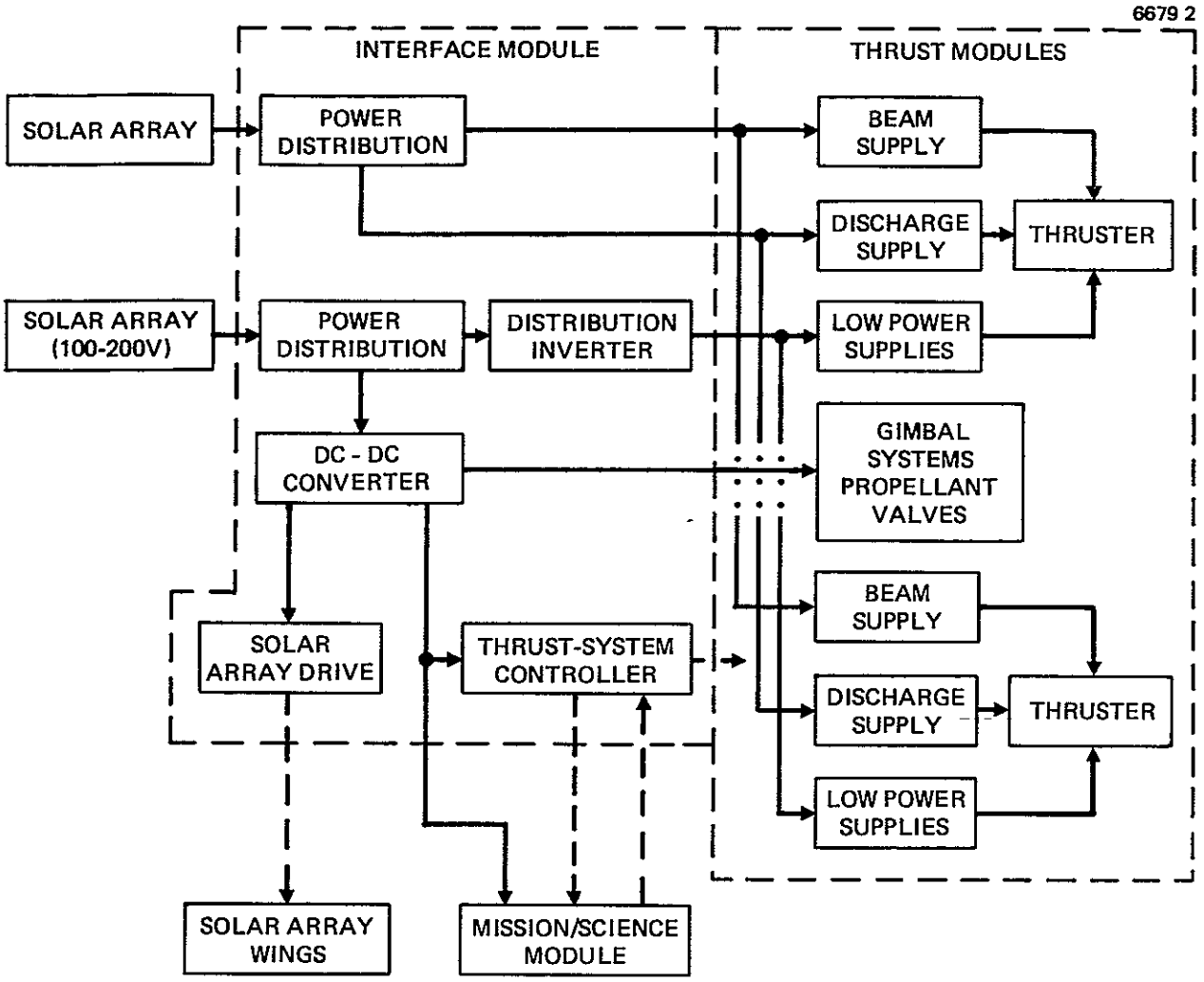

Figure 14. Block diagram of the conventional PMaC subsystem (furnished by NASA LeRC).

Table 4. Thruster Power Requirements

Supply Number	Supply	Maximum Ratings[b]			Static Load Regulations Type and Percent	Static Load Ripple, Percent, F-P
		Voltage, V	Current, A	Power, W		
1	Main vaporizer	9	1 5	13.5	1 ± 5	10[c]
2	Cathode vaporizer	6	1.5	9	1 ± 10	10[c]
3	Cathode heater	15	4.4	66	1 ± 5	10[c]
4	Main isolator and cathode isolator	9	4.0	36	V ± 10	10[c]
5	Neutralizer heater	15	4.4	66	1 ± 5	10[c]
6	Neutralizer vaporizer	6	1 5	9	1 ± 10	10[c]
7	Neutralizer keeper[a]	25 (20)	2.5 (2.1)	62.5	1 ± 5	2
8	Cathode keeper[a]	15 (5)	1.0 (0.5)	15	1 ± 10	10
9	Discharge	60	16.3	815	1 ± 1	2
10	Accelerator	500	0.02	10	V ± 10	10
11	Screen	3000	2.0	6000	V ± 10	10
12	Magnetic baffle	2	5 0	10	1 ± 5	5

[a]Boost supply. 400 V at 10 mA, 25 V at 100 mA.

[b]Maximum rating is defined to that voltage and current level that each supply can deliver continuously to the thruster Where two V/I characteristics are indicated, a condition during startup is shown and the norminal condition is bracketed.

[c]Applies only to dc heaters.

5903

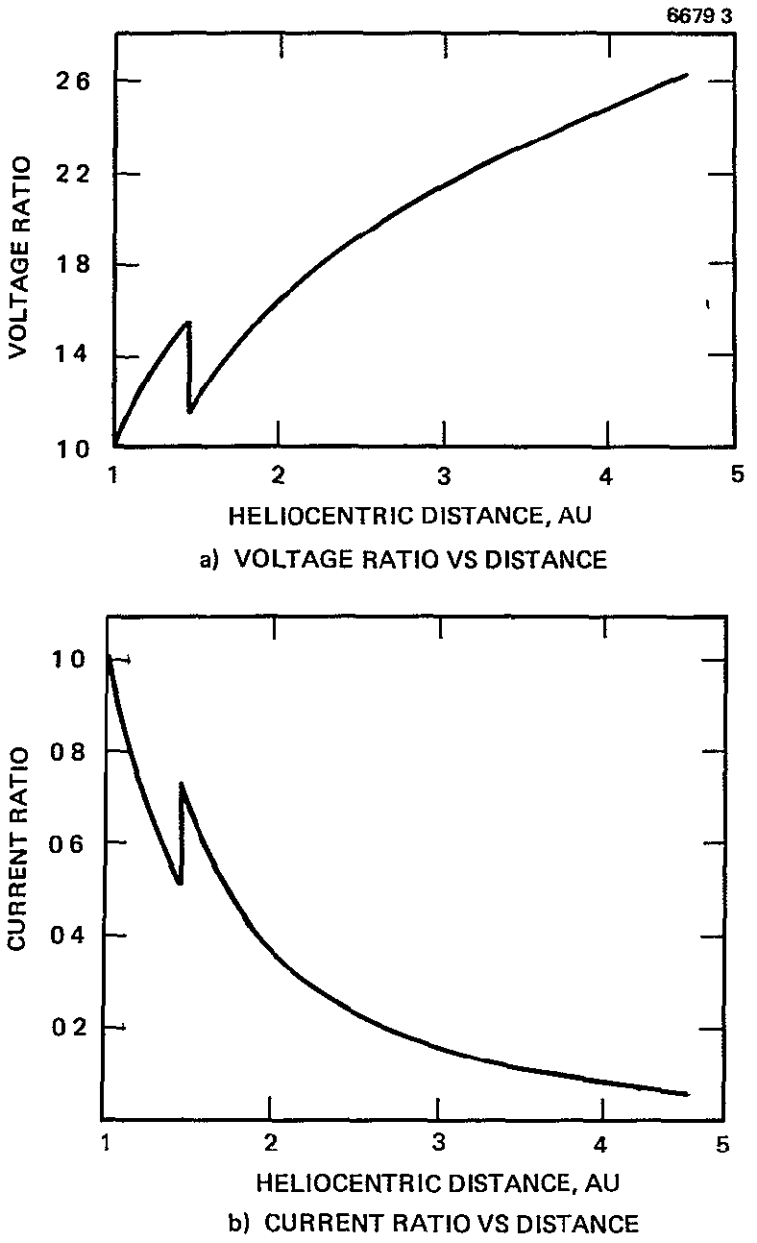

Figure 15. Normalized characteristics of the 3:1 concentrator solar array.

concurrent extended-performance power-processor design study was sponsored by NASA LeRC. Although the thrust system design study reported herein provided system design information to that effort, the first results from the power-processor design effort only became available after the thrust system technical effort had been completed.

PMaC housekeeping and mission module power requirements are summarized in Table 5. The ±15 V and 0 to 5 V requirements are for beam and discharge supply logic power and analog reference The system battery, provided in the mission module, furnishes power before the solar array is deployed. This includes power for thrust system housekeeping, firing the release squibs, and deploying the solar array

The logic to perform the thruster control functions and the other thrust system management functions is centrally placed in a controller (one of the PMaC interface module units). The controller must be capable of ensuring autonomous thruster operation for an extended period, its functions include sensing the operating parameters of the power supplies, analyzing the PMaC system and thruster operation, generating and executing control signals, exchanging data with the ground via the mission module.

The following additional general design requirements and ground rules were adopted for PMaC subsystem design:

- A common (single) bus for power distribution.
- The thruster ground must be isolated from the spacecraft ground.

Table 5. PMaC Housekeeping and Mission-Module Power Requirements

Power Source	Voltage Requirements, V	Power Requirements, W
Mission module	+30 ± 2	400 (during thrusting phase)
		650 (during rendezvous)
PMaC system housekeeping[a]	+30 ± 2	75
	+15	140 (max)
	-5	10 (max)

[a]During thrusting phase

5903

- All thruster power supplies must be capable of withstanding transient or sustained shorts.
- A thruster grid clearing circuit must be provided.
- The input/output power bus must have fault protection for all inverters.
- A malfunction of a single thruster/PMaC subsystem should not influence the operation of the rest of the thrust system
- Redundancy for critical units must be provided.
- PMaC component mounting surface temperature range must be maintained between -30° and +50°C

2. Selection of Design Parameters

Certain options became available during the system- and unit-level design work on the PMaC subsystem. Where a particular option was easily evaluated on the basis of engineering judgement as superior, the option was incorporated in the baseline PMaC design without further analysis. Where the selection was not obvious, trade-off studies were conducted in sufficient detail to make the appropriate selection. Principal trade-off studies involved the distribution inverter, the low-voltage power supplies, and the dc/dc converter.

a. Distribution Inverter

The distribution inverter may be designed to run any number of thrusters between 1 and 10 Reliability considerations dictated that one spare inverter be provided for the system. As discussed in Section B, one thruster is assumed to be started at a time.

Figure 16 shows the estimated efficiency of a typical distribution inverter as a function of the percentage of full load. It is based on measured efficiencies of similar type units and indicates how efficiency declines as inverter utilization falls. Table 6 establishes the inverter maximum power condition for various configurations. Power to run a thruster was assumed to be 62 W for steady-state operation and 200 W during start-up.

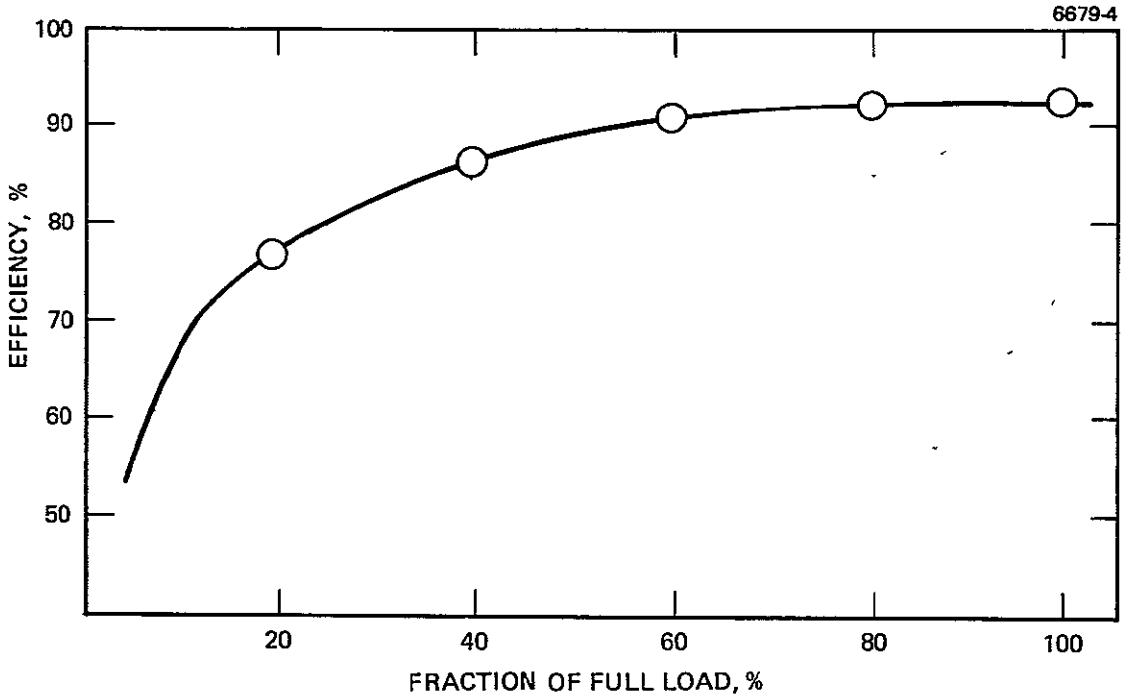

Figure 16 Utilization of the distribution inverter

Table 6. Distribution Inverter Power Levels

Number of Thrusters Per Inverter	Number of Operating Thrusters	P_{Out}, W	Efficiency %	P_{Max} (Start Up),[a] W	P_{In} (Steady-State), W
1	1	62	84 2	200	73.6
2	2	124	88.7	262	139 8
3	3	186	89.7	324	207.4
4	4	248	90 1	386	275 4
5	5	310	90.3	448	343.3
10	10	620	91 2	758	679 8

[a]Design power level.

5903

Table 7 was generated by determining the input power to each inverter as a function of the number of thrusters supplied by each inverter during steady-state thruster operation Inverter weights are based on actual unit weights for inverters of a similar design and scaled to the appropriate power levels. The weights shown in Table 7 were obtained under the assumption that one spare inverter is required in the system Weights and input power shown in Table 7 indicate that five thrusters per inverter is nearly optimal. The baseline design for the distribution inverter should therefore include two operating and one standby inverter. Each inverter should be sized for approximately 343 W while the thrusters are operated steady-state and 448 W while four thrusters are operated steady-state and one is being started up Output power when five thrusters are operating will be 310 W with 33 W dissipated within the inverter.

Table 7 Input Power and Weight of the Distribution Inverter

Number of Thrusters Per Inverter	Input Power, W					Mass of Inverter System, kg-(lb)
	Number of Operating Thruster					
	2	4	6	8	10	
1	147	294	442	589	736	20 8 (46 2)
2	140	280	419	559	699	14 0 (31 2)
3	143	286	415	558	701	14.0 (31.0)
4	146	275	419	551	695	13 0 (28.8)
5	150	277	425	554	587	11.1 (24.6)
10	169	292	419	551	680	11.9 (26 4)

5903

b. Inverter Design Alternatives

The ac distribution inverter is required to supply square-wave drive power at 90 V to the low-power supplies for five thrusters. It is assumed that only one thruster at a time will be started The maximum power that the inverter is required to supply will therefore be the starting power for one thruster plus the running power for four thrusters The inverter must also be short-circuit protected. Several alternative ways of meeting these requirements are available:

- A series-resonant silicon-controlled rectifier (SCR) inverter.
- A transistor bridge inverter, pulsewidth modulated (PWM) for regulation, with a redundant standby inverter, switched to standby by an electromechanical circuit breaker.
- A transistor bridge inverter, PWM for regulation with a solid-state switch in series with the solar panels. To minimize drive power to the switch, a rectified drive would be used.
- A transistor bridge inverter, with a transistor PWM series regulator and switch.

The last three alternatives were compared with the first alternative. The second alternative was not selected because it requires further development of a circuit breaker. The third alternative was eliminated because it requires a current-limiting choke in the transistor switch circuit to limit the rate-of-rise of a faulty current. Although the fourth alternative also requires current limiting, the required inductor size is adequate to serve as a filter for the pulsewidth modulated switch replacing an equal size inductor in the rectified output of a PWM bridge inverter.

A comparison of the first and fourth alternatives indicated very little difference in terms of weight, efficiency, or reliability The series-resonant SCR inverter has been extensively developed by NASA LeRC. Hughes has comparable experience with transistor bridge switching inverters Current state-of-the-art technology can be applied to either alternative. The transistor bridge inverter, the fourth alternative, was selected as the baseline design primarily because appropriate designs

were immediately available for use in this study. Figure 17 is a block diagram of the distribution inverter, Figure 18 is a schematic of it

Referring to the schematic, an input line choke L1 supplies solar panel power to an input capacitor C1; this capacitor in turn supplies quasi-square wave current to switching transistors Q1 and Q2. Input current to each converter is sensed in a hybrid circuit current sensor. Base drive for transistors Q1 and Q2 is supplied by an energy-storage transformer, with fly-back commutation providing reverse turn-off.

The input capacitor C1 consists of four capacitors in parallel for redundancy, each fused to protect against single-point failures. The capacitors must supply a fast rise-time current to the switch with a small voltage drop. Since the voltage on the capacitors can be 200 V maximum, a 300-V low-ESR, tantalum-foil capacitor with low equivalent source resistance was selected and sized to tolerate ripple current without overheating.

The PWM output of the switch is filtered by L2 and C2. L2 and C2 are sized to sufficiently limit the rate-of-rise of fault current to 50 µsec The current sensing circuitry would have 50 µsec in which to

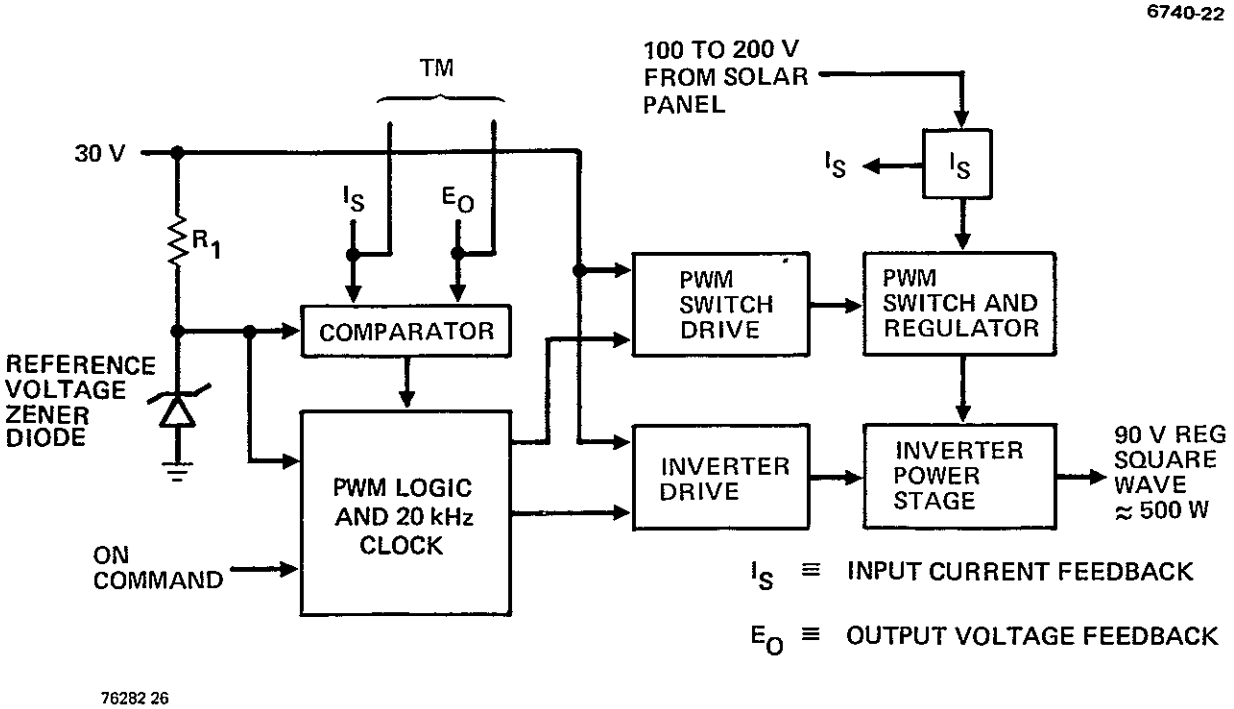

Figure 17. Block diagram of the distribution inverter.

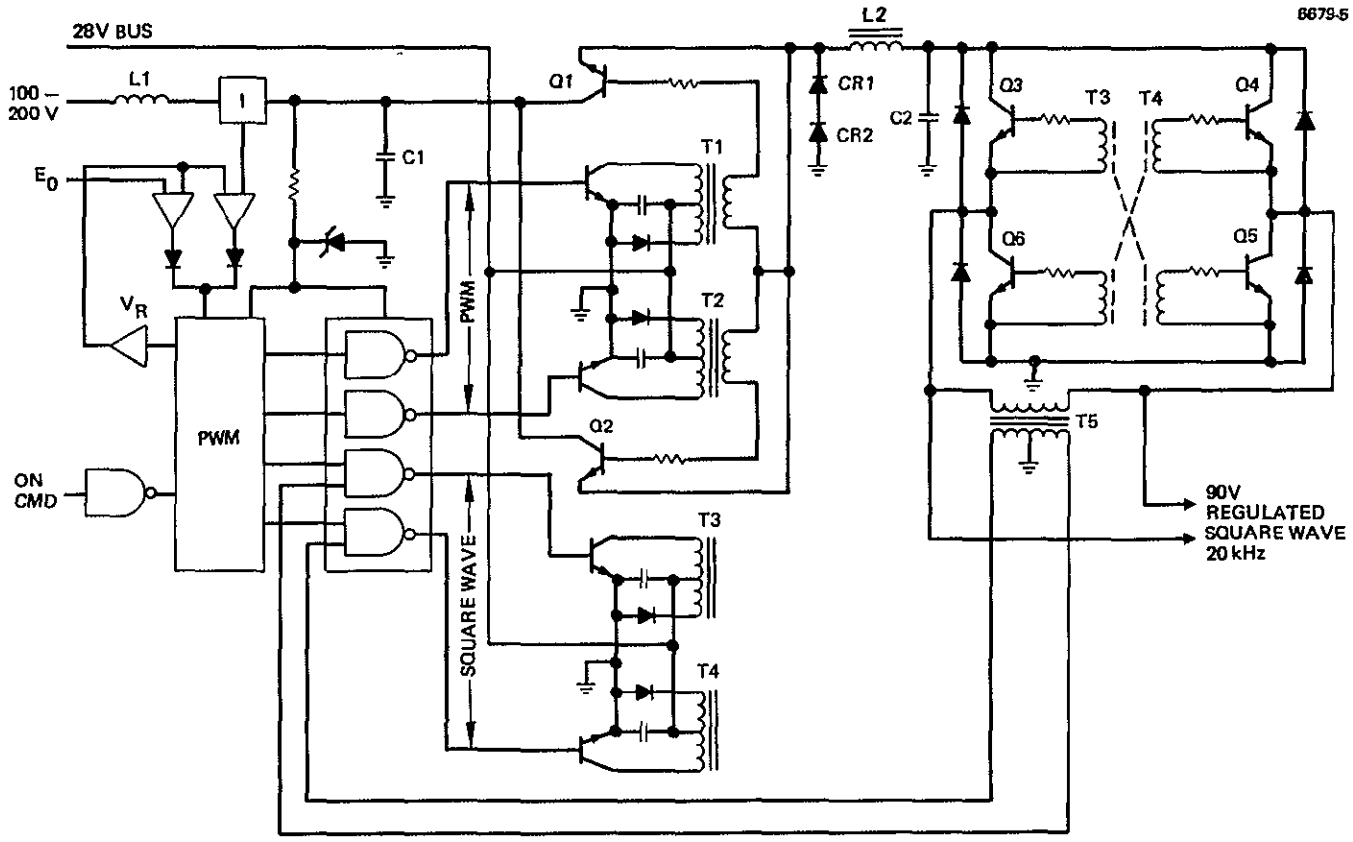

Figure 18. Schematic of the distribution inverter.

respond to an over-current or fault condition. Although 50 μsec is standard for the existing design for Hughes hybrid sensors, this could be significantly reduced if required.

The output of the current-sensor is compared to a reference in a comparator, and when the reference is exceeded, drive to the PWM switch current and to the square-wave inverter is cut off.

The filtered output of the PWM switch is supplied to a transistor bridge square-wave inverter. Since off-time in the inverter is very short (0.5 μsec turn-off and 1 μsec storage, C2 may be fairly small. Ripple current and losses are small in this capacitor.

Also affected by the fast turn-around time in the transistor bridge are the commutating diodes across transistors Q3 and Q5 They could be small-axial-lead, low-wattage diodes, since they commutate for a very short time

To prevent cross-over short-circuit currents in the bridge caused by transistor storage times, transformer 75 feeds a clock drive that holds off the turn-on signal until the opposite side has turned off. This feature must be implemented with the separate drive transformers T3 and T4, which provide turn-off drive from energy-storage in transformers

The operating frequency of the PWM switch and bridge inverter has been tentatively chosen as 20 kHz. Initial comparison showed that, although efficiency is slightly lower at 20 kHz than at 10 kHz, the weight reduction in the magnetics at 20 kHz exceeded substantially the weight reduction in the solar panel with a better inverter efficiency. The details of frequency selection are included under the low-voltage power supply options.

c. Physical Design

For efficient heat transfer, the distribution inverter circuitry is packaged on a mounting surface that is thermally controlled by heat pipes. Principal heat sources should be closely coupled to the mounting surface Since fast rise-time currents are prevalent, components should be closely spaced to minimize the inductance of the wiring between components. Weight of the package is minimized if the temperature gradients are minimized. A component layout and configuration summary is shown in Figure 19.

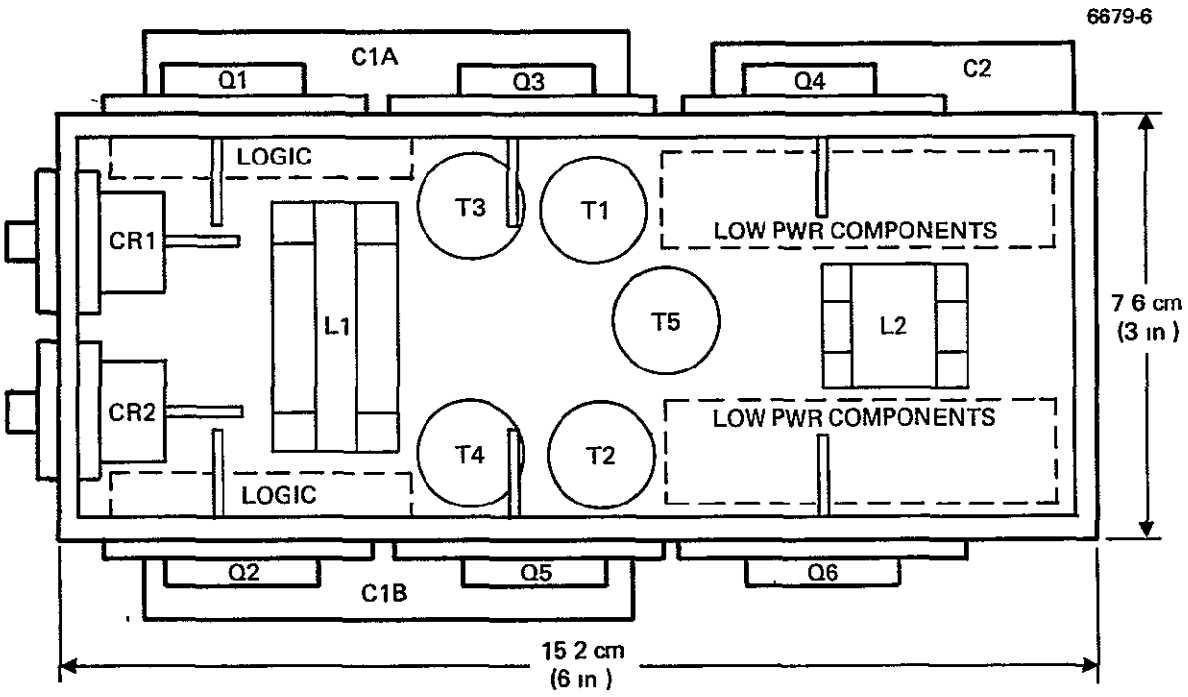

CONFIGURATION SUMMARY

SIZE 7 6 cm X 7 6 cm X 15 2 cm (3 IN X 3 IN X 6 IN)

WEIGHT 1 0 Kg (2 2 LBS)

POWER DISSIPATION 30 WATTS (MAXIMUM)

Figure 19. Distribution inverter component layout.

d The DC/DC Converter

The dc/dc converter and distribution inverter are similar in design except for automatic trip and rectification circuitry in the converter. Based on the trade-off options already discussed in Section 2.b and also those discussed later in Sections 2.f and g, we selected a design that uses a transistor bridge, pulse-width-modulation to regulate outputs, and operates at 20 kHz to obtain a low converter mass. The converter is sized for 700 W. Figure 20 is a block diagram of the dc/dc converter.

Figure 21 is a schematic of the dc/dc converter. The basic converter power circuitry is identical to that of the distribution inverter. But they differ significantly in the automatic trip logic, output power rectification, and filtering. The automatic trip logic compares input current to a reference If the input current exceeds the reference, a trip signal will be generated that will automatically turn-off the PWM series regulator in the faulted converter and initiate a command to turn on the standby converter. Switching from the primary to the secondary converter is done automatically because the output power busses are considered critical. The output busses from the primary and standby converters are diode coupled to eliminate the potential "off" period of a relay during transfer. In addition, output filters on each power bus can be sized to provide necessary ripple filtering and provide energy to support the bus during short periods of a fault

Three output voltages and their power requirements have been identified. A 30 ± 2 V bus is required to provide 650 W maximum to the mission module and housekeeping loads within the PMaC. A +15 V and a -5 V bus, providing 150 W and 10 W, respectively, will be used by the drive logic circuitry in all switching inverters Each bus is isolated from the other by separate taps on the output transformer and separate rectifier/filter circuits. Different voltages can be made available by adding more taps or varying the turns ratio

Estimated losses in the converter occur in the auxiliary solar panel bus (100 to 200 V) and in a 28 V bus supported by the battery

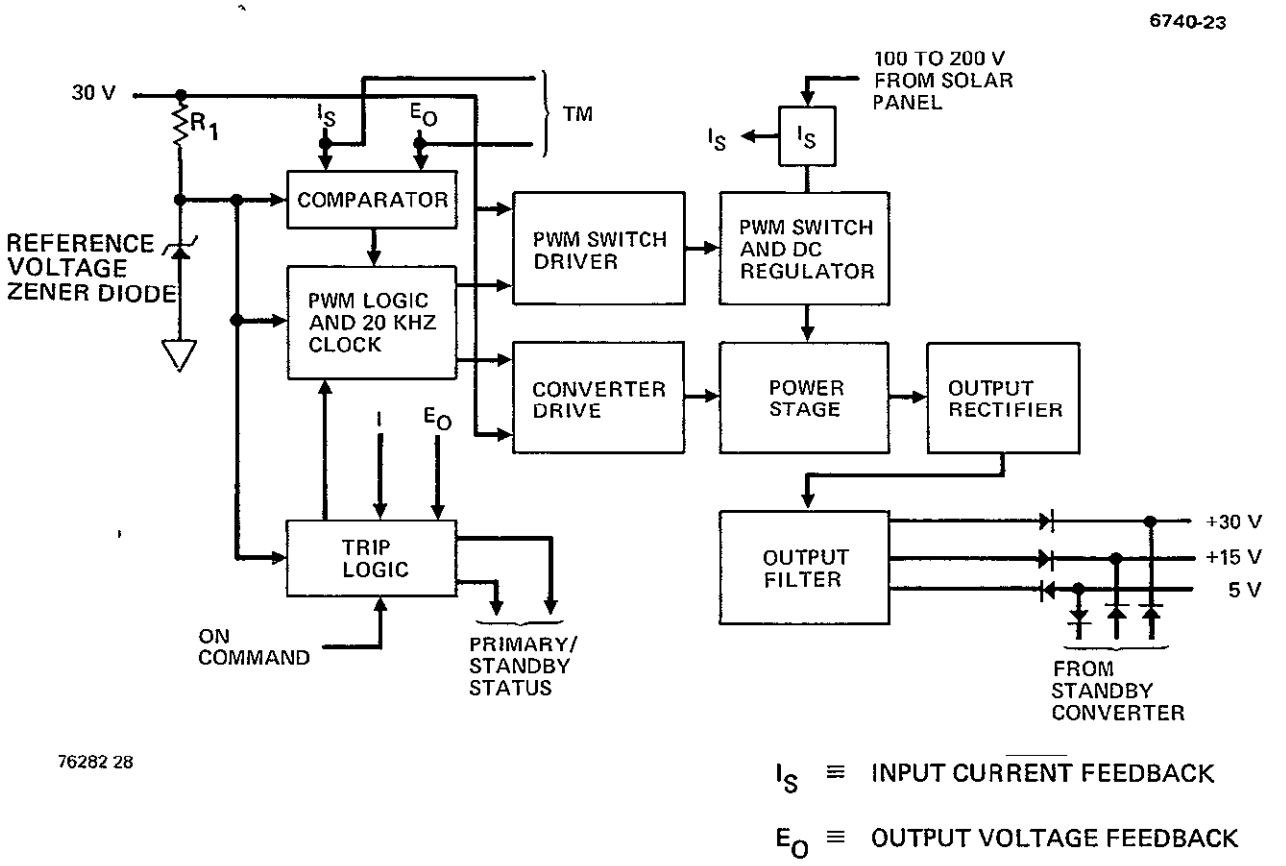

Figure 20. Block diagram of the dc/dc converter.

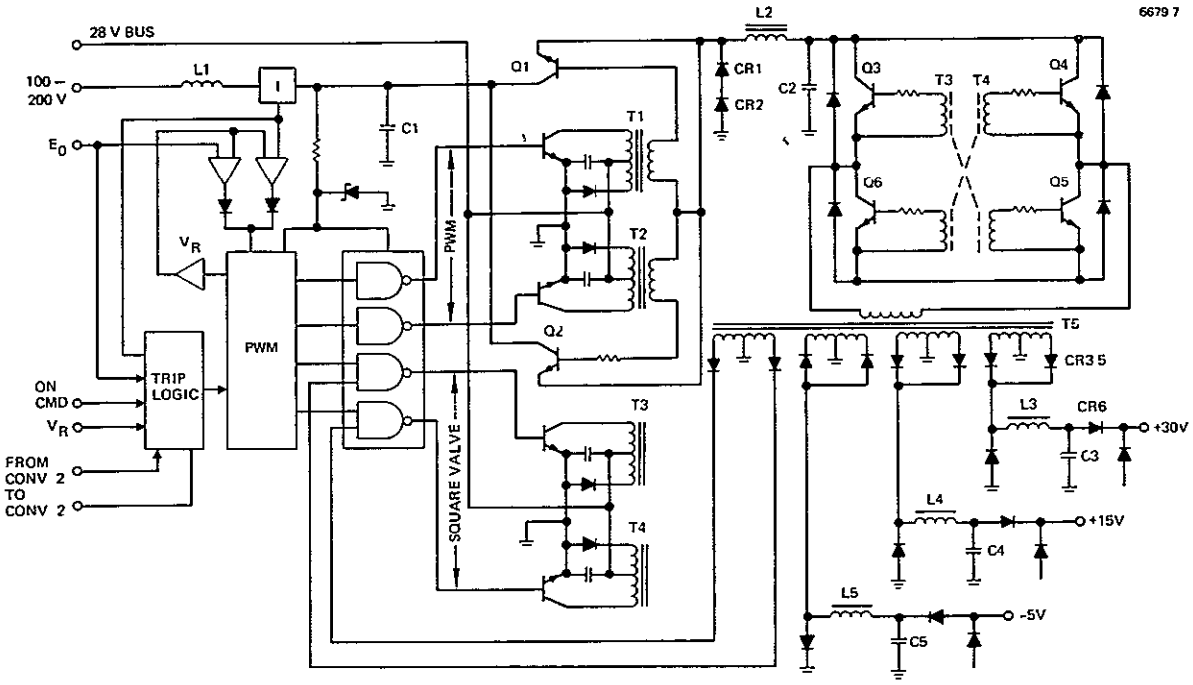

Figure 21. Schematic of the dc/dc converter.

in the mission module Input power for transistor drive is approximately 9 W from the 28 V battery bus. From the auxiliary solar array, power dissipation will be 77 W at high line voltage (200 V) and 70 W at low line voltage (100 V) for an output power level of 735 W Thus total input power will be the sum of the loss (77.0 W) and the drive (9 W), or 86.0 W, at high line voltage with 735 W output for an efficiency of 89.5%. At low line, with approximately 10 W drive, 70 0 W loss, and 80.0 W total input power, efficiency will be 90%. This represents a maximum power condition for the converter. The converter would be required to operate at half the maximum power during the thrusting phase.

The magnetics design for input inductor L1 and output inductor L2 are optimized with small 0.05 mm (+0.002 in.) thick silicon steel "C" cores. Since ac flux swing will be small, high dc flux will dominate the design. A single coil design will provide a simple and efficient implementation. Inductor L2 must carry relatively high dc current and sustain substantial ac voltage with low core loss The optimum core for this design would be a C core of 0.025 mm (0.001 in.) thick Orthonol, which would provide low core loss at high dc flux density and relatively high ac flux density to 40 kHz. For high efficiency (minimum resistance), a shell construction would be used (two C-cores and a single coil)

The magnetics design for output transformer T5 would be most efficiently implemented with a ferrite cup core, which would have low core loss at 20 kHz and a fairly high flux density of 2 kG The principal concern in this design is the high current in the secondary, which is a square wave with high harmonics and substantial skin effect The large-diameter conductor necessary for such high current would have an ac resistance many times its dc resistance if magnet wire were used To minimize skin effect, a coil can be designed using 0.013 mm (0.005 in.) thick copper foil. The step-down design has few turns, low winding capacity, and high bandwidth (fast rise-time) Even so, the primary ac resistance, because of the adverse effects of many

layers, will be 2 25 times the dc resistance, while the secondary, with fewer layers, will have an ac resistance of 1.2 times the dc resistance This design will still be 99 3% efficient

Power losses in principal components have been estimated for thermal control design and are summarized in Table 8.

The worst case single component is the output isolation diode with 19.2 W. This, plus the output diodes, must therefore be mounted with low thermal impedance to a mounting heat sink The worst case transistors are the switching transistors, each with 5.26 W maximum. These should preferably be mounted with minimum thermal contribution from other components and closely coupled to a mounting heat sink. Ferrite material was selected for transformer T5 because high-frequency core losses were low. Since ferrite material is thermally sensitive, close thermal coupling to the mounting surface is required.

This circuit must be packaged for efficient heat transfer to a mounting surface thermally controlled by heat pipes. Principal heat sources should be closely coupled to the mounting surface. Since fast rise-time currents are prevalent, components should be closely spaced to minimize the inductance from the wiring between components Weight of the package should be minimized by mounting the heat sources near the mounting surfaces of the package. Figure 22 shows a preliminary layout of a suitable package design.

Using the package design shown in Figure 21, Table 9 gives the weight distribution of the converter assembly

e. The Low-Voltage Power Supplies

Several supplies within the low-voltage power-supply system are referenced to the screen voltage to maintain proper thruster operation. A basic ground rule established by NASA LeRC stipulates that a fault in any one thruster must not influence the normal operation of adjacent thrusters Several failure modes exist within a thruster that could create a 3-kV potential between the screen grid of a faulted

Table 8 Power Dissipation in the DC/DC Converter

Component	Power Dissipation, W
Input choke L1	0 3
Input storage capacitors	0.8 (4 x 0.2)
Switch transistor Q1	5.26 (high line) 4 21 (low line)
Switch transistor Q2	5.26 (high line) 4.21 (low line)
Switch commutating diodes CR1, CR2	5.4 (2 x 2 95) (high line) 0 (low line)
Bridge transistors Q3 to Q6	12.9 (4 x 3.2) (high and low line)
Switch filter choke L2	3.5
Output transformer T5	6.6 (high and low line)
Output choke L3	0 9
Output diodes CR3 to CR5	19.2 (2 x 9 6) (CR5 ≃ 0)
Output isolation diode CR6	19.2
Transformers T1 to T4	0 6 (4 x 0 15)
Total loss per power units	75.2 W max (high line) 68.6 W min (low line)
Estimated control and drive losses	11.0 W (high line) 12 0 W (low line)
Total loss	≃ 86 W max (high line) ≃ 80 W min (low line)

5903

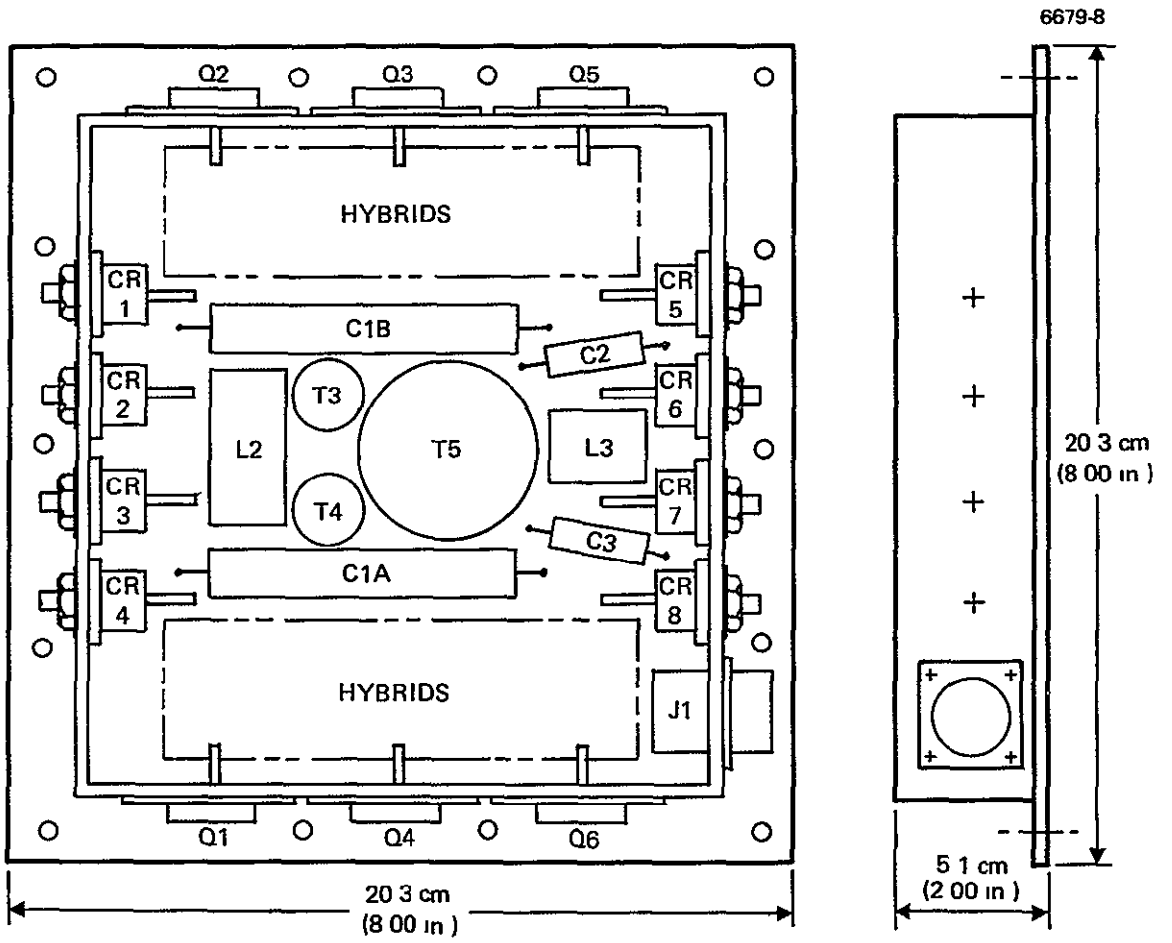

Figure 22. Component layout of the dc/dc converter.

Table 9 Weight Distribution of the DC/DC Converter

Component	Weight, lb
Input choke L1	22.5 (0.05)
Input storage capacitors 24.8 (4 x 0.005 lb)	99.0 (0 22)
Switching transistors Q1, Q2 2 x 18 (2 x 0.04)	36.0 (0.08
Switch filter choke L2	162.0 (0.36)
Switch filter capacitor C2	22.5 (0.05)
Bridge transistors Q3 to Q6 4 x 18 (4 x 0.04)	72 0 (0 16)
Output transformer T5	500.0 (1 11)
Output choke L3	22.5 (0 05)
Output capacitor C3	13.5 (0 03
Switch commutating diodes CR1, CR2 2 x 11 7 (2 x 0 026)	23 4 (0.052)
Output diodes CR3 to CR6 4 x 11.7 (4 x 0.026)	46.8 (0 104)
Hybrid circuit block	90.0 (0 2)
Chassis	517.5 (1 15)
Wiring	135.0 (0.3)
Total weight (1 converter)	1737.0 (3.86)
Contingency - 10%	171.0 (0 38)
Total weight (1 converter)	1908 0 (4 24)

Configuration Summary

Size 5 1 cm x 20.3 cm x 20.3 cm (2 in. x 8 in. x 8 in)

Weight (1.7 kg) 4.24 lbs

Power dissipation 86 W (max)

thruster and a normally operating thruster If the low-voltage heater supplies were common to several thrusters and referenced to high voltage, the affected supplies would act as a bridge coupling the fault from one thruster to another Since this would be an unacceptable perturbation to the thrust system, a separate complement of low-voltage power supplies must be provided for each thruster so that faults within a thruster or its associated power supplies will be confined to only that thruster. The same rationale applies to the beam, discharge, and accelerator supplies. Isolating a fault to a single thruster power supply system makes the task of removing the fault from the system and of eliminating any impact of the fault on the rest of the system less significant in terms of hardware complexity

Although the supplies referenced to the neutralizer return are all operated at low voltage, transformation must be used in these supplies so that peak currents in the distribution inverter may be kept to reasonable levels. In addition, since each thruster must be neutralized separately, each thruster must be supplied separately with those supplies referenced to the thruster. A common accelerator supply could be used for the system, but this option probably has no significant weight advantage since each accelerator grid must be independently current limited.

Since each of the power supplies must be isolated from the solar panel and also from other thrusters, the isolation is accomplished with a transformer between the distribution inverter and the individual low-voltage power supplies One of these transformers is located in the low-voltage power supply unit in each thrust module.

f Operating Frequency and Transformer Configuration

Transformation can be achieved with either a single transformer or two transformers (one for starting the heaters, the other for running the thruster). Table 10 shows the tradeoff for these transformers of configuration versus operating frequency (for 10 kHz, 20 kHz, and 40 kHz) Transformer weight, transformer dissipation, and inverter switching losses are shown for the starting, running, and combined transformers.

Table 10. Transformer Configuration versus Operating Frequency

Frequency	Starting Transformer	Running Transformer	Combined Transformer
10 kHz			
Xfmr weight, kg (lb)	0.11 (0.25)	0.16 (0.36)	0 35 (0.78)
Xfmr dissipation, W	9.80	4.03	[a]
Inverter switching loss, W	0.83	0.30	1 12
20 kHz			
Xfmr weight, kg (lb)	0 08 (0.185)	0.14 (0 30)	0.22 (0.49)
Xfmr dissipation, W	8.80	3.41	[a]
Inverter switching loss, W	1 65	0.60	2 25
30 kHz			
Xfmr weight, kg (lb)	0 05 (0.12)	0.09 (0.20)	[a]
Xfmr dissipation, W	6 60	2 33	[a]
Inverter switching loss, W	3 30	1 20	4.50

[a]Insufficient time to evaluate the design fully.

5903

Since skin effect in the transformer wire becomes significant above 20 kHz, 20 kHz appears to be a reasonable frequency. There appears to be no advantage in weight or power dissipation in using a combined transformer, and it has the disadvantage of having numerous leads to terminate The two-transformer approach also has the advantage that the starting transformer can be turned off after the thruster has started, thus eliminating excitation losses. This feature can be added if the weight of the switch is offset by the power savings

g. Starting Heater Modulation Techniques

Starting heater voltages may be modulated by using any one of the following options:

- AC heaters
- Magnetic amplifiers (mag amps)
- Silicon-controlled rectifier (SCR) circuits

- Transistor circuits
- Sharing of a power supply normally not used during starting (e g., the discharge power supply)

As discussed earlier, general commonality of power supplies is not feasible However, the cathode heater, the cathode isolator heater, and the main isolator heater have been successfully operated in the startup mode in series-parallel combination using a single power supply (the discharge power supply). Consequently, we considered combinations of the options listed above for combined cathode and isolator heaters plus a neutralizer heater

The starting heater tradeoff summary for combinations of the options listed above is shown in Table 11 Generally it can be said that SCR's switch faster than mag amps and that transistors switch faster than SCR's Also, EMI generally increases with faster transition times Since currents are limited with inductors in the ac supplies, current rise and fall times are slow and EMI generated should be held to a minimum

To compare the starter heaters, we assumed that the equivalent mass of the finished unit is 1.8 times the mass of the power supply components plus the mass of the additional solar array that is required to supply the power dissipated (the solar panel mass was assessed at 7 g/W, or 16 mlb/W). As shown in Table 11, the combination of options that has the lowest mass uses transistor circuitry for the neutralizer heater and the discharge supply (with appropriate switching) for the combined cathode and isolator heaters Table 11 also indicates that use of the discharge supply for the cathode and isolator heaters combined with either the mag amp or the SCR circuitry for the neutralizer heater offers alternatives that would also yield a low equivalent mass.

However, the parts count is higher for the transistor system than for the SCR system, and it is higher for the SCR system than for the mag-amp system The parts count of the ac system should be the lowest of all Since system reliability (assuming series component failure modes) is generally inversely proportional to parts count, the mag-amp system should be more reliable than either the transistor system or the

Table 11. Starting Heater Modulator Configuration

Type of Starting Heater Supply		Component Mass, kg (lb)	Power Dissipation, (W)	Equivalent Mass,[a] kg (lb)
Neutralizer Heater	Cathode and Isolator Heaters			
AC (no modulation)	AC (no modulation)	0.29(0 64)	2.42	0 54(1.19)
Mag amp	Mag amp	0.23(0.50)	16 33	0 52(1 16)
Mag amp	Discharge Power Supply	0 18(0.41)	7 79	0 39(0.87)
Transistor	Transistor	0.16(0 35)	21.10	0.44(0 98)
Transistor	Discharge Power Supply	0.16(0.35)	10 43	0 36(0 79)
SCR	SCR	0.17(0 38)	30 09	0.53(1 17)
SCR	Discharge Power Supply	0 17(0.37)	15 06	0 41(0.91)

[a]Equivalent mass is defined as 1 8 times the component mass plus the solar panel mass required to supply dissipation

5903

SCR system The starting heater technique, which uses the mag-amp for the neutralizer heater and the discharge power supply for the combined cathode and isolator heaters appears to be the best overall choice. The mag-amp system has also been extensively tested and been used in several thruster power processors.

h Circuit Design Alternatives

Since most of the power used by the low-voltage power supplies is used by the heaters for thruster start-up, and since earlier trade-offs have indicated that mag amps are the best choice for modulation, mag amps have also been selected as the baseline design for the other low-power supplies.

In the main vaporizer supply, shown in Figure 23, isolated ac power is applied to the mag amp by the power transformer. The mag amp modulates this power and feeds the output inductor L through rectifier diodes CR1 and CR2. Diode CR3 supplies commutating current when the mag amp is supporting the input voltage. The inductor supplies current to the main vaporizer through the transductor current sensor. The isolated winding, N_1, supplies input voltage to the transductor. The output of the transductor is rectified by the diode bridge consisting of diodes CR4 through CR7, which feeds the load resistor R. The voltage across the load resistor, which is proportional to the main vaporizer current, is buffered for telemetry (TM) and is also used as feedback to the control amplifier AR1. The control amplifier compares the feedback with the analog control and develops an error voltage to feed buffer amplifier AR2. Amplifier AR2 drives the control winding of the mag amp power stage.

Current-sensor transformers generally require many turns of very small wire. The smallest wire size that can be wound on the core governs the size of the current sensor. The current sensor is a unity feedback mag-amp type that requires a core window area approximately twice that required by the transductor type. Although the transductor type requires a separate excitation voltage winding, its total weight is less. Therefore, we selected the transductor-type current sensor.

Similar circuitry is used in the power supplies for the neutralizer vaporizer, cathode vaporizer, magnetic baffle, neutralizer heater, and low-voltage portions of the neutralizer keeper and cathode keeper. Referring to the neutralizer keeper supply shown in Figure 24, inductor L limits the primary current in transformer T_1. The peak voltage on the secondary winding of transformer T_1 is rectified by the diode bridge consisting of diodes CR9 through CR12, and is applied to capacitor C. This peaking supply is used to start the keeper. The neutralizer keeper voltage is buffered for TM and control. The cathode keeper supply works similarly to the neutralizer keeper supply

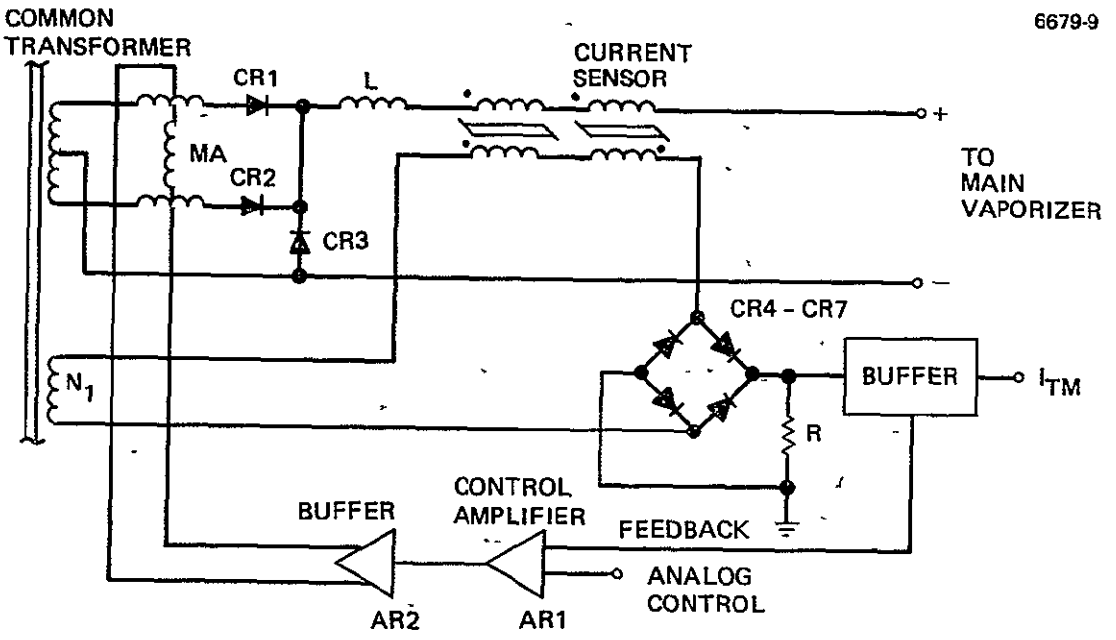

Figure 23. Main vaporizer supply.

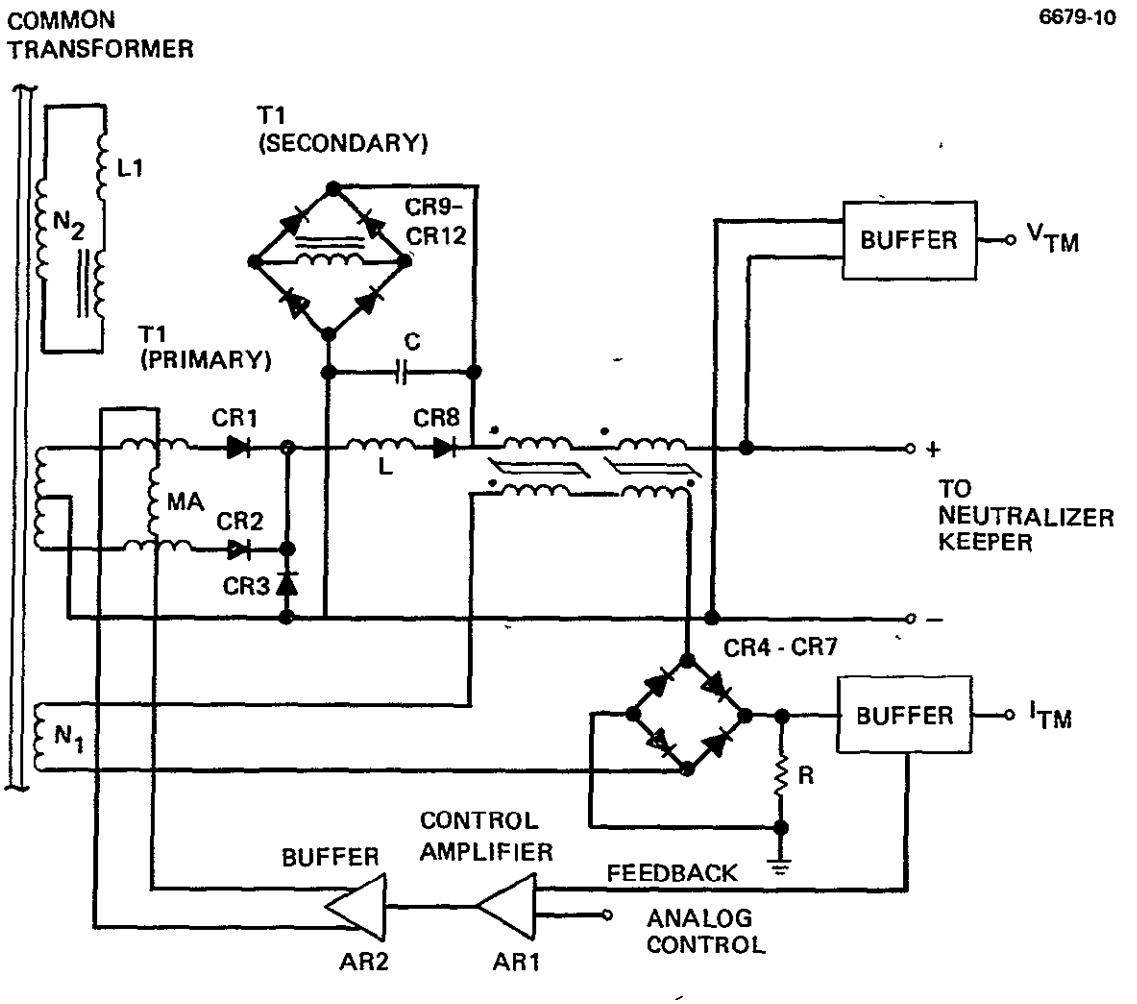

Figure 24 Neutralizer keeper supply

The main and cathode isolators are wired in parallel and the combination is connected in series with the cathode heater. Power is supplied to this combination of heaters during starting by the discharge supply (as shown in Figure 25). Relay K1 is energized by a command from the controller. Load current is sensed by the transductor The transductor output is buffered for TM

3. Description of the Baseline PMaC Subsystem

A block diagram of the generalized PMaC subsystem is shown in Figure 26. The solar array consists of two identical wings, each of which is divided into sections; a beam/discharge section and an auxiliary or housekeeping section Each array section is electrically isolated from the others and provides power to its respective thrust system element via separately dedicated harnesses.. The solar array harnesses for the beam and discharge supplies are connected to a solar array control unit (one unit per wing).

The solar array control unit manipulates the current-voltage (I-V) characteristics of the array in such a manner that the voltage to the power distribution unit remains within the 200 to 400 V range and the power does not exceed 48 kW throughout the mission. Although the way the I-V characteristics of the solar array are controlled will not be discussed until later, we assume here that solar array sections would need to be reconfigured. The output of each solar array control unit is a single beam/discharge power bus that is routed to each of five power distribution units.

The power distribution function is performed by five boxes, each of which contains two beam and two discharge supply filters. The input filter suppresses current transients that may be reflected on the common bus and ultimately appear on the solar array. Individual filters for each high-power inverter reduce conducted noise on the common bus and potential crosstalk between operating inverters Ten filters are required for the beam supplies and 10 filters for the discharge supplies.

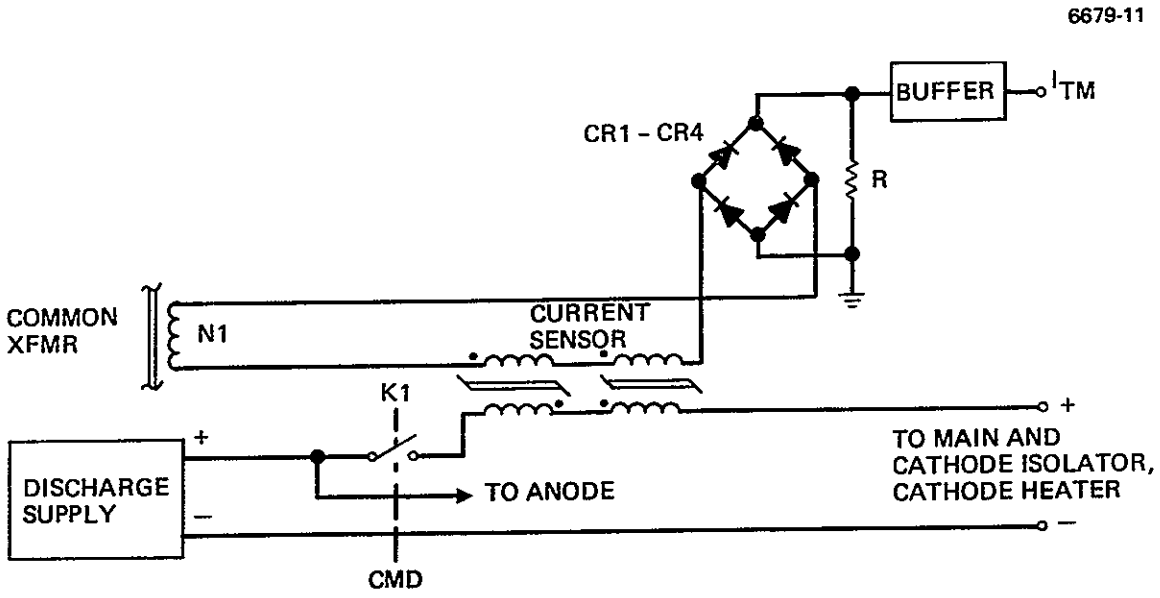

Figure 25. Main and cathode isolator heaters and cathode heater.

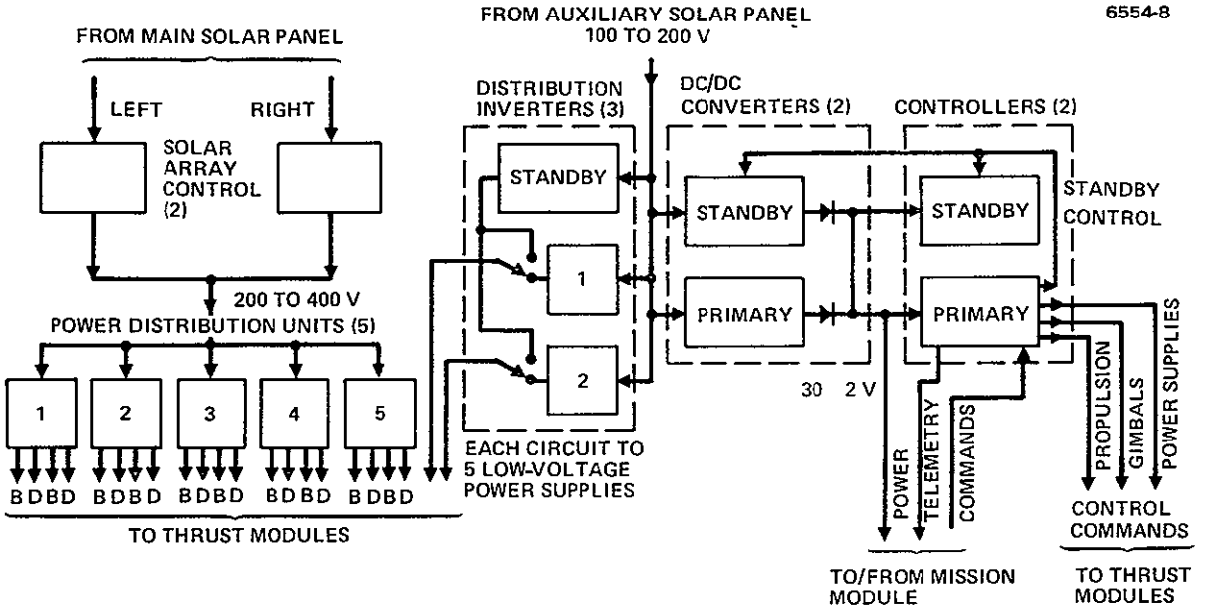

(a) Interface module

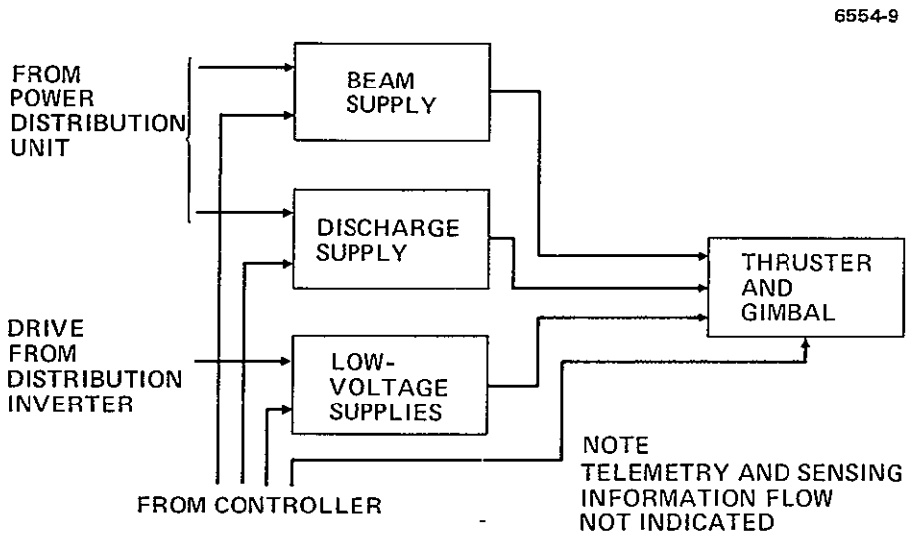

(b) Half of thrust module (one thruster)

Figure 26. Block diagram of the PMaC system.

Filtered power is routed to each beam and discharge supply. The beam supply provides the high voltage and current requirements for the thruster screen (3,000 V, 2 A) and is rated at 6 kW maximum The beam supply can turn off the high voltage should a malfunction occur in the thruster. Thruster malfunctions that indicate a short from the screen to the accelerator grids can be cleared with a burst of stored energy from a grid-clearing circuit The beam supply also provides the accelerator potential (-500 V) at low power. The beam, discharge, and low-voltage supplies are located in the thrust module using packaging techniques developed by NASA LeRC.

Discharge power comes from the high-power solar array and is filtered in the power-distribution unit Both the beam and discharge supplies are series resonant inverter designs, they utilize SCR power devices and are being conceptually designed under a separate NASA LeRC contract. The low-voltage, high-current (36 V, 16 A) output of the discharge supply is referenced to the 3,000 V beam voltage. Analog current control of the discharge supply allows the discharge current to track the beam current to maintain a prescribed ratio. With the exception of the minor quantities of logic and control power that are provided by the auxiliary panel, the high power requirements of the beam and discharge supplies are provided by the main array.

The auxiliary panel is sized to provide approximately 1.3 kW total from two wings when seven thrusters are operating The power bus from each array wing is combined to provide a common bus with a voltage characteristic of 100 to 200 V Power is then routed to the dc/dc converters and to the distribution inverters.

The distribution inverter processes the dc input voltage and produces a 90 V, amplitude-regulated, square-wave drive at 20 Hz for the low-voltage power supplies. The basic inverter, located within the interface module, consists of two active and one standby units. Each active inverter provides drive power to five low-voltage power supplies located in the thrust modules. Signals from the thrust system controller provide on/off and standby switching in case of a unit or system malfunction

The dc/dc converter is also powered from the auxiliary solar panel; it provides several regulated output voltages for housekeeping functions and for mission module power requirements. Both a primary and a standby dc/dc converter, both with automatic transfer capability to switch from one to the other, are required because the functions performed by the systems that are supplied by the housekeeping buses are critical. The most significant output voltage bus is 30 V, it provides power to electro-mechanical devices (such as thruster gimbals and propellant distribution valves), to the controller, and to the mission module Power furnished to the mission module is 400 W (max) during the thrust phase, and 650 W (max) after the thrust phase (as specified in Table 1, Section 2 A) Additional output buses of ±15 and 0 to 5 V, rated at 150 W total, provide logic power to all beam, discharge, and interface module inverters

The last unit in the interface module, the thrust system controller, contains all the logic functions necessary to control the PMaC subsystems from solar array to thruster. Logic functions within the controller can be generalized into unique categories The major logic function relates to thruster operation in both the normal and malfunction modes. Control signals are generated within the controller by comparing the key PMaC electronics and thruster parameters with preprogrammed standards; these signals are sent to individual power supplies to modify the power output levels to the thruster In addition to thruster control, the controller provides housekeeping logic and command processing for the following functions pyrotechnic control, gimbal actuator control, solar array and thrust system bus control, solar array drive control, propellant distribution system control, and primary/standby switching of PMaC units. The thrust system controller is under the direction of the mission module The controller provides to the mission module on demand the necessary status and engineering information for the mission module to control the vehicle and to relay data to the ground. Since the controller is the major intelligence unit in terms of thrust system reliability, a fully redundant controller is required

Neither the thrust system nor the mission module requires any electrical power during the shuttle launch phase. But after separation from the shuttle bay, a source of power will be required for numerous tasks A battery system located in the mission module will be the sole source of power until the solar array is deployed. The battery must be sized to provide both a steady-state voltage of approximately 30 V and sufficient current to fire squibs and drive motors. Table 12 summarizes the operations requiring battery power. Many operations require substantial amounts of battery power To keep the mass of the battery system low, the period between separation from the shuttle bay and deployment of the auxiliary solar array must be minimized. After the solar array has been deployed and initially oriented, the battery can be recharged and maintained to support the 30 V bus. Battery power can again be used if the solar array loses the proper orientation to the sun or if a low-impedance fault occurs that requires a higher clearing current than the auxiliary solar array can provide

a. Description of the Solar Array Control Unit

The I-V characteristics of the beam discharge solar array have not been explicitly defined. However, the latest information available in the study indicates that, for the 3·1 concentrator array rated at 48 kW, a voltage swing of 2.6:1 is possible rather than the 2 1 of the baseline design. This excessive voltage swing would seriously complicate power supply design in areas of component stress, output regulation, and inverter efficiency. A solar array control unit was therefore included in the baseline PMaC system primarily to provide a weight allocation for the structural configuration study and system mass description. The solar array control unit must perform two major tasks

First, it must limit the voltage swing to 2:1 This can be done either by tilting the panel with respect to the sun or by reconfiguring the solar panel while normal to the sun. Tilting is undesirable because, to maintain voltage within the allowable range, it may cause the maximum output power of the solar panel to fall significantly less than 48 kW (voltage would control the tilt angle rather than the output

Table 12. Battery System Requirements

Before Deployment of the Solar Array

1. Squib firing to separate the thrust system from the IUS and uncage the solar array
2. DC/DC converter for generation of housekeeping power
3. Controller for
   a. Solar array drive electronics (logic)
   b. Command and telemetry interface with ground via the mission module
4. Solar array deployment motors
5. Solar array articulation motors
6. Solar concentrator drive
7. Mission module communications subsystem

After Deployment of the Solar Array

1. Charging the battery to the standby level
2. Maintaining the battery support of 30 V bus during
   a. Disorientation of the solar panel
   b. Fault clearing

5903

power level). The power level would be variable and probably significantly less than the desired 48 kW. The second solution — reconfiguration — appears more desirable. The solar panel can be divided into several sections with known characteristics when oriented normal to the sun. Sections can be switched into series-parallel combinations that will keep the voltage within a 2·1 voltage range and take full advantage of the maximum power capability of the panel. Switching will be accomplished by relays and commanded by the controller. A maximum power tracking capability will be included in the controller that will monitor the solar panel I-V characteristics to determine when reconfiguration is required.

The second major function of the solar array control unit is to ensure that the power output to the PMaC system does not greatly exceed 48 kW. Tilting the main array with respect to the sun does not ensure that 48 kW will be the maximum The baseline solar panel design has peak power capability well above 48 kW when oriented normal to the sun at a heliocentric distance of 1 AU. Consider a fault in spacecraft attitude control or solar array deployment or control that would orient the panel normal to the sun. The voltage and current design limits for the PMaC system would be exceeded since the thrusters have a limited capability to load the panel. The result would be a voltage exceeding the 200 to 400 V range, which would jeopardize all electronic circuits. Reconfiguration eliminates this potentially catastrophic failure mode. The panel would always remain normal to the sun vector, the voltage would remain within the 200 to 400 V range, and the 48 kW power level would be fully used but not exceeded. Additional flexibility would be available in adjusting the loads to maximum solar panel power conditions. Actual circuit design of a solar array control unit will require further study of the solar array characteristics and mission profile.

Although the final design of such a unit is now only conjectural, it would appear logical to have twin units one for each array wing. And since a solar array control unit does appear necessary, a mass allocation is required as one basis of a configuration study We estimated 5 kg/unit, 10 kg total, on the basis of the design of a similar reconfiguration unit used with the CDVM. Output power characteristics would be 200 to 400 V at 48 kW maximum via a single bus to the power distribution units.

b Description of the Power Distribution Unit

The power distribution unit is basically an input filter for the beam and discharge supplies Since explicit information about the beam and discharge supply inverter input characteristics was not available, the filter requirements were only generally assessed Using weight and power dissipation data taken from NASA LeRC initialization

studies the filter requirements were analyzed sufficiently to justify the unit parameters Weight was estimated at 86 kg, and power dissipation at 531 W for 80 kW (scaled to 300 W for 48 kW)

The power distribution unit acts as a conducted interference filter between the beam supply and the solar panel or between the discharge supply and the solar panel, thus suppressing large ripple currents on the solar panel lines to a level permitted by MIL-STD-461 The large ripple currents that will remain on the lines between the filter and the inverter will cause high cable losses and be a source of substantial radiated interference The influence of radiated interference should be minimized by twisting and shielding the power leads and by minimizing the distance between units. Two recommendations become apparent

- Since the output capacitors of the filter act as input capacitors to the series-resonant inverter, they should be located in the inverters. This would substantially reduce cable loss and radiated noise In addition, inductance between the capacitor and the switching inverter should be minimized

- The very large ratio of thruster power to instrumentation power suggests that optimum weight may be achieved with higher thruster EMI limits, more shielding and filtering of instrumentation lines, and a relaxation of MIL-STD-461 requirements for the thrust system

The three-section filter proposed is the result of comparisons made with filters of one and two sections. Fewer sections resulted in greater weight and power dissipation Tuned filters are not suitable since the lowest ripple frequency is a function of duty cycle, which is variable

Figure 27 shows the equivalent circuit of a single inverter filter The capacitance of the output capacitor, 200 μF, is determined by allowable ripple current at high frequency, which is limited by heating losses in the capacitor The output capacitor is a composite of many capacitors selected to handle the heating losses

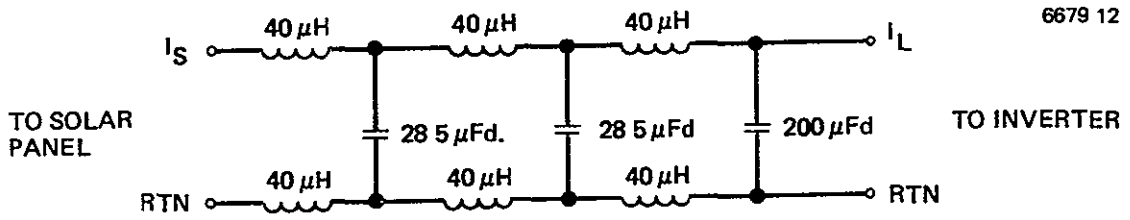

Figure 27. Equivalent circuit of the filter.

All capacitors must be connected serially in pairs because of dc voltage stress Since the input voltage can reach 400 V and capacitors of this type are generally not rated for greater than 300 V, two in series will provide a 600 V capability. The reliability of a capacitor circuit operating at 400 V with a rating of 600 V is acceptable To equalize dc voltage stresses in the series capacitor pair, resistor shunts can be added in parallel with each capacitor. A fuse in series with each series string is required to remove the capacitor string from the bus in case one capacitor fails With one capacitor failed, the other capacitor would probably also fail because its voltage rating would be exceeded The only adverse effect of such a failure would be a relatively small increase in the ripple (10 to 15%)

Components are housed in an aluminum box and mounted to the interface module side of the heat sink. Components are arranged for efficient heat conduction to the heat sink Each unit contains two beam filters and two discharge filters If all supplies were operating at near full load, power dissipation within each power distribution unit would be 65 W. Capacitors dissipate the majority of power lost and should be coupled as closely as possible to the heat sink. Dimensions of the box are 10.2 cm x 12.7 cm x 30 5 cm (4 in. x 5 in. x 12 in.), and its mass is 17 3 kg.

c. Description of the Beam and Discharge Supplies

To facilitate integrating the supplies in the PMaC system, NASA LeRC provided the input and output interface requirements for the beam and discharge supplies Figure 28 shows interface requirements for and implementation of an emission current sensor for the beam and discharge supplies and for the switching necessary for discharge power to be used for thruster startup.

The beam supply requires 6 kW of input power at 200 to 400 V, ±15 V for logic drive, an analog control signal for screen voltage, and associated command and telemetry channels. The accelerator supply is also included in the beam supply Output voltage, positive and return, are connected between the screen grid and neutralizer return on the thruster

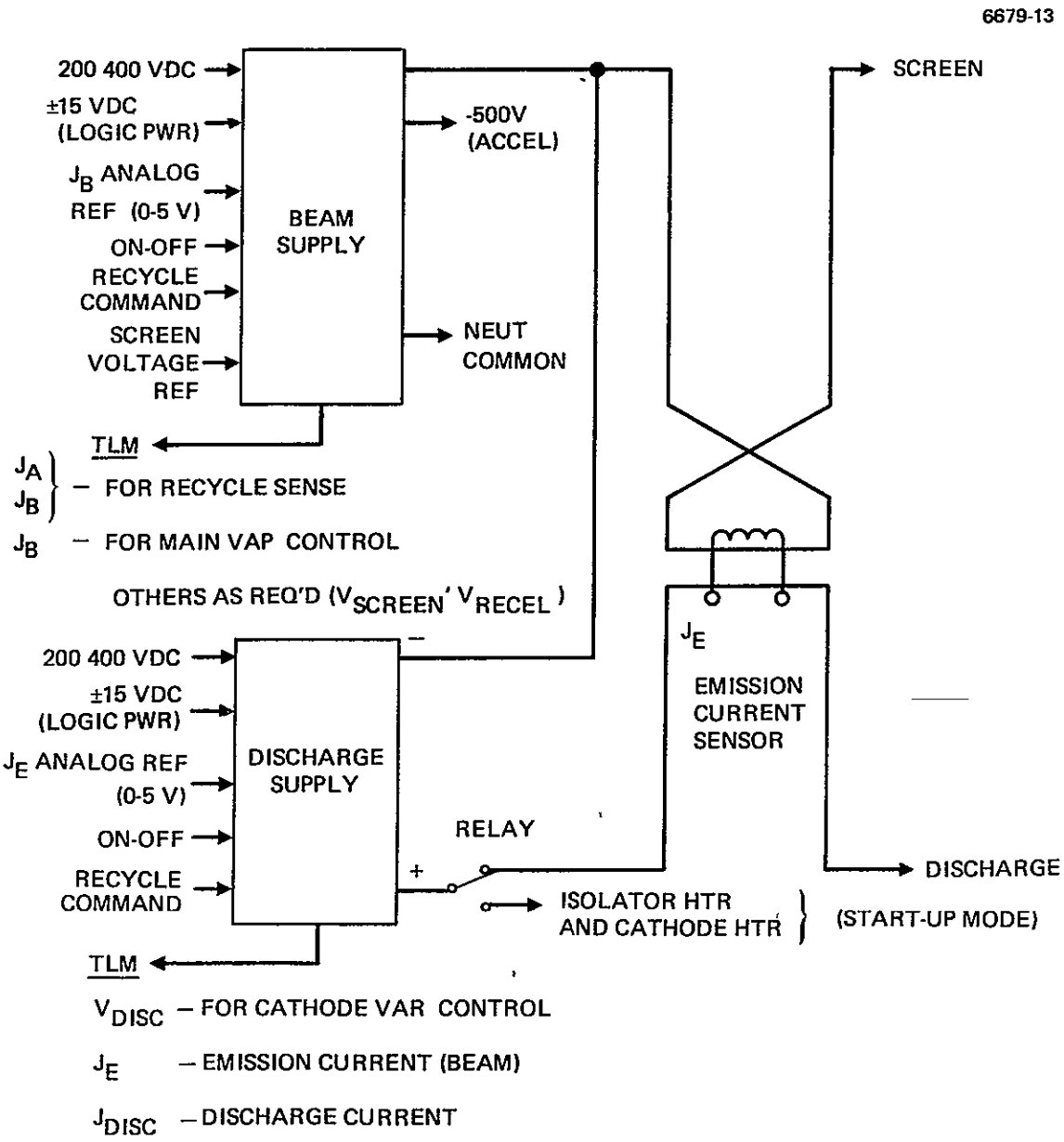

Figure 28. Interfaces of the beam and discharge supplies.

The discharge supply requires approximately 700 W of input power at 200 to 400 V, ±15 V for logic drive, an analog control signal for discharge current, and the associated command and telemetry channels The low-voltage output of the discharge supply is referenced to the high-voltage screen supply by connecting the discharge return lead to the screen positive lead. The discharge positive lead is connected to the discharge anode in the thruster During the thruster start-up mode and before the application of high voltage, the discharge supply can power the combined cathode and isolator heaters of the thruster.

The packaging requirements for thrust module electronics utilizes the "Z"-frame packaging technique developed by NASA LeRC. Each thrust module contains two thruster power supply systems, each consisting of a beam, discharge, and low-voltage power supply. The overall dimensions of each power supply assembly are 38.1 cm x 101 6 cm x 15.2 cm (15 in x 40 in. x 6 in.) high The lengths of the individual modules are 48 8 cm (19.2 in) for the beam, 27.4 cm (10.8 in.) for the discharge, and 25.4 cm (10 in.) for the low-voltage power supplies and other miscellaneous circuits. The masses are 20.0 kg for beam and 5.0 kg for discharge

Figure 29 describes the basic current paths through the thruster for the beam, discharge, and accelerator supplies. The actual current through each of the major supplies is important to the PMaC unit design The discharge supply carries discharge plus screen current and the screen supply carries both screen and accelerator currents. The discharge supply is floating at the screen voltage (3,000 V) and the screen and accelerator supplies are referenced to the neutralizer return. A detailed analysis of thruster operation will be needed to determine the requirements for the bias supply

Studies conducted at NASA LeRC and at Hughes Research Laboratories indicate that a spark-gap type of grid-clearing circuit is adequate to clear a grid short in the 30-cm thruster. The grid-clearing circuitry is shown in Figure 30 Relay K is in position 1 when the thruster is in normal operation When a fault between the screen and the accelerator grid occurs, a command will transfer relay K to position 2 and the

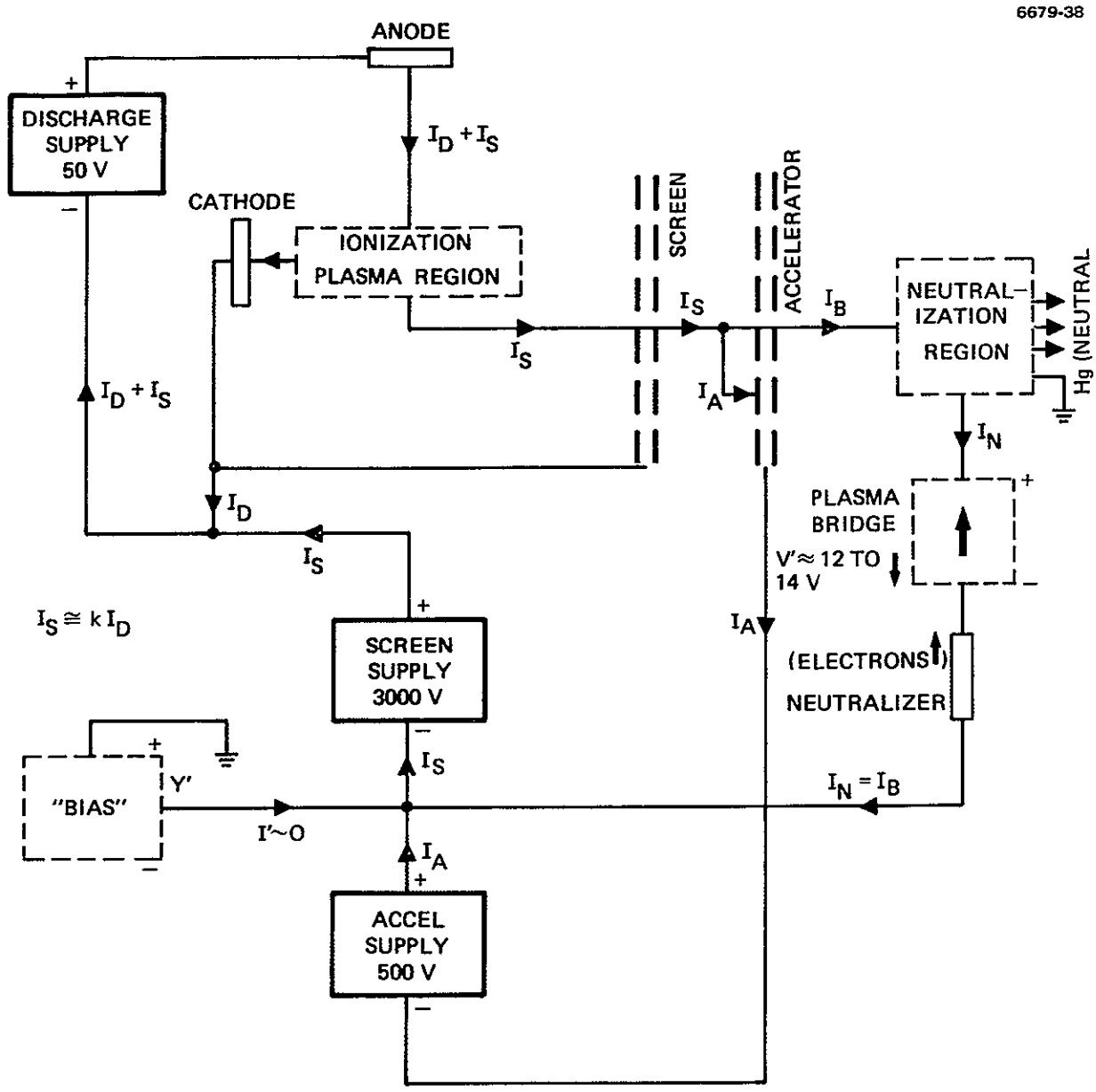

Figure 29. Basic current paths.

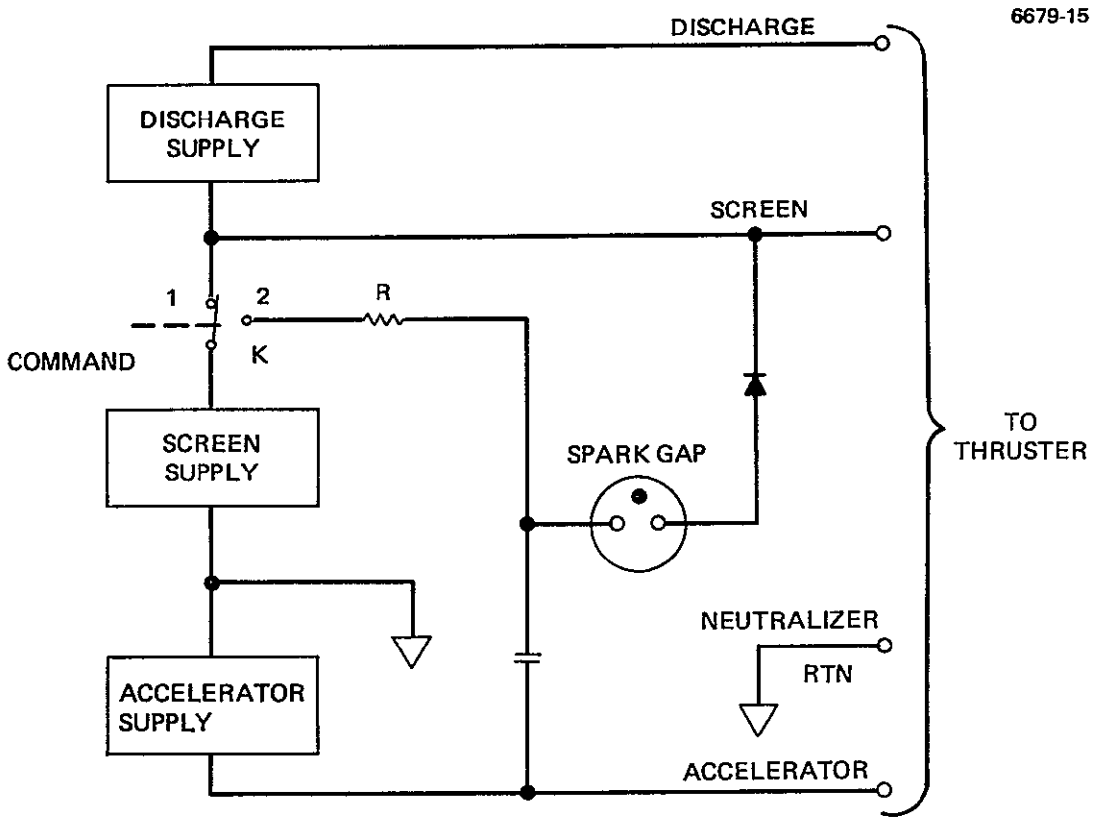

Figure 30. Grid-clearing circuit

screen supply will begin to charge capacitor C through resistor R. The voltage across C rises exponentially with time towards the sum of the voltage of the screen supply and that of the accelerator supply. When the voltage across the spark gap reaches its rated voltage, the spark gap arcs and most of the energy in the capacitor will be dumped into the fault between the grids When the current in the spark gap drops enough to extinguish the arc the capacitor will again charge, this cycle will repeat itself until the short circuit is removed and there is no return path to discharge the capacitor.

d. Description of the Low-Voltage Power Supplies

Figure 31 is a block diagram of the baseline design for the low-power supply system. Voltage standoff requirements established by the thruster dictate that the magnetic baffle and the cathode keeper

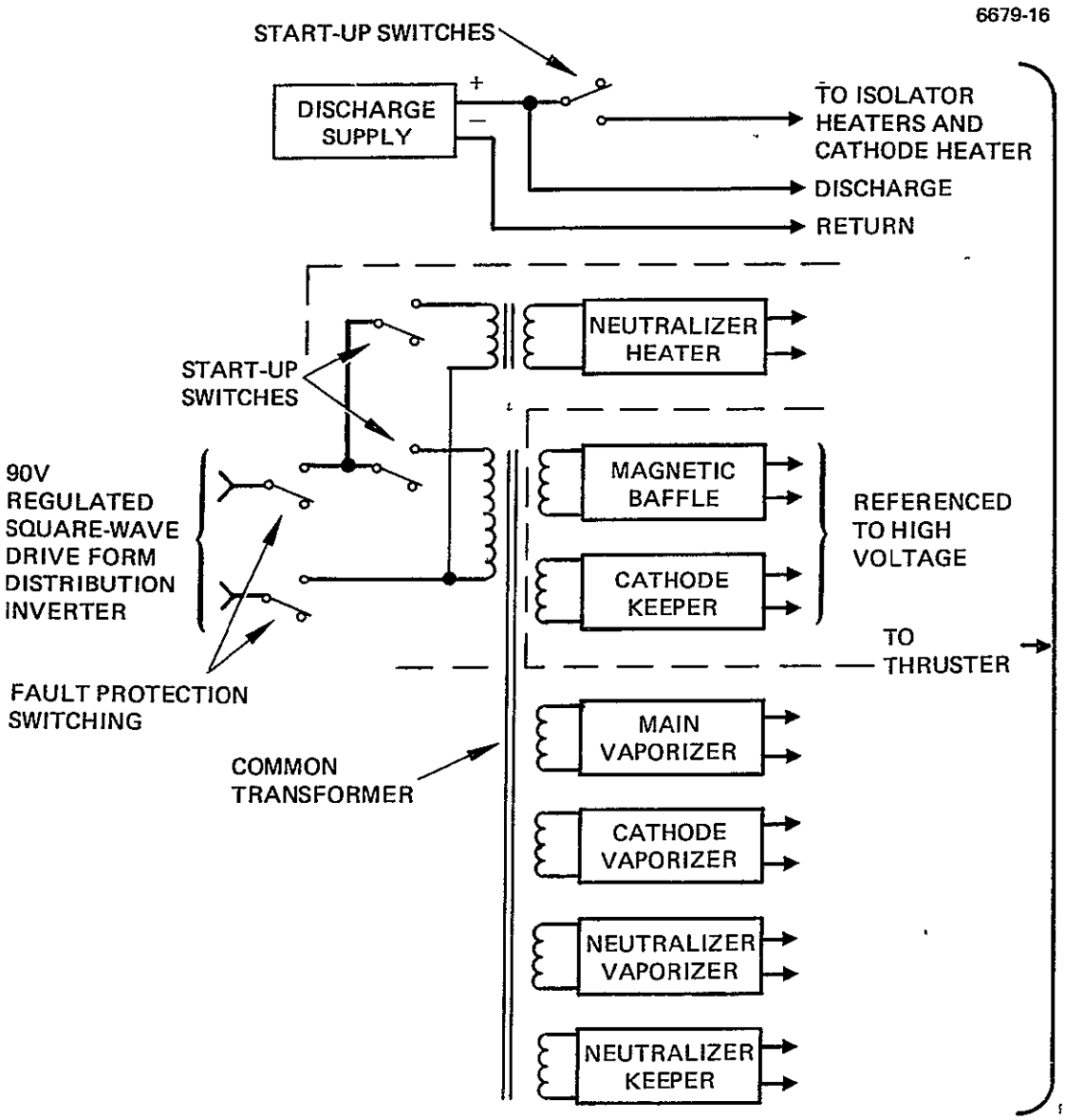

Figure 31. Block diagram of the low-voltage power supply.

must be referenced to the beam supply during normal thruster operation. The magnetic baffle requires a current-regulated dc supply with low ripple content because a variation in the magnetic baffle current significantly modulates the discharge current The cathode keeper requires a current-regulated dc supply with several hundred volts of peaking at low current output so that the keeper discharge can be ignited A high-voltage pulse could also be used to ignite the keeper discharge. The three vaporizers and the neutralizer heater represent loads with long thermal time constants, they can accommodate either ac or dc power The neutralizer keeper requires a current-regulated dc supply with starting characteristics similar to the cathode keeper: The neutralizer heater and keeper supplies must be controllable with an adequate number of setpoints, either analog or discrete. The three vaporizer supplies must be continuously analog controlled Current TM must be available from all supplies; in addition, voltage TM must be available from the neutralizer keeper Commands and TM are referenced to spacecraft return Control for the low-power supplies must be compatible with outputs of the controller Both analog and digital commands could be used. TM outputs from the low-voltage power supplies must also be compatible with the inputs to the controller.

Figure 32 describes the interface between the distribution inverters (located in the interface module) and the low-voltage power supplies (located in the thrust module) A switching network demonstrates how the standby distribution inverter can replace either primary inverter. Both the input and output of a faulted inverter can be removed from the remaining system. The output drive from each distribution inverter is connected to five parallel output transformers, each located in a low-voltage power supply unit. A switching matrix on the primary of each output transformer performs a dual function. First, it controls the sequencing of applying heater power to the thruster during start-up as determined by programming stored in the controller After start-up, heater power is removed and the thruster is operated without the start-up heaters Second, if a failure occurs in the low-voltage

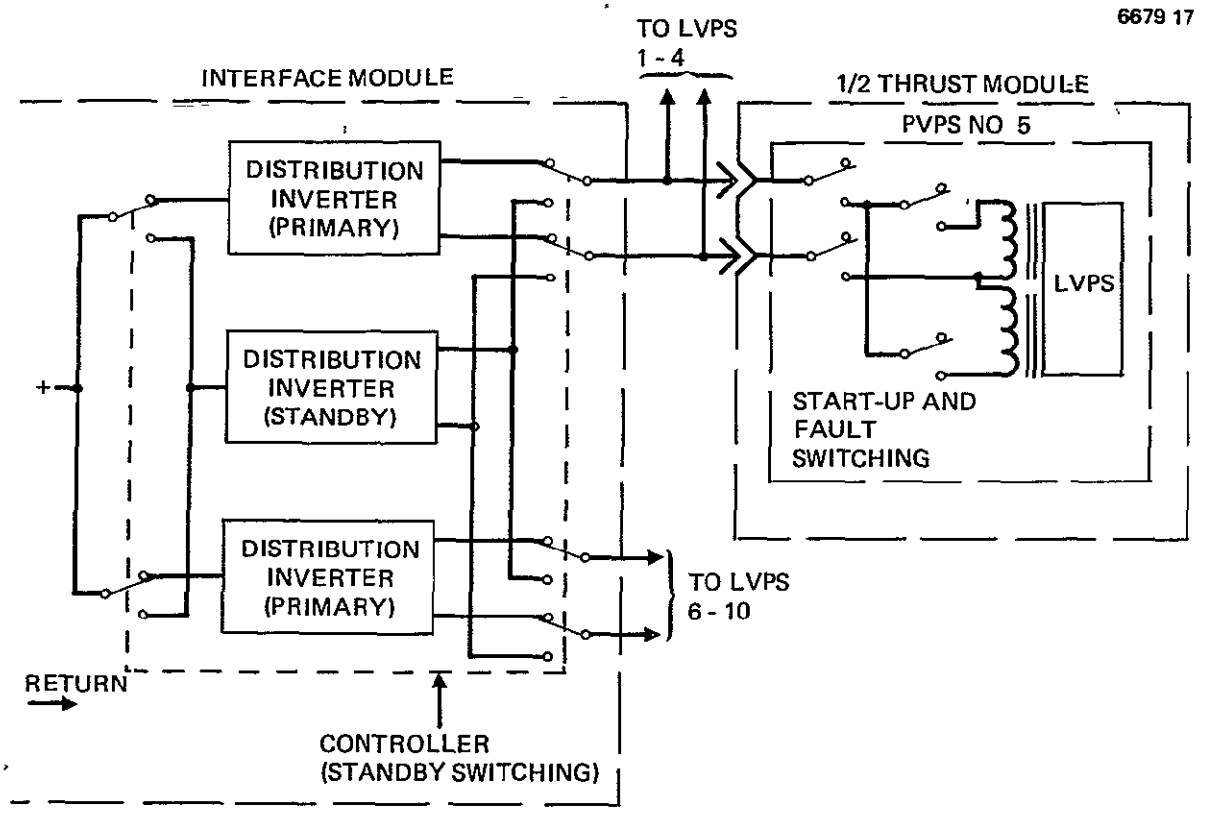

Figure 32. Interface between the distribution inverter and the low-voltage power supply.

power supply or in the thruster and an undesirable load results, relays on the primary of the output transformer will open and isolate the fault from the rest of the system.

The low-voltage power supply components are enclosed in a Z-frame module, this module, which measures 15.2 cm x 38 1 cm x 12 7 cm (6 in. x 15 in x 5 in.), is physically compatible with the beam and discharge supplies. Since the magnetic baffle and cathode keeper are referenced to the beam voltage, a separate high-voltage section provides the necessary isolation The remaining supplies can be distributed through the unit with the principal requirement being a close thermal coupling between major heat-dissipating components and the heat sink. Total power dissipation is estimated at 26 W; the input transformer and rectifier diodes are the principal contributors. Weight of the components plus chassis is estimated at 6.3 kg.

e. Description of the DC/DC Converter and the Distribution Inverter

The dc/dc converter and the distribution inverter are similar in design except that the converter has automatic overload interruption and rectification circuitry Tradeoff studies indicated that a minimum-weight design utilizes a transistor bridge, pulse-width-modulation to regulate outputs, and operating at 20 kHz The converter is sized for 700 W and the inverter for approximately 500 W.

Fault protection is critical because much of the PMaC system relies on outputs from both units. Each unit is protected from internal failures by a series dc regulator that acts as a switch and is driven by logic sensitive to an overcurrent. The primary converter is incorporated in the PMaC system with a standby unit; output buses of the standby unit are diode coupled to the output of the primary converter. Interruption logic is cross-coupled between the converters and automatic transfer occurs when a fault is detected The combination of diode-coupled buses and automatic switching eliminates potential "off" periods on the critical buses, which could disrupt logic and programmed circuits Although the distribution inverter is less critical with respect to the timing of the transfer from primary to standby, it is a single-point failure that could be catastrophic to the mission Transfer logic can originate in the controller or from ground command

f Description of the Controller

The controller will be designed to process the majority of thrust system control functions autonomously under the direction of the mission module. Transmittal of command and status information is the main electrical interface between the thrust system and mission module This implies that all thrust system control functions and most of the fault protection will be handled within the controller. To do this, all conceivable system operating and failure modes must be explicitly defined so that the controller can be programmed. For those tasks that cannot be clearly defined or adequately programmed, information will be communicated to ground where corrective action can be assessed. Implicit in

our approach to thrust system control is the partitioning of logic functions. It was considered desirable to have a central control unit to perform all control and logic functions rather than to use distributed logic. For example, each power supply that operates closed loop with a thruster will have its set-point evaluated by the controller rather than by the supply. Within the controller, each thruster or power supply set-point can be compared to a programmed set-point. If we assume that a single thruster control program can be used to control several thrusters, a centralized controller appears most efficient The logic format to implement the electrical interface will be established by the mission module and adapted in the controller.

Controller operation can be divided into normal and malfunction/failure operating modes Under normal operation, telemetry provides information on solar array characteristics, thruster power-supply performance, thrust-system housekeeping status, propellant distribution, and thruster operation. Thruster operation is a major logic category in terms of complexity. It includes startup and shutdown sequence commands; beam, discharge, and low-voltage supply control to preprogrammed set-points, and propellant control (reservoir valves, thruster valves). The maximum number of thrusters (seven) must be controlled simultaneously on a real-time basis All simultaneous thruster and PMaC command and control should be time-multiplexed to reduce hardware and increase reliability.

The solar array drive is commanded by the thrust system controller under the direction of the mission module to rotate the solar array wings to maintain proper orientation to the sun. The drive mechanism and an angle resolver are located on the pivotal axis at the base of the astromast Two motors are included for reliability. Motor drive electronics are based on a NASA LeRC design and included in the controller. Thruster gimbal actuators are commanded to their selected position via the thrust system controller under the direction of the mission module. Gimbal actuator position feedback is provided by shaft encoders.

The second logic category relates to the malfunction/failure mode of thrust-system operation. Failures in the PMaC unit, once identified, are corrected by switching on the appropriate standby units For

recoverable thruster malfunctions, the controller generates commands to autonomously correct them. This involves identifying the malfunction by comparing the parameters that are out of tolerance with preprogrammed deviation patterns associated with specific malfunction modes Commands are then generated and transmitted to the power supply(s) or thruster to initiate remedial procedures; this continues until operation of the thruster is restored For all malfunction/failure conditions that are not programmed or are beyond the programming limits for the controller, a flag or alert is transmitted to ground and a parallel thruster shut-down command goes to the supplies. This allows ground control to analyze the problem without the thruster or the thrust system being jeopardized by continued operation.

Table 13 describes the most common recoverable thruster malfunction modes that can be characterized with respect to power-supply operating conditions. Using this information, a program can be written and incorporated in the controller to identify specific malfunctions.

The controller is a digital-processing machine that uses programmed microprocessors and time-sharing techniques for thruster control. Central to the controller is a microprocessor-controlled central processing unit (CPU). Figure 33 is a block diagram of the controller

The electronics accepts and processes both digital and analog status information. The analog inputs are converted to digital on a time-shared basis, before being transferred to the CPU Computations are performed on the digital data and the results are stored in random-access memories or are output from the CPU The outputs from the CPU consist of control signals and processed data A time-shared digital-to-analog converter (DAC) and multiple sample-and-hold circuits are used to output the required analog control signals.

Input and output data multiplexers provide a controllable link for transferring digital data into and out of the CPU Serial command data from the mission module is transformed by the command processor to the data formats required by the processor and various user logic elements The TM data formatter uses external synchronization signals from the

Table 13. Recoverable Thruster Malfunction Modes

Malfunction	Manifestation (Parameter Deviation)	Cause/Source of Malfunction	Remedial Action Required
Screen (beam) overcurrent	I_{Screen} > 3 5 A for 0 5 sec[a] I_{Acc} > 0 2 A for 1 sec[a] I_{Acc} > 0 4 A for 0 1 sec[a]	Momentary high plasma density between extraction grids	Disconnect high voltage Reduce I_{Dischg} Restore high voltage
Discharge shifts to low mode operation	Low cathode Hg flow rate High main Hg flow rate High I_{Acc} I_{Screen} 10% below set point	Excess Hg in discharge chamber	Shut down main vaporizer until· Cathode vaporizer power reaches normal I_{Acc} reaches 0 3% of I_{Beam}
Screen accelerator breakdown	I_{Acc} repeatedly exceeds 0 4 A for 0 1 sec	Metallic flakes between grids (conductive path)	Activate grid clearing circuits (remove conductive path)
Isolator contamination	I_{Screen} repeatedly exceeds 3 5 A for 0 5 sec	Coated isolators[a] Foreign material between isolator shields[a] Liquid penetration[a]	Operate thruster with isolator heater and with discharge power

[a]Any one of these

5903

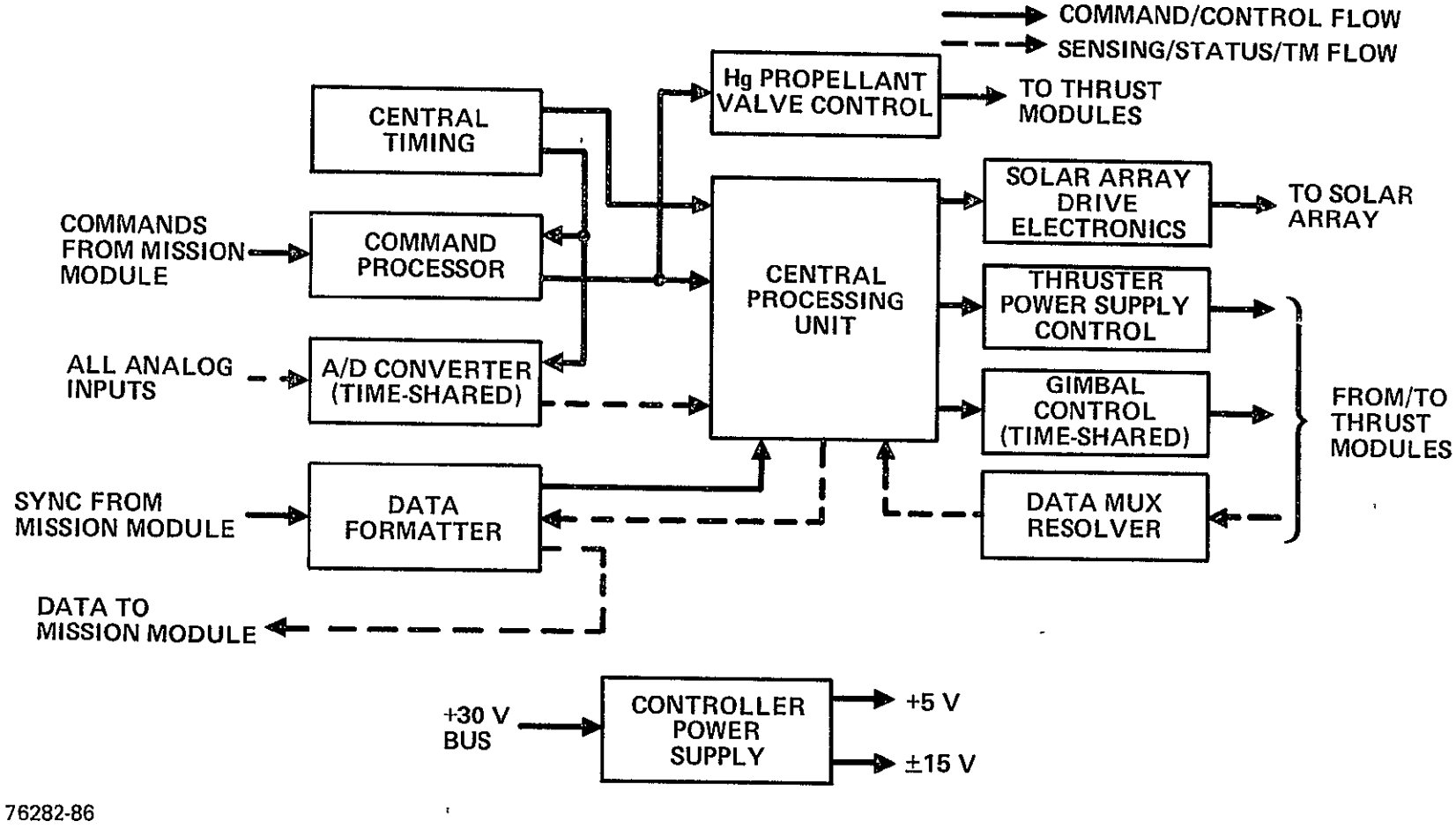

Figure 33. Controller block diagram.

mission module interface to transfer parallel data from the processor and reformat it to a serial data stream that is sent to the mission module.

The CPU is the primary process and control element of the control module electronics The CPU provides the onboard logic, monitoring, and control functions for the thruster and interface modules The CPU shown in Figure 34 is a programmed digital microprocessor. All command, digital TM, and control algorithm data processing is accomplished on a 4-bit byte-serial basis. This byte-serial architecture reduces the parts count and power consumption in comparison to a fully parallel design and provides an effective means for reducing data storage requirements and for accommodating mixed precision arithmetic The advantages of the byte-serial architecture more than outweigh the disadvantage of slower control-algorithm execution times because the execution time for any control mode is a small fraction of the available period.

Control algorithm parameters and variables are stored in a data memory that is physically and architecturally distinct from the microprocessor program, or control, memory. Parameters are stored in a nonvolatile programmable read-only-memory (PROM) Variables are stored in random-access memory (RAM) The control algorithms themselves, implemented as microprocessor programs, are stored in the control memory that is implemented with nonvolatile PROM. The nonvolatile memories guarantee that the control logic is hardwired and unalterable. Separate RAMs will be used to provide a reprogramming capability that will allow ground-generated programs to be substituted for fixed programs

The heart of the CPU is a single 4-bit bipolar microprocessor slice used for performing arithmetic. The microprocessor performs complement addition, subtraction, and Boolean logic operations on byte-serial (4 bits at a time) input data, the control algorithm, or product data Temporary storage for arithmetic results are provided by a 16-byte scratch-pad memory internal to the arithmetic logic function Final arithmetic results are transferred back into data memory, into

C-2

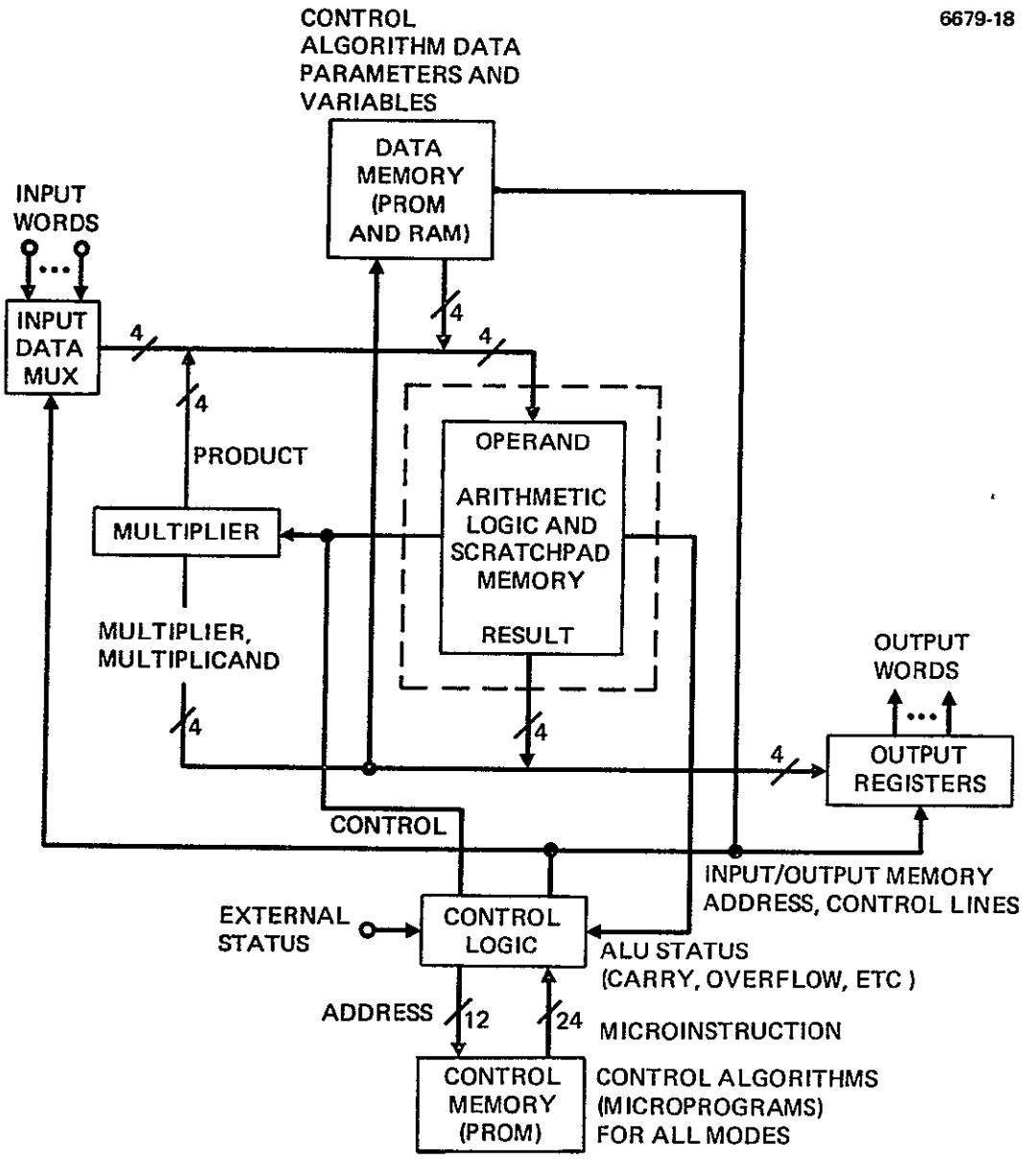

Figure 34. Central processing unit.

an output register, or into the multiplier, as determined by the control algorithm in control memory. All arithmetic operands and results are processed or transferred in 4-bit byte-serial form.

Binary complement multiplication is performed by a multiplier under programmed microprocessor control Both the multiplier and the multiplicand are loaded in byte-serial format and the product is read in byte-serial format The length of the multiplication operation performed is variable as determined by the microprocessor program

The instructions to the microprocessor comprising a program are sequentially retrieved from the control memory and executed by the control logic. Execution consists of appropriately decoding these instructions to produce the memory addresses of the inputs, outputs, and data and to produce the control signals that yield the desired operand and resultant data flow and processing.

4 Physical Configuration of the PMaC System

Table 14 lists the components of the baseline PMaC design, indicating their size, mass, power consumption, and redundancy Units are located in either the interface module or one of five thrust modules. Each thrust module is identical to another and directly interchangeable.

The information summarized in Table 14 was used in determining the arrangement of the interface module units on the top side of each thrust module heat sink. The general layout of the units was determined by optimizing three parameters: electrical function, thermal balance, and mass distribution on each heat sink Module heat sinks (numbered 1 through 5) and an optimized grouping of units is shown in Figure 35 along with a summary of weight and power dissipation per module heat sink The numbers directed toward the unit with an arrow indicate the unit power distribution Power dissipation varies from 65 W to 113 W for the operation of primary units with no standby units operating A worst-case power dissipation of 128 W could occur if standby units were operating In addition, operating all 10 thrusters rather than 7 of 10, which is the baseline, was considered because the power dissipation of individual modules is the controlling design parameter rather than power dissipation

Table 14. PMaC Units

Unit	Unit Size, m (in.)	Unit Weight, kg	Unit Power Dissipation, W	Number of Units	
				Active	Standby
Interface module					
Power distribution	0.102 x 0.127 x 0.304 (4 x 5 x 12)	17.3	66	5	0
Solar array control	0.102 x 0.203 x 0.304 (4 x 8 x 12)	5.0	0	2	0
Distribution inverter	0.076 x 0.152 x 0.076 (3 x 6 x 3)	1.0	30	2	1
DC/DC converter	0.102 x 0.152 x 0.152 (4 x 6 x 6)	1.7	73	1	1
Controller	0.102 x 0 203 x 0.304 (4 x 8 x 12)	4.0	15	1	1
Thrust module				Per Module	
Beam supply	0.152 x 0.381 x 0.487 (6 x 15 x 19.2)	200	390	2	0
Discharge supply	0.152 x 0.381 x 0.274 (6 x 15 x 10.8)	5 0	52	2	0
Low-power supplies	0.152 x 0.381 x 0.127 (6 x 15 x 5)	6.3	26	2	0

5903

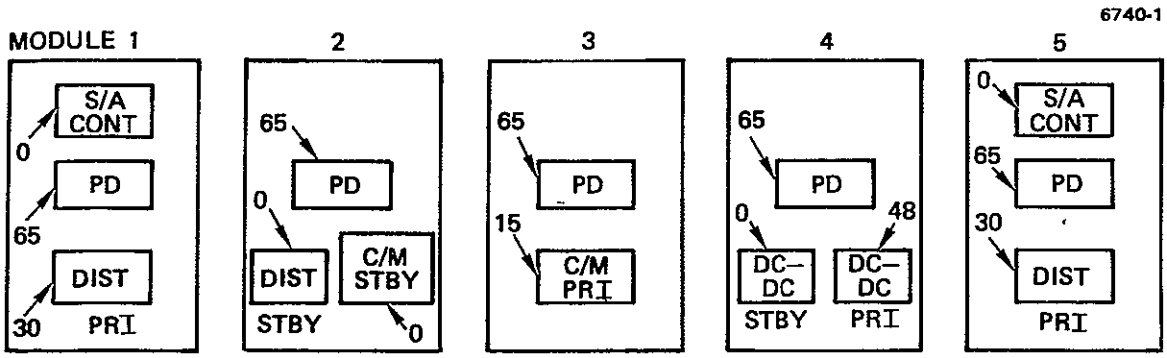

S/A CONT ≡ SOLAR ARRAY CONTROL
PD ≡ POWER DISTRIBUTION
DIST ≡ DISTRIBUTION INVERTER
C/M ≡ CONTROLLER
DC–DC ≡ DC–DC CONVERTER
PRI ≡ PRIMARY UNIT(S)
STBY ≡ STANDBY UNIT

	MODULE NUMBER					
	1	2	3	4	5	1 THROUGH 5
POWER DISSIPATION, W	95	65	80	113	95	449
MASS, kg	28 7	27 7	26 8	26 2	28 7	138 1

Figure 35. Layout of the interface module unit.

of the total system. Each module must be designed to dissipate the maximum heat generated during the full-power operation of the equipment mounted on both sides of the heat sink.

The arrangement of the units of the thrust module PMaC system is shown in Figure 36 A standard Z-frame modular structure as used in present NASA LeRC power processor designs with overall dimensions of 76.2 cm wide x 101.6 cm long x 15.2 cm high (30 in wide x 40 in long x 6 in. high) can accommodate the beam, discharge, and low-power supplies for two thrusters. Space remains to provide access for the feedthrough harness and propellant lines. Thrust module units mount to the thruster side of each heat sink. A rotation of 180° between the supplies for each thruster evenly distributes the power dissipation over the heat sink.

Unit layout, power dissipation, and weight for thrust modules 1 through 5 are shown in Figure 37 The power dissipation entry represents the case for 7 out of 10 thrusters operating. Figure 38 shows the combined thrust module and interface module summary. The maximum total power dissipation for any single module is 1029 W. The total PMaC system power dissipation is 3654 W. The mass distribution for each module is well balanced (93.8 kg to 96.3 kg) for a total of 476.1 kg With this information, the heat sink, heat pipes, radiators, and general thrust system structural and thermal control configuration can be evaluated.

5 PMaC Unit Reliability

PMaC units were designed to the point that a reasonable assessment of hardware complexity and parts count was established. Every effort was made to simplify the PMaC subsystem to improve its reliability. Although we attempted to keep the number of units to a minimum, it was necessary to add some redundant units to eliminate the possibility that the failure of a single unit would be catastrophic to the entire mission. The baseline PMaC subsystem is a compromise between minimum complexity and maximum reliability.

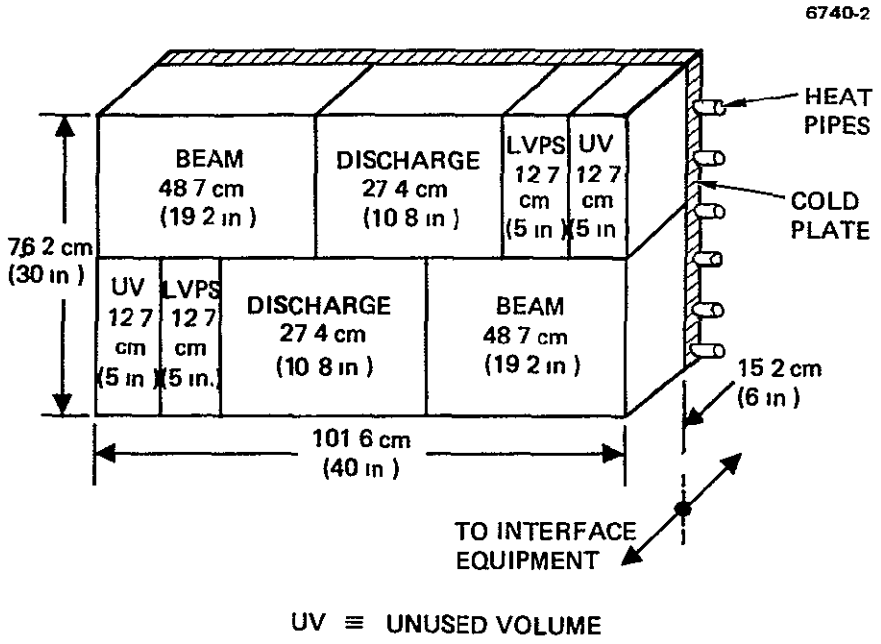

Figure 36. Thrust module electronics.

6740-3

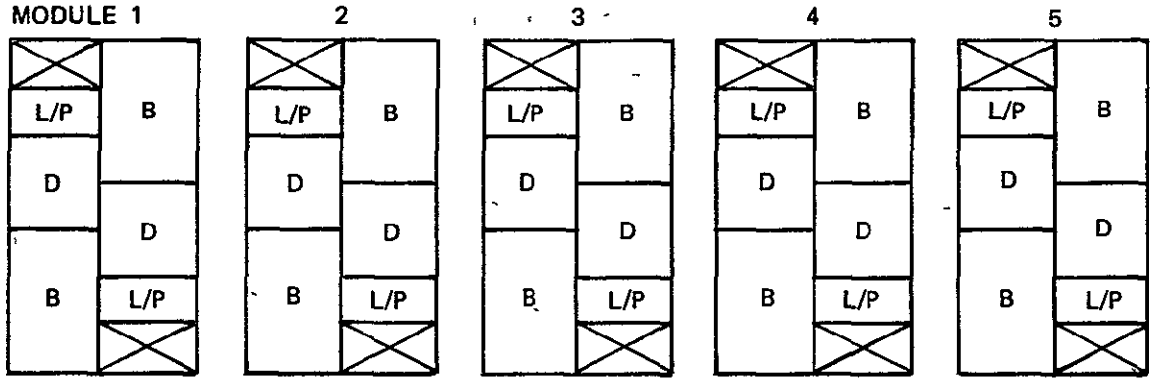

B = BEAM SUPPLY
D = DISCHARGE SUPPLY
L/P = LOW VOLTAGE POWER SUPPLIES

	MODULE NUMBER					
	1	2	3	4	5	1 THROUGH 5
NUMBER OF THRUSTERS OPERATING	1	0	2	2	2	7
POWER DISSIPATON, W	458	0	916	916	916	3206 [a]
MASS , kg	67 6	67 6	67 6	67 6	67 6	338 0

[a]FOR 7 OUT OF 10 THRUSTERS OPERATING

Figure 37. Layout of the thrust module unit.

6740-4

	MODULE NUMBER					
	1	2	3	4	5	1 THROUGH 5
POWER DISSIPATION, W	553	65	996	1029	1011	3654
WEIGHT, kg	96 3	95 3	94 4	93 8	96 3	476 1

Figure 38 Combined thrust module and interface module power dissipation and weight summary of baseline design

Since the PMaC subsystem contains units in various stages of development, an estimate of parts count is the only common denominator appropriate to a reliability assessment of all units A basic parts count for each unit was divided into several component categories: integrated and hybrid circuits, active discrete, passive discrete, and magnetics. A failure rate based on Hughes experience with similar hardware programs was determined for each type of component. Figure 39 summarizes the quantities of each type of component for each unit Also included is a unit and effective (functional) unit reliability number based on the mission lifetime

Failure rates have been established for components operating within specified bounds of voltage and current stress and temperature A reliable design must take into account appropriate component derating factors for operation outside these bounds. Failure rates were also assigned by classifying components in operating and nonoperating modes based on the duty cycle of components within a circuit design, redundancy of units, and the number of operating thrusters. Then, after a basic unit reliability was calculated using weighted failure rates, an experience factor was applied. This was based on Hughes experience with high-reliability spaceflight hardware in space and had the effect of increasing the estimated system reliability

Where the estimated reliability of a single unit is less than 0.97 or failure of the unit would be catastrophic, redundant units were included The effective (functional) reliability is therefore considerably higher than the reliability without redundancy, as exemplified by the controller Redundancy improves the reliability of the interface module by providing backup units to perform a given function. Although there is no redundancy in the thruster and power-supply systems, it would be possible to lose one or possibly several thruster or power-supply systems and still successfully complete the mission Adding redundant units for the beam, discharge, or low-voltage power supplies would result in a tremendous weight penalty. The baseline design,

6740-5

UNIT	ESTIMATED PARTS COUNT					RELIABILITY	
	INTEGRATED AND HYBRID CIRCUITS	ACTIVE DISCRETE	PASSIVE DISCRETE	MAGNETICS	TOTAL	SINGLE UNIT	EFFECTIVE[a] (FUNCTIONAL) PER UNIT
INTERFACE MODULE							
POWER DISTRIBUTION AND SOLAR ARRAY CONTROL	0	0	1180	0	1180	0 985	0 985
DISTRIBUTION INVERTER	5	18	37	3	63	0 984	0 999
DC/DC CONVERTER	6	34	71	4	115	0 979	0 999
CONTROLLER	366	78	1715	0	2159	0 797	0 970
RELIABILITY OF THE COMPLETED MODULE							0 955
ONE-HALF THRUST MODULE							
BEAM SUPPLY	b	b	b	b	b	0 977[c]	0 977
DISCHARGE SUPPLY	b	b	b	b	b	0 983[c]	0 983
LOW-VOLTAGE POWER SUPPLIES	20	25	539	20	604	0 967	0 967
RELIABILITY OF THE HALF-MODULE						0 930	

[a] ACCOUNTING FOR REDUNDANT UNITS
[b] NOT AVAILABLE
[c] CALCULATED FROM FAILURE RATES FURNISHED BY NASA LeRC

Figure 39. Summary of PMaC unit reliability.

therefore, includes a redundant half-module rather than redundant power supplies or thrusters. Reliability for a half-module (one thruster and its associated power supplies) is 0 93 Reliability of the interface module is 0.955

D. ANALYSIS AND DESIGN OF THE THRUST SYSTEM STRUCTURE AND THERMAL CONTROL SYSTEM

This subsection presents the design of the thrust system structure and the thermal control subsystem In addition, the subsystems not previously discussed are described the mercury propellant subsystems and solar array drive.

The objectives in designing the thrust system structure and thermal control subsystem were to achieve minimum mass and maximum reliability using available technology and existing fabrication techniques The design evolved from several goals and constraints:

- Modular construction
- Minimum mass of the deployed thrust system
- Solar array stowage and deployment requirements
- IUS and shuttle load requirements
- Maintenance of all subsystems within their operational temperature range
- Viable interfaces with the mission module and with the IUS
- Easy assembly and good accessibility

The requirements imposed on the design of the structure and of the thermal control subsystem, including those posed by other components of the Halley's comet mission spacecraft, are reflected in the data base in Section 2 A The general design approaches adopted are presented in Section D.1 Results of an analysis conducted to establish design parameters are presented in Section D 2 These analyses include structural loads analysis, thermal control tradeoff analyses to select optimum design parameters, tradeoff analysis of alternate propellant tank configurations, and materials analysis to select structural

materials. Section D 3 describes the design characteristics established for the baseline system.

The composite mass breakdown — including the mass of the thrusters and gimbals and of the PMaC system — and the thrust system mass properties are presented in Section 3 as part of system performance projection.

1 Design Requirements and Approach

Structural design requirements (identified in Figure 1) consist of the interface with the IUS, the interface between the thrust system interface module and the mission module, the attachment of the solar array drives to the interface module cross-shaft, and the attachment to the space shuttle cradle Interfaces within the thrust system (also illustrated in Figure 1) entail the attachment of the adapter to and the separation of it from the interface module

The overall dimensions of the structure are primarily dictated by the stowed solar array, the envelope of which is shown in Figure 4. As shown below, the required radiator length is 0 4 m less than the height of the stowed array. Therefore, the radiator would have to grow at least 0 4 m before its length would govern the length of the thrust system

The design approach adopted was to generate a simple structural layout with direct, nonredundant load paths that would minimize the mass of the structure. The location of the solar array canister at the center line of the thrust system structure prohibits a direct diagonal load path to the IUS bolt circle (Figure 49(a)) The required position of the thrust system release points does not permit the attachment of the required adapter base bolt pattern to the IUS interface ring, which is 2.985 m in diameter. Consequently, two cross-beams were added to the IUS interface ring; these efficiently transmit lateral shears from the separation plane, thereby reducing the axial loads in the tube members. The interface requirements of the mission module and of the solar array drive are readily achieved

The bulk of the thrust system, mission module, and payload fits comfortably within the 4.572 m diameter space shuttle envelope (Figure 50), except for the extreme corners of the solar array package where only a small clearance is available. The amount of clearance is strictly a function of solar array design, and further analysis of the solar array is required to either reduce its dimensions or to validate the adequacy of this design for the shuttle environment.

The design is required to provide for, on command, the removal of the tie bolts, a separation (push-off) force, and an unobstructed egress for separation of the entire vehicle from the IUS. These requirements are fulfilled by electro-explosive separation nuts, with bolt catchers, and with an adapter design which results in its collapse out of the exit path immediately upon separation

The design of the thrust system structure was further constrained by the requirement for design modularity, by PMaC packaging specifications, and by the requirements to provide the requisite degree of thermal control. Dimensions of the cold plate were established from a consideration of the thermal requirements associated with the modular packaging approach adapted for the PMaC units. Each thrust module houses two sets of PMaC units serving two thrusters and has a specified base dimension of 76.2 cm x 101.6 cm (30 in. x 40 in.) The minimum dimensions of the cold plate needed to accommodate each module is 81.3 cm x 106 7 cm (32 in x 42 in), this allows 2.5 cm (1 in.) around the periphery of each for the attachment to the interface module.

The requirements for thermal control were determined by the thermal interface data provided in the data base, and by the requirement to maintain all subsystems within their operational temperature range throughout the mission. Subsystem operational temperature ranges are itemized in Table 15. The minimum temperature limit is the non-operating survival temperature limit. The design analysis, which provided the defined thermal parameters, considered the limiting hot and cold conditions encountered during the mission. Using variable conductance heat pipe (VCHP) radiators as the primary thermal control device ensures that all environmental and operational conditions that will exist between these limiting points will be adequately satisfied

Table 15 Subsystem Operational Temperature Ranges

Unit/Subsystem	Allowable Temperature Limits, ^{o}C	
	Maximum	Minimum
PMaC/Interface Module Unit Mounting Surface	50	-30
Propellant Tanks	150	-40
Propellant Lines	150	-40
Thrusters	300	-100
Gimbals.	125	-65
Solar Array Drive	60	-30
Structure	200	-185

5903

The maximum thermal load case occurs at the start of the mission at 1 0 AU. At this point the spacecraft subsystems that determine the thrust system thermal environment (mission module and solar array) are at their maximum temperatures, the sun is shining on one end of the thrust system, seven thrusters are operating, and power dissipation from the PMaC units are maximum. These conditions establish the design requirements for the radiator area, the number of VCHPs, and the thermal conductance of the cold plate.

The minimum thermal load occurs at the greatest distance from the sun (4.5 AU) At this point the mission module and the solar arrays are at their minimum temperatures, if all of the thrusters and PMaC units are off, the system is in a minimum dissipation mode. By analyzing this case, heater sizing for each subsystem can be determined.

Estimated power dissipation from the various subsystems was determined above, the results are summarized in Table 16. These results were the basis for the thermal analysis Thermal interface data are presented in Section 2. Solar array characteristics — emittances and temperatures of solar array components as functions of heliocentric

Table 16. Subsystem Heat Dissipation

Unit/Subsystem	Power Dissipation, W	
	Maximum	Minimum
Thrusters, each module	750	0
PMaC system, each module	936	0
Interface module	113	65
Solar array drive	4 5	0

5903

distance — are shown in Figure 3. The mission module is conductively and radiatively coupled to the interface module. The effective conductance across the attachment from the module to the interface truss has been specified to be 0.01 W/°C. The mission module is enclosed in a multilayer insulation (MLI) blanket (effective emittance of 0.025), with 1.13 m^2 area within the field of view of the thrust module. The temperature swing of the module is between 5°C and 50°C.

The design of the thermal control subsystem includes a modified version of the Communications Technology Satellite (CTS) heat pipes. This is a VCHP having the following assumed performance characteristics:

- 305 W-m (12,000 W-in.) transport capability at 50°C
- A dynamic range of 28°C (from full off to full on)
- 1 W leakage per VCHP (full off)
- Weight: 0 26 kg/m (0 173 lb/ft) — heat pipe
  0.15 kg (0.34 lb) per reservoir.

To minimize mass, the baseline design did not provide for any VCHP redundancy. Tradeoffs available between an alternate design approach that has VCHP redundancy and potential schedule risks are discussed in Section 4.

The baseline design assumes that the Halley's comet mission spacecraft will always be oriented so that the sun does not shine on the

radiators. The design is strongly dependent on this fundamental assumption

The design approach selected for the thermal control subsystem complies with the above requirements. A cold-plate/radiator assembly is provided on each module, with two radiators per module; CTS VCHPs are embedded in the structure MLI blankets minimize thermal coupling of the thrust system to the environment, thus ensuring that the VCHP-radiator assembly is the dominant heat-rejection surface for the system Heaters are used to maintain design temperature levels when the modules are shut down.

2. Analysis of Structural Loads and Thermal Control

The key areas of structural loads and thermal design were analyzed, this subsection presents the results of that analysis. Also included are the results of the analysis that led to the selection of a dual-tank system for the mercury propellant and to the choice of structural materials. Results of these tradeoff studies defined the parameters that characterize the baseline design presented in the following subsection

a. Structural Loads Analysis

The loads used to size the structural configuration of the thrust system are shown in Table 17 These loads are based on the current understanding of the shuttle launch environment and of the IUS boost environment as given in Refs. 13 and 14, respectively. The load factors, as presented, would apply to the interface between the spacecraft and the IUS. The shuttle load factors are largely vibrational, and the IUS factors are largely a result of lateral acceleration caused by IUS turn capability, with a relatively small vibrational content. As a first approximation, the IUS factors can be considered to be constant along the length of the spacecraft. If the spacecraft is cantilevered from the IUS, the shuttle load factors would be amplified along the length of the spacecraft adapter, approximately as the first mode

Table 17. Design Load Factors

Interface	Flight Event	Axis[a]	Load Factors (G)		
			Ultimate		Limit
Shuttle	Maximum acceleration	X (longitudinal)	+4 7	Conservatively combined	+3.7
	Liftoff	Y	±1.4		±1.1
	Landing	Z	-4 0		-3 2
	Emergency landing	X (longitudinal)	-0.0	Separate	
		Y	±1.5		
		Z	+2.0 -4 5		
IUS	Earth orbital	X (longitudinal)	7.0	Combine	5 5
		Y	±4 2		±3 3
		Z	±4 2		±3 3

[a]See Figure 40

5903

of a cantilever beam This could amplify the lateral load factors by a factor of approximately three at the interface module Rather than accept the spacecraft mass that would result, the shuttle/IUS configuration shown in Figure 40 has been assumed Using a properly designed forward support cradle to couple the spacecraft to the shuttle should keep the loads coupled into the interface module from exceeding those defined for the IUS interface in Table 17

Designing the cradle and analyzing the clearances within the shuttle bay are beyond the scope of the current effort. These tasks will require coupled structural analyses involving the spacecraft, IUS, IUS cradle, shuttle, and shuttle cradle. But sufficient clearance is provided in the baseline design to give confidence that clearance will not be a significant problem Use of the loads that were specified for the IUS interface to represent the loads at the shuttle cradle

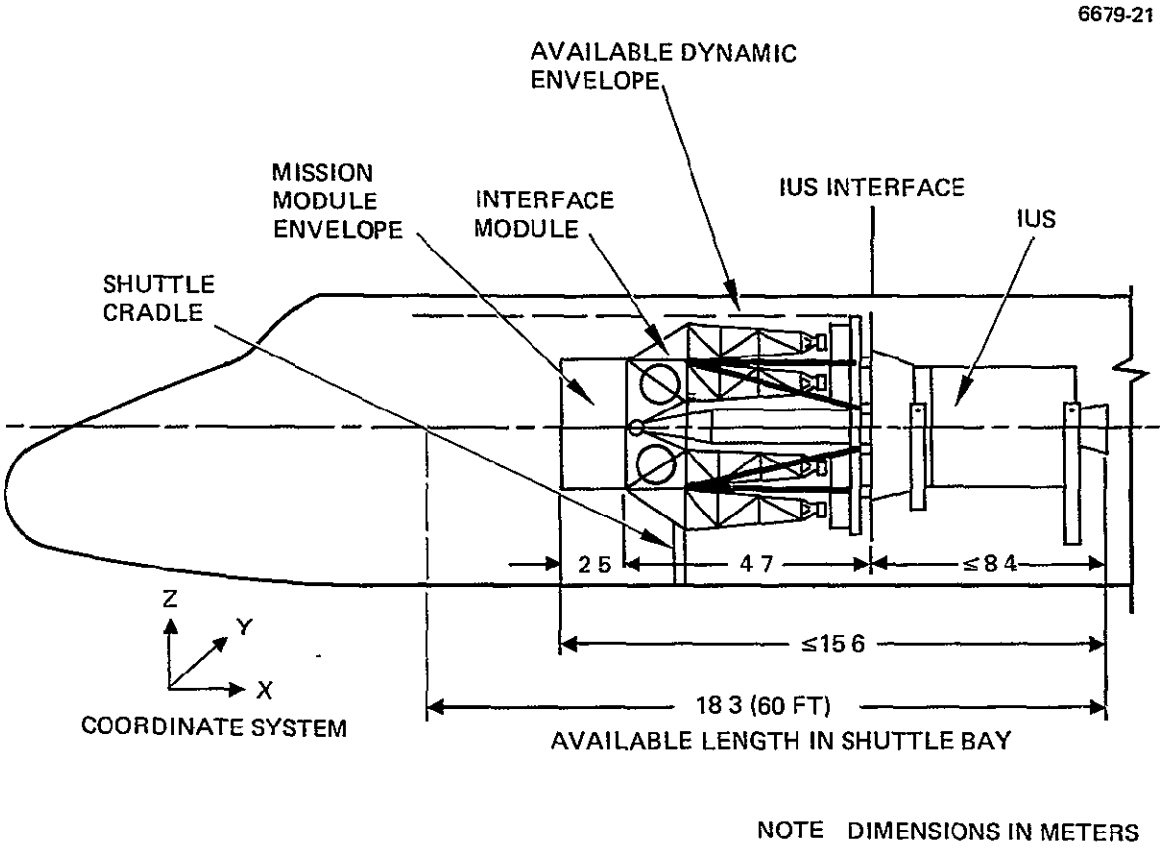

Figure 40. Thrust system/payload assembly in shuttle bay.

interface is probably also conservative, indicated from a consideration of the load amplification expected through the IUS cradle, as compared to the direct load path from the shuttle into the shuttle cradle.

This approximation to the spacecraft load input was compared to the results of recent Hughes studies of several DoD satellites, the objectives of these studies were to define the design requirements for shuttle launches using the IUS These analyses indicated that the use of a forward shuttle cradle concept, similar to the one proposed here for the baseline thrust system, results in an optimum, minimum mass design for a spacecraft structure that can withstand shuttle loads The satellite/IUS payloads (including the IUS cradle) and the forward shuttle cradle were dynamically coupled to the shuttle, and a coupled analysis of the system was conducted for modes and frequencies and for payload transient response for two critical loading events for the shuttle. These two events were (1) a symmetric and an asymmetric lift-off for the total shuttle launch vehicle and (2) an abort landing. The study revealed that the satellite loads and accelerations were extremely sensitive to the dynamic properties of the IUS and of the shuttle cradle The loads and accelerations determined for the two events showed values substantially greater than those previously predicted by NASA and furnished to shuttle users This is illustrated in Table 18, in which NASA's space vehicle load factors (from Ref 13) are compared with the results of the coupled analyses. Although these results are not directly applicable to the thrust system design, they do add credibility to the input load levels used in the tradeoff and baseline studies.

The IUS load cases will be considered to be cases of uniform lateral acceleration. The distribution of lateral acceleration for structures that are designed for shuttle mounting must also be evaluated in a way that allows comparing alternative configurations Figure 41 presents the results of detailed spacecraft/shuttle coupled analyses In this case, the structural configuration consisted of a stiff (natural frequency $f \geq 20$ Hz) and a flexible ($f \leq 10$ Hz) section Other analyses indicated that the two conic segments shown are

Table 18 Comparison of Results of Coupled Load Analysis with NASA Load Specifications

Satellite Properties	NASA Specification	Coupled Analysis Results[a]			Thrust System Baseline
		Satellite A	Satellite B	Satellite C	
Mass, kg (lb)	b	b	1193(2650)	1260(2800)	3600(8000)
Center of mass from IUS/ cradle interface, cm (in)	b	3 38(133.0)	3 28(128 9)	2 48(97 8)	3 56(140)
First bending frequency, Hz	b	5 3	9 0	10 0	c
Liftoff· limit loads at satellite center of mass, G					
Maximum transverse	1 5	3 0 - 2 5	3 9	3 6	4 7
Maximum axial	2.9	3.1	2 75	2 75	5 6
Landing limit loads at satellite center of mass, G					
Maximum transverse	2 8	7.0 - 6.7	4 6	5 2	4 7
Maximum axial	1.0	1 3	1.2	1 4	5.6

[a]Recent Hughes studies of several DoD satellites.

[b]Not available.

[c]To be determined

5903

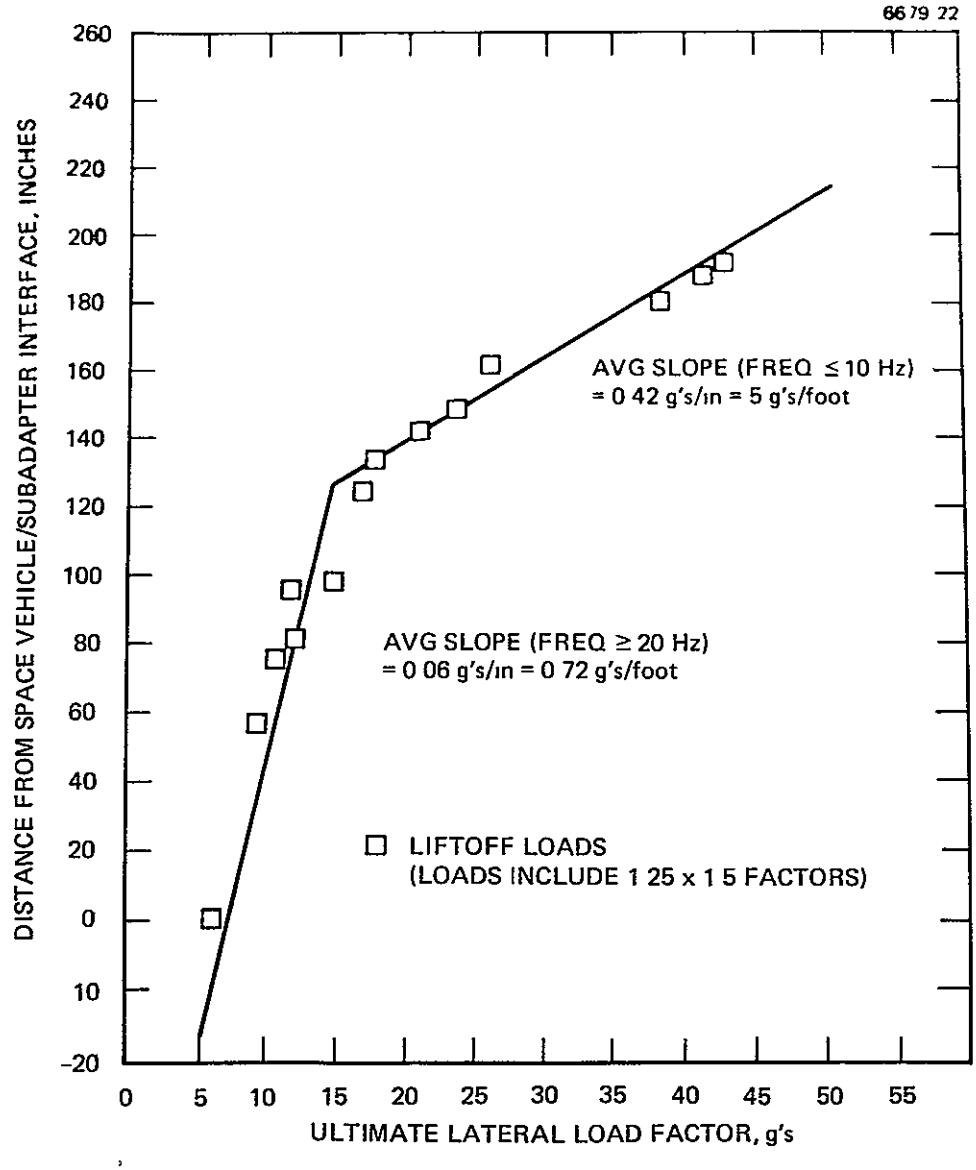

Figure 41. Lateral load versus distance from space vehicle/subadapter interface for different spacecraft configurations.

probably better represented by a quadratic. However, a linear fit was used as a guide in using data available to obtain Figure 42. This data, represented by curve T_1 in Figure 42, was generated by assuming that the frequency of the long, unsupported thrust module will be low. Adding a snubber as the single support at the IUS end of the module will change the vibrational modes and raise the frequency. This is illustrated in Figure 42 by curves T_3 through T_6 (representing different thruster module lengths). When a short module is used, the frequency will be high ($f \geq 20$ Hz), and curve T_2 may be assumed to hold Since definitive data for the mission module is not available, a stiff section ($f \geq 20$ Hz) has been assumed. The numerical values used are shown in Table 19

The load assumptions made may be summarized as follows

- When mounted on the IUS and cradle, the thrust and mission modules were considered to be beams cantilevered from the interface, with a load distribution based upon their length and free-end condition
- The IUS flight loads have been considered to be uniformly distributed over the length of the spacecraft and the adaptor

These assumptions have permitted a uniform comparison between grossly different configurations and the development of a baseline design

A comprehensive load study must be conducted during the development phase to verify these assumptions This will require coordination with the many shuttle environmental studies that are expected to be performed by shuttle users for many other satellites to define the shuttle acoustic, shock, and vibration environments. Early shuttle flight data from other satellite programs will be very helpful in defining the basic input levels. As the characteristics of the IUS, IUS cradle, shuttle cradle, and Halley's comet spacecraft become more clearly defined, transient coupled analyses can be performed The results from these analyses will be used to validate the design loads, provide a basis for the static test levels, and provide peak limiting (notching) levels for structural vibration tests of the system

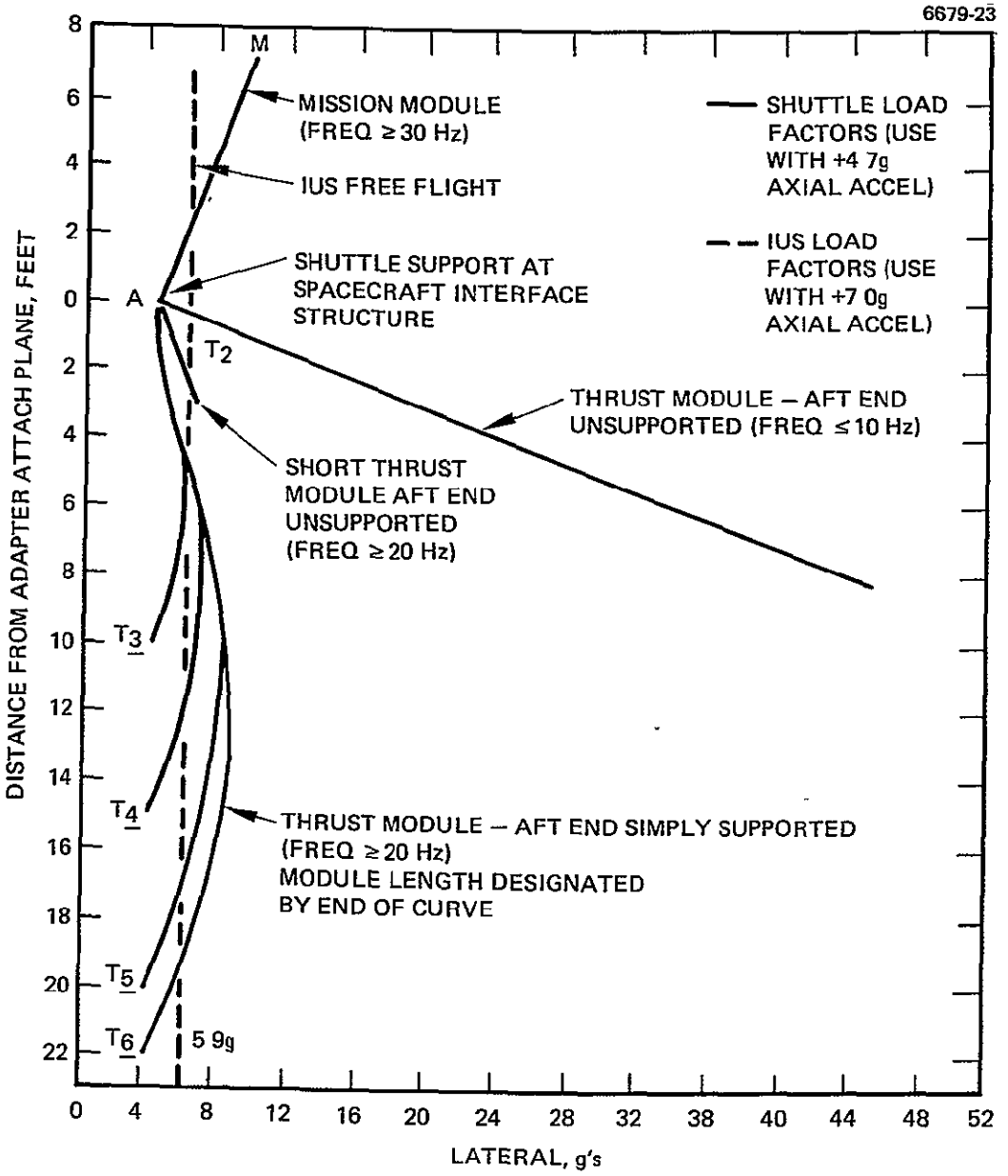

Figure 42. Design loads used in this study.

Table 19. Derived Curves for Local Lateral Acceleration on Thrust Module[a]

Curve Designation[b]	Type of Structure	Acceleration Variation with Distance from Interfaces
A-M	Mission module Assumed f ≥ 30 Hz	$a = 4.24 + 0\ 72\ \ell$
$A\text{-}T_1$	Long, unsupported thrust modules	$a = 4.24 + 5\ 0\ \ell$
$A\text{-}T_2$	Short, unsupported thrust module	$a = 4.24 + 0.72\ \ell$
$A\text{-}T_3$	Aft end supported by snubber to IUS interface structure	$a = 4.24 + 0\ 72\ \alpha^2 L\ (2\alpha^2 - 5\alpha + 3)$
$A\text{-}T_4$		
$A\text{-}T_5$		
$A\text{-}T_6$		

[a]Data used for design of thrust and interface modules Adapter design based upon IUS free-flight condition, a = 5 9 G.

[b]Refers to curves in Figure 42.

KEY

a ≡ Local lateral acceleration (4 24 = root square sum of lateral liftoff acceleration values)

ℓ ≡ Distance from plane of adapter/cradle support

$\alpha \equiv \ell/L$

L ≡ Total length of thrust module from plane of adapter/cradle support to thruster supports.

5903

Appropriate static tests should be conducted on parts and assemblies that have complex load paths and are not amenable to analysis Bending and axial forces can be simulated by multiple point loadings, with critical stresses and displacement being monitored throughout such testing

The qualification thrust system test vehicle tentatively defined in Table 20 could be assembled from a combination of flight, qualification, and simulated parts to provide mass and stiffness representation of the flight system. This simulation will also be valuable for correlating analytic and test data A combination of analyses and tests at an early stage in the design effort will provide a very high level of confidence that the safety and strength requirements can be satisfied within the stringent mass budget of the configuration.

b. Thermal Control Analysis

To define the design of the thrust system thermal control subsystem required specifying the following parameters:

- Effective fin thickness of the cold plate
- Radiator dimensions and surface finish
- Number and spacing of the VCHPs in the cold plate and radiator
- Location and effective emittance of the MLI blankets
- Thermal finish requirements for each subsystem
- Heater requirements for each subsystem.

Specifying the first three parameters constitutes an integrated design task, the objective of which is to provide a maximum cold plate temperature of 50°C (Table 15). The peak temperature is the sum of: (1) the temperature drop (ΔT) in the cold plate, (2) the ΔT across the interface between the cold plate and the heat pipe, (3) the ΔT across the interface between the heat pipe and the radiator, and (4) the maximum radiator temperature.

The sequence used to design the cold plate and radiator assemblies began with an analysis of the cold plate This analysis correlated cold plate ΔT as a function of fin thickness (with the number of heat pipes as a parameter) This data was used to select the operating temperature (vapor temperature) of the VCHP The next step was to perform a radiator design study to determine the desired VCHP temperature.

Table 20. Thrust System Vibration Qualification Vehicle

Subsystem	Flight	Hardware Qualification	Simulated
Interface Module		Truss structure Tank supports 2 solar array drives	PMaC dummy units
Thrust module		2 Ti trusses 2 PMaC modules 4 Thrusters 4 Gimbals	3 Dummy thrust modules
Propellant storage and distribution	1810 kg Hg	2 Tanks Field joints[a] Manifold Latching valves[a] 4 Flex lines	
Thermal		4 Cold plates 4 Radiators 16 Heat pipes	
Adapter	4 Tripods 4 Shear cones 4 Pushoff springs and retainers	4 Separation bolts 4 EE Separation nuts	
Ground Support Equipment (GSE)			Mission module and solar array packaging

[a]Number to be determined

These studies provided a design for the cold plate and radiator based on a uniform heat distribution into the cold plate The final step in the design process was to evaluate and modify the idealized design on the basis of the actual heat distribution of one of the PMaC units

Figure 43 contains the results of the analysis of the cold plate It was assumed for the analysis that the heat flux into the cold plate is uniform and that all of the heat generated is conducted to the VCHP (i.e , there are no radiation losses) The analytical model represented

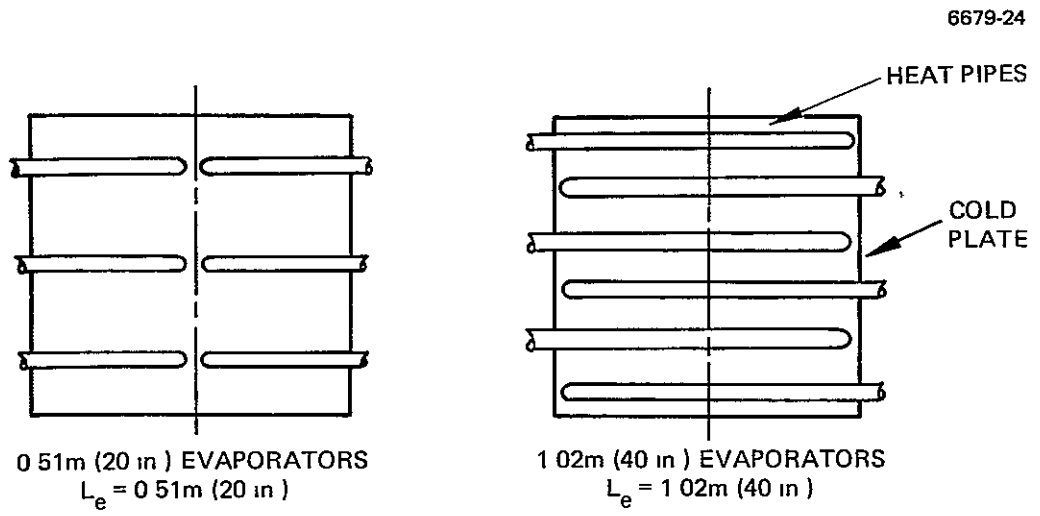

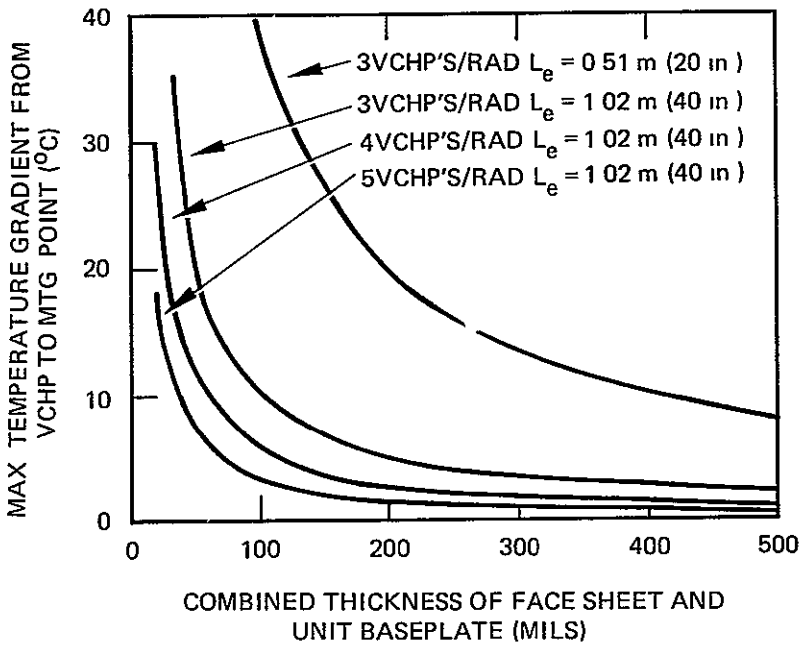

Figure 43. Effect of the number of heat pipes and of the thickness of the facesheet plus the thickness of the baseplate on component mounting point temperatures for a uniform unit heat flux of 2045 3 W/m^2.

the section of cold plate under the footprint of a 3 kW beam supply and the heat flux associated with its maximum dissipation The figure shows the maximum cold plate ΔT as a function of fin thickness with the number of heat pipes as a parameter Fin thickness consists of the unit baseplate thickness of 1 mm (0 040 in.) plus the cold plate face-sheet thickness, the latter being the design variable.

The data in this curve permits evaluating two approaches to the design concept, as illustrated in Figure 43. The cold plate could be built with the evaporator section of each heat pipe extending halfway into the cold plate With this approach, each radiator would be identical and each heat pipe would have a 50 1 cm (20 in.) evaporator An alternate approach would be to run the heat pipes completely across the cold plate by using longer, 1 02 m (40 in.), evaporators. This would result in a module's two radiators being mirror images rather than identical Comparing the two curves in Figure 43 representing these heat pipes per radiator — one for a 0 51 m (20 in.) evaporator and the other for a 1 02 m (40 in) evaporator — shows that, for a given ΔT, the requirements for fin thickness vary considerably The effective halving of the distance between pipes causes this. The 1 02 m (40 in) evaporator was selected for the baseline design because of the reduction in fin thickness requirement Estimated performance data for the cold plate with three 1 02-m (40-in) heat pipes running across it was used in designing the radiator. Should more than three heat pipes be used, the design would be conservative A ΔT of 12°C for the cold plate was selected as the design point, the slope of the curve for higher ΔTs indicates considerable sensitivity to fin thickness. A cold plate fin thickness of 2 mm (0 080 in) was selected, with an attendant ΔT of 12°C in the cold plate A vapor temperature of 38°C is thus required to maintain the cold plate at or below 50°C

The radiator design is based on hot-case environment and dissipation. View factors from the radiator to the solar array are dependent on which module is being considered and the relative orientation of the array with respect to the radiators Monte Carlo techniques were

used to obtain view factors as a function of these variables. The worst case (with the radiator view factor to the solar array at maximum) was selected to ensure that the design would be adequate. Figure 44 contains a table of the view factors used in the analysis. A maximum heat dissipation of 1000 W per module was used for the radiator sizing. A silver-teflon finish was selected for the radiator; it would provide high emittance and low solar absorptance should the radiator be exposed to solar radiation. But the design is based on the assumption of no solar loads would be placed on the radiator, if illumination occurred near earth, the operating units would exceed the design temperature for them. The magnitude of this excess would be a function of the angle of incidence and of the actual distance from the sun If the trajectory makes radiator illumination likely, the radiator would need to be resized As the vehicle gets further from the sun, it will become more tolerant of solar loads because the solar array will be cooler and the IR backloading lower As long as the total of absorbed solar load and solar array backloading remains less than or equal to the latter at 1 AU, adequate temperature control will be maintained.

Based on the environmental and operational parameters described above, we performed a radiator optimization study. Figure 44 shows the parameters involved in the analysis The results of this study are presented in Figures 45, 46, and 47.

Figure 45 correlates radiator width w with heat-pipe spacing L_s The curve is based on a radiator thickness of 0 5 mm (0 020 in), which is the minimum thickness consistent with adequate structural characteristics Structurally, the lightest system is attained when the radiator width is maximum The width of the thrust module, 0 81 m, is the maximum radiator width attainable with this design As shown in the figure, two designs are available to provide the desired radiator performance 20 3 cm (8 in.) spacing with four heat pipes or 26.7 cm (10 7 in) spacing with three heat pipes The discontinuities represent changes in the number of heat pipes.

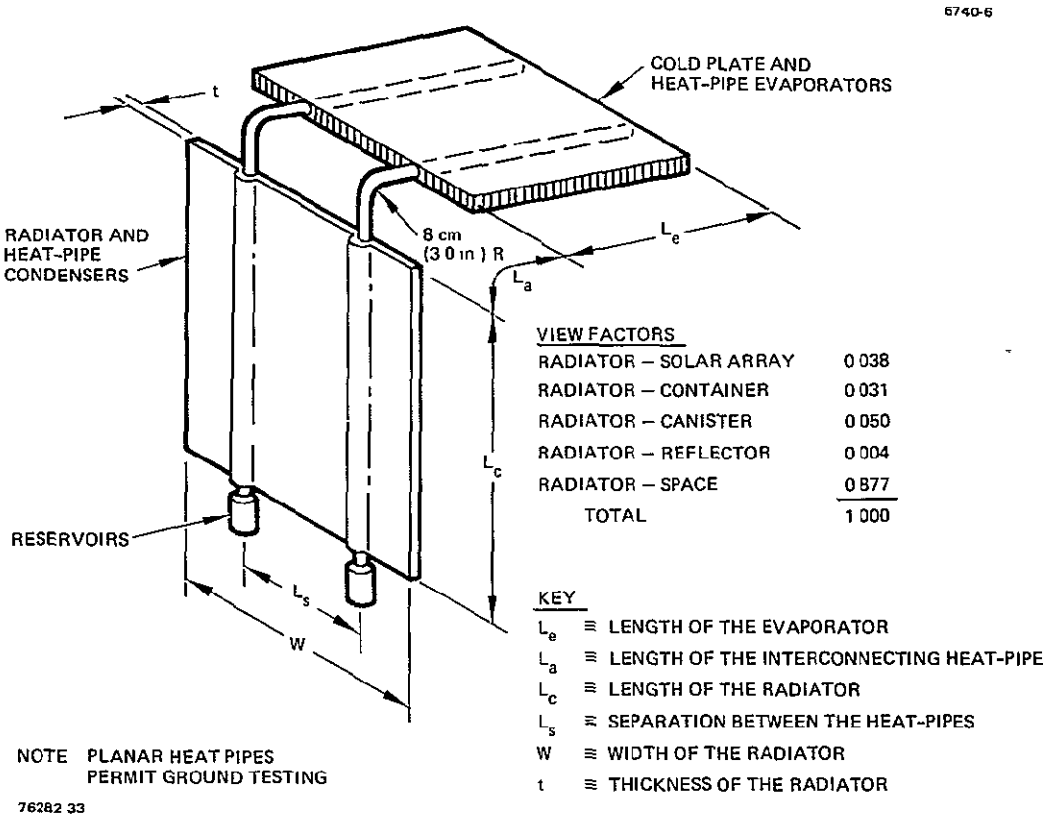

Figure 44. Heat pipe-radiator optimization of the parameters.

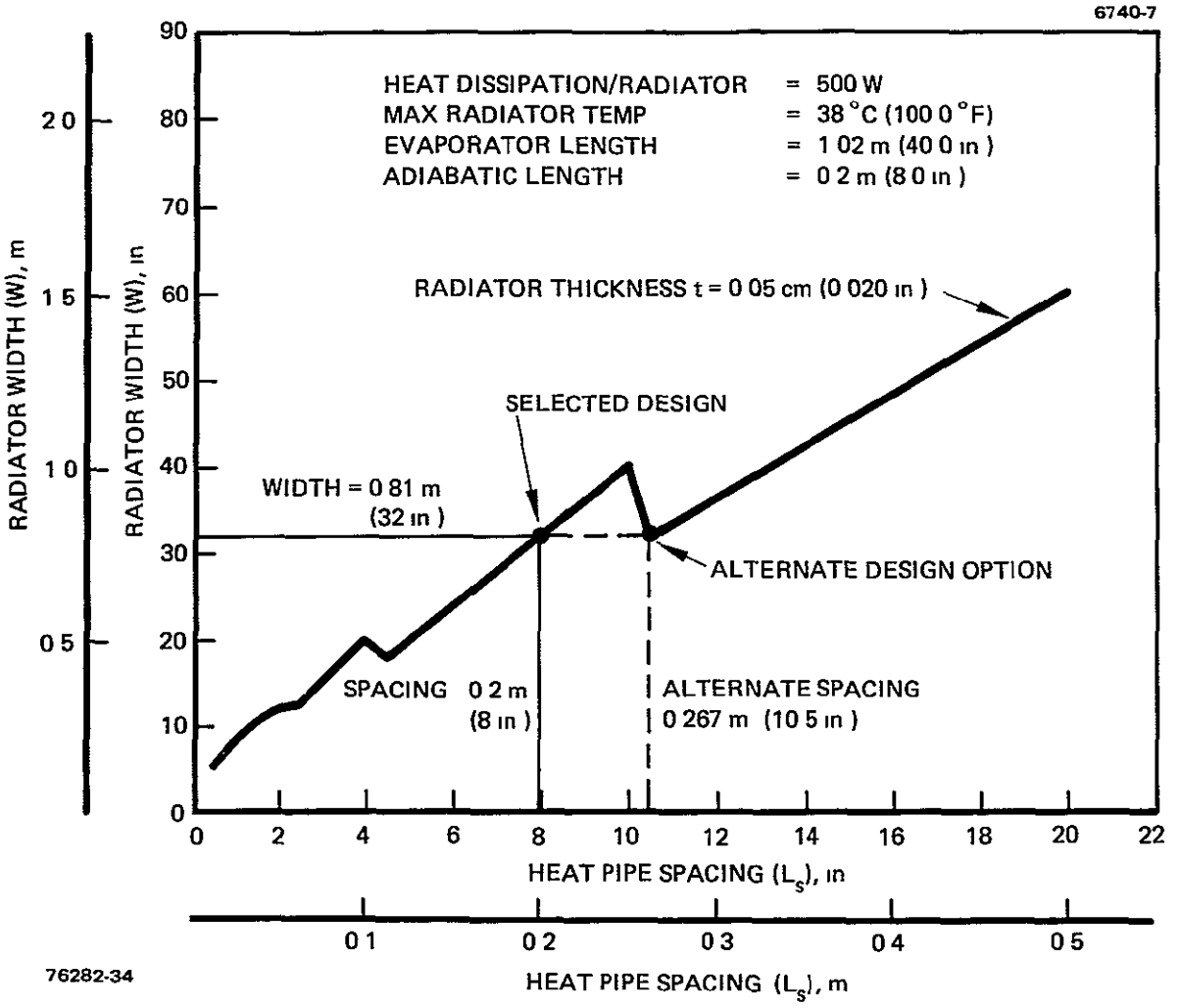

Figure 45. Width of the thermal radiator versus heat pipe spacing.

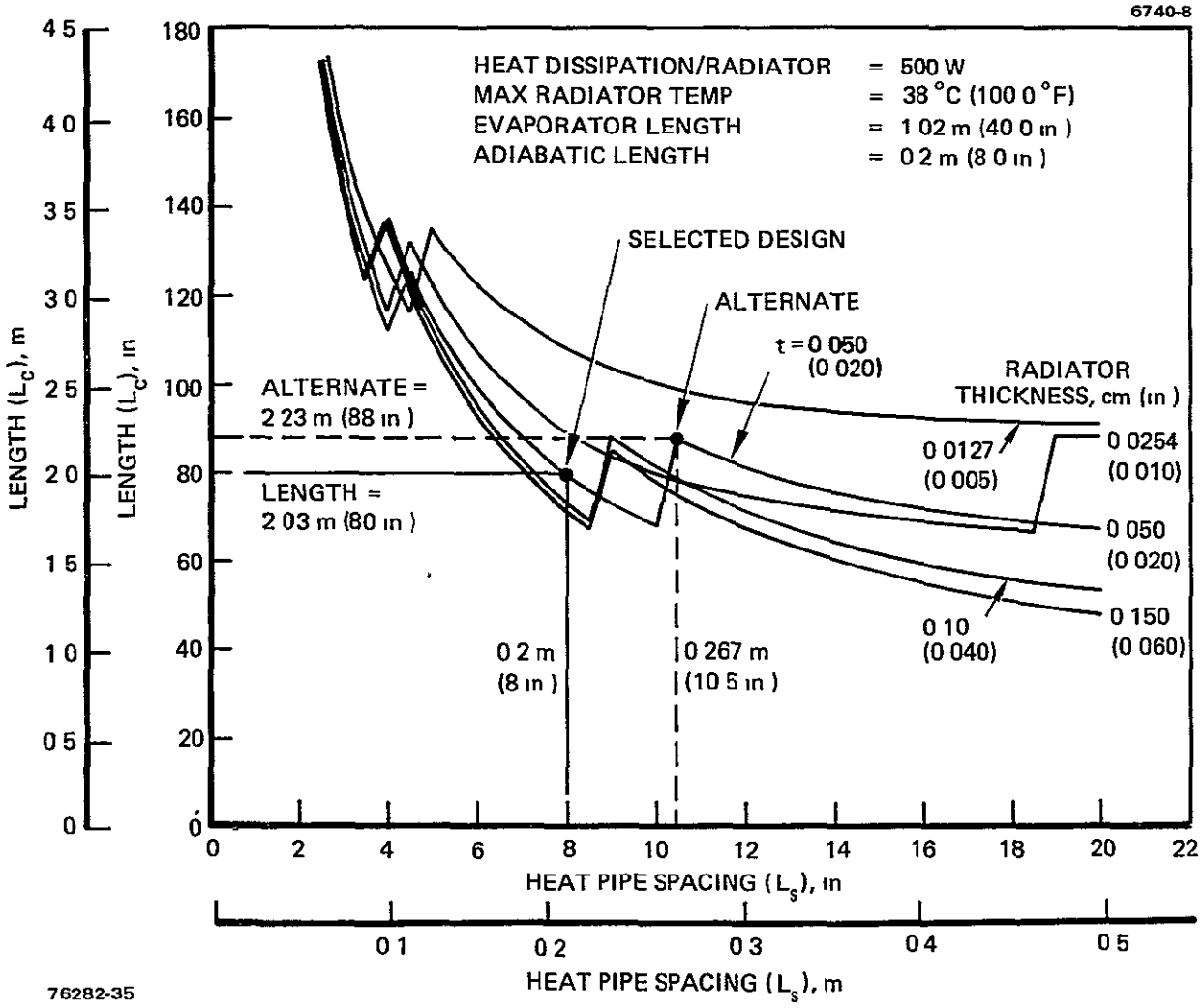

Figure 46. Condenser/radiator length versus heat pipe spacing.

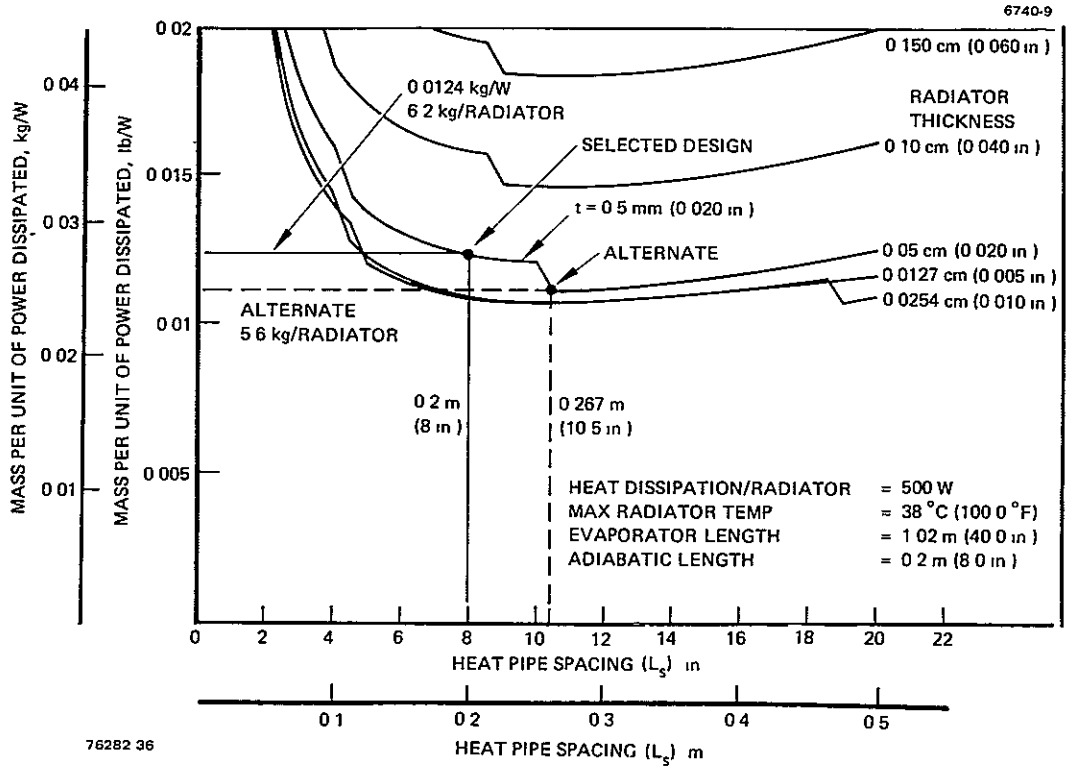

Figure 47. Radiator/heat pipe mass per watt dissipation versus heat pipe spacing.

Figure 46 shows the length of the heat-pipe condenser (or radiator length) as a function of heat-pipe spacing with radiator thickness as a parameter The required radiator lengths for each of the candidate designs are shown to be 2.23 m and 2.03 m for the 26.7 cm (10.5 in) and 20 3 cm (8 in) spacings, respectively A longer radiator is needed for wider spacing because the fin is less efficient

Figure 47 shows the normalized system mass (total heat pipe and radiator per unit of heat dissipation by the radiator as a function of heat pipe spacing. Table 21 summarizes the significant parameters for each of the candidate designs. Selection of Option 1 was based on the margin between the heat transport required and the capability of the heat pipes Assuming uniform heat distribution (all pipes transport equal loads), Option 2 requires operation that is essentially at the limit of transport capability for this type of heat pipe (305 W-m, or 12,000 W-in.) The selected design has a shorter radiator; this allows more potential for an increase in radiator if necessary and is slightly heavier

At this point, the assumption of uniform heat dissipation on the cold plate was dropped. Using the power dissipation distribution of the PMaC beam supply, the design was modified (heat pipe spacing) to accommodate the actual, nonuniform heat distribution The final design for the radiator and cold plate is presented in Section 2 D.3.

Two candidate approaches were considered for insulating the thrust modules (1) enclosing all of the thrust modules within a common blanket and (2) using individual blankets for each module. The first approach does provide a weight advantage. But since it would be impractical from an assembly and installation standpoint, the second approach was selected. In addition, the second approach is consistent with the modular concept for the thrust system The interface module will be enclosed by an MLI blanket The size and geometry of these blankets will make an effective emittance of 0.025 readily attainable

Subsystem thermal finish and heater requirements were established from computer analysis of a bulk model of the thrust system Heaters were sized to maintain subsystem temperatures above the minimum

Table 21. Radiator Design Alternatives — Heat Pipe Spacing Options

Design Parameter	Option 1 (Selected Baseline)	Option 2
Heat pipe spacing, cm (in)	20 3 (8)	26.7 (10.5)
Radiator length, m (in.)	2.0 (78.7)	2 2 (86 6)
Radiator width, m (in)	0.81 (32)	0 81 (32)
Radiator thickness, mm (in.)	0.5 (0 02)	0.5 (0.02)
No of heat pipes	4	3
Weight per radiator, kg	6.2	5.6
Weight of 10 radiators, kg	62	56
Effective length of heat pipe, m (in.)	1.71 (67 4)	1 82 (71 8)
Average heat load per heat pipe, W	125	167
Average transport requirement, W-m (W-in.)	216 (8,425)	305 (11,990)

allowable design temperatures. The analytical model was also used to verify the adequacy of the cold-plate/radiator design and the MLI blanket under both the extreme hot and cold cases.

c. Number of Propellant Tanks

A dual-tank system was selected for the baseline through a brief tradeoff analysis. The results of the study comparing the one- and two-tank alternative are summarized in Table 22. The mass of one large tank would be 0.4 kg more than the combined mass of two smaller tanks. Placing the large tank in the center of the interface module truss members adds 1 5 kg. The local structure for supporting the two small tanks is 0.2 kg heavier than the large tank local support structure. There is a negligible mass gain involved in increasing the large tank pressure by 55 kPa (8 psi) to provide the same pressure as does the small tank. A summary of the estimated mass differences indicates that the two-tank system provides a net mass savings of 0.9 kg over the one tank system.

The cost of development is about the same because both tank systems have approximately the same size. Cost of six smaller tanks may

Table 22. Comparison of the Single- and Dual-Tank Propulsion Systems

Tradeoff	Dual-Tank System (Baseline)	Single-Tank System
Mass of tank(s)	+2.4%	-
Number of tanks to be developed.	6	4
Tank diameter, m	0 61	0 99
Cost of development	Same	Same
Manufacturing difficulty	Same	Same
Unbalance potential (with respect to the center of mass)	Yes	No
Reliability (single-point failures)	-	Better
Accessibility	Better	-
Flexibility (tank center of mass and cross shaft axial location)	Better	-
Vibration	Stiffer	-
Pressure, kPa (psi)	311 (45)	366 (53)
Mass comparisons		
Tanks, kg	+0.4	-
Local support structure, kg	+0 2	-
Interface module truss structure, kg	-	+1.5
Additional N_2 (pressure increase), kg	-	Negligible
Total	+0 6	+1 5
Net mass difference, kg	-	+0.9

5903

be greater than the cost of four larger tanks. Both tanks are within the state of the art and can be readily manufactured

The two-tank system, located in thrust module bays two and four, is easier to assemble and more accessible after integration because neither tank is obscured by the solar array boom The smaller tanks can be moved further fore or aft for a more favorable center-of-mass location, and there is the flexibility to move the solar array cross-shaft fore or aft in the unoccupied center bay With respect to vibration, two small tanks are better than one large one because smaller tanks are inherently stiffer

The single-tank design is somewhat more reliable because it has fewer parts, although this difference may not significantly affect overall system reliability.

d. Selection of Materials

Selection of materials was governed by considerations of mass, thermal and load requirements, and ease of manufacture. Results of the analysis conducted during this preliminary study are presented in Table 23. This analysis is considered sufficient to provide the basis for structural sizing and for estimating program costs, but further analysis during the development phase will be required.

Wherever possible, aluminum is used as the basic structural material because it is inexpensive, readily available, and possesses good mechanical properties. However, the truss tubes in the interface module and adapter are attractive candidates for weight savings because they serve single load paths and are simple to assemble in bonded socket joints The prime failure mode of the tubes is column buckling, therefore, stiffness is an important design parameter Therefore, graphite/epoxy and beryllium, materials which have high specific moduli were considered for the truss tubes. Figure 48 compares the specific strengths and moduli of candidate and other materials Table 23 also shows that the strength of both materials compares favorably with that of aluminum. Although the density of the graphite/epoxy material

Table 23 Structural Materials

Structural Element	Material	Selection Consideration
Interface truss		
Lower frame	Aluminum	Strength and manufacturability (forming)
Fittings	Aluminum	Strength and machinability
Tubes	Beryllium	Low mass and high stiffness
Tanks	Stainless steel	Per NASA/LeRC specification
Thrust modules		
Cold plate honeycomb core and face sheets	Aluminum	High thermal conductivity
Radiators	Aluminum	High thermal conductivity
Heat pipes	Stainless steel	Proven CTS design
Truss tubes	Titanium	Strength and low thermal conductivity
Fittings	Aluminum	Strength and machinability
Adapter		
Tubes	Beryllium	Low mass and high stiffness
Beams	Beryllium	Low mass and high stiffness
Fittings	Aluminum	Strength and machinability

5903

is higher, the mass of the finished tube is predicted to be at least equal to that of the beryllium tube Graphite/epoxy material is designed and fabricated by a thermoset process, it requires additional plies for shear and torsional stiffness, while beryllium is homogeneous and isotropic with good omnidirectional mechanical properties.

The thickness needed for the beryllium tubes will not be accurately determined during the definition phase of the design effort But extra-thick tubes can be ordered before this and then chem-milled to

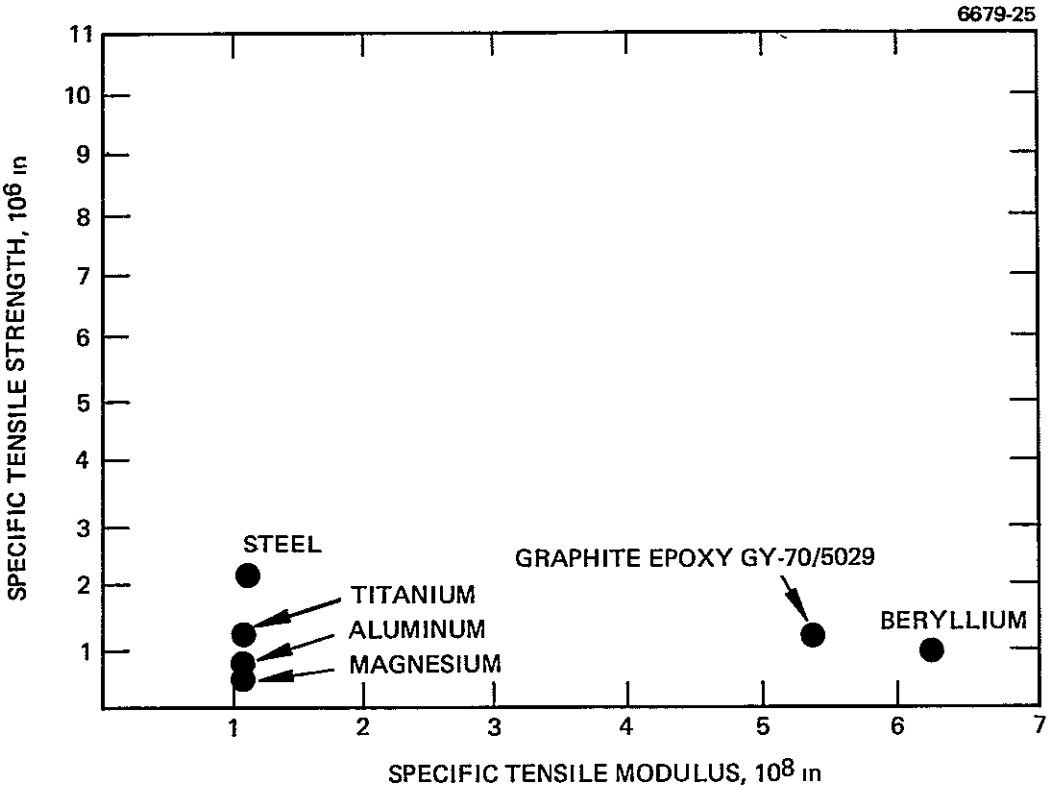

Figure 48. Specific tensile strength versus specific tensile modulus.

dimensions based on final loads On the other hand, graphite/epoxy tubes have to be fabricated to a definite thickness and have a lower tolerance on thickness because of the unique orientation of its plies. The extruded beryllium tube can be fabricated with less eccentricity, which is an important stability factor.

After considering the above tradeoff factors, beryllium, although costlier, was selected as the baseline material for the truss tubes because it is predicted to be lighter and provide less risk to the program schedules

To use beryllium in this design, in which the loads are limited to compression and/or tension, would require little additional development. The maximum longitudinal strength is obtained from extrusions. The major factors affecting physical properties are grain size, orientation, and purity (particularly with respect to oxygen, silicon, iron, and aluminum) Strength, ductility, and resistance to crack propagation are highest when the grain size is fine ($\leq$ 10 μm) and uniform

Disadvantages of using beryllium are procurement time, cost, and toxicity. The latter disadvantage can be easily overcome by closer coordination between engineering and manufacturing and by equipping manufacturing facilities with filtered venting systems for chemical milling operations and a standard portable filtering vacuum system for machining and grinding operations.

The cold plate thickness was established by the selection of the 1 27-cm (0.5 in) diameter heat pipes For efficient heat transfer, the heat pipes must contact both face sheets of the sandwich structure. Honeycomb core was selected as the filler because of its low density and high bi-direction shear strength The heat pipes are embedded in the core between the aluminum face sheets

3. Description of the Structural and Thermal Control Designs for the Baseline Thrust System

a Thrust System Structure

An isometric of the thrust system with the solar array in the stowed position is shown in Figure 49 to provide the reference for the discussion of the structural design. The structure is comprised of an interface module, five thrust modules, and an adapter which connects the thrust system structure to the IUS interface ring A shuttle cradle, not shown in Figure 49, supports the cantilevered thrust system with its mission module payload attached to the interface module; the cradle attaches to the thrust system at the separation plane between the interface module and the mission module

The structural configuration is designed to make efficient use of the available volume, to provide a direct load path to the IUS, and to provide a protective environment for the various subsystems. The structure accommodates the stowed solar array; its members have been designed to withstand the expected load environments discussed in Section 2 D 2. The design minimizes injected thrust system mass, and features relatively easy assembly and good accessibility. Although further design effort will be needed during the development phase (including load definition based on coupled load analyses), the design is believed to be near optimal with respect to the specifications.

The thrust system layout is presented in Figure 50 Figures 49 and 50 provide the basis for the discussion which follows of the interface module, thrust module, and adapter designs. Although explicit design of the shuttle support cradle is excluded because it is not considered within the scope of this study, this is not expected to present any significant problems.

b. Interface Module

The interface module shown in Figure 51 is a spatial truss structure, its functions are to· (1) provide an interface between the mission module and the IUS through the adapter, (2) support the thrust

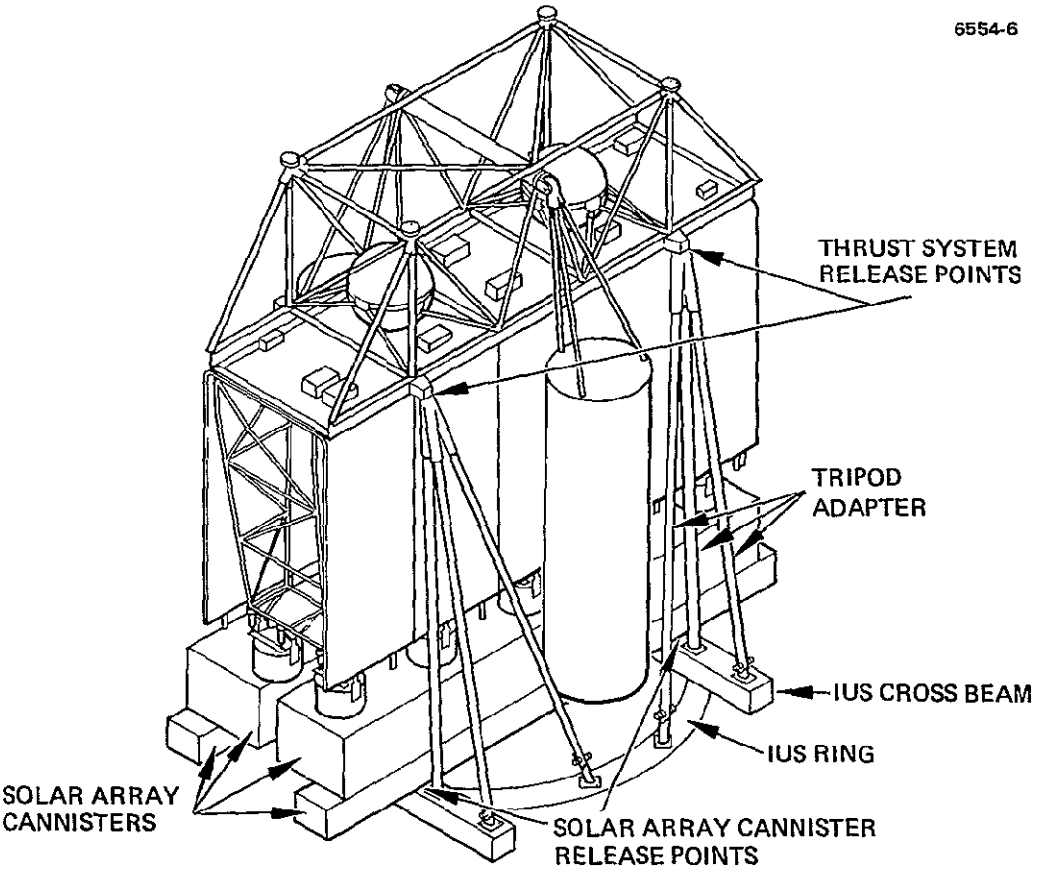

(a) Stowed configuration

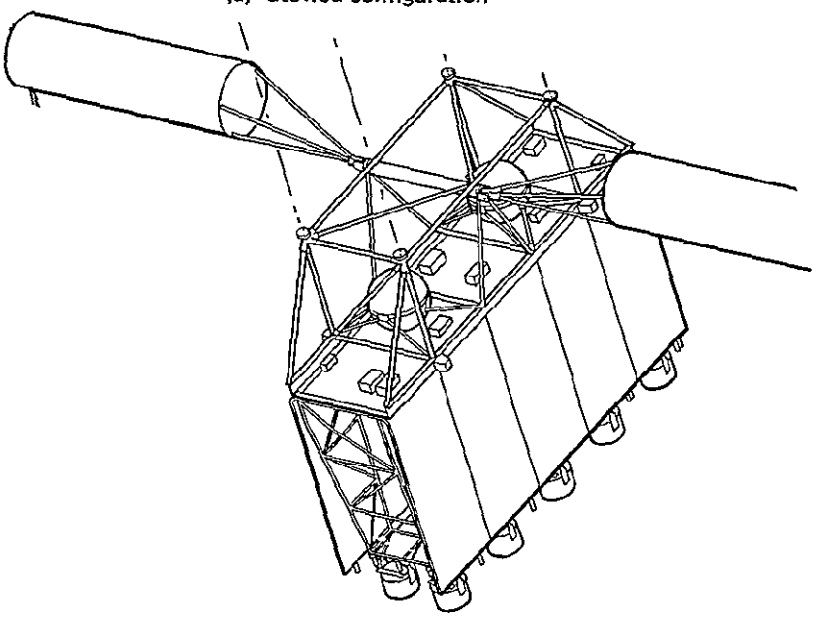

(b) Flight configuration

Figure 49. Thrust system isometric.

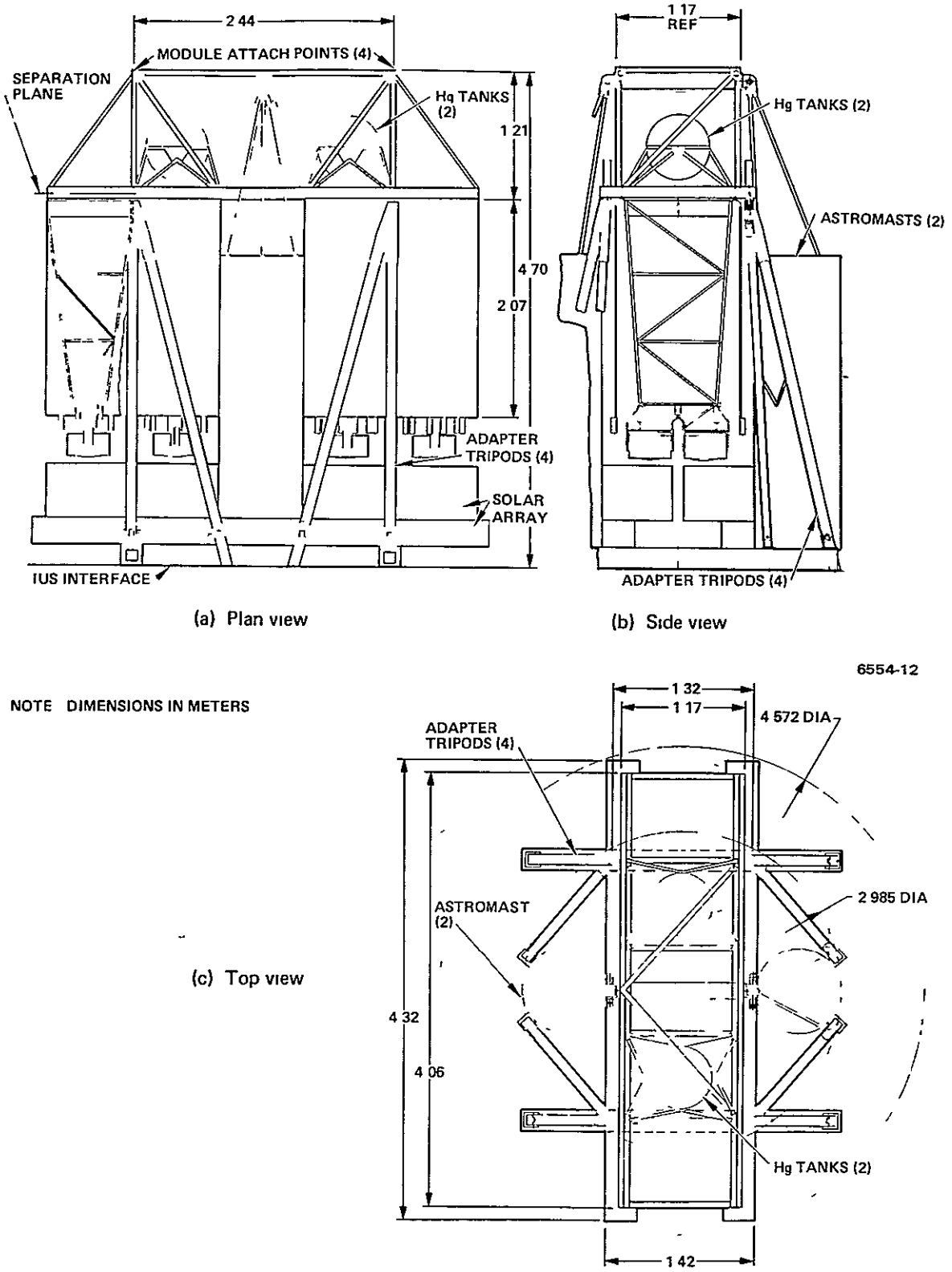

Figure 50 Thrust system layout.

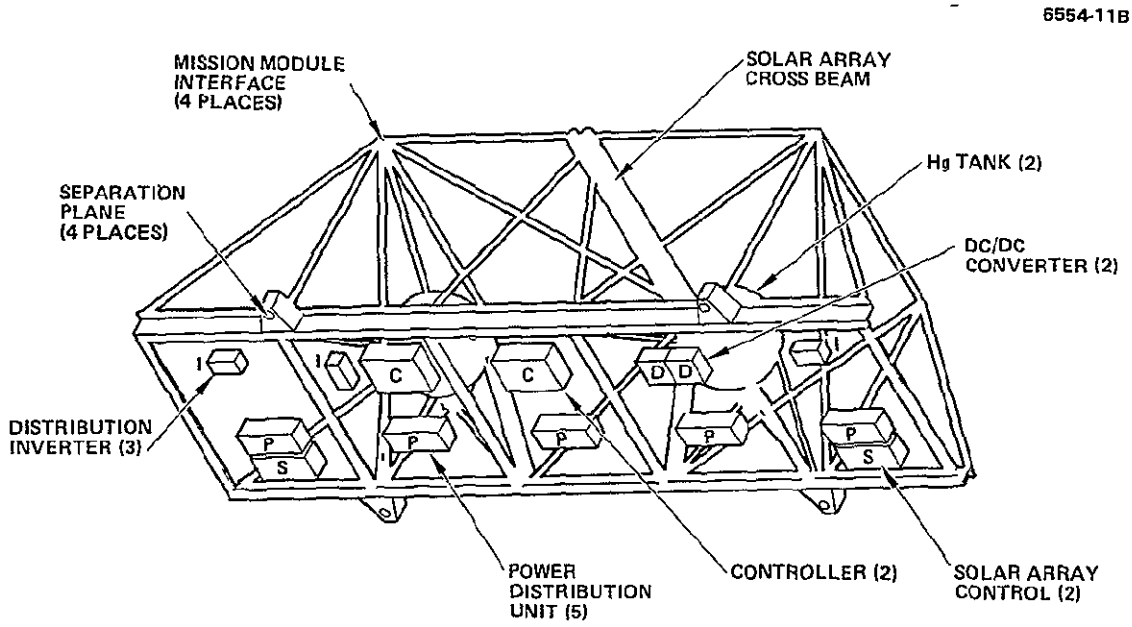

Figure 51. Design of the interface module.

modules, (3) house the mercury propellant tanks, (4) support the solar array system, and (5) provide a separation interface with the adapter The interface module occupies a volume bounded by approximately 1 1 x 1 1 x 4 1 m. The lower structure consists of (1) two extruded aluminum Z-members that are the lower chords of the truss and (2) six extruded aluminum transverse T-members that divide the lower truss into five framed bays to which the five thrust modules attach at the perimeter of the cold plates The combination of Z-chord members and cold-plate shear webs form a stiff and strong lower truss beam that is capable of carrying the required in-plane loads to the adapter The propellant tanks are each supported in bays 2 and 4 by four bipods The tank supports provide the necessary omnidirectional stiffness and detune the large masses from the IUS/shuttle structural frequencies Transverse extension fittings on both sides of bays 2 and 4 provide the separation interfaces.

The separation planes between the interface module and the adapter (as shown in Figure 52) contain four conical seats: separation bolts, electro-explosive nuts, separation bolt catchers, and push-off springs. After the electro-explosive separation nuts are fired, the bolts eject and are captured by bolt catchers mounted in the tripod end fittings

The interface module PMaC units are distributed in the five thrust module bays so as to provide approximately equal mass distribution and heat dissipation. The PMaC units are mounted on the forward side of the cold plates after the thrust modules have been assembled with the interface module. A common mounting hole pattern is provided on the cold plate to allow for full thrust module interchangeability.

c. Thrust Modules

Each thrust module shown in Figure 53 is comprised of a horizontal cold plate, a spatial thruster/gimbal support truss, two vertical 0 5 mm (0 020 in.) thick aluminum radiator panels, and eight L-shaped heat pipes (The heat pipe design is described later.) All eight legs are embedded in the common cold plate; four of the eight legs are

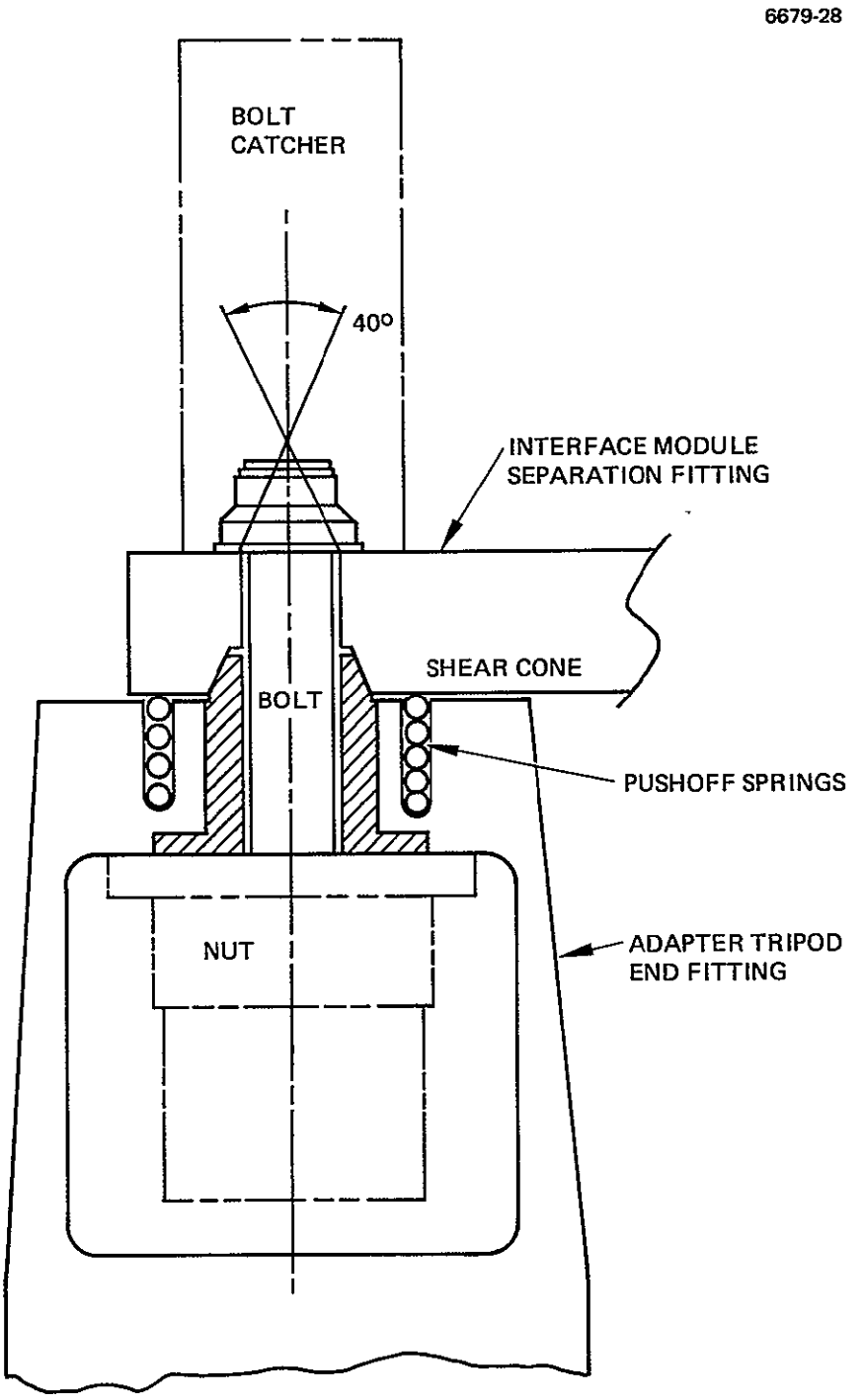

Figure 52. Separation plane.

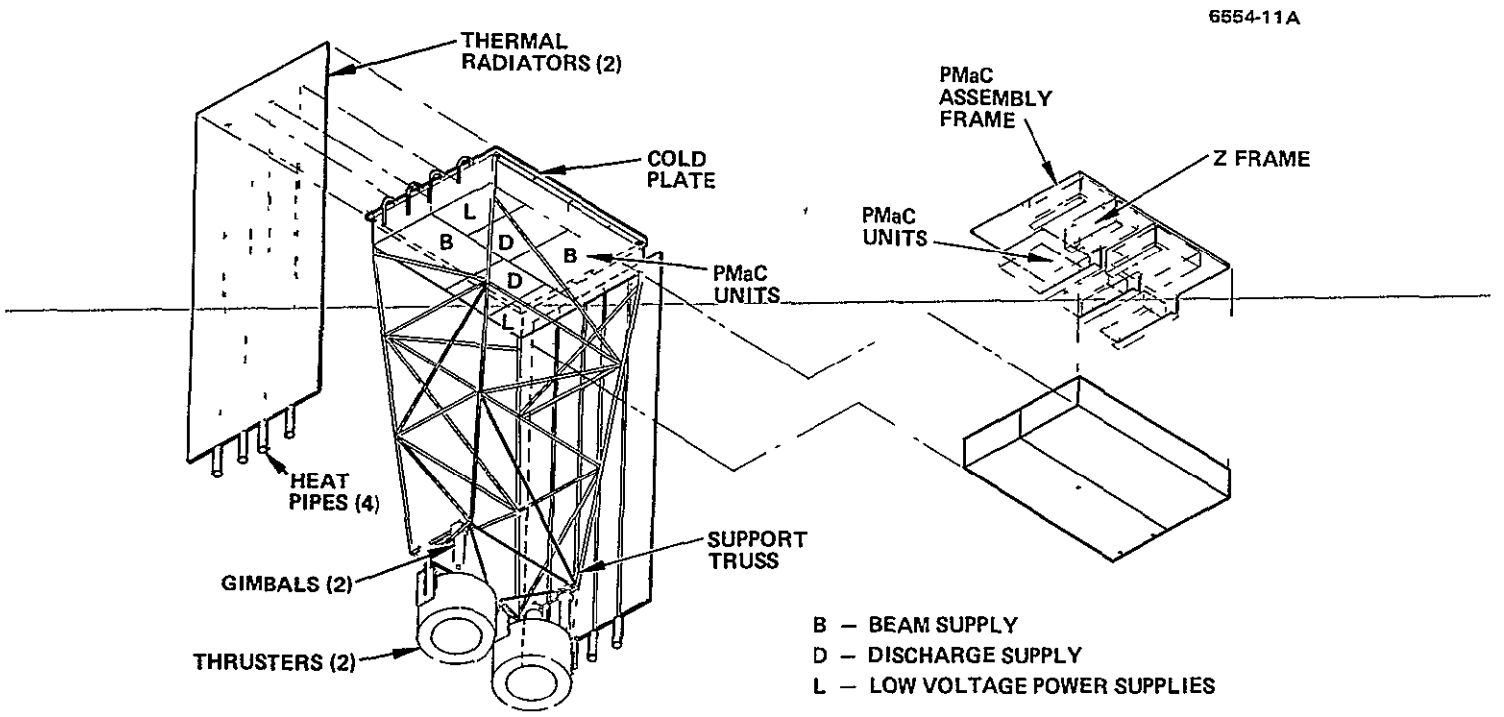

Figure 53. Thrust module design.

embedded in each radiator. The cold plate dimensions are 81.3 cm x 106 7 cm (32 x 42 in.), the minimum required to accommodate the specified dimensions of the modular PMaC package. The PMaC package is joined to the cold plate by screws that fasten to inserts potted into the aluminum honeycomb core with a foam-type epoxy. Similar inserts are used on the other side of the cold plate for mounting the interface PMaC units. The upper facesheet of the cold plate is a 0.5 mm (0 020 in) thick 6061-T6 aluminum sheet, and the lower facesheet is 1.5 mm (0.060 in.) thick of the same material Both facesheets are bonded to the aluminum honeycomb core (5052-.001P, 3/16 cell) with a 0 15 mm (0 006 in.) sheet bond material.

The method for embedding the heat pipes into the core was left open pending the outcome of future development tests However, two viable alternatives are available. (1) bonding in aluminum tubes during the thermoset process followed by post-cure bonding of the heat pipes into the aluminum tubes and (2) bonding the heat pipes in the honeycomb sandwich during fabrication and curing the cold plate The former method is the simplest to assemble but results in the largest mass

The truss that bridges the gap between the cold plate and the thruster gimbals consists of titanium tubes ≈ 1.6 cm (0.625 in.) in diameter. The tubes are welded at the truss joints to reduce the mass of the fittings The truss tapers from a maximum at the cold plate to a minimum where it attaches to the thruster/gimbal assembly The environmental loads from the thruster/gimbal assemblies are carried by the cantilevered truss (through the cold plate) to the interface module structure Brackets on this truss also support the radiator panels

The radiator panels are crimped along their lengths to receive and retain the heat pipes. Even though the crimping acts as a retention spring, supplementary structural attachments, such as bonding or brazing, will provide a positive radiator/heat pipe attachment The four heat pipes also provide longitudinal stiffening and reinforcement to the radiators

d Adapter

The adapter design, shown in Figure 54, consists of four independent tripods and two IUS cross-beams. This design minimizes the injected spacecraft mass and provides a stable structure without resorting to moment-carrying joints at the separation plane. The adapter extends about 3.5 m above the IUS interface. Each tripod has a triangular footprint the sides of which are approximately 1 0 m x 0.8 m x 0 5 m. The two outboard tripod legs are connected to a machined fitting at the separation plane and are articulated outward by preloaded torsion springs located at the base hinges. The tripod inner leg has its own machined fitting, which is connected to the other two legs by the separation bolt. This leg, which does not have its own torsion spring, is pulled outward by a folded drag link connected to the outer leg. The cross-beams, which are bolted at four places to the IUS interface ring, support the adapter legs that fall outside the IUS bolt circle Using the cross-beams yields a broader moment base for the adapter, which reduces the axial loads in the tripod tubes The diagonal inboard leg of each tripod bolts directly to the IUS bolt circle. The adapter tubes are fabricated from extruded beryllium tubes, and the end fittings are machined from aluminum bars

e. Thermal Control

Figure 55 shows an overview of the thermal control subsystem. Primary thermal control of the insulated enclosures is provided by a cold-plate/VCHP/radiator assembly for each thrust module. PMaC units are mounted on both sides of the cold plate (as discussed earlier) Each thrust module is enclosed in an MLI blanket A low-conductance titanium truss supports the cold plates, gimbals, thrusters, and propellant lines within each module The exterior surfaces of the interface module are enclosed in an MLI blanket, within which are located the solar array drive mechanism and the propellant tanks The cold plates provide the interface between the thrust modules and the interface module The temperature levels within the enclosures are

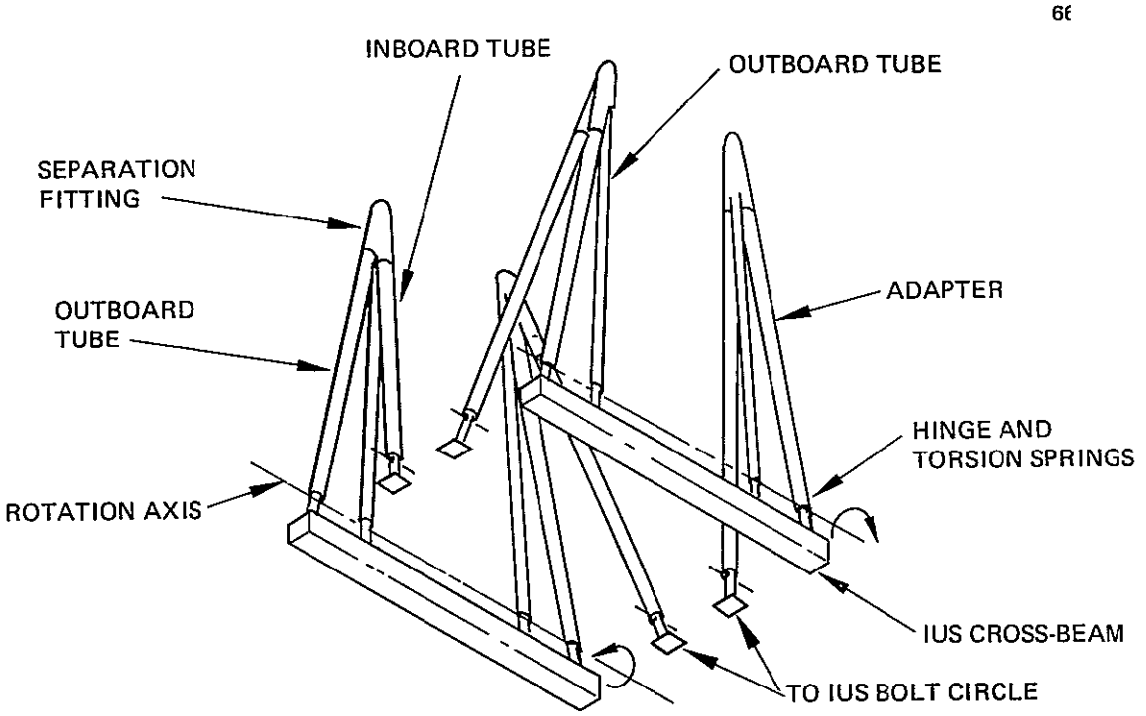

Figure 54 Adapter design for configurations 1A, 1AX, 2A, and 3A

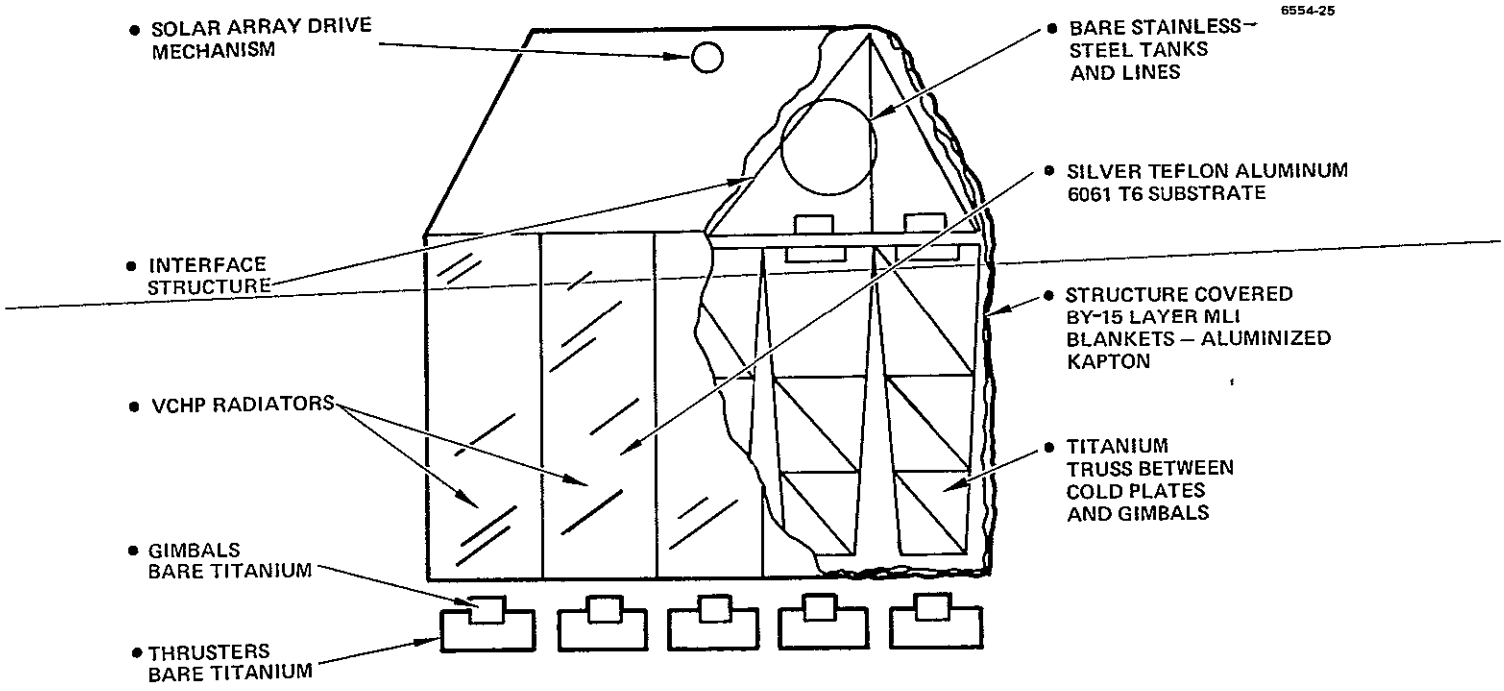

Figure 55. General description of thermal control design

established by the controlled temperature of the cold plates Heaters are provided to maintain suitable temperatures during non-operational periods

The design of the cold-plate/VCHP/radiator assembly is shown in detail in Figure 56. In addition to the mechanical attachment discussed in c, each PMaC unit is thermally bonded to the cold plates using 0 127 mm (0.005 in) of nonstructural epoxy (equivalent interface conductance equals 360 BTU/hr-ft^2-°F) to minimize interface temperature differences To minimize temperature gradients in the cold plate and to keep the maximum mounting surface temperature below 50°C, cold plate facesheet thicknesses are 1 5 mm (0 060 in) on the thrust module side and 0.5 mm (0.020 in) on the interface module side A titanium truss is used to minimize conductive coupling between the thruster/gimbal assembly and the cold plate.

A silver-teflon finish provides a high-emittance (ε = 0.78) radiator surface. The VCHP spacing is based on nonuniform dissipation in the beam supply The heat pipes are planar to facilitate ground testing the thrust modules (i.e , in a 1 G environment). Table 24 summarizes the design parameters and characteristics of the VCHP/radiator assembly The table shows the variation in heat load and transport requirements for the VCHPs Actual transport requirements are between 203 and 269 W-m (8,000 and 10,600 W-in.) These levels are sufficiently below the 305 W-m (12,000 W-in.) projected transport capability of the CTS-type heat pipe

The MLI blanket consists of 15 layers of Al-Kapton; it will provide a maximum effective emittance of 0 025 Except for the radiator, the nature of the design does not impose any thermal finish requirements on any of the subsystems.

At the "cold" design limit, internal dissipations and solar irradiations are at their minimum This causes the VCHPs to shut off with only a 1 W heat leak per pipe and makes it necessary to provide heater power to the various subsystems to maintain their temperatures above the minimum design temperatures. The maximum heater power required for each subsystem at the "cold" case is listed in Table 25.

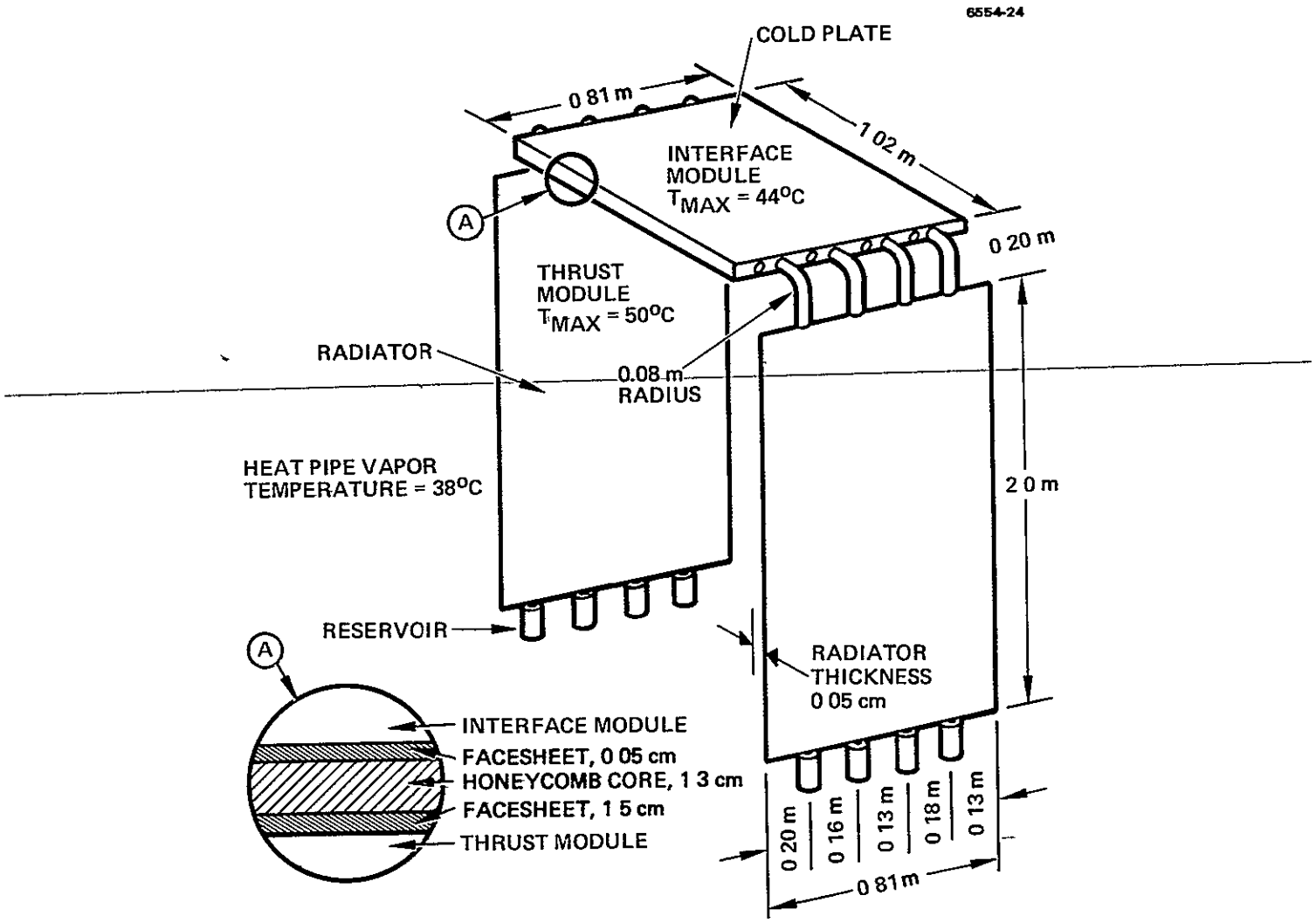

Figure 56. Radiator/ VCHP design description.

Table 24 Radiator/VCHP Design Parameters

Radiator width	0.81 m (32 in.)
Radiator thickness	0 5 mm (0.020 in)
Average heat pipe spacing	0 2 m (8 in)
Radiator length	2 0 m (79 4 in)
No of heat pipes	4
Effective length of heat pipe	1 71 m (67 4 in)
Average load per heat pipe (actual load range 119 to 157 W)	125 W
Average transport requirement[a]	214 W-m (8425 W-in)
Weight per radiator	6 2 kg
Total weight, 10 radiators	62 kg

[a]Actual transport requirement 204 W-m to 269 W-m (8,020 W-in to 10,600 W-in.)

5903

Table 25. Heater Requirements

Subsystem or Unit	Maximum Heater Power Required, W[a]	Comments
PMaC	12 (per module)	Required to maintain T > -30°C with all units off
Propellant tanks	2 (each)	
Propellant lines	5 (total)	Variable during mission
Solar array drive	6 (total)	Variable during mission
Thrusters	6 (each)	Power to existing thruster heaters produced by low-voltage supplies (100 W capability per thruster)
Gimbals	3 (each)	Required only when both module thrusters are off

[a]Worst case condition, i.e., all unit power off.
NOTE: All heaters could be on continuously without exceeding upper temperature limits.

5903

Propellant-line, thruster, and gimbal heater power is required if both thrusters in a module are off, the need for solar array drive and propellant tank heater power depends on which thrust modules are on If necessary, all heaters could be left on during the entire mission without the upper temperature limits being exceeded.

Predicted subsystem temperature ranges for the thrust system are given in Table 26. All are within the required design limits. These predictions were obtained from a system bulk thermal analysis.

A detailed thermal analysis was conducted for the PMaC subsystem for the "hot" design case The predicted maximum unit temperatures and the assumptions made in the analysis are shown in Table 27. As indicated, all units except the beam supply were assumed to have uniformly distributed dissipation

The beam supply was then analyzed in detail to verify that the components of the beam supply can be maintained at or below 50°C The analysis was based on the information available on the component layout and power dissipation of an existing 3 kW beam supply design provided in NASA LeRC drawing CF637300. We consider this reasonable because to a first approximation a 6-kW beam supply is achieved by doubling the number of components and the baseplate area of the 3 kW unit Conservative one-dimensional calculations were used in the analysis to calculate the maximum temperatures in all but the largest dissipation components. These large dissipators, the transformer and SCRs, were modeled using two-dimensional finite-difference models of the baseplate region local to the component. Results of the beam supply analysis, presented in Table 28, show that all dissipating components of the beam supply have maximum mounting temperatures at or below 50°C From this we conclude that all other nondissipating components will have maximum temperatures at or below 50°C

f Mercury Propellant Storage and Distribution Subsystem

The propellant storage and distribution system (shown schematically in Figure 57) consists of two stainless-steel mercury storage tanks, stainless-steel feed lines, nitrogen and mercury feed

Table 26 Predicted Thermal Performance at the System Level

Unit or Subsystem	Maximum Temperature, °C[a]		Minimum Temperature, °C[b]	
	Predicted	Allowable	Predicted	Allowable
PMaC	49	50	-21	-30
Propellant tanks	36	150	-31	-40
Propellant lines	45	150	-15	-40
Solar array drive	47	60	-20	-30
Thrusters	254	300	-68	-100
Gimbals	112	125	-57	-65
Structure	65	200	-43	-185

[a]All thrusters on, at 1 AU

[b]All thrusters off, at 4 5 AU

5903

valves, a distribution manifold, solenoid latching valves, field joints, flexible gimbal lines, and tank temperature and pressure transducers. The storage tank selected uses a nitrogen gas expulsion technique to supply propellant to the thruster This design is based on the approach employed for the SERT II spacecraft, but the shape of the bladder support liner has been modified so that only the required volume of mercury is supported by the liner. This bladder support technique minimizes slosh effects during launch. An operating pressure of 310 kPa (45 psi) for a full tank, with 104 kPa (15 psi) at depletion is compatible with thruster propellant interface requirements. Field joints are used to simplify the assembly and disassembly of the system The latching valves isolate the mercury propellant from the thruster vaporizers during launch

Table 27 Summary Results of Thermal Analysis

Unit or Subsystem	Unit Power Dissipation, W	Predicted Maximum Temperature, ^{o}C
Thrust module		
Beam supply	390	50
Discharge supply	52	44
Low-voltage supplies	26	45
Interface module		
Power distribution unit	66	44
Distribution inverter	30	44
DC/DC converter	73	46
Control module	15	40
Solar array drive	0	38

Analytical assumptions

Unit baseplates same material as cold-plate facesheet. Aluminum 6061-T6 (K = 97 BTU/hr-ft-^{o}C) 1 mm (0 040 in.) thick

All units bonded to cold plates using 0 127 mm (0.0005 in.) non-structural RTV.

Heat pipe vapor temperature = 38^{o}C.

Conduction through honeycomb core neglected (conservative).

Radiation effects neglected (conservative).

Uniform dissipation assumed over unit footprint area for all units except beam power supply

5903

Table 28. Summary of Beam Power Supply Thermal Analysis

Component	Dissipation, mW	Maximum Baseplate Temperature, °C
SCR1[a]	23,900	47[b]
SCR2	23,900	47[b]
L1	7,000	46
L2	7,000	46
R1	2,500	46
R2	2,500	46
R3	213	40
R4	213	40
R5	213	40
R6	2,860	43
R7	2,860	39
R8	2,860	41
R9	121	38
R13	100	38
R17	50	38
C3	1,000	44
C4	1,000	39
C5	333	38
C6	333	39
C7	333	39
C8	333	39
C9	333	39
C10	333	38
C11	1,000	49
C12	1,000	49
T6	26,000	49
CR5-CR16	7,200	46
A3A4A	2,692	47
A3A4B	2,371	47
A3A2	1,492	50
A3A3	1,885	39
A3A5	3,046	47
A3A6	339	39

[a]Nomenclature and dissipations per NASA LeRC drawing CF637300

[b]Obtained with computer model of local baseplate

5903

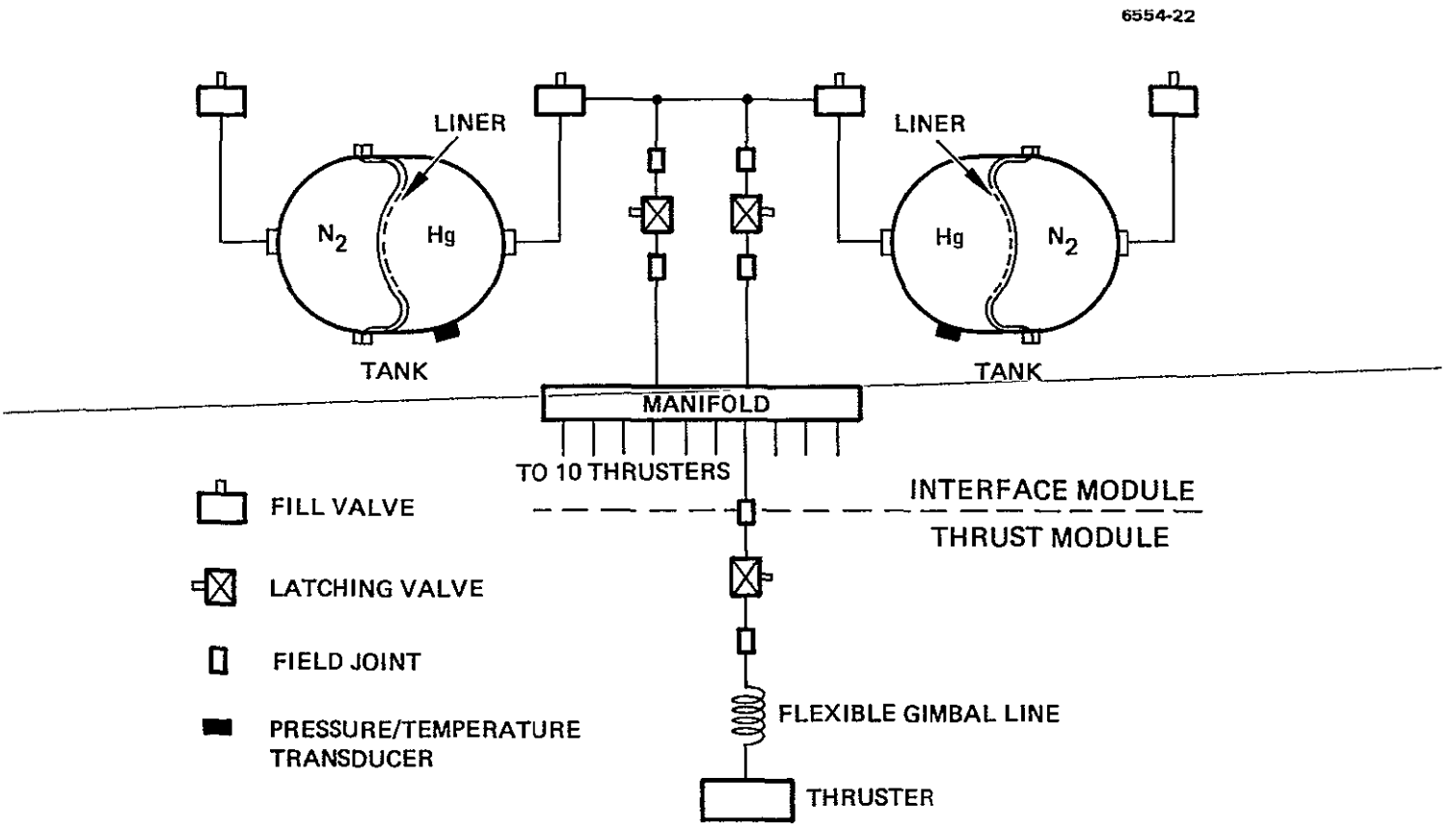

Figure 57. Schematic of the propellant storage and distribution system.

g. Solar Array Drive System

A solar array drive system, consisting of two solar array drive mechanisms and the corresponding electronics, is used to rotate the spacecraft solar arrays during the mission. The solar array drive has a bi-directional operating capability for redundancy and/or increased output The design, which is based on the solar array drive system being developed[15] for NASA LeRC, is shown in Figure 58 The required life, rotation rate, and minimum torque capability will be determined during the development phase in response to the requirements that will be generated by a more thorough mission analysis System operation must be controllable either by ground command or autonomously from the spacecraft. An extended duration test of flight configuration units is needed to determine the potential failure modes.

6 Assembly and Integration of the Thrust System

The thrust system assembly and integration sequence is illustrated in Figure 59, which shows how the thrust modules, interface module, and adapter are integrated to form the assembled configuration. The spacecraft-level assembly definition requires specification of interface information that will not be generated until the development phase of the project. The assembly and integration sequence are discussed below

a. Thrust Module

The titanium tube truss is fabricated by welding the joints together The gimbals and thrusters are assembled to the lower end of the truss structure. This assembly of the truss-structure, gimbals, and thrusters is bolted to the cold plate. The shorter segments of the eight L-shaped heat pipes are then bonded into the cold plate with the longer segments protruding on each side of the truss (four on each side). The radiators are attached and bonded to the exposed heat pipes and the radiator is supported by brackets on the truss. The next step is the installation of the PMaC module on the lower face of the cold plate. The propellant lines and wire harnesses are then added, completing the thrust module assembly

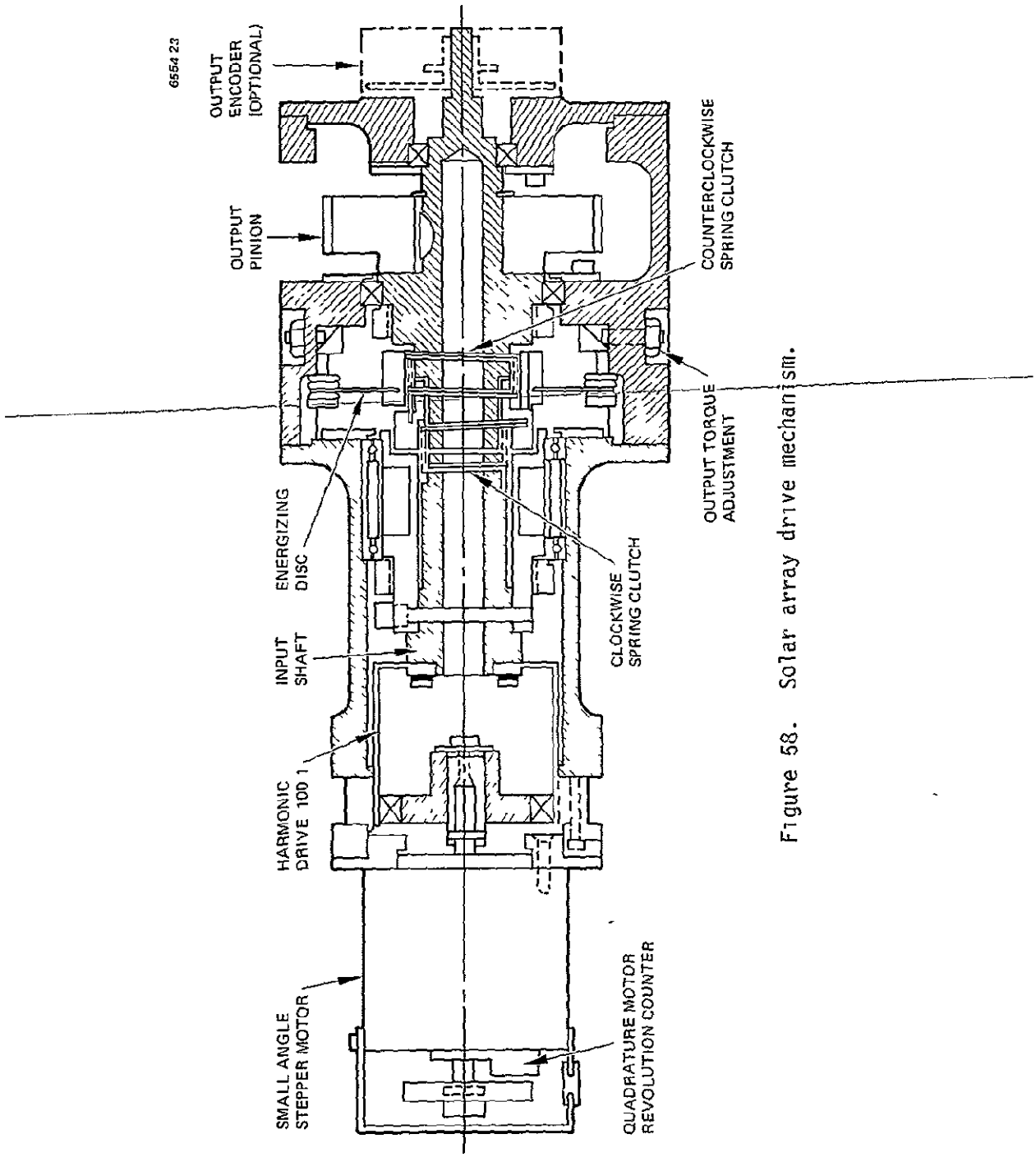

Figure 58. Solar array drive mechanism.

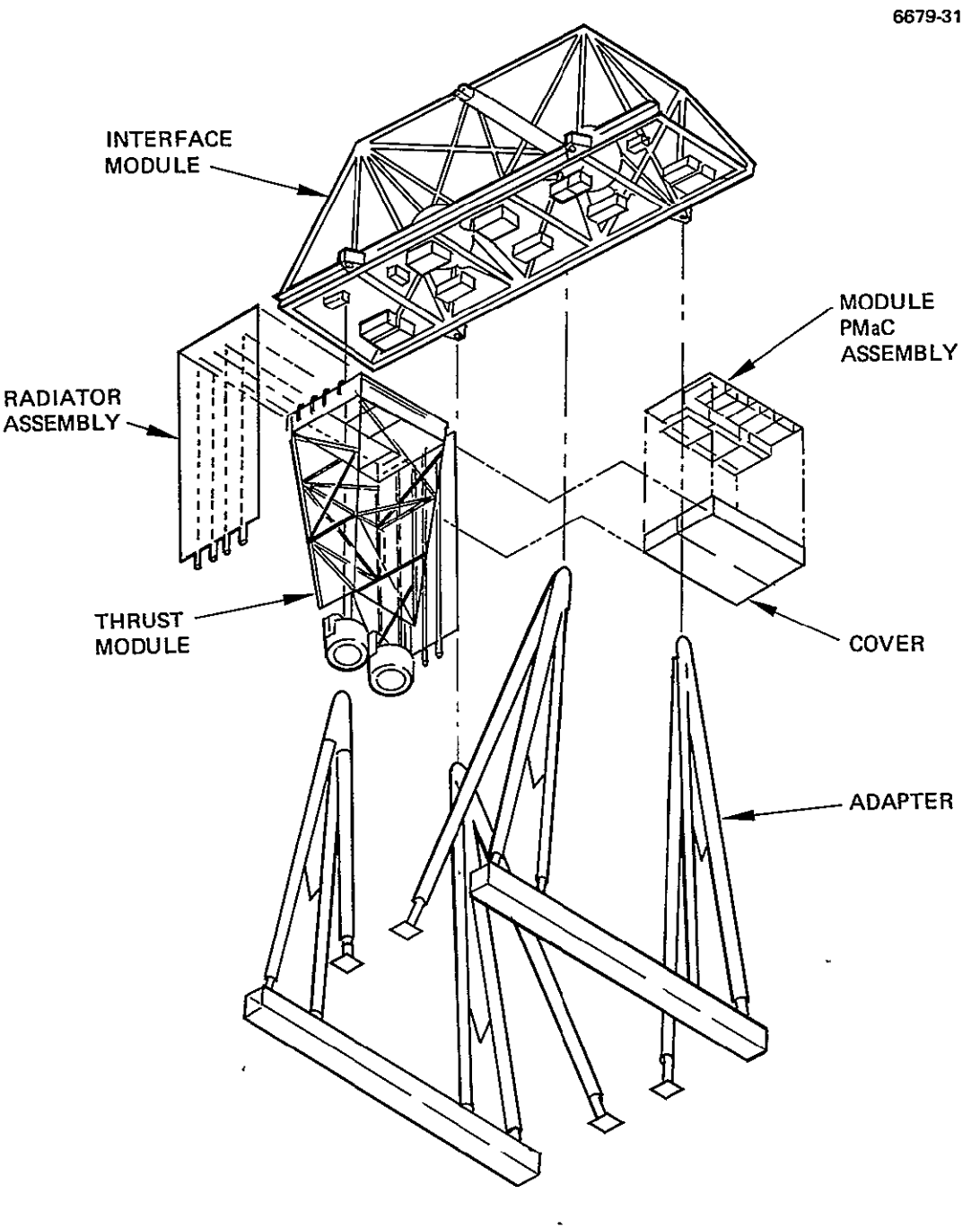

Figure 59. Assembly and integration of the thrust system.

b. Interface Module

The bottom face of the interface module truss is assembled using conventional hardware attachments The upright titanium tubes are bonded into the aluminum sockets using special fixtures to maintain the geometry within dimensional tolerances during the assembly process. The mercury tank support structure is an integral part of the truss, and the tanks are installed before the truss is completed. The cross shaft supporting the solar array drive is bolted across the center of the upper truss structure The wire harness is then installed, followed by the fill valves, lines, and latching valves of the propellant system The solar array drives are bolted to each end of the cross shaft.

c Adapter/IUS Beams

The IUS beams are fabricated from beryllium sheet metal with a square cross section, 20.3 cm (8 in) on a side Built-in bulkheads are placed at the highly loaded points. The beams are bolted directly to the bolt circle of the IUS interface ring and provide an interface for attaching 8 of the 12 adapter legs. The outboard tubes are bonded into a common aluminum socket, at the interface module attachment end. Dimensional tolerances are maintained during assembly with tooling. These tubes are hinged at the IUS attachment points with preloaded torsion spring assemblies. One tube attaches to the IUS cross-beam and the other attaches directly to the IUS interface ring The inboard leg, attached to a separate upper fitting, is hinged to the IUS cross-beam A folded drag link connects this leg to the outboard leg The inboard leg, which separates at the top to make rotation possible, is dragged along and collapses with the other tubes to provide a clear egress for separation of the spacecraft from the IUS

d. Thrust System

The thrust modules are placed in the five bays of the interface module, with 2 54 cm (1 in) of the periphery of the cold plates resting against the flanges of the lower interface module truss. Screws

passing through sleeves potted in the cold plate attach to nut plates on the interface module flanges. Interface module PMaC units are then attached to the upper cold plate faces in the five bays. The interface connectors for the electrical system are assembled, and the field joints for the propellant supplies to the thrusters are connected.

- The interface-module/thrust-module assembly is placed on the adapter, which is already bolted to the IUS and beams. Push-off springs placed in retainer fittings are compressed as the thrust system is lowered onto the four conical fittings. The electro-explosive separation nuts are installed on the adapter side, and bolts and bolt catchers are installed on the thrust module separation fittings. The bolts are torqued to a predetermined value, and the separation nut is wired into the command and power circuits.

The interface for attaching the mission module is provided on the upper plane of the interface module. The dimensional accuracy of the tie bolt pattern is maintained by using a common drill fixture. Close flatness, perpendicularity, and concentric tolerances must be maintained on all the interfaces to ensure a satisfactory fit and to prevent preloading the structure on either side of the interface. Connectors supplying power and signals across the interface are then installed.

E ANALYSIS OF THE SENSITIVITY OF THE BASELINE DESIGN TO VARIATIONS IN SPECIFICATIONS

After the baseline design had been defined, we performed a study of the effects on design characteristics and system performance of changes in the assumed design parameters and in the characteristics of the solar array. The objectives were to determine how critically the estimated performance depends on the assumed parameters and to explore possibilities for performance improvement. Table 29 lists the parameters varied and the corresponding impact on the baseline.

Table 29. Scope of Sensitivity Analysis

Variations From the Baseline	Impact on the Thrust System			
	Design Impact	Mass	Efficiency	Reliability
Power dissipation (Thermal control)	Radiator length VCHP Transport capability	Yes	—	—
Replacement of conventional beam supply with CDVM	PMaC design Thermal control	yes	yes	yes
Variation in beam supply efficiency	Thermal control	yes	yes	—
Varation in solar array maximum power	Thermal control only (Baseline thruster and PMaC design postulated)	yes	yes	—
Alternate solar array design (Stowed configuration)	Structural Thermal	yes	—	—
Reduction in number of thrusters from 10 to 8	Different thruster parameters and operation profiles Structural Thermal PMaC	yes	yes	yes
Solar array maximum capability (60 kW and 36 kW)	Different thruster parameters and operation profiles Different configurations (no of modules) Structural Thermal PMaC	yes	yes	yes

5903

1. Thermal Control Design Sensitivity to Power Dissipation

The impact of power dissipation on thermal design was examined to provide an input to the subsequent determination of thrust system mass dependence on various design parameters (power supply efficiency, variation of solar array power, etc.). Results are summarized in Figure 60, which shows the following key parameters as a function of the change in power dissipation per module relative to baseline·

- Required change in radiator length (Figure 60(a))
- Resulting change in the mass of the thermal control subsystem (Figure 60(b))
- Required (average and peak) heat transport capability of heat pipes (Figure 60(c)).

Basic relationships — radiator length and heat pipe transport requirements versus power dissipation — are plotted as families of curves with the number of heat pipes as the parameter The origin in Figure 60(a) and (b) corresponds to the baseline design· four heat pipes per radiator, 1,000 W of dissipation per module, and 2.0m radiator length Design variables are plotted over a range of ± 500 W of relative power dissipation, which corresponds to ± 50% of the baseline value.

The change in the mass of the thermal control system is shown in Figure 60(b) as a function of changes in power dissipation module. The change in mass varies along the baseline design curve (for four heat pipes) until limits imposed by consideration of component capabilities require a change in the number of heat pipes. These limits are

- Heat transport capability is limited to 30.5 kW-cm (12 kW-in); this limit can be obtained by reference to Figure 60(c).
- Radiator length is limited to 0.4m (without major configuration impact*), this limit can be obtained by reference to Figure 60(a).

*If radiator length were allowed to increase beyond 0.4m, the corresponding increase in thermal control mass in Figure 60(b) would be lower relative to the heavy line, because the four heat pipe design could be retained; however, the net increase in the mass of the configuration, resulting from the design modifications to accommodate a length increase beyond 0.4m, would overshadow this saving.

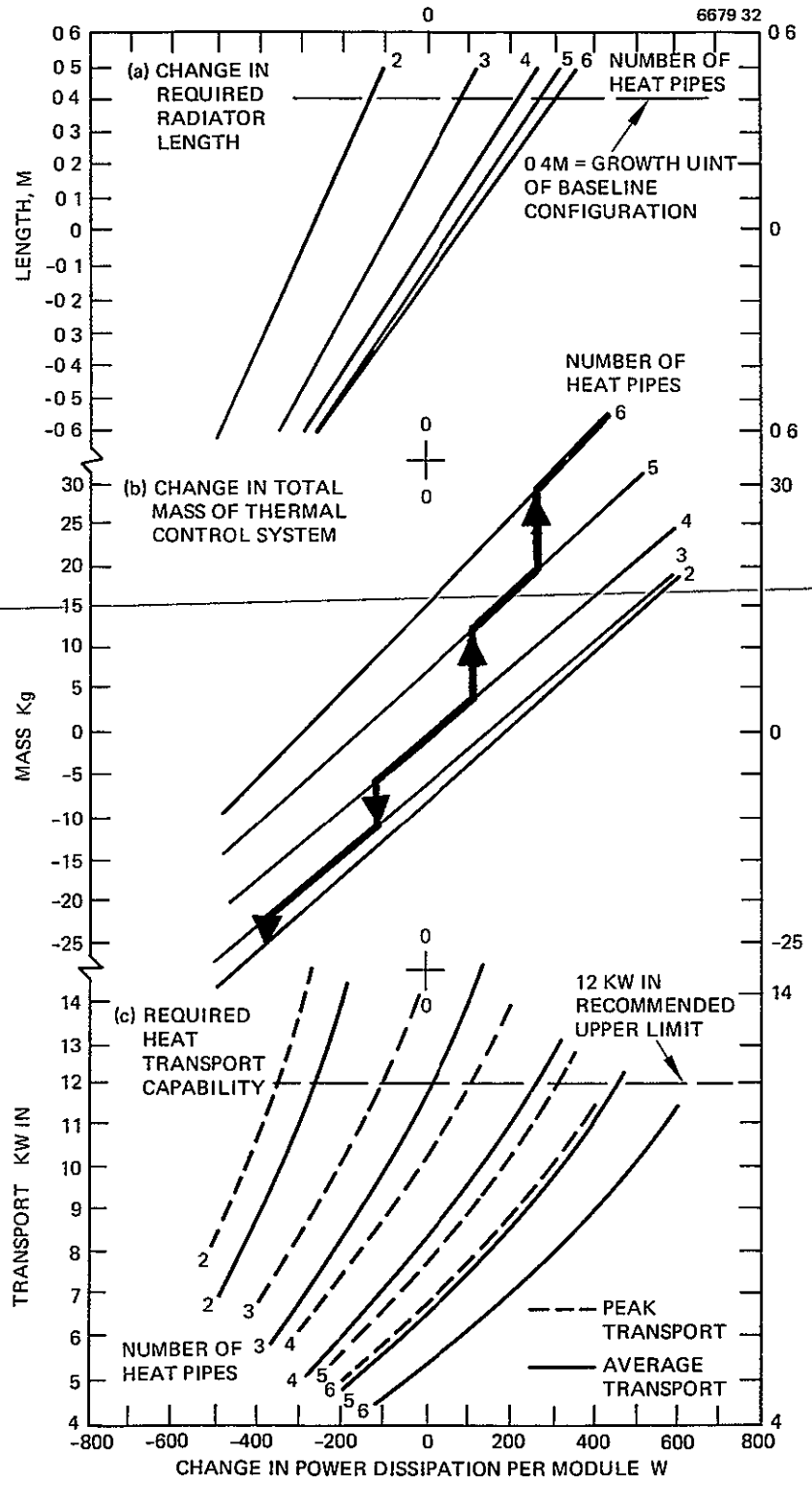

Figure 60. Thermal control parameters versus heat dissipation.

The heavy curve of Figure 60(b) was obtained by observing these limits, using the plots in Figure 60(a) and (c), as indicated. This curve defines the sensitivity of the thermal control mass to power dissipation.

2. Replacement of Conventional Beam Supply with a CDVM

Significant benefits in mass, reliability, and, possibly, in efficiency of the CDVM could merit its use in lieu of the conventional design This is dependent on the development of the CDVM to a level of maturity to confirm these benefits and attain an acceptable risk level. Accordingly, a preliminary analysis was conducted to estimate these potential thrust system benefits

Using results available from a parallel study of a DCVM breadboard model, reported in Volume V, the calculated potential benefits are summarized in Table 30. The CDVM is projected to be 9 kg lighter per unit than the conventional beam supply, allowing for about 0 5 kg for the required separate accelerator supply. The unregulated* CDVM is conservatively expected to be 95% efficient, compared to 94% efficiency for the conventional beam supply. Furthermore, the power distribution units on the interface module would be replaced by lighter reconfiguration units that would dissipate very little power: this would result in a further mass saving of $\approx$75 kg and in a reduction of system power dissipation of $\approx$330 W The lower power dissipation coupled with greater CDVM efficiency would allow the mass of the thermal control system to be reduced by $\approx$10 kg. The net reduction in the mass of the thrust system from all of these changed would be about 200 kg (including contingency). Calculations based on design analysis (which included a parts count) led to the projected reliability improvements shown in Table 30.

*Incorporating regulation circuits in the CDVM — which may or may not be required for this application — would lower its efficiency to a value comparable with that for the conventional supply.

Table 30. Impact on the Thrust System of Replacing the Conventional Beam Supply with a CDVM

Thruster System Parameter	Parameter Value	
	Conventional Beam Supply	CDVM
Mass, kg	1010	810
Average efficiency, %	70	71.2
Reliability (range), %		
Lower bound	37	40
Upper bound	72	75

5903

3. Variations in Beam Supply Efficiency and Solar Array Power

Expected variations in the efficiency of the conventional beam supply (from the design value of 94%) and independent changes in the power level from the solar array (from the 48 kW design value at 1AU) both effect thrust system mass and efficiency. Results of the analysis of these effects are presented in Figure 61(a) for variations in efficiency and in Figure 61(b) for variations in power level.

Variations in beam supply efficiency are assumed to require that solar array power be adjusted correspondingly to keep the power level to the thrusters the same as the baseline case Analogously, changes in solar array power (at a constant beam supply efficiency) would require corresponding changes in thruster power levels. We assumed that changes in thruster power were obtained by varying the beam voltage up to the 3 3 kV limit shown at a constant beam current of 2 A.

In both cases investigated, the associated power dissipation changes, indicated in Figure 61, translated into system mass changes using the data from Figure 60(b) because only thermal control mass is affected. Figure 61 shows that thrust system performance is not very sensitive to beam supply efficiency over the 93% to 95% range of interest. The thrust

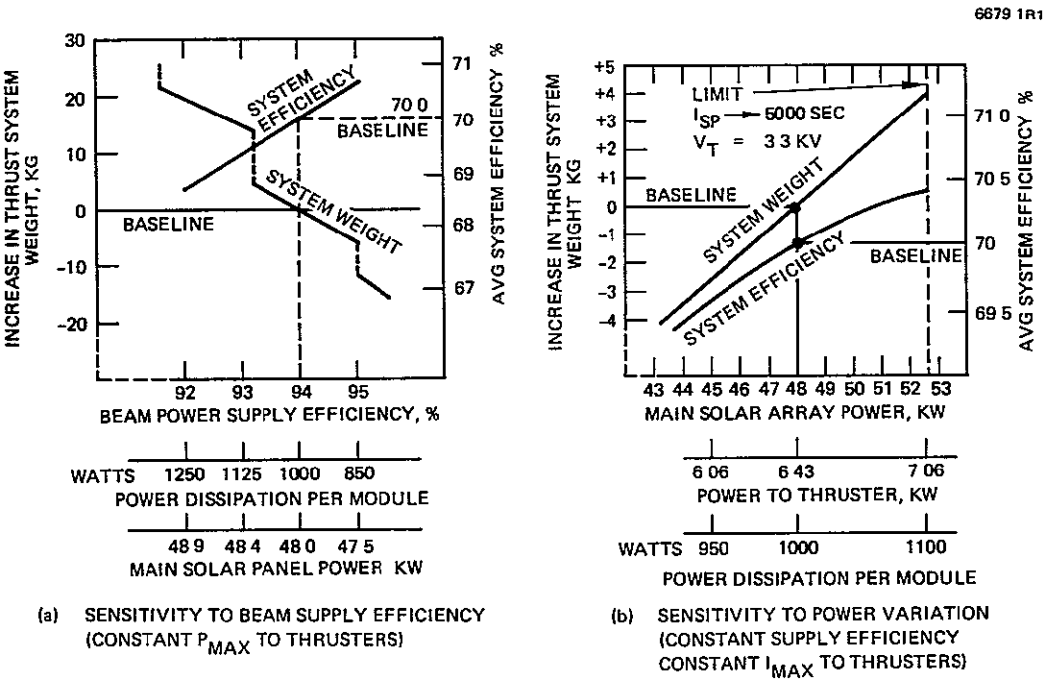

Figure 61. Sensitivity of baseline design to beam supply efficiency and solar array power variation.

system is even less sensitive to variations in the solar array power level in the range of ± 10% about 48 kW.

4. Effect of Reducing the Number of Thrusters and of Changing the Solar Array Power Level

We examined the consequences of changing the solar array power level (to 60 kW and to 36 kW) and of changing the number of thrusters (from 10 to 8). Changes in solar array power level were introduced by postulating modifications in the baseline power profile. the 48 kW initial and final power levels were first raised to 60 kW and then decreased to 36 kW, as indicated in Figure 62. Eight-thruster configurations were considered when the configurations were judged feasible and potentially desirable. It was possible to consider reducing the number of thrusters from 10 to 8 because the modular design of the baseline thrust system design allows any one of the five modules to be eliminated without a major redesign. In effect, therefore, a full matrix of possibilities was examined 36-, 48-, and 60 kW power levels versus 8- and 10-thruster configurations. This analysis only considered the impact on thrust system performance A complete-mission/trajectory analysis, which was beyond the scope of this study, would be required to assure that the thrust system configurations defined here for the 36 and 60 kW solar array could fulfill the mission and trajectory requirements Iterations of mission and trajectory analysis using the properties of conceptual thrust system configurations would be required to optimize the design parameters.

a 48-kW Array Power, 8 Thruster System

With only 8 thrusters available, all thrusters must be used during the mission (i.e., none treated as spare, unlike the baseline) to avoid prohibitively high operating time per thruster. The maximum power per thruster remains at 6.5 kW for reasons previously given in Section 2.B.3, and evident from Table 3. In comparison with the baseline, reducing the number of thrusters decreases the mass of the thrust system at the cost of lowering the estimated reliability, the efficiency of the thrust system is unaffected. A tradeoff analysis of these two opposing factors would be required to determine the viability of this 8-thruster option

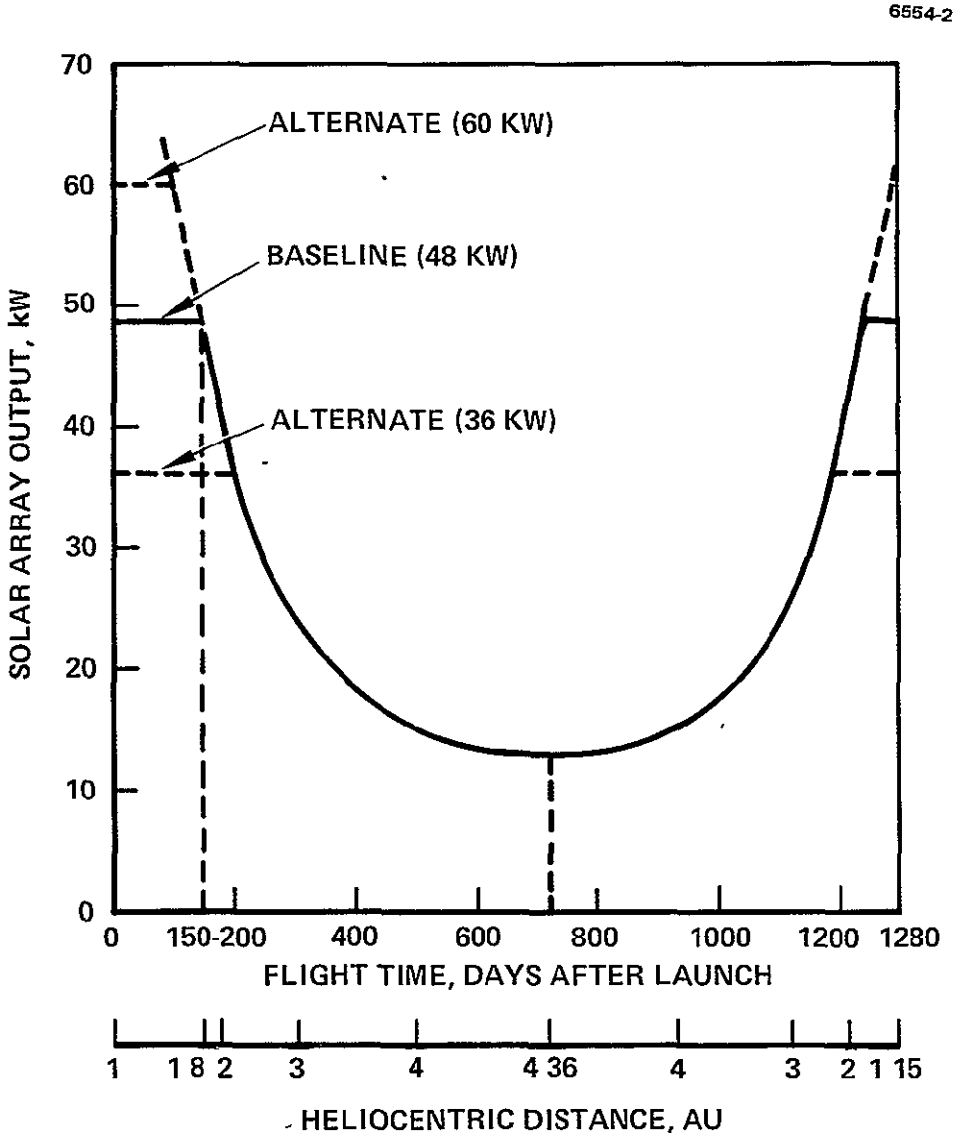

Figure 62. Power profile of the main solar array.

The reduction in mass from eliminating one module was calculated to be about 150 kg on orbit and 160 kg on IUS as shown in Table 31.

The lower reliability of the 8-thruster system results from two effects: (1) operating time per thruster is increased from 13,600 hr to about 15,000 hr and (2) loss of the benefit of one spare. Calculations indicate that:

- The lower bound for estimated reliability decreased from 37% to 15%.
- The upper bound for estimated reliability decreased from 72% to 44.5%.

The thruster operation plan for the 8-thruster case is shown in Figure 63.

It appears from these findings that the 8-thruster alternative is not attractive unless overall system analysis indicates that the 150 kg mass saving is mandatory (e.g., to provide sufficient science payload mass). If it is required, however, the resulting lower reliability estimate would make the viability of the mission questionable.

Table 31. Comparison of Component Mass for 8 and 10 Thruster Configurations of the Baseline Thrust System

Thrust System Configuration	Component Mass, kg	
	Thrust System	Adapter
10 Thrusters	1010	130
8 Thrusters	860	120
Difference between configurations	150	10
Total injected mass difference = 160 kg.		

5903

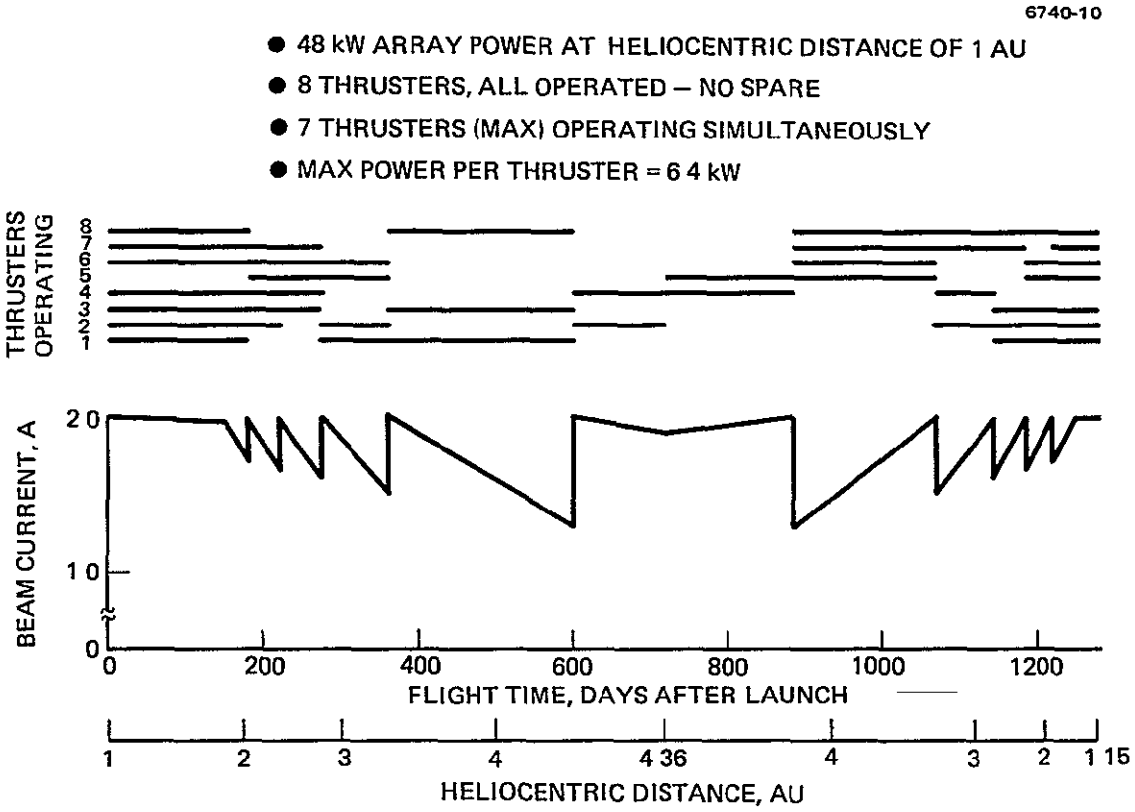

Figure 63. Effect of reducing number of thrusters to eight, thruster operation plan.

b. 60 kW Array Power

To make use of the full power output of a 60 kW solar array with 8-thrusters, all thrusters would have to be operated at the beginning and at the end of the mission. Thus, a spare thruster could not be held in reserve. Moreover, the maximum power level of the thrusters would have to be increased to 7 kW or more; but, as discussed in Section 2.B.3 (see Table 3), 7 kW was considered to be somewhat higher than 'optimium " The power available can be used by operating 9 thrusters at the 6 4 kW. Consequently, keeping a spare thruster in reserve again becomes a feasible option. Because of reliability considerations, we selected the option using 10 thrusters with 1 held as a spare for a solar array that has a 60 kW output. The parameters for this configuration are shown in Table 32 as alternative 1. The number of hours that each thruster is required to operate under this alternative is very close to the limit of 15,000 hr in this study. Figure 64 shows a thruster operations plan for scheduling the beam current level and thruster utilization over the duration of the mission.

Compared with the baseline, estimated reliability is somewhat lower and system mass higher by 90 kg. The higher mass was caused by increased Hg propellant requirement. Average thrust system efficiency was unaffected because thruster power levels were not altered. The analysis did not take into account the effects on the PMaC system of increasing the solar array power level to 60 kW, (e.g., potential reconfiguration requirements of the potential increased voltage swing, with an associated probable increase in interface module power dissipation). With respect to the baseline, the analysis dealt only with the impact on the thrust system. From that standpoint alone, it is evident from Table 29 that the 60 kW alternative is inferior to the baseline, although the disadvantages are not serious. It remains for the mission/trajectory analysis to assess these results against potential advantages from a total system standpoint. Such an analysis might indicate that reduced flight time would reverse the above conclusions on reliability and that the mass of the science payload could be higher in spite of the higher thrust system mass.

Table 32. Comparison of Parameters for the Baseline Thrust System With Alternative Configurations

Thrust System Parameters	Thrust System Configuration			
	Baseline	Alternative 1	Alternative 2	Alternative 3
Solar Array Power at 1 AU, KW	48	60	36	36
Number of Thrusters	10	10	8	8
Operational	9	9	7	8
Spare	1	1	1	0
Number of Thrusters Operating Simultaneously				
At 1 AU	7	9	5	5
At large AU	2	2	2	2
Maximum Power per Thruster, KW	6 4	6 4	6 7	7 7
Hg Propellant Required, Kg	1810	1900	1620	1620
Mass, Kg				
On Orbit, at IUS Separation	3970	4060	3630	3630
On IUS	4100	4190	3750	3750
Average Hours per Operational Thruster	13,600	14,450	15,540	13,600
Reliability (Range), %				
Estimated Lower Bound	37	35	44[a]	17
Estimated Upper Bound	72	72	77[a]	45
Average Efficiency, %	70	70	b	b

[a]Assuming reliability data is valid for operating period of 15, 540 hours

[b]Not calculated (approximately same as baseline)

5903

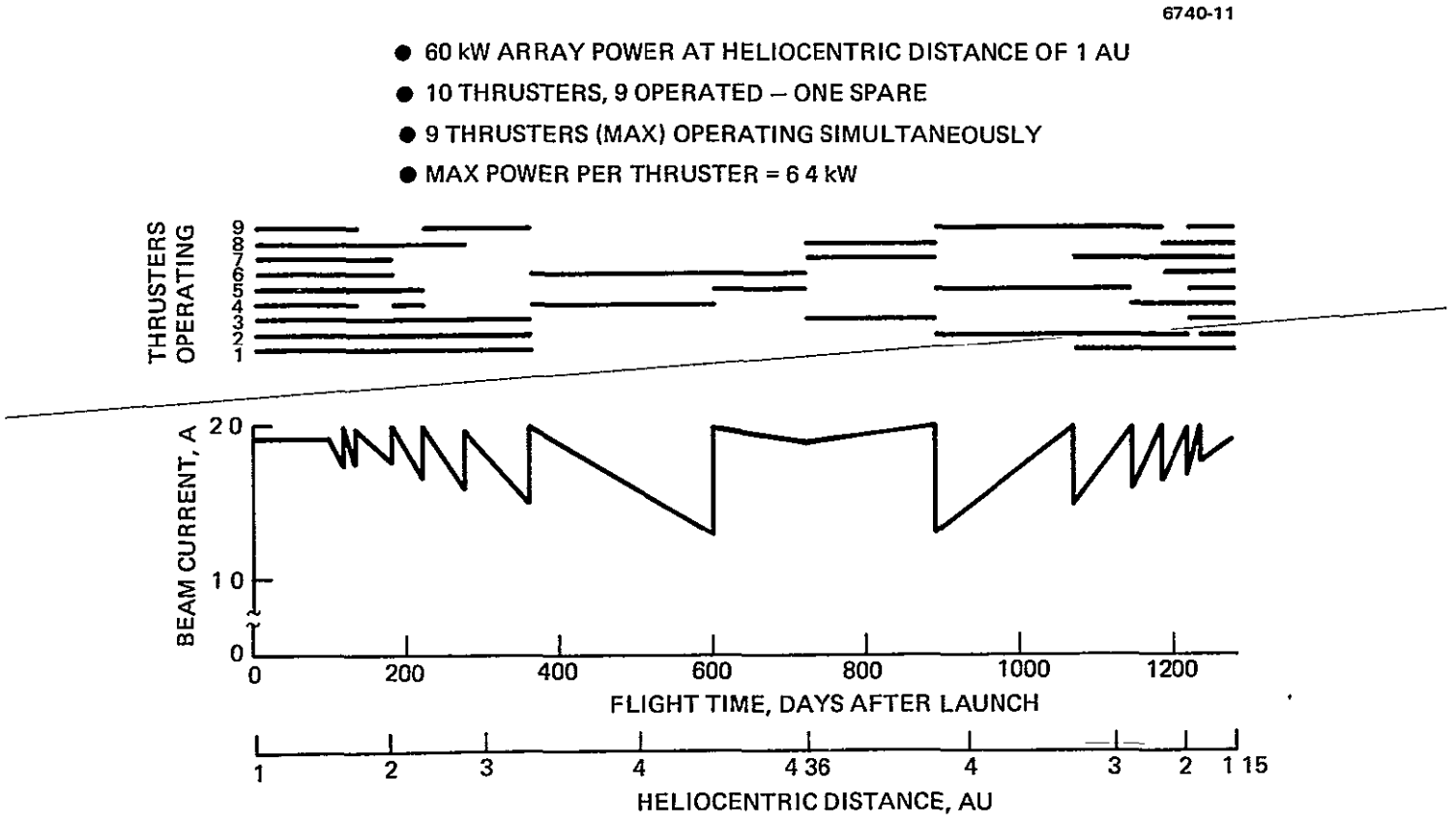

Figure 64. Effect of increasing solar array power to 60 kW at low heliocentric distance thruster operation plan.

c. 36 kW array Power

The number of thrusters selected for this alternative was governed by the fact that, with only 36 kW available at low heliocentric distance, the maximum number of thrusters that could be operated simultaneously with a reasonable degree of efficiency is five. This also follows from the discussion of the baseline in Section 2.B.3. Operating more than five thrusters simultaneously would increase Hg propellant mass requirements, and, more importantly, it would be an inferior design because it would require the prolonged operation of thrusters at a correspondingly lower power level: if this lower power level were chosen as the maximum-power design baseline, then the total operating time per thruster would be excessive, alternately, if a higher maximum power level were chosen as the design baseline, then inefficient prolonged operation in a throttled mode would result.

With a maximum of five thrusters operating simultaneously (as indicated by the above analysis) a 10-thruster system would result in an unwarranted thrust system mass penalty. The 8-thruster system would therefore be preferred, provided that it did not result in excessive total operating times per thruster.

The 8-thruster system was explored further for the two options available — with and without one thruster retained as a spare. These two options are indicated in Table 30. Since at most only 5 of the 8 available thrusters would operate simultaneously, two additional options are hypothetically also available: 6 operational thrusters with 2 spares and 5 operational thrusters with 3 spares These additional options were disregarded because the resulting total operating time required per thruster would greatly exceed the 15,000 hr limit that has been specified as the thruster lifetime.

Results of the analysis of the 36 kW alternative for the two options, and a comparison with the baseline, are presented in Table 20 as alternatives 2 and 3. An operating plan for the option that maintains one spare thruster, alternative 2 is shown in Figure 65. With both options,

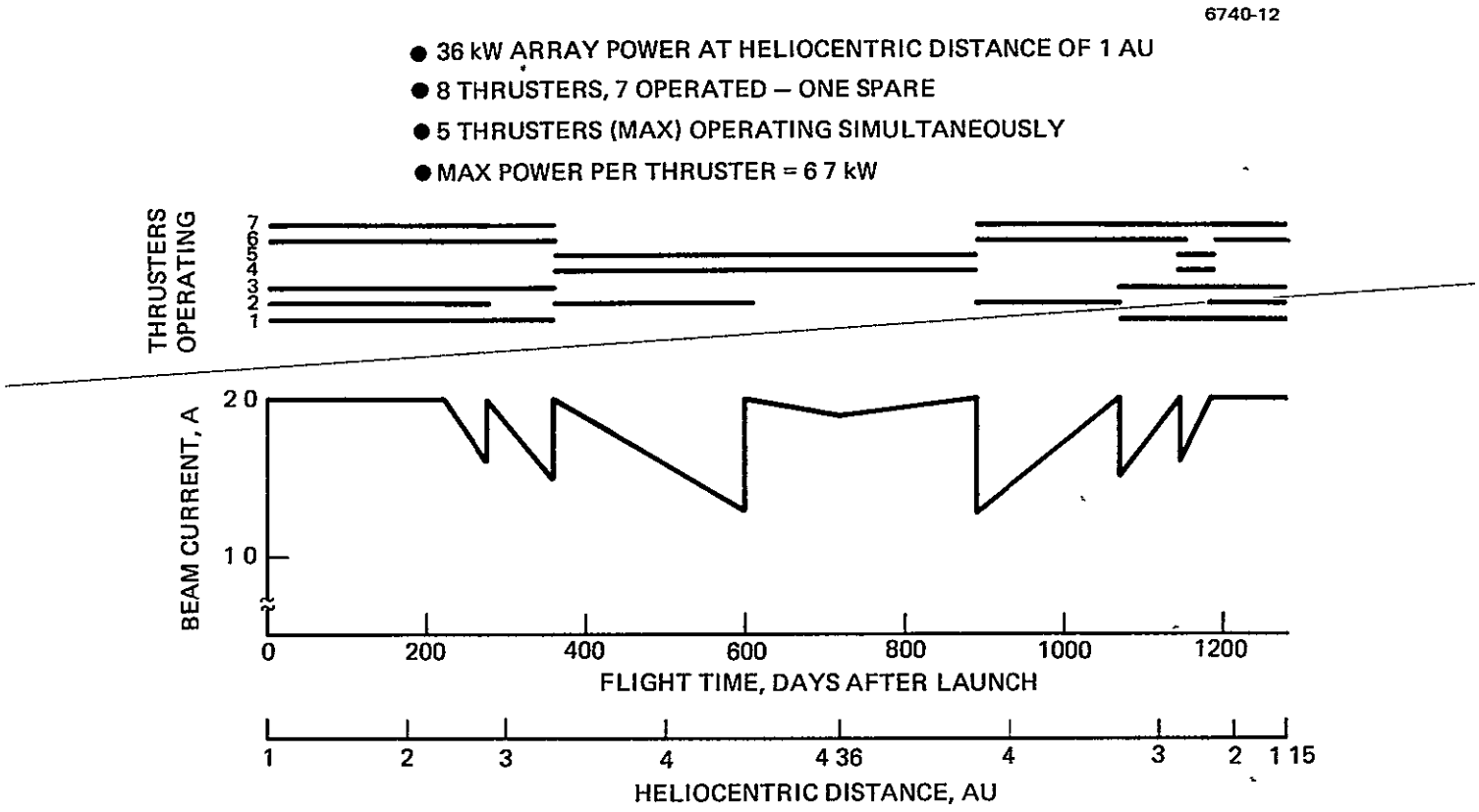

Figure 65. Effect of reducing solar array power to 36 kW at helicocentric distance of 1 AU thruster operations plan for alternate 2.

a significant reduction in thrust system mass, about 350 kg, could be achieved. about 150 kg from the deletion of one module and an additional 200 kg from a reduced Hg propellant requirement However, both options would significantly reduce reliability: total operating time per thruster would slightly exeed 15,000 hr if 1 spare thruster were retained, and estimated system reliability would be low if all 8 were operational.

As before, these findings must be assessed in the context of an overall, iterative mission/trajectory and thrust system analysis. This would determine whether these alternatives would result in a viable mission profile, and whether the potential mass re-uction would warrant the lowered reliability

SECTION 3

BASELINE DESIGN PERFORMANCE, RISK ASSESSMENT, AND INTERFACE MANAGEMENT

This section describes the thrust system performance characteristics that are projected for it on the basis of the design analyses presented in Section 2. System reliability and technical risk are also included in this section, since these properties relate to the entire system (although some iteration to improve reliability and reduce risks took place in unit design considerations during the study) The types and management of system interfaces are discussed

A PERFORMANCE DESCRIPTION OF THE THRUST SYSTEM

This subsection reviews the subassemblies that comprise the system and lists the parameters that are used to characterize its capabilities. The system characteristics are based on an interpretation of the mission requirements in terms of thruster operating parameters (listed earlier in Figure 13) The 3-kV constant beam voltage and 2-A power thruster maximum beam current selected defined the maximum PMaC power supply capacities. Thus, the PMaC units must supply 6.4 kW per thruster To utilize the available solar array power and meet the thruster lifetime and reliability requirements, 10 thrusters (5 thrust modules) are required to perform the mission All the parameters that are listed or described in the following sections were determined during design of the five-module thrust system, an interface module, and an IUS adapter to provide the capability for operating the thrusters as described in Section 2 B, Figure 13

1. Mass Properties

A mass breakdown for the baseline system is presented in Tables 33 and 34, using data for the masses of the individual component parts of the thrust system. The 15% contingency (given in Table 33) is considered ample We have used similar contingency factors on other space programs at this stage of design Fifteen percent will be more than

Table 33 Thrust System Mass Breakdown

Thrust Modules (5)	Mass, kg	Interface Module	Mass, kg	Adapter	Mass, kg
Thrusters	87.8	Electronics and harness	138 1	Main truss	54.4
Gimbals	29.5	Structure	38 4	IUS support beams	45 4
Electronics and harness	338 0	Thermal blankets	6 1	Solar array support	3.6
Structure	36 3	Propellant tanks, lines, and support residuals	25 3	Separation subsystem	11.8
Radiators and cold plates	100 2	Launch locks	2 7		
Thermal blanket	15.4	Solar array positioner cross-shaft and beam	2.7		
Propellant lines and valves	8.4	Solar array positioners	9 0		
Subtotal	615 6	Subtotal	258 5	Subtotal	115.2
15% contingency	92.4	15% contingency	38 5	13% contingency	14 8
TOTAL	710	TOTAL	300	TOTAL	130

T5903

Table 34 Subsystem Mass Breakdown

Subsystem	Mass, kg
Thrust Module Electronics and Harness	
Beam supply	40.0
Discharge supply	10.0
Low-voltage power supplies	12 6
Harness	5 0
Total per module	67.6
Total for 5 modules	338.0
Thrust Module Structure	
Titanium tubes	4.22
Radiator supports	0.23
Propulsion line supports	0 18
Gimbal support pads	0 23
Cold plate support	0.09
Miscellaneous attach hardware	2.31
Total per module	7.26
Total for 5 modules	36.3
Thrust Module Thermal Control	
Cold plate	
Facesheets (0.020 and 0.060)	4.34
Core	0.25
Bond	0.22
Edge fill (epoxy)	0 09
Inserts for attachments	0 09
Heat pipe clips	1.36
Subtotal	6.35
Heat pipes	7.80
Radiators	4.54
Radiator standoffs	1 35
Total per module	20.04
Total for 5 modules	100.2
Interface module electronics and harness	
Solar array controls (2)	10.0
Power distribution (5)	86.5
Distribution inverters (3)	3.0
DC-DC converter (2)	3.4
Control module (2)	8 0
Harness	27.4
Total	138 1
Interface Module Structure	
Aluminum lower truss Z-members	17.5
Aluminum lower truss T-members	9.8
Aluminum tube joints	2 7
Beryllium tubes	8 4
Total	38.4

sufficient if the input parameters and interface data are not changed, since sufficient analysis was conducted during this study to lend confidence to the mass estimates The principal uncertainty is probably in the area of the PMaC subsystem. Second, any significant changes to the solar array mass and to the stowed solar array envelope affect the structural configuration and its mass (notably adapter mass). Furthermore, the contingency includes provisions for the additional mass that the thermal control system would have if more heat pipes were used More heat pipes will be needed if a lower transport capability is ultimately selected as the design baseline (pending heat pipe development, procurement, and testing) or if additional redundance against potential breakage is deemed desirable. Table 35 summarizes the data presented in Table 33 and includes the Hg propellant mass allocation (from Section 2 B) and the mission module and solar array estimates furnished by NASA LeRC This total mass breakdown is presented for reference only, final values must be compiled at the total system level, pending results of mission/ trajectory analysis The key quantity in Table 35 is the estimated IUS payload of 4100 kg (including the 150 kg mass contingency for the thrust system), which includes a comfortable margin relative to the projected IUS payload capability.

The resulting mass properties of the thrust system (including total mass, location of the center of mass, moments of inertia, and products of inertia) are presented in Table 36. The inherent symmetry of the design is reflected in the very low products of inertia The quantities shown provide the required input to the system-level analysis of mass and system control characteristics

2. Efficiency

The efficiency η_T of an ion-propulsion thrust system is defined as

$$\eta_T \equiv \frac{T^2}{2\dot{m}P}$$

where T is the thrust in newtons, $\dot{m}$ is the time rate of change in system mass in kg per sec and P is the total power input to the thrust system The system efficiency varies as the number of thrusters being operated is varied and also as the power level per thruster is varied. The reason

Table 35. Mass Summary for a Spacecraft for the Halley's Comet Rendezvous Mission

System Element	Mass, kg[a]	
	Including 15% Contingency for Thrust System	Excluding Contingency
Thrust modules	710	615
Interface module	300	260
Thrust system, dry[b]	1,010	875
Hg propellant	1,810	1,810
Thrust system, wet	2,820	2,685
Solar array[c]	700	700
Mission module[c]	450	450
Spacecraft, injected on trajectory	3,970	3,835
Adapter	130	115
IUS payload	4,100	3,950

T5903

[a]To nearest 5 kg.

[b]Including residuals

[c]Assumed, per NASA/LeRC direction.

Table 36. Summary of the Mass Properties of the Thrust System[a]

Time on Orbit	Mass, kg	Center of Mass,[b] M	Moments of Inertia, kg-m^2			Products of Inertia,[c] kg-m^2		
			I_X	I_Y	I_Z	P_{XY}	P_{XZ}	P_{YZ}
After separation from IUS (tanks full)	2820	3.6	2800	4000	1100	0	0	15
Upon completion of thrust phase (including residuals; 1810 kg of Hg expended)	1010	3.1	1500	2200	500	0	0	15

[a]Excluding solar array, mission module, adapter.

[b]Above IUS interface plane (+X).

[c]About center of mass.

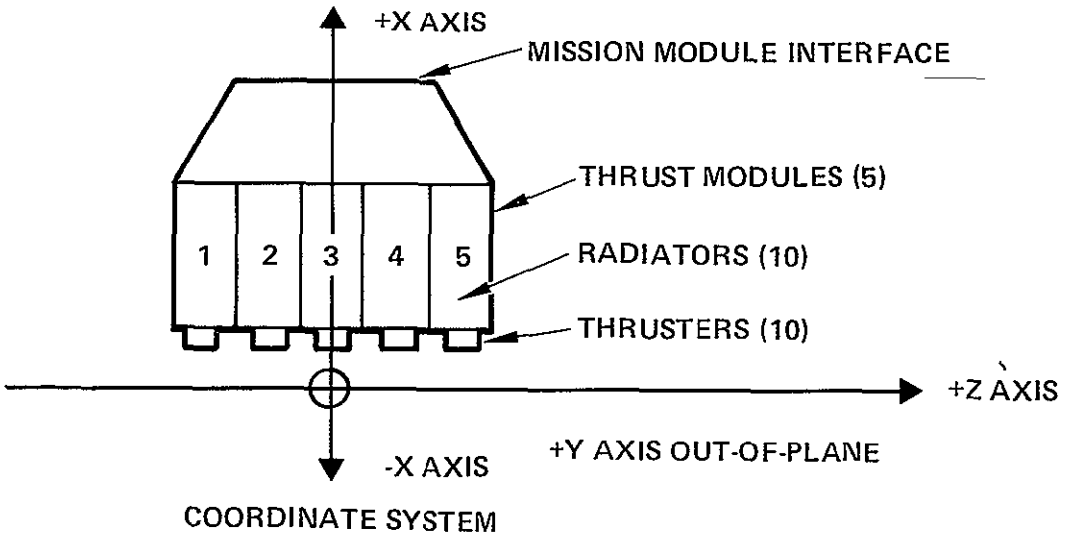

T5903

for this is that a portion of the power furnished to the thrust system remains nearly constant, independent of the number of thrusters operating or the power level at which they operate. Thrust system efficiency is a significant performance parameter because it must be specified to perform trajectory analysis. For initial trajectory computations, it is sufficiently accurate to specify the thrust system efficiency based on operating the average number of thrusters at the average power per thruster. The thrust system efficiency can then be written

$$\eta_T = \langle\eta_P\rangle\langle\eta_t\rangle$$

where $\langle\eta_P\rangle$ is the ratio of the power supplied to the operating thrusters to the solar array input power under the average operating conditions and $\langle\eta_t\rangle$ is the thruster efficiency, as defined in Volume IV, at the average thruster power.

Referring to the baseline thruster operation plan (discussed in Section 3), the average thruster beam current is 1.83 A and the average thruster input power is 5.9 kW. At this power level, the thruster efficiency, $\langle\eta_t\rangle$, is 76.2%. To determine the efficiency of the PMaC system, we computed the average thrust system power level as follows. The total energy input, E_T, supplied to the thrusters over the entire mission is given by.

$E_T \equiv$ N (average power per thruster) (operating time per thruster)

where N is the number of thrusters.

The average power input to the thrusters, P_T (avg), is

$$P_T \text{ (avg)} \equiv \frac{E_T}{\text{total mission time}}$$

$$= \frac{722{,}160}{30{,}720} = 23.5 \text{ kW}$$

Consequently, the PMaC system efficiency was based on the power input required to deliver 23.5 kW to the thrusters (operation of 4 thrusters at the average thruster power).

The block diagram shown in Figure 66 shows the power distribution of the PMaC system power during thruster operation, and Figure 67 itemizes the power inputs required for each block to obtain full power output Figure 66 also indicates how the power requirements vary with the thruster power level and with the number of operating thrusters. Proportioning the power requirements (as indicated in Figure 67) results in the values shown in Table 37 and an average efficiency, $\langle \eta_p \rangle$, of 92.2% for the PMaC system. The overall thrust system efficiency is therefore 70 2%.

3 Reliability

Thrust system reliability calculations were based on the reliability data introducted in Sections 2.B and 2.C for the thrusters/gimbals and the PMaC system components, respectively. To make the calculations we utilized the simplified reliability model developed for the thrust system In addition, estimates were made for the reliability of the other thrust system components (the reliability of these components is less critical with respect to overall system reliability). Three examples, including the baseline are discussed in this section

The reliability model starts with the calculation of r_M, the reliability of one-half of a thrust module (one thruster and all associated equipment). There are 10 such half-modules, 9 of which are required to be operational through the entire mission (i e , 9 of 10, with one space that will be used only if one of these operations fails Using the unit reliability values provided in Section 2.B and 2 C yields

$$r_M \equiv r_p \, r_T = 0.930 \, e^{-\lambda T_T} \quad ,$$

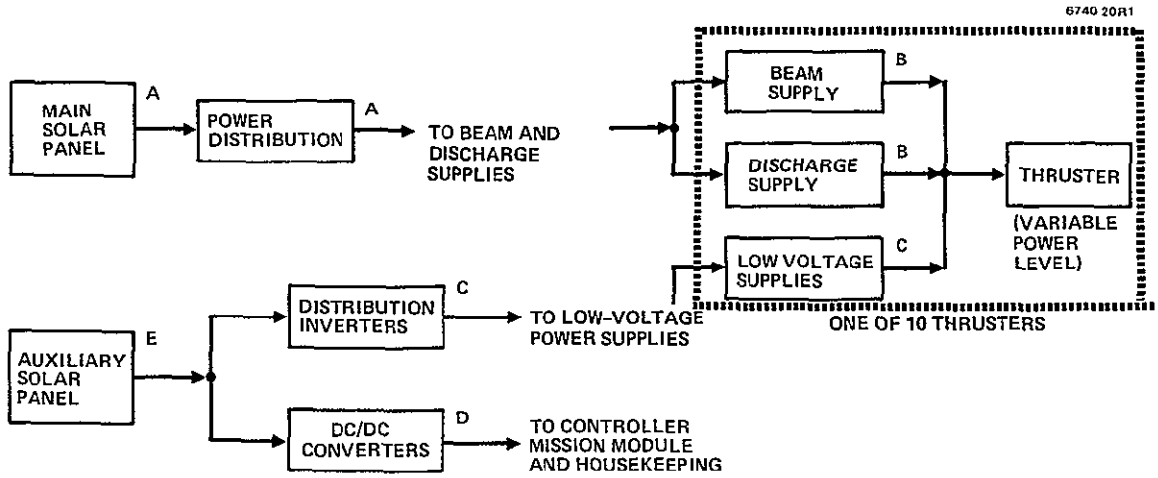

A PROPORTIONAL TO THRUSTER POWER LEVEL AND NO OF THRUSTERS OPERATING

B PROPORTIONAL TO THRUSTER POWER LEVEL

C PROPORTIONAL TO NUMBER OF THRUSTERS OPERATING, INDEPENDENT OF THRUSTER POWER LEVEL

D CONSTANT OVER 30,720 hr OF THRUST PHASE

E VARIABLE, DEPENDING ON C AND D

Figure 66. Block diagram showing power distribution for thruster operation and proportional dependence.

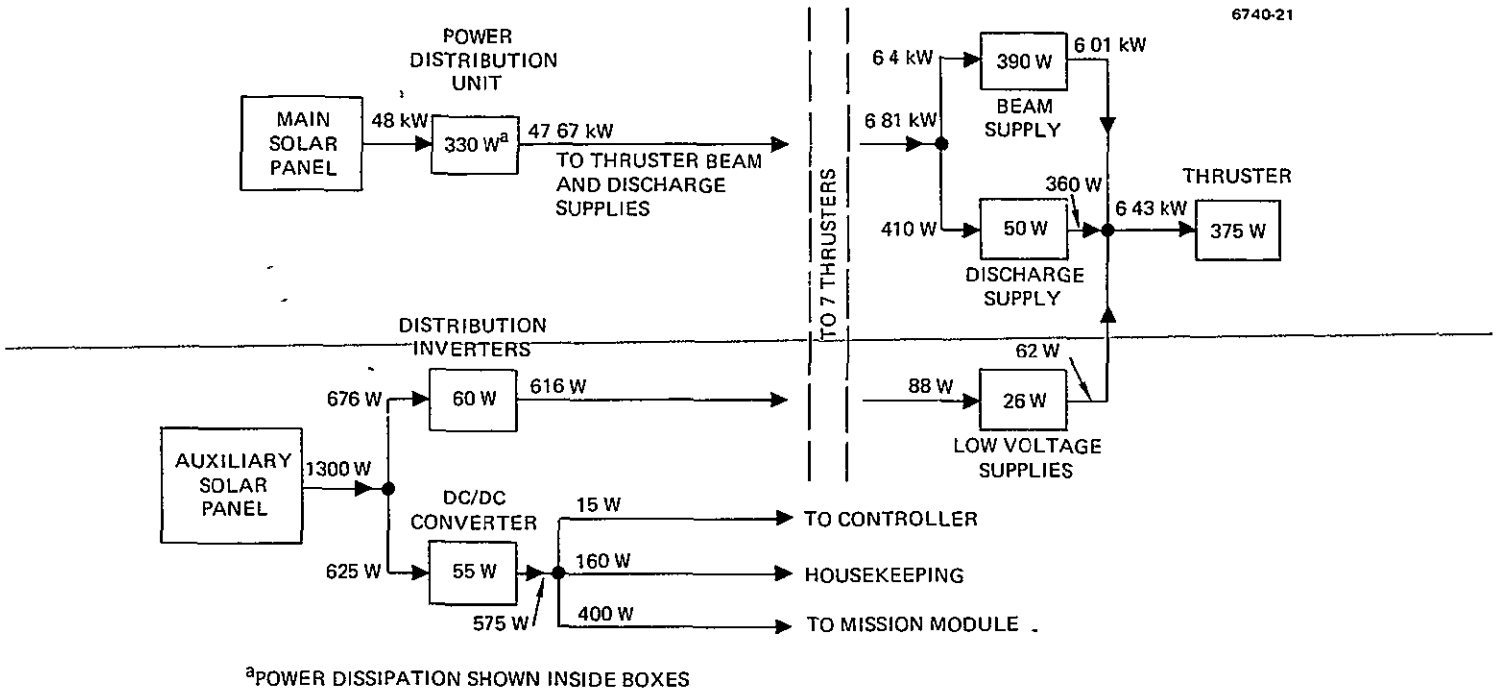

Figure 67. Block diagram showing power input, output, and dissipation for blocks within the PMaC system operating at full power.

Table 37 Power Requirement for Operation of Four Thrusters 23.5 kW Input

PMaC Element	Power, W
Beam supply output	21,734
Discharge supply output	1,518
Low-voltage supply output	248
Total thruster input	23,500
Beam supply input	23,145
Discharge supply input	1,729
Low-voltage supply input	352
Input to power distribution unit	24,886
Input to distribution inverters	386
Input to dc/dc converter	189
Total thrust system input	25,461

T5903

where

$r_p \equiv$ reliability of the set of PMAC power supplies required for one-half module = (0.977) (0.983) (0 967) = 0.930

$r_T \equiv$ reliability of one thruster/gimbal assembly = $e^{-\lambda T_T}$

$T_T \equiv$ average operating time per thruster = 13,600 hr

$\lambda \equiv$ failure rate, in failures per hr

$10^{-6} \leq \lambda \leq 10^{-5}$.

The values used to calculate r_p were taken from Section 2.C for beam, discharge, and low-voltage supplies. The reliability of the thruster/gimbal units can only be estimated in terms of the expected range of the prewearout failure rate, λ, as discussed in Section 2.B. Substituting into Eq. 11 yields the following limiting values for r_M:

$$r_M \text{ (minimum)} = 0.812 \quad r_M \text{ (maximum)} = 0.917 \tag{12}$$

The reliability of the thrust modules as a group, R_M, with 9 of the 10 thrusters operational over the full mission, is given by

$$R_M = r_M^{10} + 10\, r_M^9 (1 - r_M) = r_M^9 \cdot (10 - 9\, r_M) \quad . \tag{13}$$

In general, with (n + 1) sets of which n are operational and one is a spare, system reliability is

$$R_M = r_M^n [(n + 1) - n\, r_M] \quad . \tag{14}$$

Substituting the limiting values for r_M from Eq 12 into Eq 13 yield

$$R_M \text{ (min)} = 0.413 \quad R_M \text{ (max)} = 0.801 \tag{15}$$

The overall thrust system reliability, R, can now be estimated by multiplying R_M by the reliabilities of the other components:

$$R \equiv (R_P \cdot R_S \quad R_H)\, R_M \quad , \tag{16}$$

where

$R_P \equiv$ reliability of interface module PMaC units = 0 955

$R_S \equiv$ reliability of the structure = 1.0

$R_H \equiv$ reliability of other subsystems, including mercury propellant storage and distribution subsystem and solar array drive.

The value of 0.955 for R_P was derived in Section 2.C, where sufficient redundancy was incorporated to ensure an overall reliability above 95% R_H may be conservatively estimated to also be in the 95% range The reliability model is shown in Figure 68. This leads to an overall estimate of thrust system reliability of·

$$R \cong 0.9\, R_M \quad , \tag{17}$$

or, using Eq 15,

$$0\ 37 \leq R \leq 0.72 \quad , \tag{18}$$

which corresponds to

$$10^{-5} \geq \lambda \geq 10^{-6} \quad . \tag{19}$$

The results of this first example are shown in Table 38

The above analysis provides only a relative estimate of thrust system reliability, since it is critically dependent on the thruster/gimbal prewearout failure rate. The analysis is also intended to demonstrate the advantage of providing one spare unit. The important

conclusion is that a reasonable level of reliability — above 70% — is achievable. This confidence stems from three factors:

- The thruster/gimbal failure rate is expected to be closer to the 10^{-6} limit, although further confirmation is necessary.
- Redundancy in the thrust module (i.e , provision of one spare thruster) and in the interface module PMaC designs significantly contribute to the achievement of high reliability.
- The estimates are predicted on the very conservative requirement of 9 thrusters operational for the full mission

The importance of retaining one thrust module as a spare is easily demonstrated with example 2, which utilizes all 10 thrusters. With no spare thrusters, the average hours per thruster, T_T, would be reduced by a factor of 0.9 from 13,600 hr to 12,240 hr. The corresponding improvement in single thruster reliability would increase the r_M in Eq. 12 from 0 812 to 0.823 and from 0.917 to 0 919, respectively. However, Eq. 13 for R_M would now become $R_M = r_M^{10}$. The resulting values for R_M in Eq. 15 would be lowered from 0.413 to 0.142 and from 0 801 to 0.426, respectively This is easily shown mathematically Denoting the non-redundant case with primes, the equations for r'_M and R'_M become:

$$r'_M = r_P \, e^{-0.9\lambda T_T} \tag{20}$$

$$R'_M = (r'_M)^{10} \quad . \tag{21}$$

Dividing Eq. 20 by 11 yields

$$r'_M = r_M \, e^{\lambda T_T/10} \quad . \tag{22}$$

Substituting Eq. 22 into Eq. 21 yields

$$R'_M = r_M^{10} \, e^{\lambda T_T} = r_M^9 \, (r_M \, e^{\lambda T_T}),$$

which Eq. 11 allows us to restate as

$$R'_M = r_M^9 \, r_P \quad . \tag{23}$$

Dividing Eq. 13 by Eq. 23 yields the relative reliability improvement factor

$$R_M/R'_M = (10 - 9\ r_M)/r_P = (10 - 9\ r_M)/0\ 93 \quad . \tag{24}$$

This general improvement factor is seen to be always greater than unity The lowest value, corresponding to $r_M = r_P$ (i e , $T_T = \infty$), is $(10/r_P) - 9$, or 1 75. Applying Eq. 24 to the values of R_M in Eq 12 yields the factors

$$R_M/R'_M = 2.9 \text{ for } r_M = 0.812$$

$$R_M/R'_M = 1.88 \text{ for } r_M = 0.917.$$

Applying these factors to Eq 15 reduces R_M to the 0.142 to 0.426 range

The improvement from using one spare thruster would actually be somewhat lower than indicated because it would be necessary to provide switching equipment to insert the spare thruster/PMaC string after a failure of one of the 9 operating thrusters. However, with only a minimal weight penalty, sufficient switching redundancy can be incorporated to ensure that the impact on thrust system reliability is not significant, although additional, more detailed analysis is needed.

The impact of relaxing the conservative requirement that 9 thrusters be operational throughout the mission merits consideration The thruster operation plan shown in Figure 13 indicates that only 7 thrusters would be operational over the last 15% of the thrust phase Eq. 14 can be used to obtain a measure of how much estimated thrust system reliability would be improved by reducing the thruster requirement. If, as in example 3, only 8 thrusters were required to be operational at the end of

the mission * Using this equation, the improvement factor can be estimated to be:

$$\frac{r_M^8 (9 - 8 r_M)}{r_M^9 (10 - 9 r_M)} = \frac{1}{r_M} \cdot \left[\frac{9 - 8 r_M}{10 - 9 r_M}\right] .$$

For r_M = 0 917 the factor would be 1 04, and the corresponding maximum R_M would increase from 0.801 to 0.833 The factor would be 1.145 for r_M = 0.812, which would increase R_M from 0.413 to 0.473.

Further studies using actual mission profiles obtained from an integrated system mission/trajectory analysis, are needed to generate a more realistic (and presumably less conservative) thrust system reliability estimate.

B. ASSESSMENT OF TECHNICAL RISKS

The analysis of potential technical risks leads to the conclusion that the proposed baseline is an inherently low-risk design. Areas of highest potential risk (discussed below) are believed to be amenable to a timely and successful solution. The most significant risks associated with the thrust system for the Halley's comet mission is in the area of program schedule compliance.

The analysis leads us to have high confidence in the technical integrity of the baseline design from the following factors

- Electric propulsion technology, which will be the basis for the proposed ion thruster, is well established.
- Supporting analysis and tests conducted during this study demonstrate that the required extended performance of the 30-cm thruster can be achieved.

*This might somewhat increase the distance at rendezvous between the spacecraft and Halley's comet, but the mission could still be successfully completed.

Table 38. Summary of the Reliability Analysis

	Configuration					
	Example 1[a]		Example 2		Example 3	
	Max	Min	Max	Min	Max	Min
Parameters						
Number of operational thrusters	9	9	10	10	9	9
Number of spare thrusters	1	1	0	0	1	1
Number of thrusters operating at end of mission	9	9	9	9	8	8
T_T, average operating time per thruster, hr	13,600	13,600	12,240	12,240	~13,600	~13,600
λ, thruster failure rate, failures/hr	10^{-5}	10^{-6}	10^{-5}	10^{-6}	10^{-5}	10^{-6}
Reliability range						
r_M (single string reliability of thruster/gimbal/processor)	0 812	0.917	0 823	0 919	0.812	0.917
R_M (thrust module's overall reliability)	0.413	0.801	0.142	0.426	0.473	0.833
R (thrust system reliability)	0.372	0.721	0.128	0.383	0.426	0 750

T5903

[a]Baseline

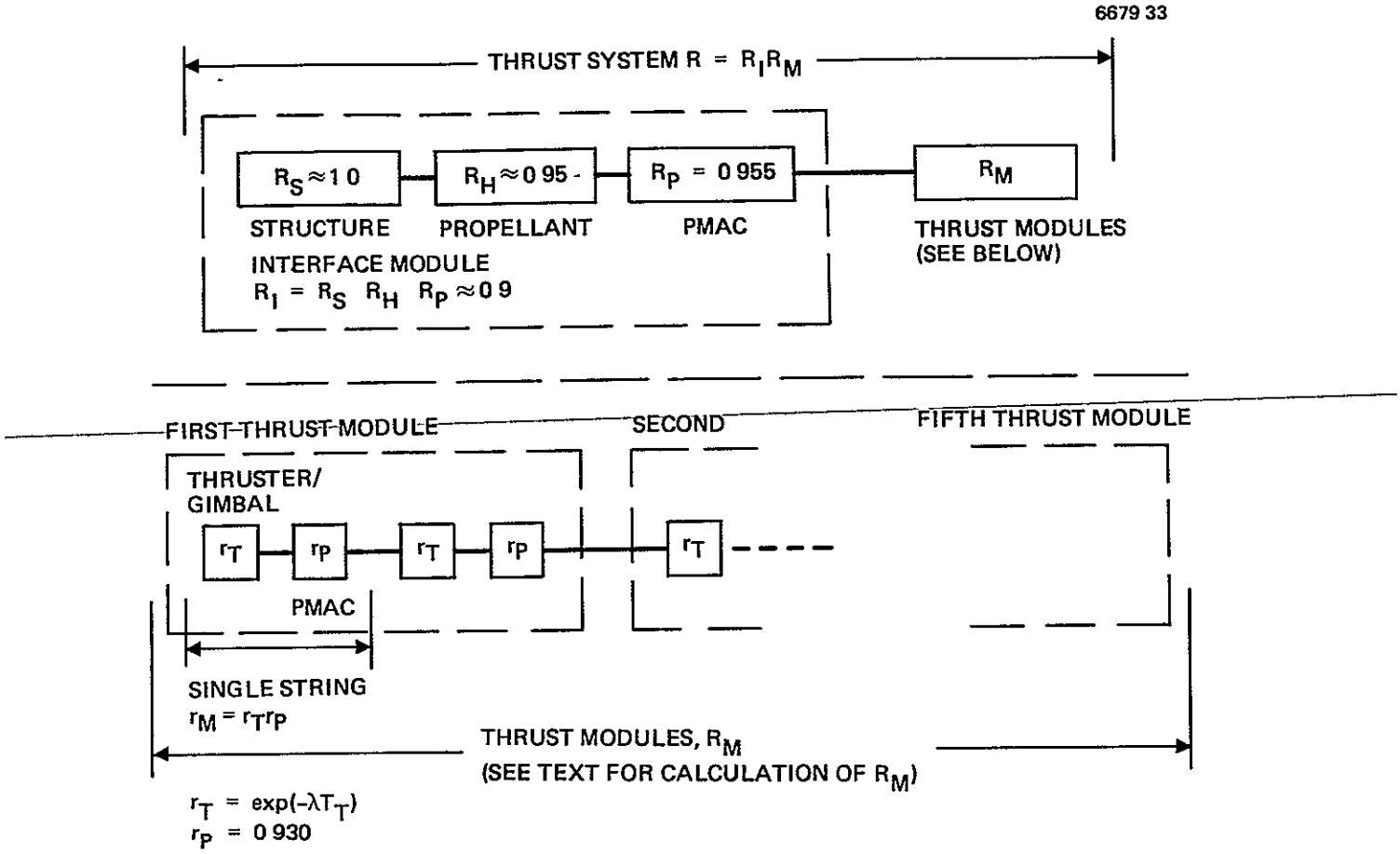

Figure 68. Reliability model.

C-3

- Power-processor technology is also well established and is directly applicable to the conventional PMaC concept adapted for the baseline

- Current (1977) technology is adequate for the proposed baseline thrust system design, and neither new components (with the exception of the high-voltage isolator) nor novel techniques appear necessary.

An overview of the electric propulsion program to date (and projected near-term activities) is presented in Figure 69, it attests to the existing technical capability. Results of the supporting technology study are presented in Volume IV and confirm the prediction of extended performance capability The milestones achieved in the development of power processor technology are the basis for the continuing development of the PMaC units for this application, these milestones include

- Initial concept 1967

- First breadboard 1969

- Thermal vacuum breadboard 1973

- Operation with ion thruster 1974

- 4,000 hr of operation with thruster demonstration 1976.

There are not believed to be any significant technical risks in the areas of structural or thermal design. But the discussion here does not consider the technical risks that may be associated with the solar array or with the mission module.

The analysis identified the most significant technical risk areas. These risks and the reasons they are considered significant are in Table 39. With the exception of thruster life, these risks are those that would normally exist at this preliminary stage of development.

Fulfilling the 13,600 hr thruster life requirement is, perhaps, the only problem with a still unconfirmed solution Intensive effort is recommended during the initial development phase of the proposed program to dispel this concern. Further testing to evaluate wear rates has a reasonable probability of showing the current design to be adequate.

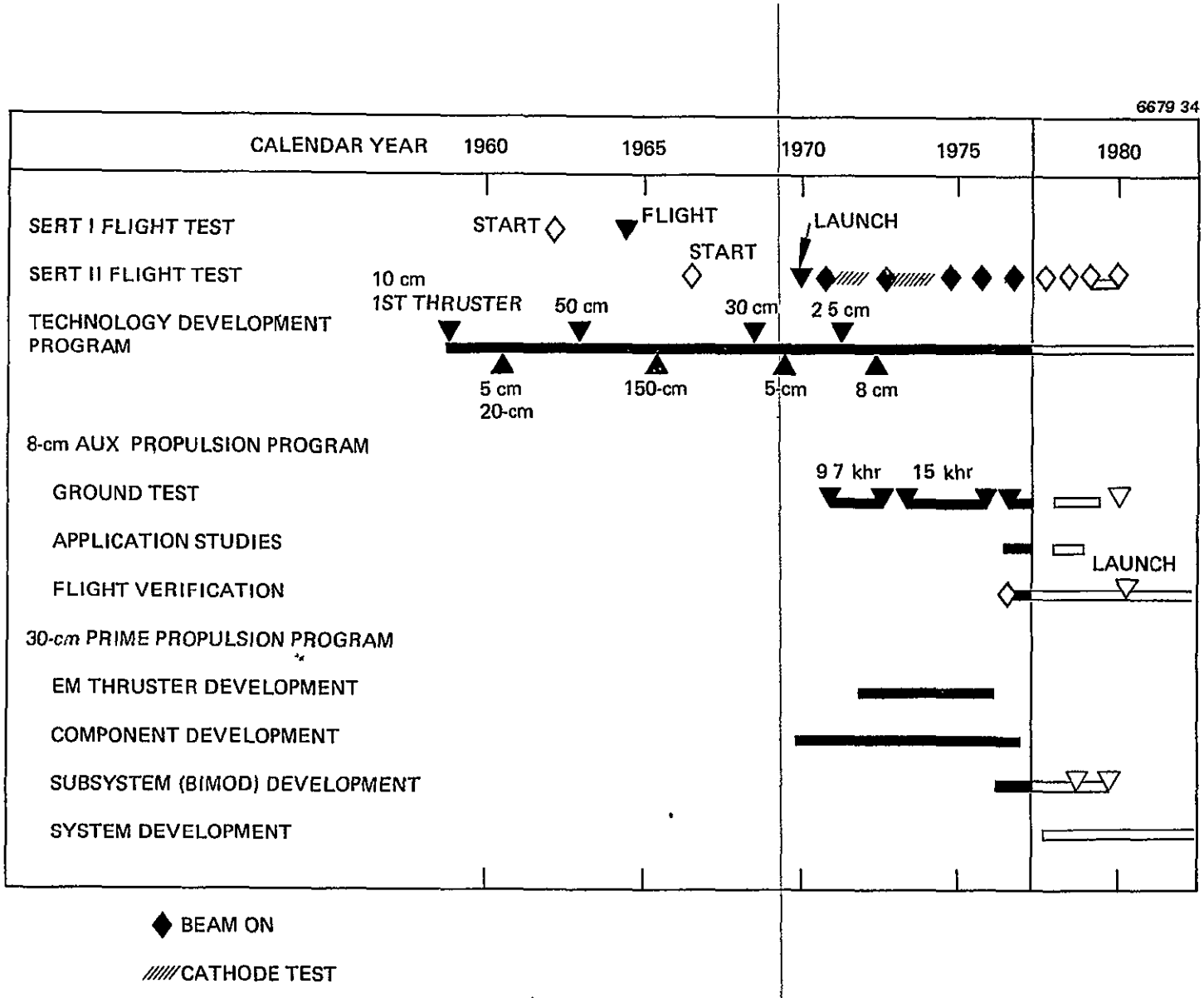

Figure 69. Electric propulsion program.

Table 39. Significant Technical Risks Associated with Thrust System Development

Technical Risk	Reason for Concern
Isolator life and performance at high voltage	New component
Thruster failure rate at high power and voltage	Greater energy into accelerater grid during arcing and increased stress on insulators
Thruster life	15,000 hr not yet demonstrated for 900-series design
Reliability of PMaC design for high power operation	High thermal loading and stress level of components (qualifiability)
	High parts count (added redundancy costly)
Controller EMI susceptibility during high-power thrusting	Nature and effects of severe EMI environments not addressed or provided for

T5903

Alternately, readily implemented design modifications are available to increase life expectancy.

The high-voltage isolator is the only novel component in the baseline design. The design effort reported on in Volume IV is believed to have resulted in an isolator design approach that can be implemented within the schedule. However, further evaluation of the isolator is necessary to confirm its performance.

High-power operation of the 30-cm thruster was, at the start of the study, considered to present a significant technical risk. But, as discussed in Volume IV, extended-performance operation (high voltage and current levels) of the 30-cm 900-series thruster was successfully demonstrated during this study Nevertheless, extended-performance operation still presents a technical risk. Under high-power operation, more energy is released into the acceleration grids under conditions of breakdown (arcing) than that known to be tolerable from endurance test results, this could increase the failure rate The potential problems should all be manageable during the development phase by the

An additional concern is the control of flake formation, since flakes caused several early failures in the SERT II program. This is not listed in Table 39 because a relatively high level of confidence exists that solutions already demonstrated for other thrusters will work for the 30-cm 900-series design and the extended performance thruster. But additional tests are needed to demonstrate that these control techniques are adequate for the 900-series and extended performance design.

Principal risks associated with the PMaC system arise from the high parts count of some of the components and from the high-power operating levels required. High parts count leads to design complexity, and this is compounded by the requirement that sufficient redundancy be provided to ensure adequate reliability. High power level operation gives rise to several concerns: high component stress levels, adequate packaging to withstand thermal loading, component qualifiability, and potential EMI effects With the possible exception of EMI effects, each of these areas, although presenting a degree of technical risk, is believed to be manageable with the application of standard engineering skills during the development phase. Potential EMI problems, however, merit further discussion. Of particular concern is the susceptibility of the controller during high-power thrusting. This rated a separate listing in Table 39 because the successful operation of this unit is critical to the success of the mission.

The results of a preliminary analysis conducted to identify the potential EMI problems and to define some of the remedial measures available to solve them are presented in Table 40. A distinction is made between unit-level problems and system-level problems. Potential unit-level problems are primarily associated with conductively coupled noise Various design measures, pertaining to the design of each unit, are available and can be readily validated by unit testing under simulated environmental conditions, as indicated in Table 40 These concerns can be alleviated by the application of standard engineering practices. System-level problems, which may arise from conductive as well as

Table 40. EMI Concerns and Available Remedial Measures

Potential Concerns			Available Remedial Measures						
			Unit Level				System Level		
Source	Cause	Effect	Isolation of High Power Components	Power Control Harness Separations	Differential Receivers/ Transmitters	Addition of Inductors	Multi-point Grounding	Twisting and Shielding of Power Interconnections	Packaging (Relative Location of Sensitive Components
Thruster noise	High power operation and/or arcing	Conducted noise affects logic in controller		X	X			X	X
		Conducted noise affects inverter operations	X	X		X		X	X
		Radiated noise couples into mission module affecting communications and housekeeping functions				X	X	X	X
Noise generated in inverters	High power operation	Internal noise affects inverter operation	X	X					X

T5903

radiative interactions, are more difficult to predict, identify, and remedy. Simulation of high-power thrusting, as well as of electrical interconnections and physical layouts, is required. The remedial measures indicated in Table 40 are expected to alleviate potential problems. However, because some of these effects are quire unpredictable and are dependent on the final design and physical layout of components, system-level EMI must be considered to be one of the most significant technical risks

Solution of system-level potential EMI problems will require special attention throughout the development, qualification, and flight system fabrication and testing phases of the program. It will be especially important to define and conduct a comprehensive testing program to complement the design effort Elements of such a testing program are summarized in Table 41 to indicate both the scope of testing required and the availability of viable test approaches to provide confidence in the final outcome. The testing program also identifies a third level of EMI concern total spacecraft system level. Previously noted system-level problems were confined to the interactions among PMaC components and between PMaC components and thrusters — all within the thrust system. But perhaps a more significant concern is the potential for the EMI interactions between the thrust system and other components of the spacecraft. The thrust system may adversely affect the mission module Conversely, the thrust system may be susceptible to radiative or conductive interference from the mission module or from the solar array (i.e., arcing effects). The design measures discussed previously (and listed in Table 40) will alleviate such spacecraft-level EMI effects. Spacecraft-level test validation, included in the test matrix in Table 41 is an essential part of this total effort to minimize EMI risks. This area of potential spacecraft-level EMI affects falls within the general consideration of thrust system interfaces, discussed in the next subsection.

There was some initial concern regarding potential impingement of mercury ions on the solar array cells or reflectors. This is no longer considered to be a significant risk, however, because tests conducted during the study indicated that no significant amount of mercury ion flux

Table 41. EMC Test Validation Program

Test Level	Test Type	Test Configuration	Objectives
Unit	Development	Engineering model	EMI design verification
Unit	Qualification	Flight configuration	Compliance with unit EMI specs[a]
Thrust Module	Qualification	Flight configuration with interface module units simulated with regard to electrical characteristics and physical location	Identification/correction of thrust module EMI effects Nominal thruster operation Malfunction mode operations Identification of potential thrust system EMI effects
Interface Module	Qualification	Flight configuration with electrical simulation of thrust modules	Identification/correction of interface module EMI effects
Thrust System	Acceptance	Flight configuration with simulated mission module electrical interface	Full assessment/validation of thrust system (internal EMI effects) Identification/assessment of potential thrust system - mission module EMI effects
System	(Pending program plan definition)	Complete spacecraft (thrust system, mission module, solar array)[b]	System level validation of electromagnetic compatibility Factory system test - design validation Launch site test - prelaunch and flight validation

[a] Per MIL-STD-461, except for high power inverters (operating during high power thrusting with science payload off, and isolated from housekeeping functions via EMI filters), which may tolerate less stringent specs

[b] Flight configuration (stowed) or simulated - exact configuration to be defined by system contractor

T5903

is present outside of a 45° cone A 50° clearance (allowing 5° for gimbaling) can be provided for the baseline by ensuring that proper deployment geometry is maintained (i.e , by specifying that the minimum separation between the deployed solar array and the thrust system be about 4.3 m (including 2.8 m for the canister) This requirement would be a part of the interface specifications.

C. SYSTEM INTERFACES

The basic interfaces between the thrust system and the other major spacecraft elements — solar array and mission module — are simple. There is, however, an intrinsic interrelationship between (1) the design and performance of the thrust system and (2) the design, requirements, and constraints of the other major elements of the spacecraft (the solar array, mission module, IUS, and shuttle).

The challenge is to affect the early specification of the major system interfaces and to manage the interfaces during the program There is no technical deterrent to the specification of the interfaces and subsequent design of the major systems by the individual responsible parties Under the plan recommended here, and presented in Section 4, a single contractor (under NASA LeRC sponsorship) is responsible for thrust system design, procurement, and delivery. It is anticipated that the thrust system contractor would participate with NASA LeRC in a total system interface working group. By establishing management of the program at this level, the challenge of the design of each major system — thrust system, solar array, and mission module — and integration of the systems into the Halley's comet mission spacecraft can be met.

Design interdependence exists in the following category.

- Thrust system design is significantly affected by the design characteristics and requirements of the other components of the spacecraft for the Halley's comet mission. Assumptions made of necessity during this study must be verified and/or changed to further improve the overall design.

- Thrust system design affects the design characteristics of the other system components.

- Overall design integrity and performance also depends on factors that involve all subsystems To resolve potential problems and assure system integrity requires a coordinated analysis and test effort by all participants.

Specific examples in each of the above categories will serve to further illustrate the nature and scope of the interface effort involved

In the first category, the following factors play a major role in defining thrust system design

- Solar array stowed envelope
- Solar array power profile
- Mission module physical and thermal characteristics and requirements
- Mission module control system constraints
- Mission module data processing design characteristics and requirements
- Mission module operations doctrine (definition of PmaC controller)
- Mission module EMI susceptibility
- Mission profile/trajectory (thruster power levels, utilization plan, life requirements)
- IUS loads
- IUS clearance requirements and tipoff rates
- Shuttle loads
- Shuttle safety and other operation constraints.

In the second category, category (b), the following subsystem designs may be affected by design characteristics of the thrust system.

- Solar array profile management plan (reconfiguration requirements)
- Solar array deployment requirements (prevention of Hg ion impingement)
- Maximum power tracking design

- Mission module control system design (including requirements for spacecraft tilting)
- Mission module data processing design
- Mission module EMC design features
- Shuttle cradle design.

In the third category, category (c), the analysis and design tasks that must be conducted at the system level include the following

- Combined iterative trajectory/mission analysis
- Integrated development of mission operations and management plan
- Coupled load analyses (IUS and shuttle)
- Coupled thermal analyses
- System level EMI analysis and tests
- Integrated system tests.

An effective management is mandatory to successfully interface these systems. The interface management plan should provide the following:

(1) Clearly defined central authority

(2) Responsive channels of direct communication between all participants and this central authority

(3) Early definition of subsystem designs

(4) Effective control of design changes

(5) Design definition and timely provision of simulators and models.

Items 1 and 2 above, are reflected in the recommended procurement plan in Section 4 Item 3 is probably the most crucial requirement from a schedule standpoint, and the most difficult one to implement Item 5 is probably the most significant risk for the mission. Program schedule risks are treated in Section 4.

SECTION 4

PROGRAM DEVELOPMENT PLAN

The program plan developed for the baseline thrust system defines the schedule and effort required to deliver a fully tested flight thrust system to the spacecraft in sufficient time for spacecraft integration and spacecraft-level tests to meet the stipulated 1 June 1982 launch date The plan encompasses three distinct programs: development, qualification and flight hardware These culminate in the delivery of an electrical development model, a thrust system qualification prototype model, and a thrust flight system, respectively The program plan does not include development of the solar array nor of the mission module; neither does it deal with total spacecraft integration checkout nor with launch and flight operations after the thrust system has been delivered Program cost estimates are included as the final subsection

The thrust system program takes full account of the stipulated contract phases· design definition (starting 1 April 1978) and the system acquisition (starting 1 October 1978) However, schedule constraints required that advanced development and procurement phase be included, for some items it would start as early as 1 September 1977. A thrust system procurement and management plan is also included as part of the program plan to account for this advanced start prior to the project-approved document (PAD) release in October 1978, and prior to an official sanction of the Halley's comet mission.· This recommended procurement plan is consistant with the proposed program development plan. Schedule constraints also dictated a certain degree of overlap between the development, qualification, and flight-system-procurement phases of the program. The resulting plan minimizes as far as possible the advanced (FY 1978) funding requirements; it calls for the delivery of the flight thrust system to the spacecraft on 1 May 1981, which is considered to provide adequate time for subsequent spacecraft-level integration and test operations

The program plan and associated schedules are presented down to Level 3 (i.e., development, design, procurement, fabrication, assembly and test operations within individual major subsystems). Sections 4 through 4.F define the overall plan down to Level 2 schedules. Proposed facilities and their utilization and the recommended procurement and management plan are presented in Sections 4.G and 4 H, respectively Section 4.I presents the more detailed Level 3 schedules.

A. GENERAL CONSIDERATIONS

In structuring the program plan, the fundamental assumption was made that the thrust system (including the adapter) should be developed, ~~designed, fabricated, and delivered as a complete major subsystem~~ Because of the intrinsic electrical, structural, and thermal interfaces inherent in the development and design of this subsystem, it is not considered technically viable to parcel out the components of this major subsystem for development and delivery by separate organizations for subsequent integration at the spacecraft level. There are several examples of such intrinsic design interfaces that require a single technical focal point if they are to be resolved during the development phase, these include (1) interactions among the thruster, the thrust module PMaC components, and the interface module PMaC components, (2) thermal design that requires full cognizance of all elements of the thrust modules and of the interface module; (3) structural design that cannot be assured or properly tested except at the thrust system level (including adapter), (4) propulsion subsystem design-tanks and distribution system that involves both the interface modules and the thrust modules. On the other hand, the interface between the thrust system and the other major elements of the complete spacecraft — solar array and mission module — is comparatively simple, and can be readily implemented by providing the required simulators and mass models In any event, the management of system interfaces poses a major program challenge (including interfaces with the shuttle and with the IUS).

B MASTER SCHEDULE — PROGRAM PLAN OVERVIEW

The program plan calls for the delivery of the fully tested flight thrust system on 1 June 1981 Figure 70 presents an overview of the thrust system program plan; key milestones and the development/ procurement time spans are shown in Figure 71, the master schedule

The proposed plan features three sequential (but partially overlapping) activities development, qualification, and flight hardware procurement. These activities are shown in the simplified flow chart overview in Figure 72. Each activity culminates in major module-level tests followed by system-level tests during the time periods shown in Figure 71 Each activity then results in delivery to the spacecraft of the:

- Thrust system electrical model on 1 March 1980 for early spacecraft-level electrical compatibility tests, as required.
- Thrust system qualification model on 1 December 1980 as a potential "pathfinder."
- Flight thrust system delivery on 1 May 1981, 13 months before launch

C. REQUIREMENTS FOR ADVANCED DEVELOPMENT AND PROCUREMENT

Although the key elements of the proposed program plan generally correspond to the stipulated two-phase definition/acquisition program, it will be necessary to begin development and procurement substantially before the scheduled initiation dates for the two phases of the program (1 April 1978 and 1 October 1978) One way these advanced development and procurement activities might be implemented is suggested in Section 4.H. The reason these advanced activities are needed is evident from the development and procurement time spans indicated in Figure 71, the need stems primarily (but not entirely) from the lead time required for the development of PMaC hardware. Specific requirements for advanced development and procurement are shown in more detail in Figure 73. In particular, considering the lead times required, it is deemed mandatory to initiate PMaC design definition no later than

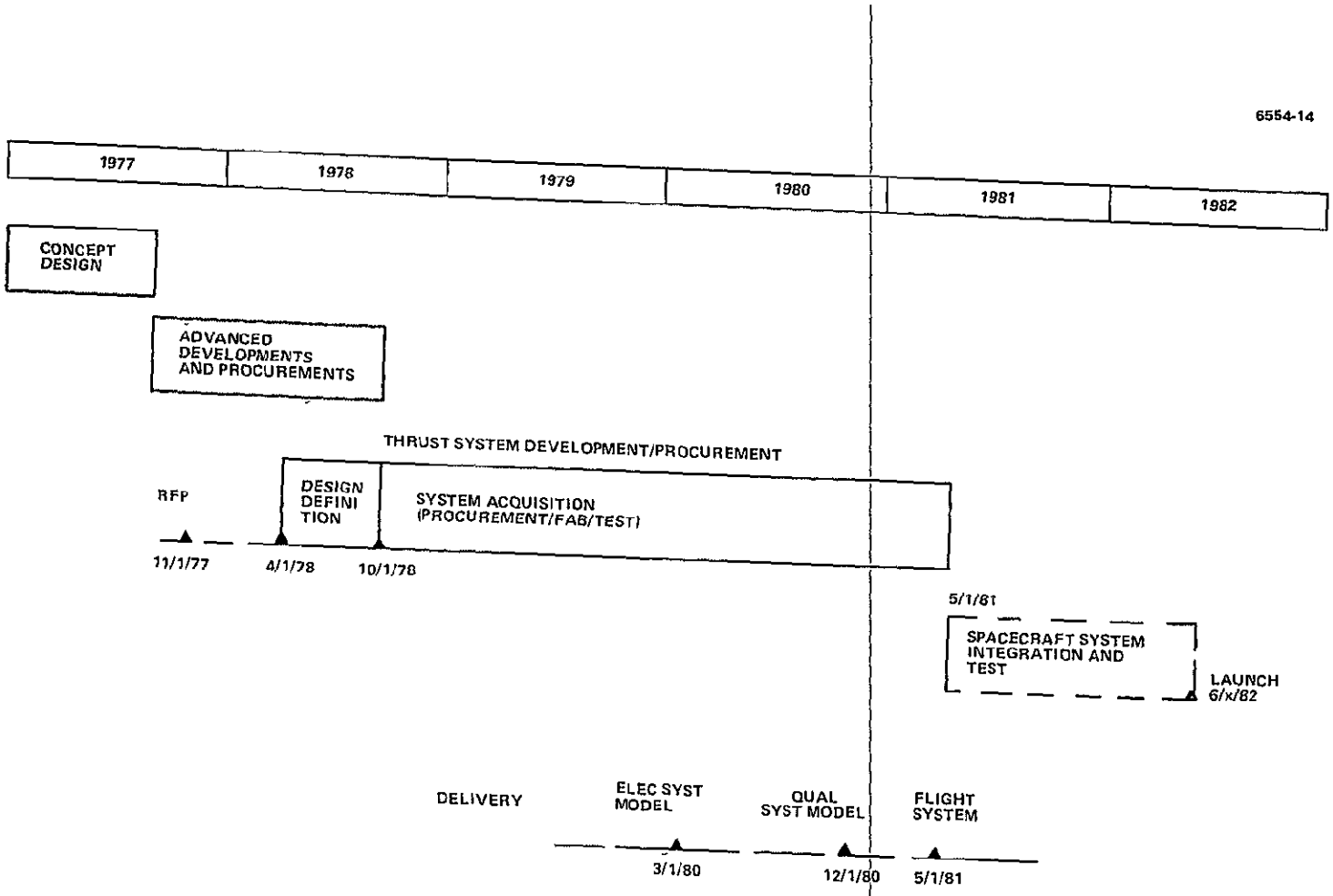

Figure 70. Overview of the thrust system program plan

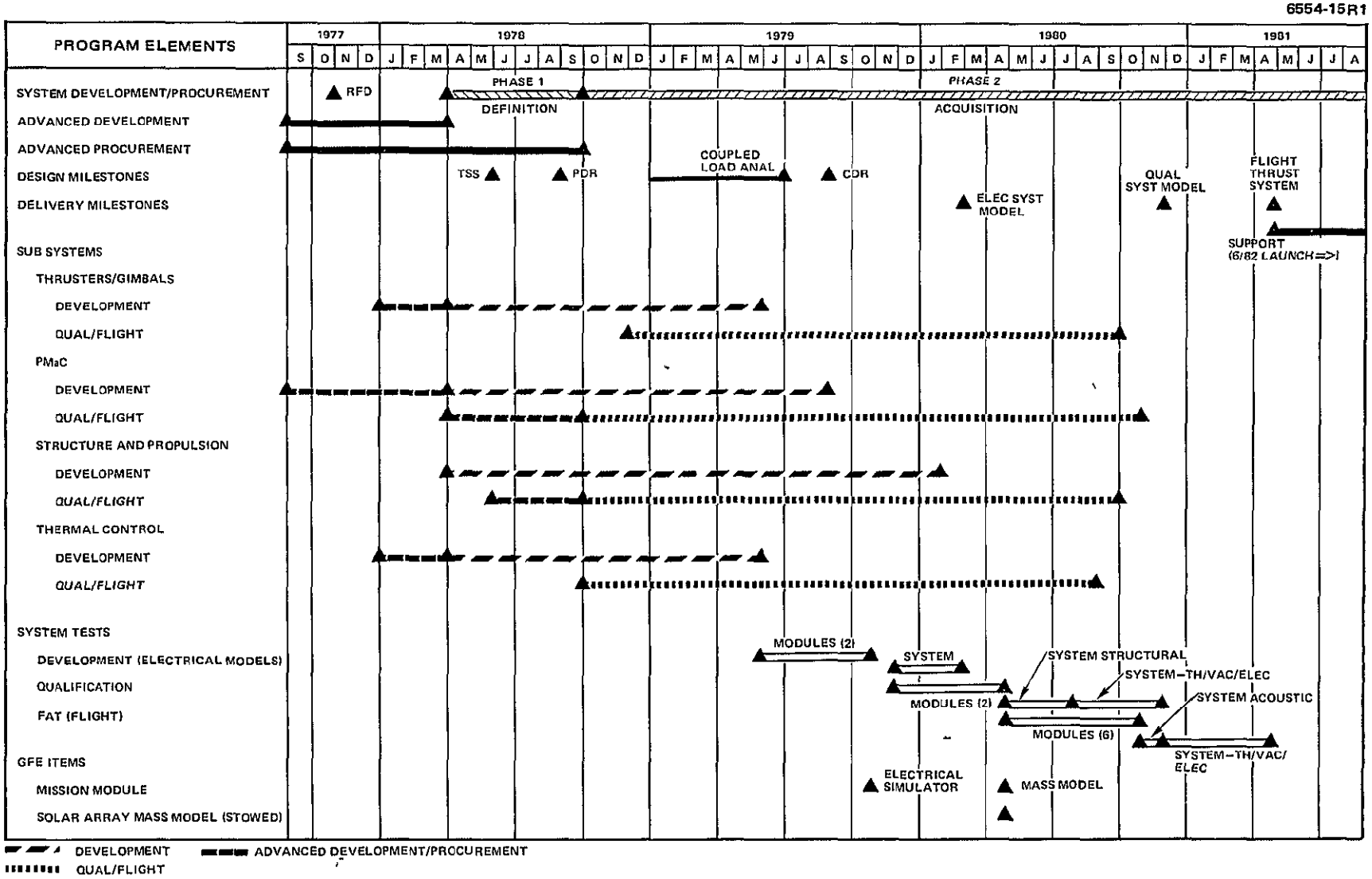

Figure 71. Master schedule for the thrust-system program

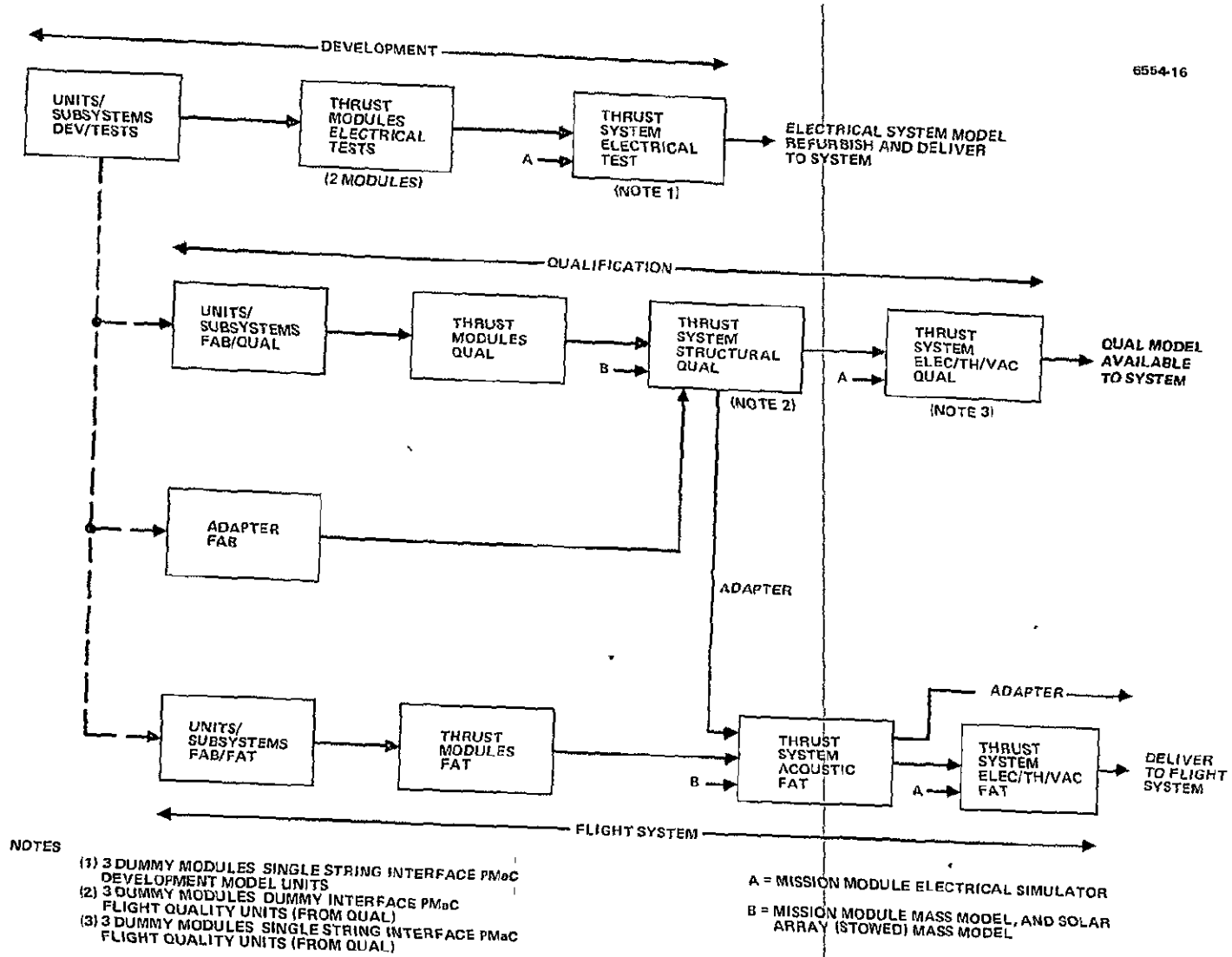

Figure 72. Simplified flow chart of program development, procurement, and testing.

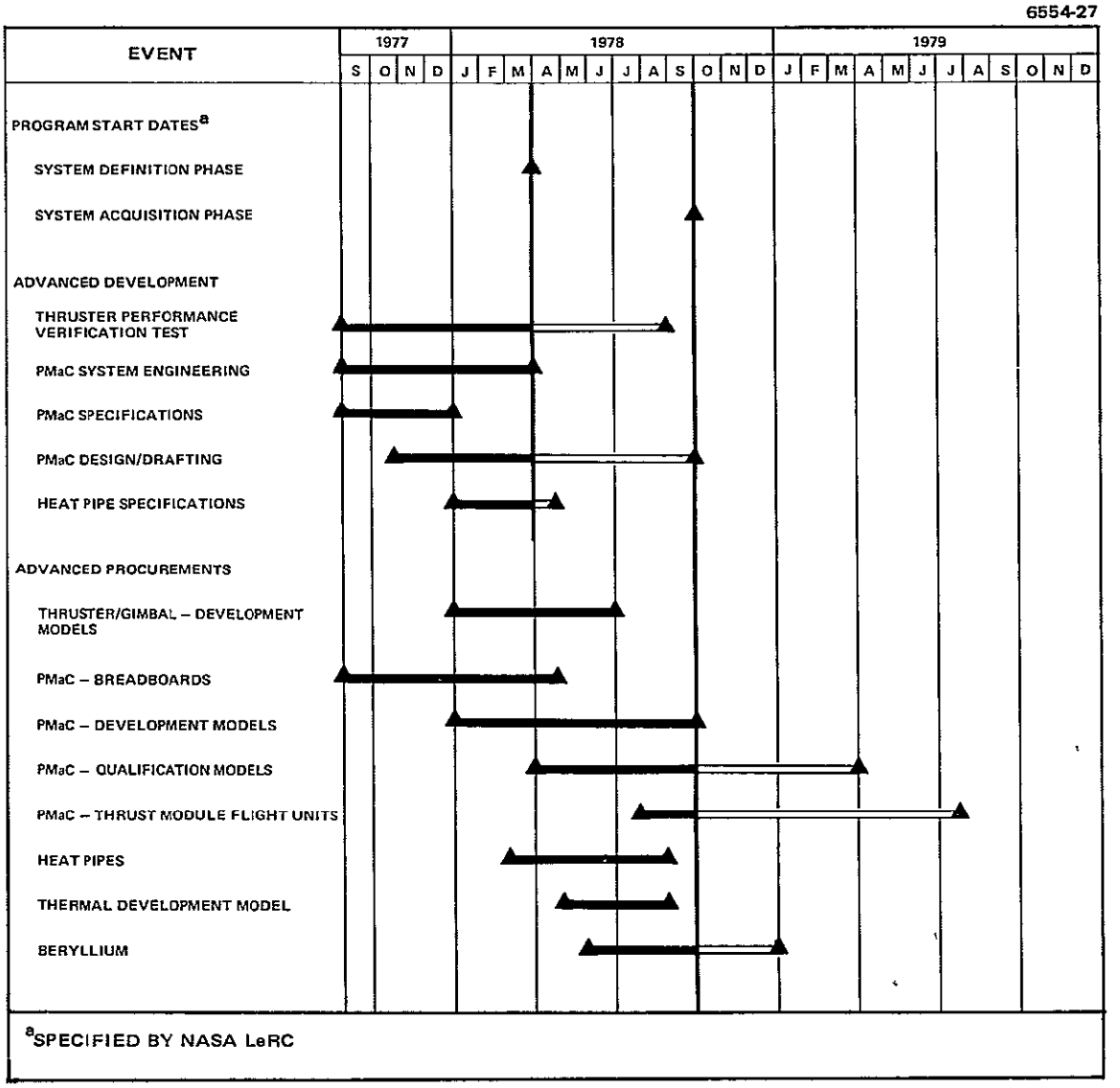

Figure 73. Requirements for advanced development procurement.

September 1977, and to start PMaC hardware procurements without delay. In addition, to meet the delivery date for the heat pipes, it is necessary to begin development of the final specifications by 1 January 1978 and to begin procurement by 1 March 1978 Beryllium delivery lead times require advanced procurement starting 1 January 1978. Figure 73 also shows the proposed immediate initiation of thruster performance verification tests using the modified 900-series thrusters

D DEVELOPMENT PROGRAM

The development activity shown in Figure 72 comprises PMaC/thruster development, and parallel developments of the other major subsystems thermal control, propellant storage, solar array drive, structure, and adapter. The PMaC-electronics/thruster development program is shown in more detail in the flow chart in Figure 74. A schedule for all the development activities is shown in Figure 75.

The PMaC-electronics/thruster development program features sequential breadboard- and development-model module-level tests, followed by tests at the thrust-system level using a single-string interface module PMaC unit and the mission module electrical simulator To ensure that major inter-module interactions are explored, two full modules will be fabricated and tested. All developmental model electronics will be flight configured, but use commercial parts. The system is therefore considered not to be flight quality, no module environmental testing is included in this development. Correspondingly, structural, thermal, and propellant storage subsystems for these configurations are either non-flight or simulated, as required. Thermal control in vacuum chambers is provided by separate means. After the thrust system electrical tests are completed, the thrusters will be replaced by equivalent electrical load simulators for subsequent spacecraft-level electrical compatibility tests (in air), as desired.

Thermal control development is a separate parallel activity that entails the designing, developing, and life testing of heat pipes and the designing and testing of a separate thermal model Corresponding parallel propellant subsystem, solar array drive, and structure/adapter

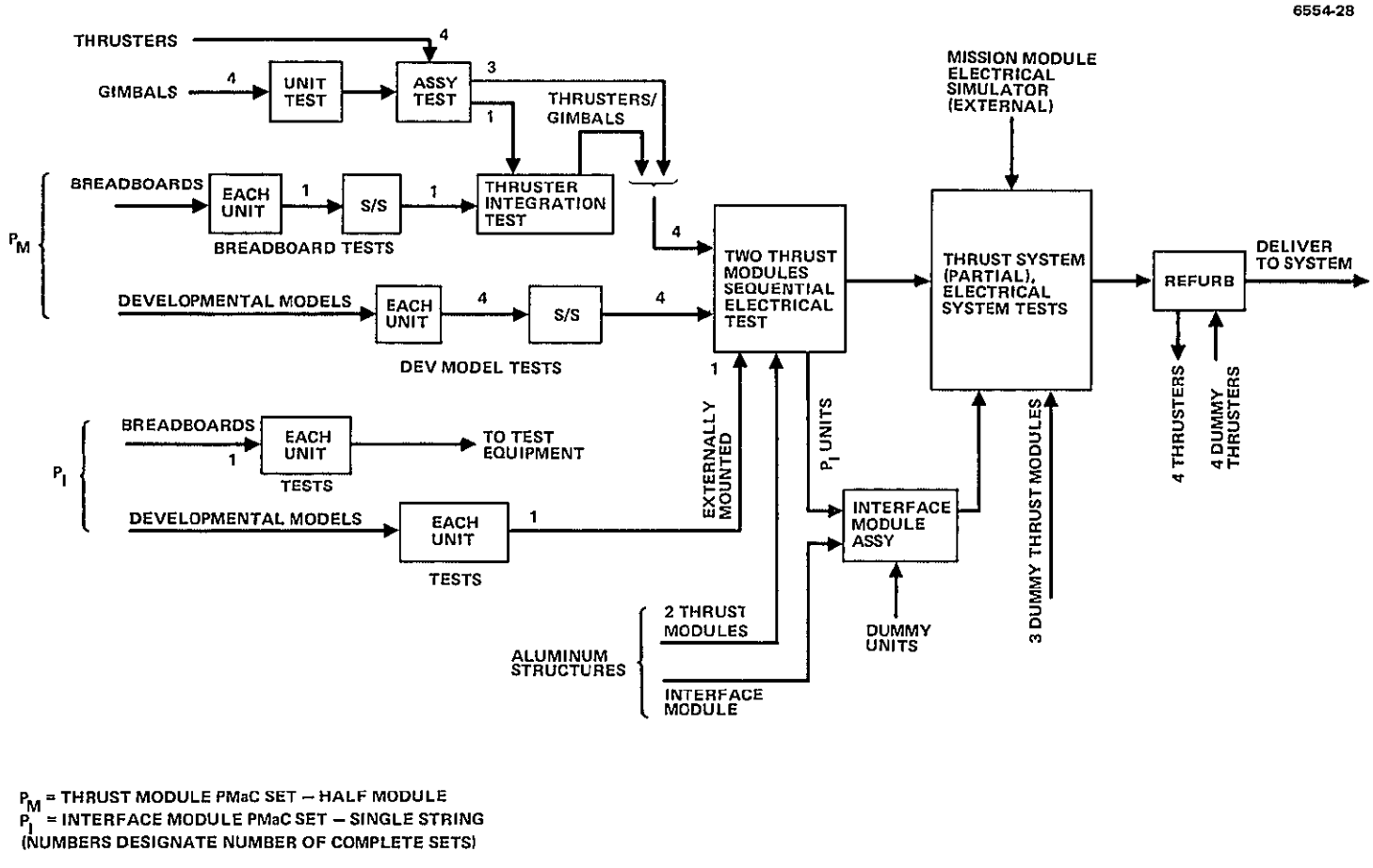

P_M = THRUST MODULE PMaC SET – HALF MODULE
P_I = INTERFACE MODULE PMaC SET – SINGLE STRING
(NUMBERS DESIGNATE NUMBER OF COMPLETE SETS)

Figure 74. Development flow chart for thrusters/PMaC-electronics subsystem

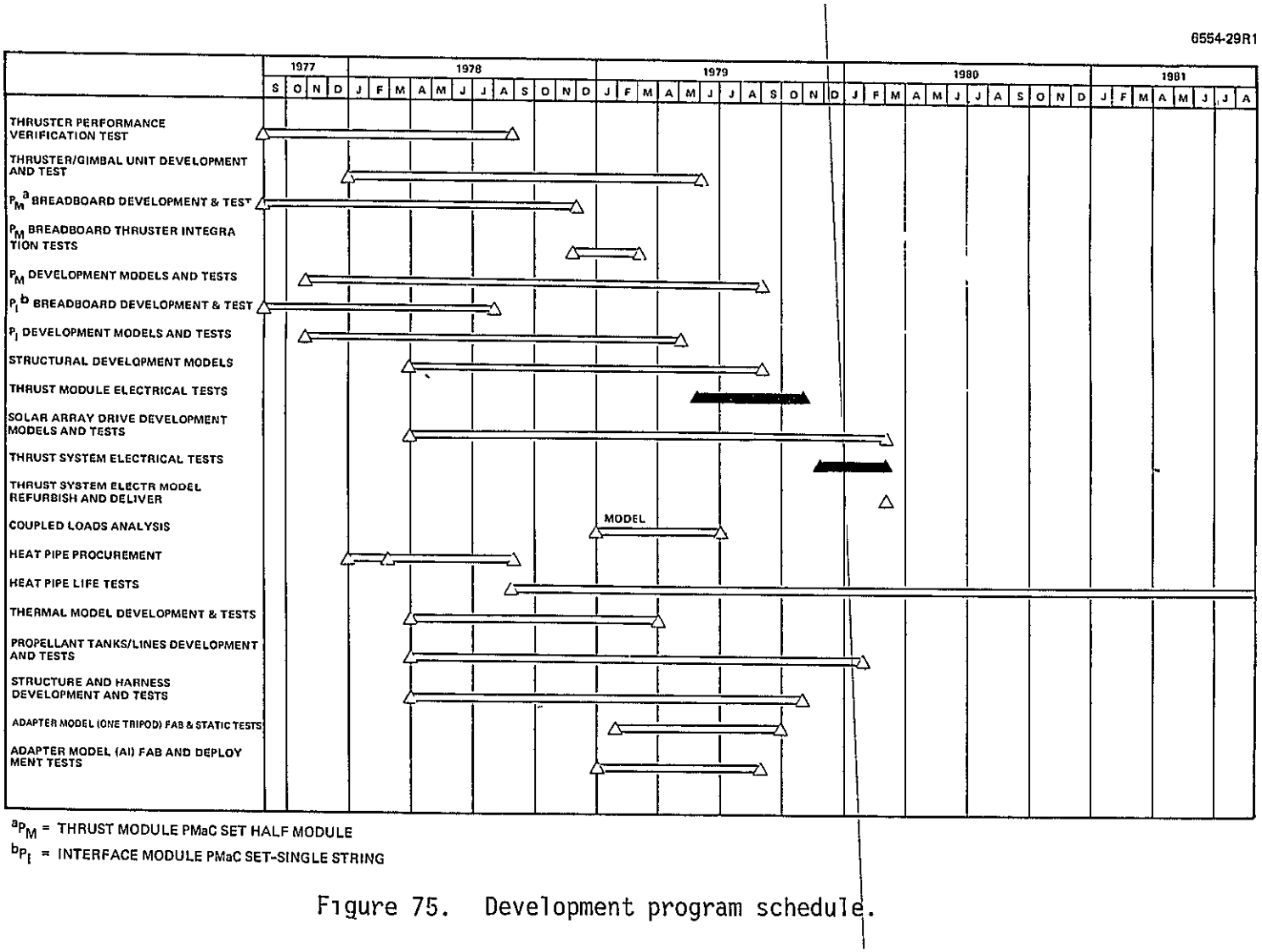

Figure 75. Development program schedule.

development is also indicated. Structural development includes static tests of one adapter tripod, the development of structural math models and coupled-load analysis, and deployment tests using an aluminum adapter model.

E. QUALIFICATION PROGRAM

A flow chart for the qualification program is shown in Figure 76, with the corresponding schedule shown in Figure 77. The proposed qualification plan features a comprehensive, albeit minimum-cost, program to assure maximum confidence in thrust system electrical and environmental integrity prior to delivery. This plan would greatly reduce the possibility of discovering problems at the spacecraft level; such a late discovery would probably cause a nonrecoverable schedule slippage.

After unit-level qualification of the thrusters and gimbals, electronics, solar array drive,-and propellant tanks, two complete thrust modules will be assembled and subjected to complete electrical testing and environmental testing (in vacuum), using externally mounted interface module PMaC electronics. Module-level tests will be used to qualify the thermal subsystem. The subsequent qualification program at the thrust-system level will consist of two distinct tests a structural qualification test in a vibration facility, and an electrical and thermal vacuum qualification test in a thermal vacuum facility.

The structural qualification test, which serves to validate system structural integrity (including the integrity of the adapter and of the propellant storage and distribution subsystem), will be performed on a simulated full structural assembly that will include the mass models of the mission module and of the stowed solar array Dummy interface PMaC units and three dummy thrust modules with simulated thermal control will be used to minimize cost; their use will not significantly jeopardize technical integrity. Then, after the mass models and the adapter are removed, and the qualification PMaC interface units are installed, the electrical and the thermal-vacuum tests will be conducted using the mission module electrical simulator

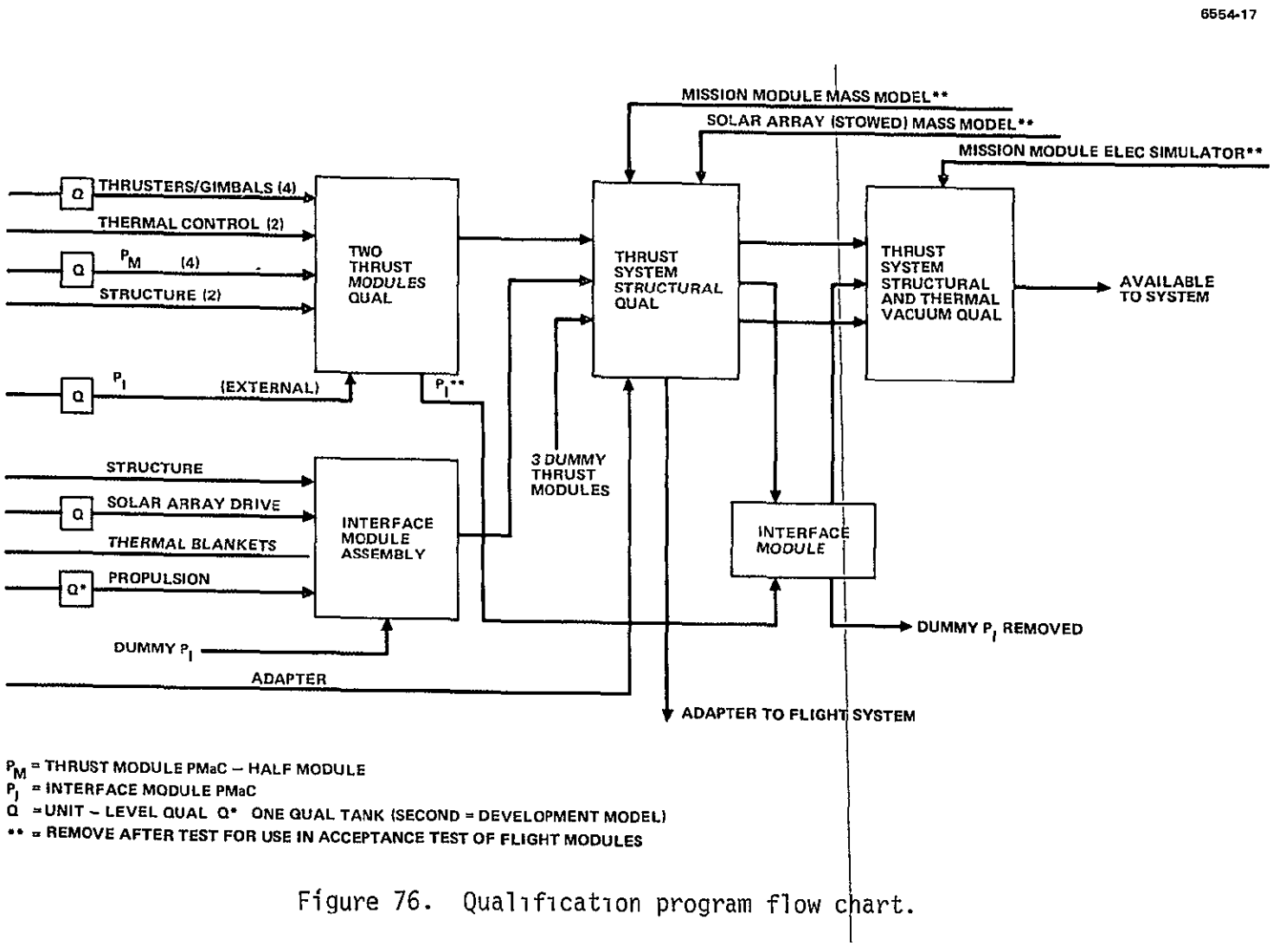

Figure 76. Qualification program flow chart.

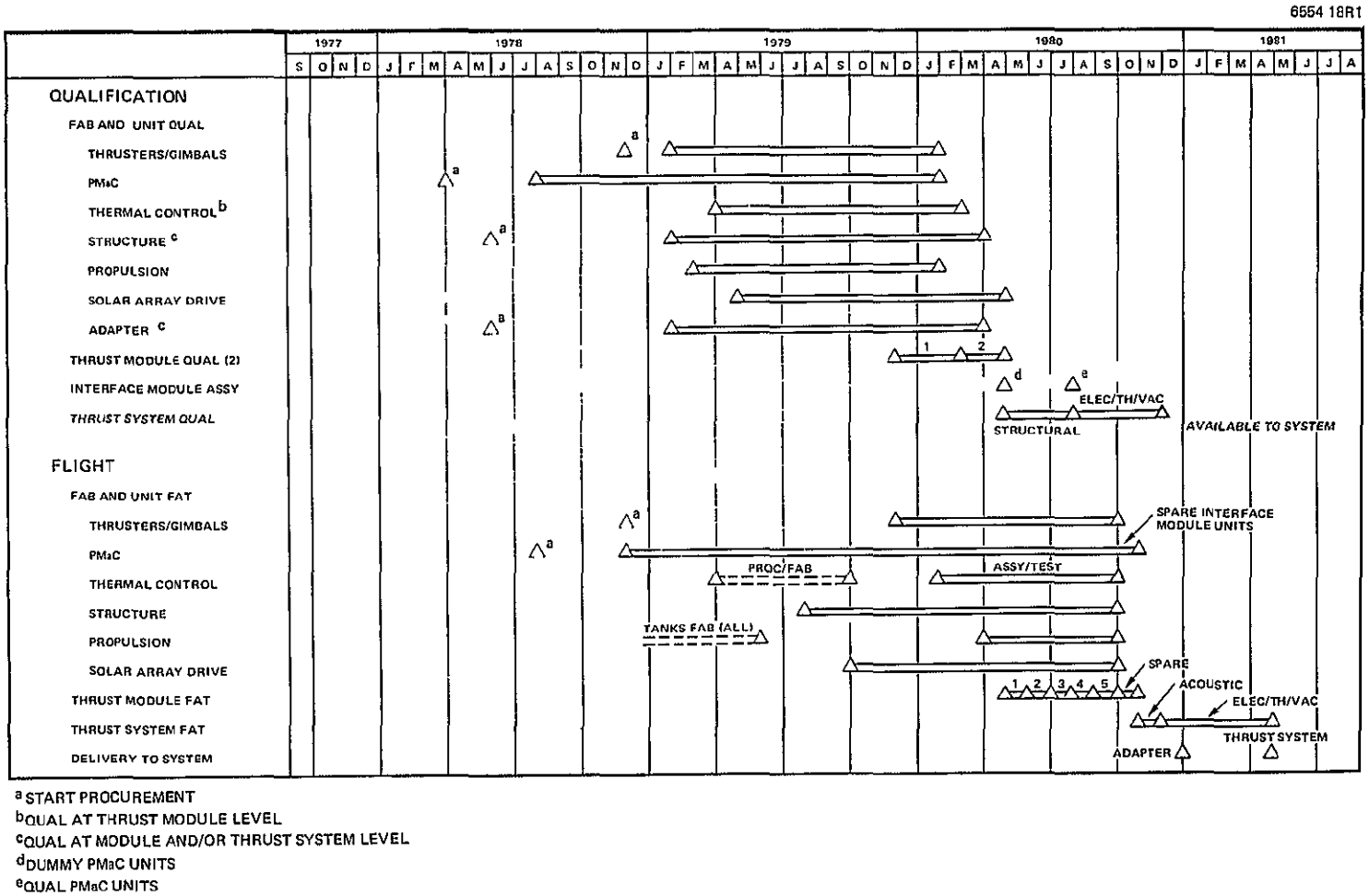

[a] START PROCUREMENT
[b] QUAL AT THRUST MODULE LEVEL
[c] QUAL AT MODULE AND/OR THRUST SYSTEM LEVEL
[d] DUMMY PMaC UNITS
[e] QUAL PMaC UNITS

Figure 77. Qualification and flight system schedule.

Using the electronic units in the qualification tests would preclude their being used for flight without first being reconditioned, and schedule considerations do not allow time for such reconditioning. Furthermore, this plan calls for the qualification thrust system to be delivered intact to the spacecraft immediately after the qualification program. Therefore, we propose that a separate set of flight units and flight spares be procured for the flight system. The significant exception to this proposal is the beryllium adapter, which is to be delivered and used in the flight system after the structural qualification program is completed.

F FLIGHT SYSTEM PROCUREMENT AND TESTING

The procurement, fabrication, assembly, and testing steps for the flight system and flight spares are indicated in the flow diagram in Figure 78 (the corresponding schedule is shown in Figure 77) This procurement and testing program will begin shortly after the qualification program because of schedule pressure, but with a sufficient lag to allow modest changes resulting from the qualification program to be incorporated; major design changes could not be made in the time allotted, however.

The flight acceptance test (FAT) program sequence is similar to the qualification program sequence, except that the test configurations and levels of testing are significantly different. Units and modules will undergo the FAT program at lower levels of environmental exposure All five modules will be tested, one additional complete module, which will serve as a flight spare, will also be tested The qualification model interface PMaC electronics will be used to acceptance test these flight modules before the flight model interface PMaC electronics become available. A single-string set of spare interface module PMaC units will also be fabricated and tested. At the thrust system level, the structural FAT program will be conducted on the completely assembled flight configuration (including the adapter and the mission-module and solar-array mass models), but an acoustic environmental exposure is deemed adequate The subsequent electrical and thermal vacuum testing of the thrust system will essentially be identical to that performed earlier on the qualification thrust system.

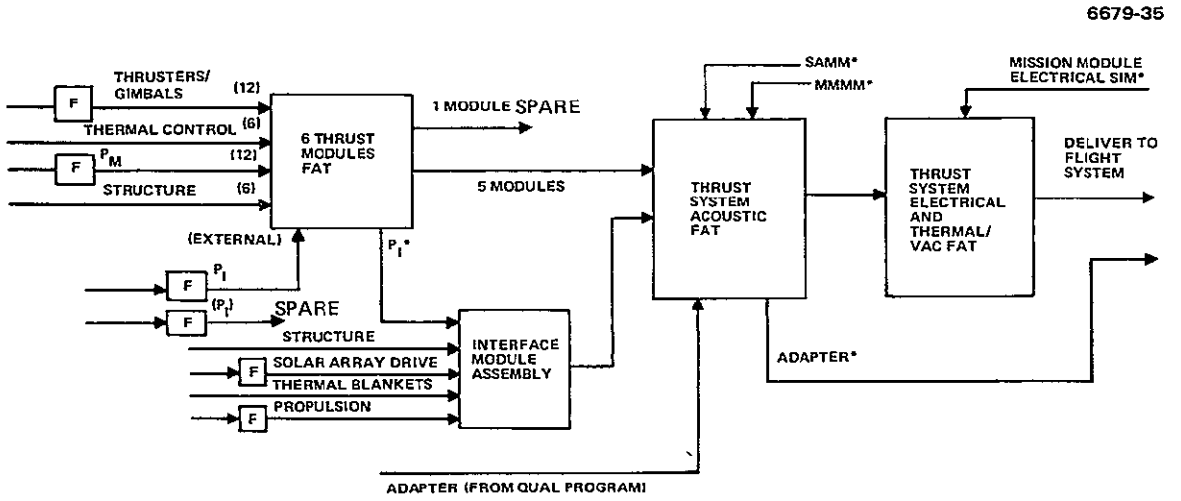

F = UNIT – LEVEL FLIGHT ACCEPTANCE TEST
P_M = THRUST MODULE PMaC – HALF MODULE P_I = INTERFACE MODULE PMaC
SAMM = SOLAR ARRAY MASS MODEL MMMM = MISSION MODULE MASS MODEL
(P_I) = SINGLE STRING P_I UNITS
* = REMOVE AFTER TEST

Figure 78. Flight system test and integration flow chart.

After the FAT program is completed, the thrust system will be delivered to the spacecraft for integration, testing, and launch The adapter will be available earlier – after the system acoustic FAT program is completed.

The required units and subsystems are summarized in Table 42. The required types and quantities of the principal units of the thrust system are indicated, these reflect the specific requirements of the program plan. The proposed plan for spare parts is also indicated in Table 42. It includes the assembled unit; module flight spares, and spares planned to be procured at the piece part and subassembly level. Table 42 also shows the dummy models of thrust system components required for the various test configurations, and the postulated GFE simulators and mass models.

G. FACILITIES PLAN

To implement the proposed program plan will require highly specialized vacuum test facilities for the development testing, qualification testing, and FAT of the thrust system components (thruster/PMaC electronics), the thrust system modules, and the full thrust system assemblies. The problem is compounded by the schedule-dictated requirement for parallel testing, by the physical size of the thrust system, and by the fact that not all of the potential facilities would be made available for use with mercury. In addition, vibration and acoustic facilities are required for the thrust system structural qualification and flight acceptance tests, respectively.

Facility requirements are further deterrents to performing thrust system qualification testing at the spacecraft level because it would be difficult to provide the much larger chamber required There is a readily available chamber for the electrical/thermal vacuum tests of the thrust system alone – the "Tank 6" facility at NASA LeRC.

Many suitable vibration and acoustic facilities are available for thrust system structural tests The proposed facility plan for electrical tests at the unit, module, and thrust system levels is shown in Figure 79. Two existing Hughes facilities should readily be able to accommodate the

Table 42. Required Units and Subsystems

Units/Assemblies	Quantities[a]					Piece Parts/ Subassemblies (Spare)
	Developmental		Flight Quality			
	B	D	Q	F	Spare	
Thrust system subsystems						
thruster/gimbal	-	4	4	10	2	1 full, plus 4 ea CIV, MIV, NIV, grid set
PMaC thrust module set (one beam/discharge/LV supply)	1	4	4	10	2	30% extra parts for all units
PMaC interface module	1[b]	1[b]	1	1	1[b]	30% extra parts for all units
Structure thrust module	-	2[c]	2	5	1	Tubes (50% of module)
Structure interface module	-	1[d]	1	1	-	Tubes (50% of module)
Thermal control	0.5[e]	1	2	5	1	30% extra pipes, one extra set all else
Tanks	-	1	2[f]	2	1	
Solar array drive	-	1	2	2	1	
Propulsion lines	-	0.5	1	1	-	One set
Adapter	0.25[g]	1[h]	1	(1)	-	50° tubes
Dummy						
Thruster (electrical simulation[i]	-	4	-	-	-	
Thrust module (mass model)	-	3[j]	3	-	-	
PMaC interface module (mass model)[k]	-	-	1	-	-	
GFE						
Mission module electrical simulation	-	1 ⟶	(1)	⟶(1)	-	
Mission module mass model	-	-	1	⟶(1)	-	
Stowed array mass model	-	-	1	⟶(1)	-	

[a] B - Breadboards or equivalent development assemblies
D - Development models (nonflight) — e g , electrical PMaC models
Q - Qualification models (flight quality) — "engineering models"
F - Flight units/assemblies

[b] Denotes single string

[c] Aluminum

[d] Aluminum

[e] Life test (half module)

[f] One to unit qualification burst test (D-tank installed on system qualification)

[g] Static (one tripod)

[h] Aluminum (articulation tests)

[i] For electrical system model

[j] Aluminum

[k] Flight simulation

5903

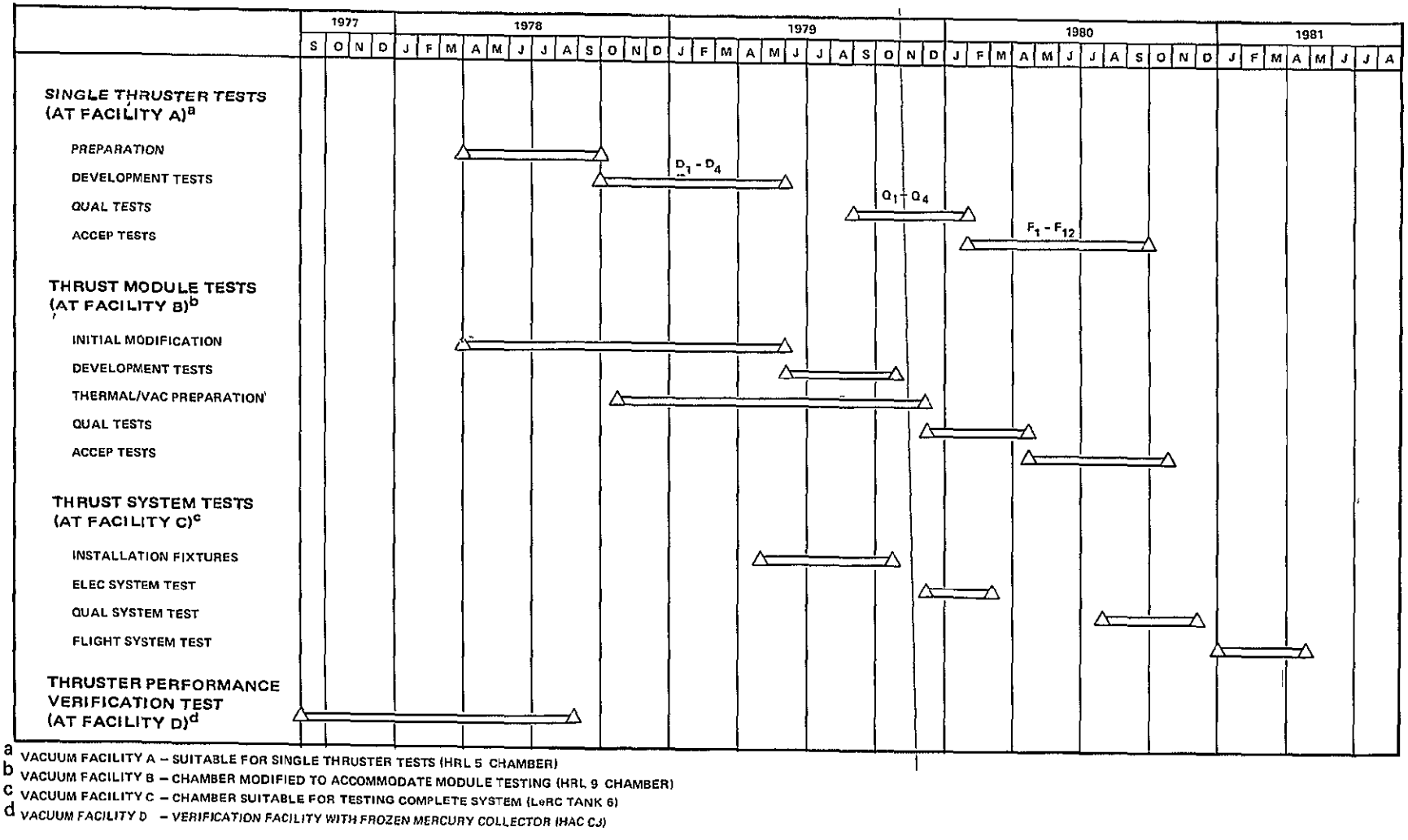

a VACUUM FACILITY A – SUITABLE FOR SINGLE THRUSTER TESTS (HRL 5 CHAMBER)
b VACUUM FACILITY B – CHAMBER MODIFIED TO ACCOMMODATE MODULE TESTING (HRL 9 CHAMBER)
c VACUUM FACILITY C – CHAMBER SUITABLE FOR TESTING COMPLETE SYSTEM (LeRC TANK 6)
d VACUUM FACILITY D – VERIFICATION FACILITY WITH FROZEN MERCURY COLLECTOR (HAC CJ)

Figure 79. Test facilities plan

parallel unit-level and module-level tests with only minor modifications The proposed schedule overlap is sufficient to allow these two facilities to be used efficiently and sequentially. To use the NASA LeRC "Tank 6" facility proposed for tests at the thrust-system level would require only that a suitable mounting adapter be provided. Scheduled phasing would permit the efficient, sequential use of this facility for the thrust system development, qualification, and FAT programs. The fourth facility shown in Figure 79 is currently available at Hughes and is used for laboratory tests of ion thrusters, this facility could be used to conduct the proposed thruster performance verification tests early in the program.

The proposed facilities plan, admittedly predicated on the assumption that the Hughes Aircraft Company will be responsible for thrust system development, is not a unique solution. But it does indicate that at least one solution is available for implementing the proposed program plan.

H RECOMMENDED THRUST-SYSTEM PROCUREMENT AND MANAGEMENT PLAN

The recommended thrust system procurement and management plan, presented in Figure 80, is consistent with the ground rules in Section 4.A.1, with the requirements for advanced development and procurement in Section 4 A 3 and with the other features of the program plan This figure illustrates that a viable procurement structure is available and makes recommendations regarding the assignment of responsibilities Admittedly, alternate procurement plans are possible

The recommended plan for a complete thrust system was developed under the supervision of NASA LeRC within the program schedule, starting with the contract award 1 April 1978. Advanced development and procurement requirements will be met by early, direct funding and management by NASA LeRC, these programs can then be phased at suitable times, as indicated in the program plan, to the responsible thrust system contractor

We recommend that the prime contractor for the thrust system be directly responsible for the specific areas indicated. This recommendation reflects the general ground rules discussed in Section 4 A.1.

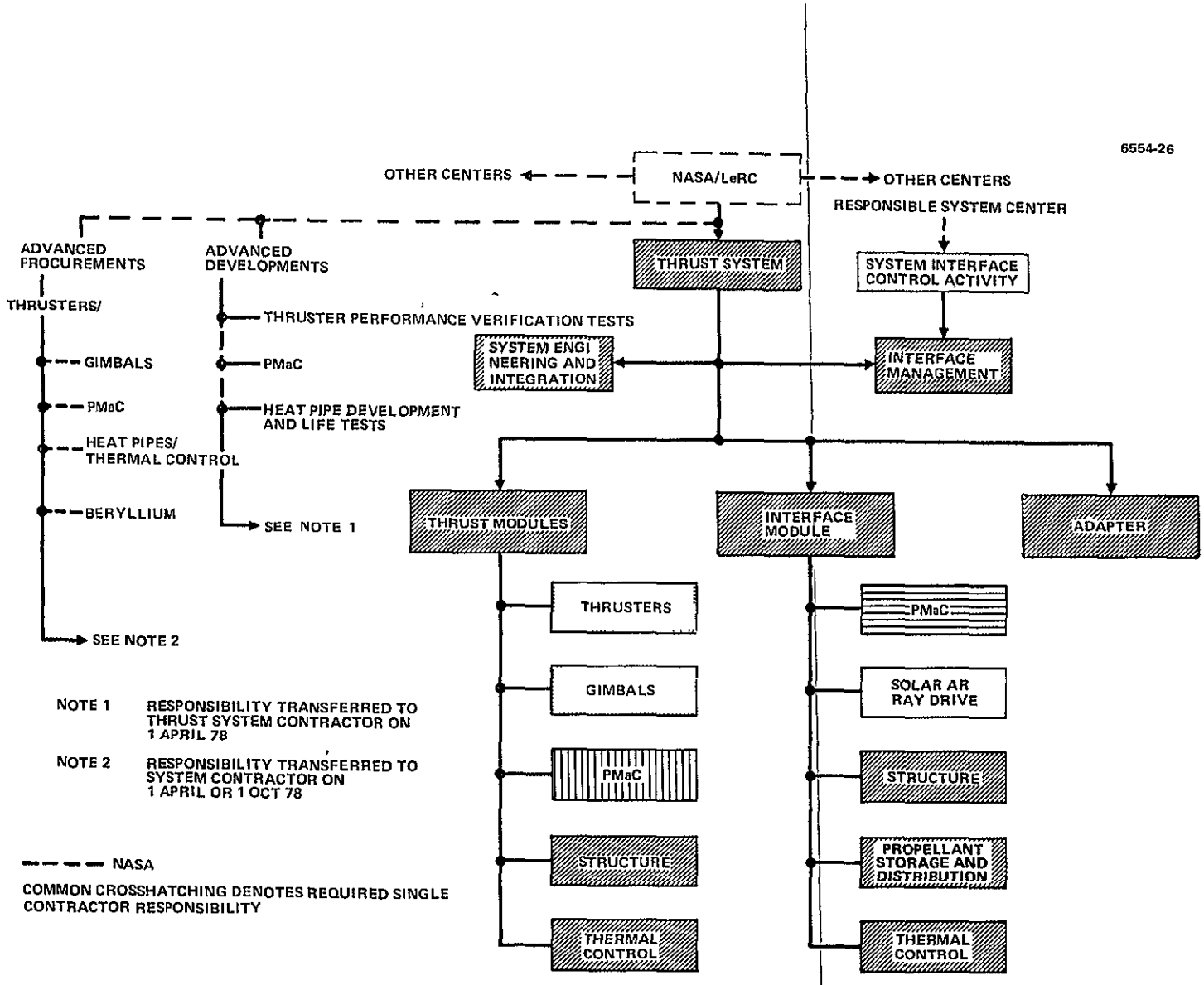

Figure 80. Recommended thrust system procurement and management plan.

We also recommend that special attention be paid to system interfaces. This is reflected in the proposed central system interface control activity and in the centralized thrust system interface management group, this group must coordinate the communication of system interface specifications.

I SUBSYSTEMS DEVELOPMENT AND PROCUREMENT SCHEDULES

Level 3 schedules were generated for the major subsystems thruster gimbal, PMaC, structure, mercury propellant, solar array drive, adapter, and thermal control. The individual schedules reflect the overlapping development/qualification/flight-procurement phases of the program and give delivery dates for the assembled and tested subsystems. The schedule for the PMaC subsystem is the most critical one from the standpoint of advanced development and procurement requirements; it is presented in three parts to highlight the rationale for an early start to design work and parts procurement.

1 Thruster and Gimbals

The development and procurement schedule for the thruster gimbal subsystem is shown in Figure 81. The schedule indicates the required 1 September 1977 start of performance verification tests using the modified 900-series 30-cm EMT (to be furnished by the government). These tests will more completely specify the thruster design modifications (to ion optics, high-voltage isolators, etc.) needed to satisfy the requirements of the Halley's comet mission. The plan for developing the thruster and gimbal assemblies and for documenting the flight program begins with the design, fabrication, and testing of four developmental thruster/gimbal assemblies. The initial design will be based on the 900-series EMT design (as defined on 1 January 1978 on the testing of the indicated verification tests and of the results from the ongoing NASA LeRC programs)

The design effort under the development phase of the project will begin by upgrading the design documentation package to meet standards appropriate to a flight project A primary objective of this phase of the program is to establish the specifications and the documentation, fabrication, and test procedures needed for the qualification of the

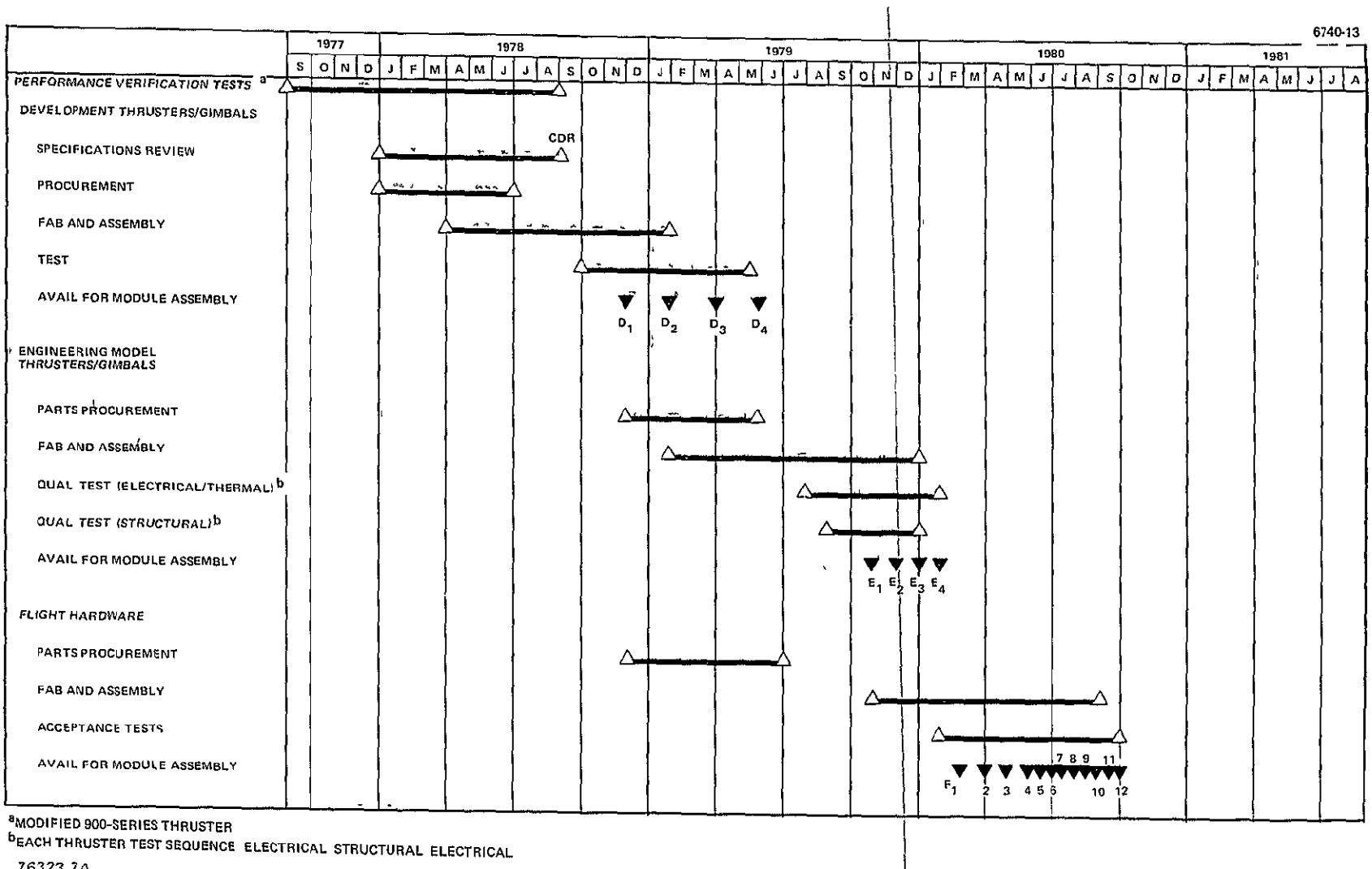

Figure 81. Development and procurement schedule for thrusters/gimbals.

thruster/gimbal assemblies. The design will be critically reviewed before the first developmental thruster/gimbal assembly is completed to evaluate all the results of the verification tests as they affect the design of the assembly The design will be considered frozen after the recommendations from this design review have been implemented Test electronics used during this development phase will be standard laboratory equipment; the test results will be used to assist in formulating procedures for qualification and flight-acceptance testing.

During the program's developmental phase, the parts needed to fabricate the qualification and flight hardware will be procured making use of the improved design documentation package. This procurement activity is phased to allow the first developmental thruster/gimbal assembly to be completely evaluated The fabrication and assembly of qualification hardware will begin as soon as parts procurement permits, with formal qualification testing beginning as the first assemblies become available. Special test equipment will be constructed from breadboard PMaC power supplies for the qualification tests If this test equipment is not available soon enough to avoid a substantial delay, laboratory equipment could be used for the qualification testing of the thruster/gimbal assemblies Qualification testing will include thermal-vacuum operational tests, performance evaluations, and structural and vibrational tests.

As soon as it is apparent that the thruster/gimbal design is able to pass qualification testing, assembly of flight hardware will begin. The thruster/gimbal assemblies will initially be produced at the same rate as are the qualification assemblies (one assembly per month) As production personnel become more familiar with the flight hardware documentation and acceptance testing procedures this rate will be increased (to two or more per month). This program phase will be complete when 12 thrusters for the thrust module assembly have been delivered.

a. PMaC

The PMaC development and procurement plan is defined in Figures 82, 83, and 84 for, respectively, the thrust module components (beam, discharge, and low-voltage supplies), for the interface module components other than controller (the distribution inverter, the dc/dc converter, the power distribution units, and the solar array control unit), and for the PMaC controller. Because the PMaC schedule is so tight, it is necessary that the effort begin on 1 September 1977 with advanced circuit design work and parts procurement. Major milestones within the program plan include designing the breadboard circuits for all units, fabricating the developmental unit (according to flight drawings), and fabricating and testing the qualification and flight units.

Designing the breadboard circuits for the PMaC units will involve defining the design and test requirements. This task must be closely integrated with the system analysis tasks. Therefore, the system characteristics and the interface parameters of the mission module must be defined quickly because they are needed for the latter task. The development of the software needed for the PMaC controller is scheduled to begin on 1 January 1978 (it is assumed that the characteristics of the interface module will have been adequately defined by then)

The circuit design and analysis leading to breadboard fabrication includes the specification of the physical and electrical performance requirements and the environmental requirements for both the qualification and acceptance levels. Breadboard tests are used to verify performance and to analyze electrical and thermal stress and failure modes. Figure 82 calls for an integration test of PMaC units with the thruster to follow the level unit tests of the PMaC module breadboards. This will be the first verification of the electrical compatibility (interaction) between the PMaC system and the thruster in the various operational modes required for the mission. After the breadboard tests, the breadboard units will be used in the assembly of the thrust system test equipment.

Breadboard development will be followed, with some overlap, by the fabrication and assembly of development models. Four sets of thrust module development models are shown in Figure 82 (as required by the master program plan). Development units will be fabricated to flight

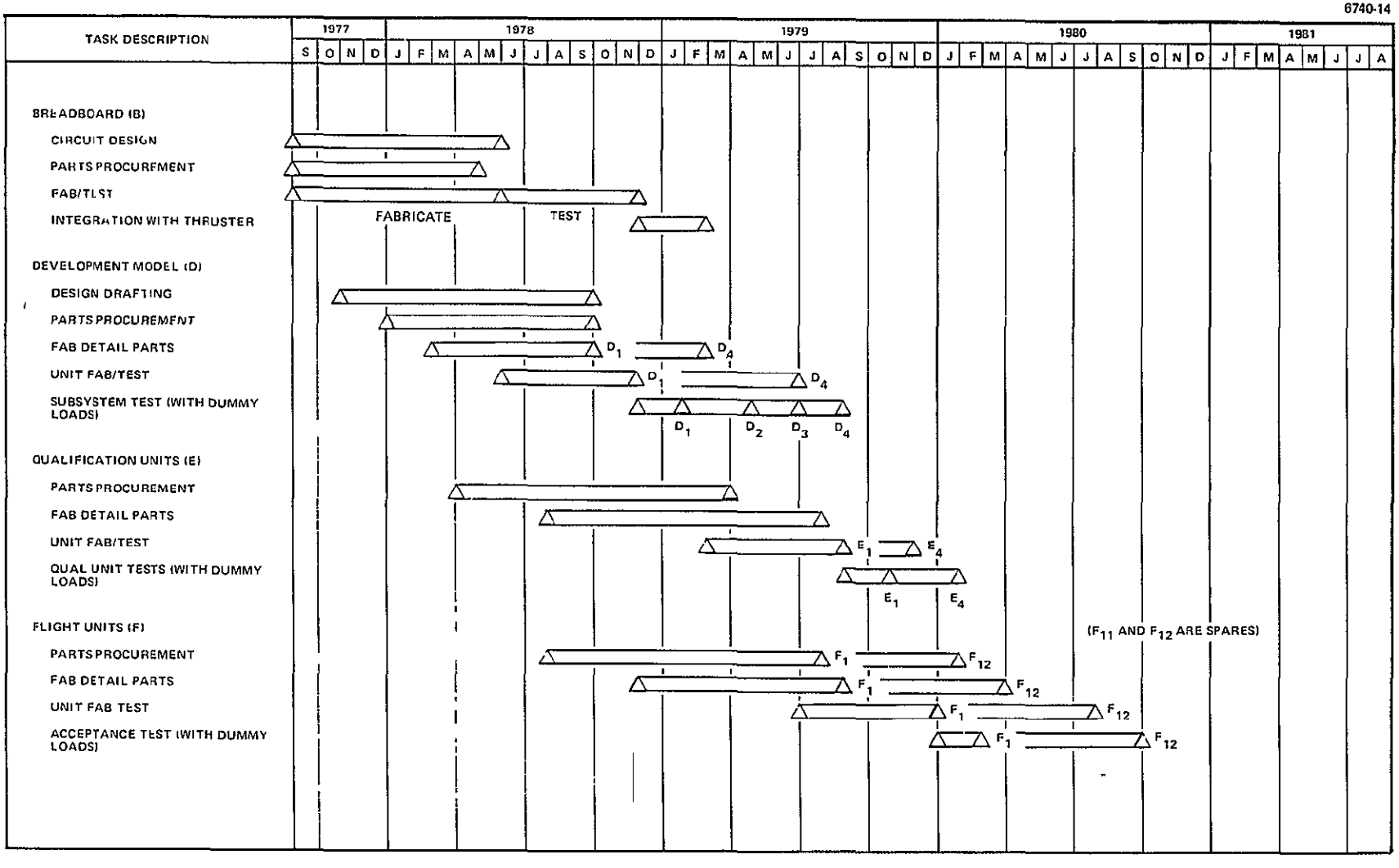

Figure 82. PMaC thrust module development and procurement schedule

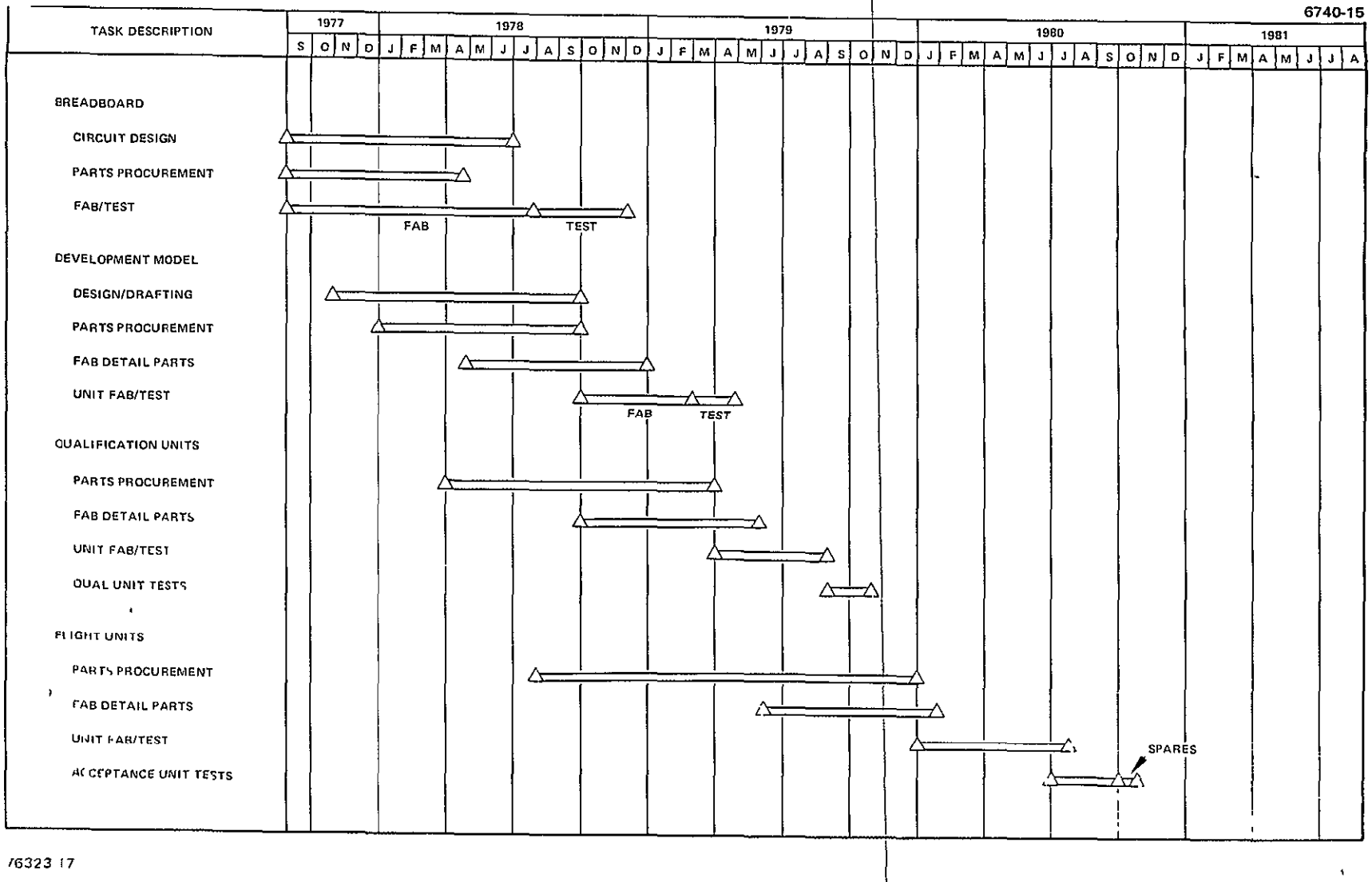

Figure 83. PMaC interface module less controller development and procurement schedule.

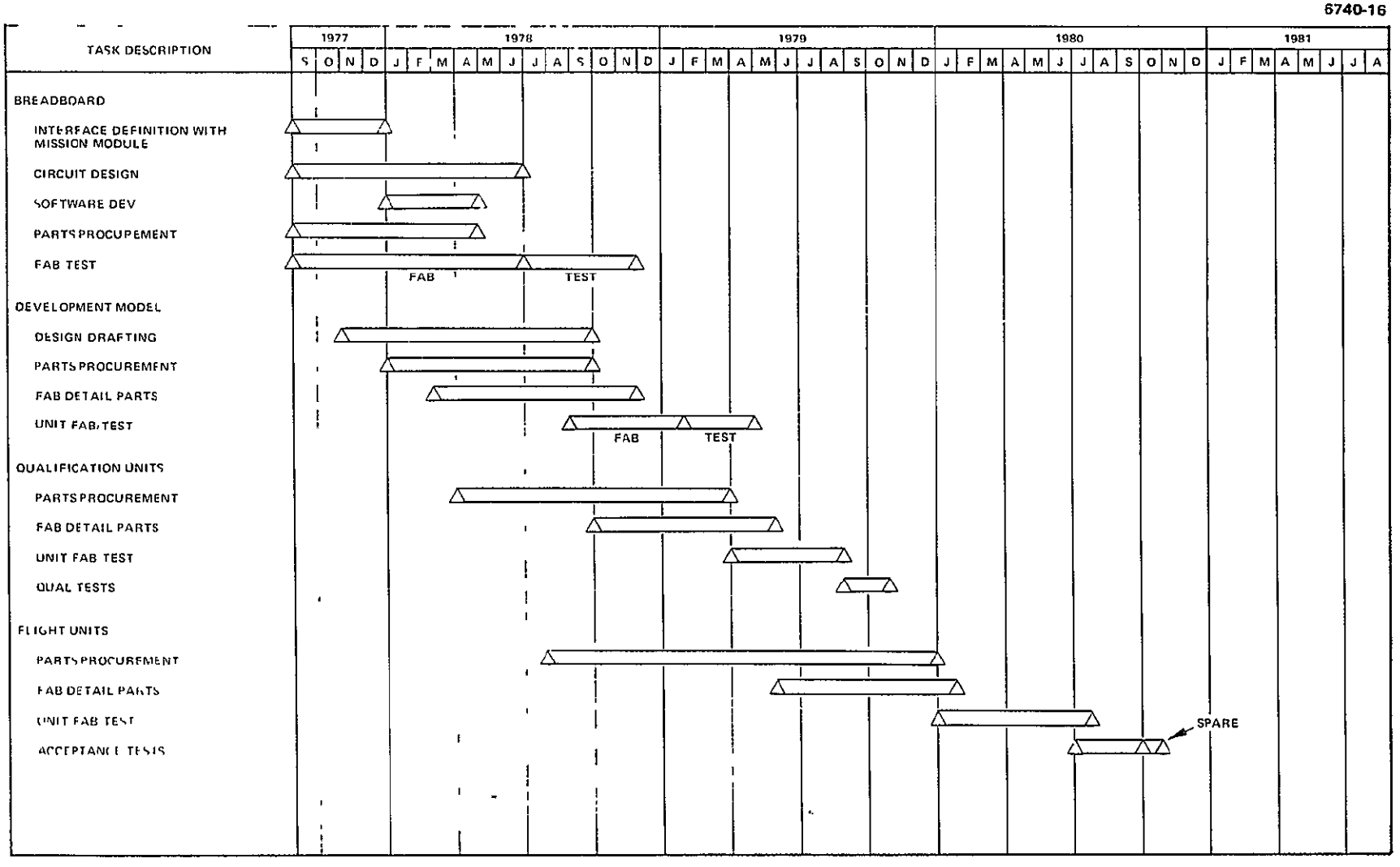

Figure 84 PMaC controller development and procurement schedule.

drawings using commercial components. Subsequently, four sets of qualification units, followed by 12 sets of flight units, will be fabricated and tested. The overlap between these fabrication, assembly, and testing operations is limited to the extent that at least one of the preceding sets (e.g., development before qualification) will be tested before the assembly of the next-level set is begun; this will allow sufficient time for any design changes to be incorporated in the subsequent set. The 12 sets of thrust module flight units will be assembled and tested within an 8-month period at the following rate: 1 per month for the first 4 months, and 2 per month for the last 4 months. This schedule, which allows ample time to meet the project schedule, takes advantage of the experience gained during the initial fabrication period. Before the system is delivered, each unit will undergo extensive tests at the unit level. Development units will be subjected to full environmental testing, except for structural vibration (since commercial parts are used). Qualification models undergo full structural and thermal vacuum testing. Flight units will undergo full acceptance-level testing. Extensive EMI tests will also be conducted at each phase of development.

Figures 82, 83, and 84 also highlight the parts procurement problem. Advanced procurement of critical parts, such as ICs, must start as early as 1 September 1977, even for flight units, some advanced procurement is required before the 1 October 1978 start of program acquisition phase.

3. Structure, Propellant Storage and Distribution

Level 3 schedules for the development, fabrication, and testing of the structural subsystems, harness, mercury propellant subsystem, solar array drive, and adapter are shown in Figure 85 and 86. No significant scheduling problems are anticipated in complying with the milestones in the master phasing schedule, and no advanced development or procurement will be required before the 1 April 1978 and 1 October 1978 start dates. There is only one possible exception: beryllium procurement may need to be begun several months before 1 October 1978 to ensure against potential slippage The reason that advanced beryllium procurement may be needed is that only one vendor who is capable of providing beryllium tubes of the required size has so far been identified

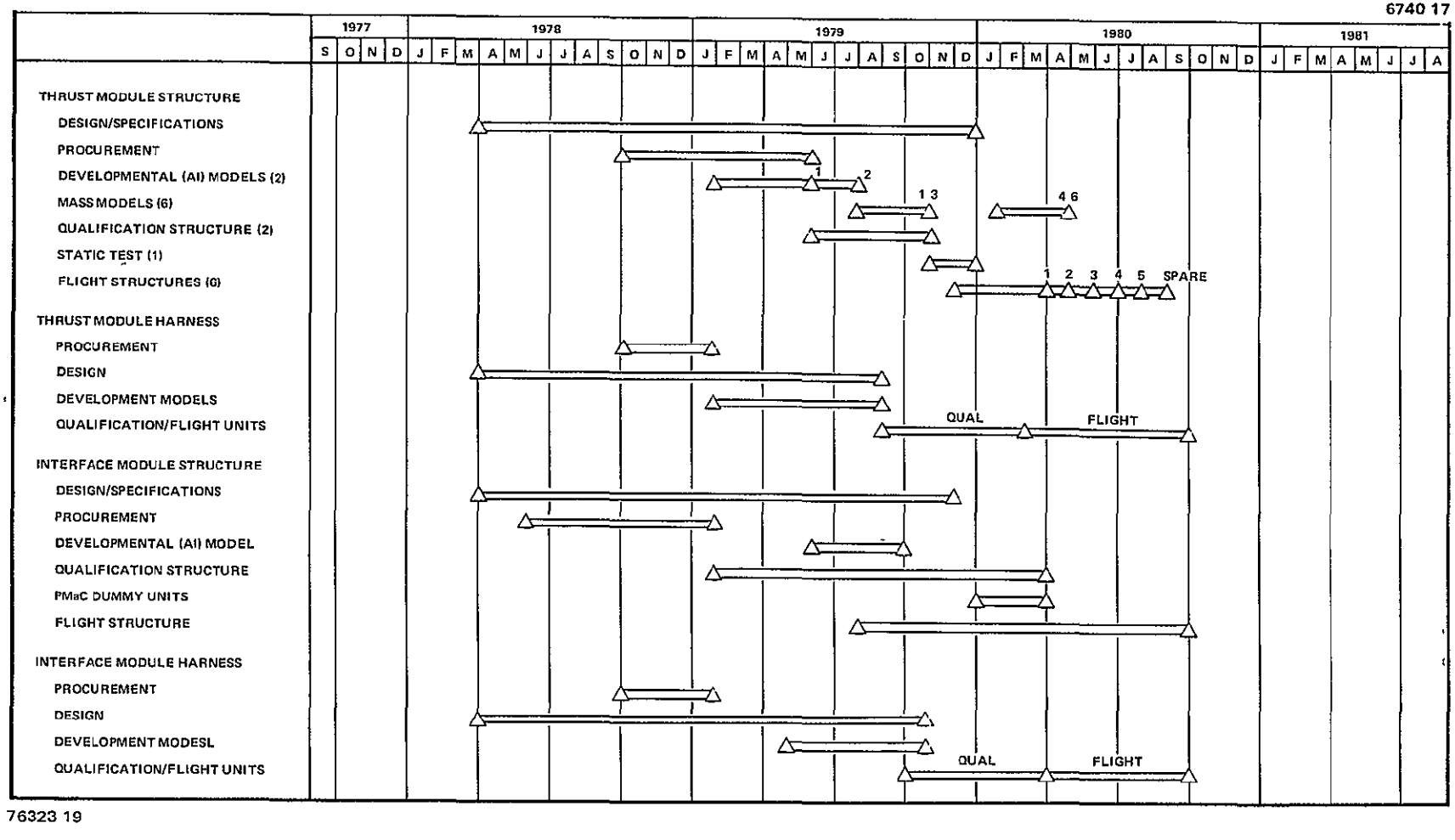

Figure 85 Development and procurement schedule for the structures and harness.

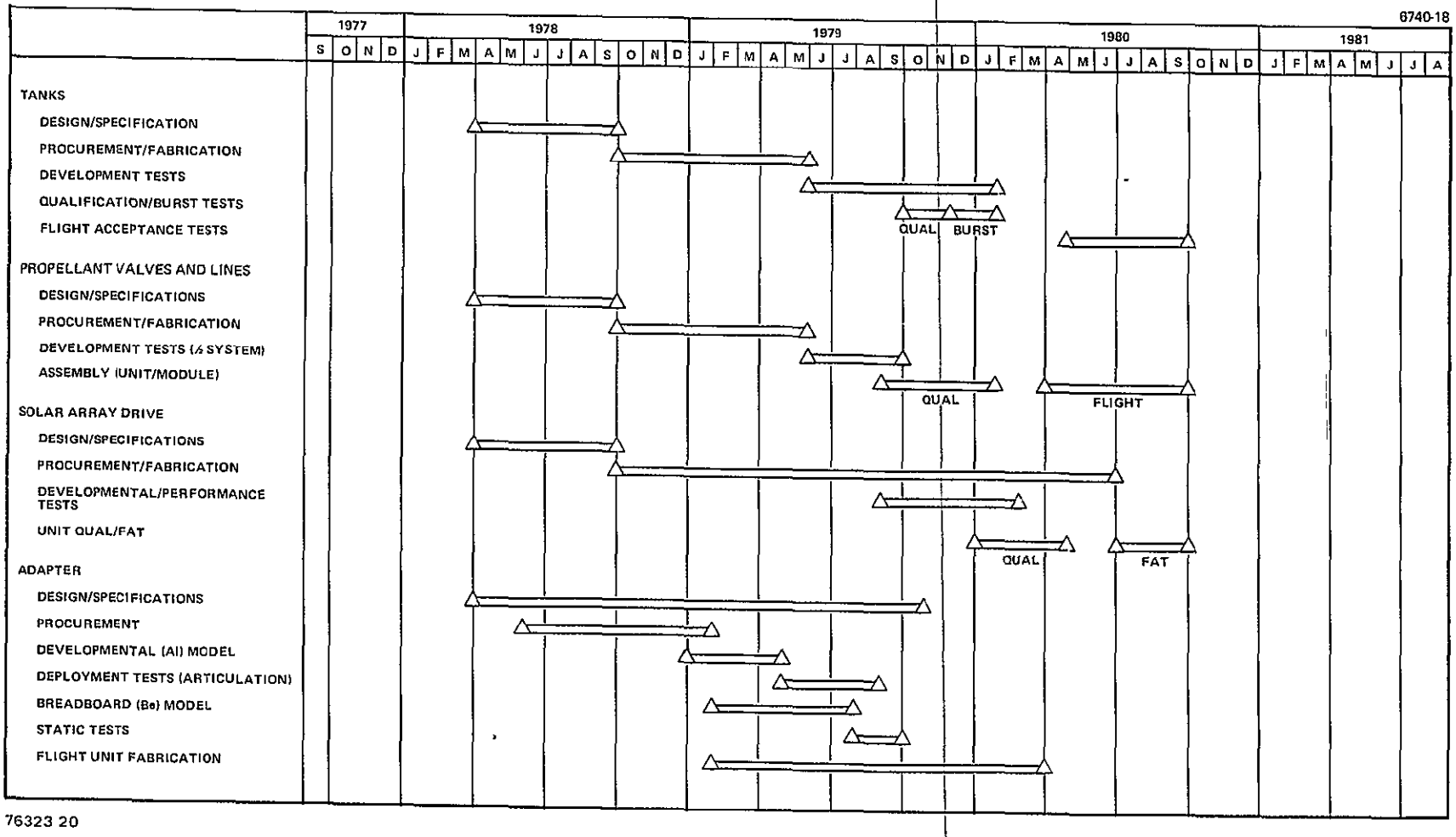

Figure 86. Development and procurement schedule for the propellant storage and distribution system, the solar array drive, and the adapter.

A final decision on the procurement date will have to await further investigation.

Accordingly, Figure 85 and 86 show the start of the design and specifications effort on 1 April 1978, also the development and procurement stage is scheduled to begin concurrent with the acquisition phase on 1 October 1978.

The structure, harness, and adapter design phases consist of designs, definition load analysis, and the analysis of all interfaces. This effort will culminate in the definition of the design and interface specifications. Detailed drawings for development parts will be released for parts procurement. All engineering development will virtually be complete before manufacturing begins. During this phase, a preliminary dynamic math model will be developed for the subsequent load analyses. Preliminary loads, which will be obtained two months after beginning this phase, will be used to establish the diameter and thickness of the beryllium tubes An uncertainty factor will be added to allow for load increases, pending results of coupled analysis. After the size is finally specified, the beryllium tubes will be chemically-milled to the appropriate thickness.

Development tests will be identified in key design areas during the development phase. The joint between the beryllium tube and the aluminum socket used on the adapter will be tested to demonstrate the structural adequacy of the bonded joints. Column buckling tests will be performed on the beryllium tubes to determine the effects of manufacturing eccentricities on column stability and to establish knockdown factors for column allowable loads. Test specimens will be fabricated to demonstrate the attachment of stainless-steel heat pipes to aluminum thermal radiators and the construction of honeycomb sandwich cold plates. A development model of a single adapter tripod (one fourth of the complete adapter) with aluminum tubes will have been designed and fabricated by 1 September 1979. This test model will be used to demonstrate the separation system and the deployment of the tripod after separation. These tests will reveal functional anomalies and clearance problems before the flight hardware is assembled. An additional single adapter

tripod will be fabricated to flight quality and static tested to demonstrate its strength and to verify stiffness predictions. This assembly will serve as a prototype for fabricating flight parts.

A partial thrust system will be fabricated and delivered on 1 November 1979 for electrical system tests This vehicle will consist of an interface module with aluminum truss tubes, two development thrust modules with aluminum tubes, and three aluminum dummy thrust modules. Since this system will only be used for electrical tests, it need not possess the strength and stiffness of the flight parts. A complete set of dummy PMaC interface module units for simulating mass will be fabricated These will have package dimensions and attachment provisions that are representative of flight hardware. The dummy modules will be fabricated to be interchangeable with their flight counterpart units

The schedule for the delivery of the mercury propellant subsystem (shown in Figure 86) reflects the design, development, qualification, and flight procurement sequence. No major schedule difficulties are anticipated. The first mercury tank is scheduled to be delivered about 32 weeks after the award of the contract (1 July 1979). Activity during the first 32 weeks of Phase II will consist of design definition, forging and diaphragm procurement, welding and machining, and assembly. The first tank, designated as the development tank, will be the prototype for the fabrication and assembly of the remaining tanks. The second tank will be designated as an engineering model It will be subjected to qualification-level vibration environments and destroyed by burst pressure. Another engineering model, two flight units, and one spare tank will also be assembled. The engineering and development tanks will be installed on the thrust system structural qualification model. Acceptance testing will be performed on the flight hardware at the unit level. Subcontracts for the units of the other propellant subsystem units (lines, valves, solenoids, etc.) will also be awarded during the first three months of Phase II. Qualification and acceptance vibration testing will be performed on all units. Thermal-vacuum tests will also be run at the unit level on the valves A complete interface module

(including two tanks filled with mercury) and two thrust modules will be installed on the thrust system structural qualification model.

The schedule for the solar array drive also calls for the design specification to be developed during the design definition phase. Six solar array drives will be fabricated during the acquisition phase. The first will be used for development tests, (including extended duration testing). Two engineering models will undergo unit qualification environmental testing, and will later be integrated into the thrust system qualification model. Three solar array drives will undergo acceptance-level tests; of the three, one will become a flight spare.

4. Thermal Control

The Level 3 thermal control program plan (shown in Figure 87) is structured around the completion of the following main items: design and analysis of the thermal control system, procurement and life testing of the heat pipes, development testing of the VCHP/radiator assembly and of the interface module blanket and support for the procurement and fabrication of flight and qualification thermal control hardware (e.g., MLI blankets and radiators).

The heat pipes must be ordered early because there will be a 6-month lead time between order and delivery of VCHPs. To establish specifications for the initial VCHP order, interface requirements and thermal control performance will be estimated. Throughout the six-month delivery period, the VCHP supplier will be monitored by the contractor for the thrust system Before delivery, the supplier will perform acceptance and qualification tests on the VCHPs. The development phase will start three-months after the initial VCHP order has been placed During this phase, mission environmental conditions will be defined, the thermal control system will be designed and analyzed, and life and development tests will be conducted Environmental definition, the first step of this phase, consists of establishing thrust system dissipations and operating modes, allowable temperature limits, and interface temperatures and couplings for the mission module and solar array Thermal control analysis and design, which will start at the

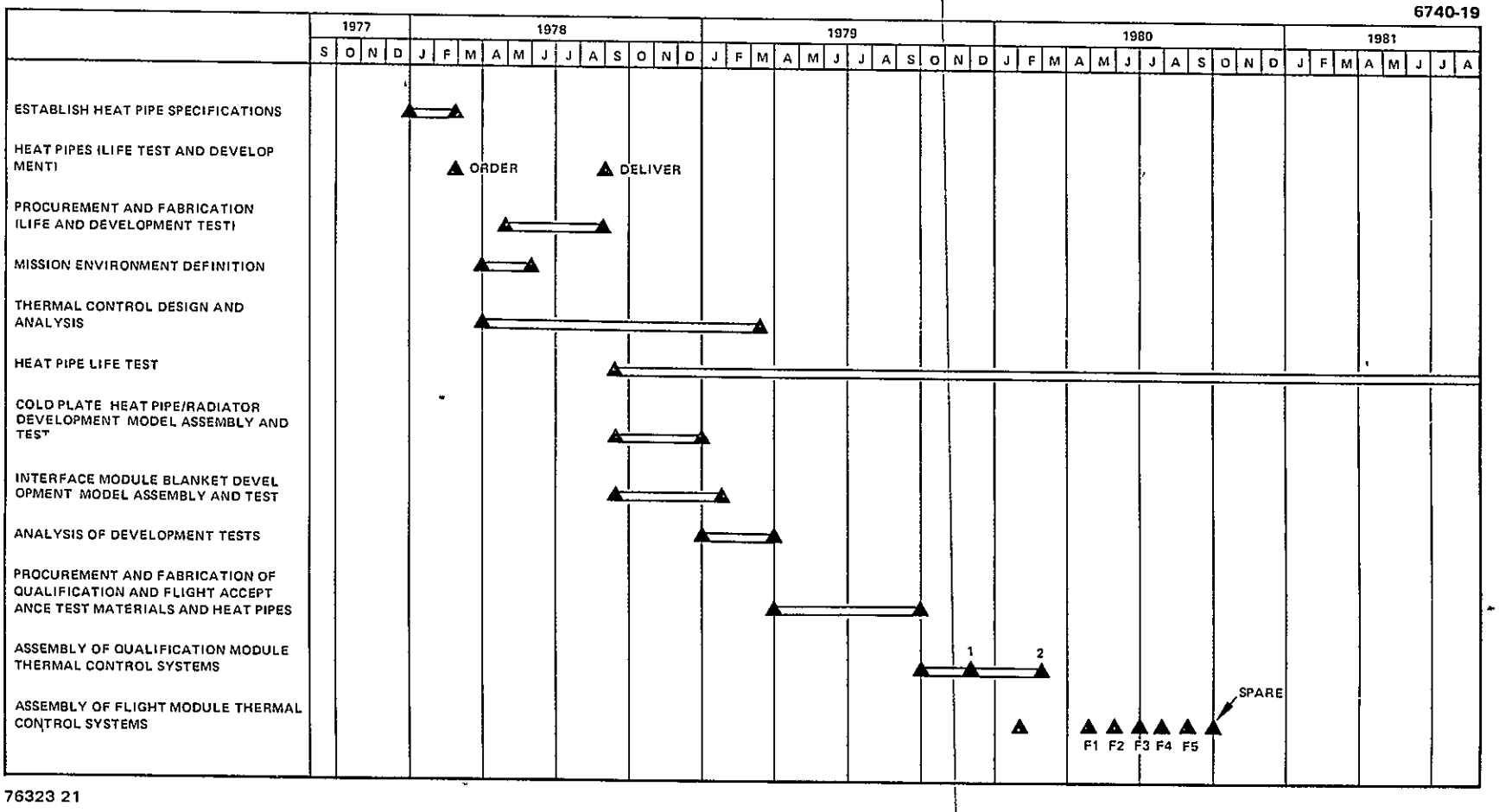

Figure 87. Thermal control development and procurement schedule.

beginning of the program, will culminate in the development of subsystem design requirements; these in turn, will define the development tests.

VCHP life tests will begin shortly after delivery of the first VCHP. These tests, intended to verify long life characteristics of the VCHPs, will consist of steady-state heat input to the VCHP evaporators with convective heat rejection to the laboratory ambient. VCHP temperature distribution will be measured Four VCHPs are to be tested at different temperature levels about the nominal design value to obtain accelerated test data.

Thermal control development tests, which will follow the life tests, will comprise interface-module-blanket and heat-pipe-radiator tests. Results of these tests will be used to verify the designs, and the analytical thermal models and, if necessary, to upgrade specifications for the second VCHP order.

Tests will be conducted to measure the performance of the blanket on the interface module and to verify the adequacy of the blanket design The data obtained will be used to upgrade the representation of the blanket in the analytical thermal models and will be an input into the VCHP/ radiator development tests. The blanket development test will be a thermal simulation of the interface module, with a thermal representation of the mission module boundary condition. Flight design MLI blankets will be tested. The cold plates and truss structure will represent the flight design geometrically and thermally. PMaC units located on the cold plates will be represented by electrical heaters. The test will be conducted in a thermal-vacuum chamber. The range of operating conditions over the mission will be simulated by setting the temperature of the cold plate at the required maximum and minimum temperatures and by varying the temperature of the mission module to cover the range of uncertainty. The heater power required at each temperature will then be measured to determine the performance of the blanket.

Development tests of the VCHPs and radiator will be used to establish the maximum and minimum performance limits, validate the assembly procedure, confirm the thermal math models and the adequacy of the thermal control systems design, and evaluate thermal performance. The following performance parameters will be measured.

- Active radiator area
- Adequacy of VCHP spacing
- Interface ΔTs
- Full-off VCHP heat leakage
- Thrust module blanket effective emittance
- Heater adequacy.

The tests of the VCHPs and the radiator will be run on a full-size thermal simulation of one flight-configured thrust module. The mockup will consist of one cold plate, eight heat pipes, two radiators, and the truss structure and blankets for the thrust module. The thermal environment produced by the interface module, adjacent thrust modules, solar arrays, and ion thrusters will be simulated. The PMaC system and its layout on the cold plate are represented thermally by masses and electrical heaters. The test will be run with the VCHPs nearly horizontal and the evaporator ends slightly above the condenser ends to guarantee operation of the heat pipe.

Steady-state and transient of the operation thrust system will be simulated. Steady-state conditions to be tested include both the "hot" and "cold" design limits, which would be achieved by operating both thrusters or none of the thrusters, respectively. Transient tests will be conducted by simulating the start up and shut down of various combinations of thrusters.

The qualification and flight procurement phases following the development phase are shown in Figure 87. Ample time is available to produce the flight hardware required for the qualification modules and the flight units

SECTION 5

ESTIMATED PROGRAM COSTS

The program plan was the basis for estimating the costs of developing, procuring, and testing the thrust system, and the costs of meeting the associated support requirements. These costs, presented in this section, were compiled in accordance with the work breakdown structure (WBS) defined below; they were also compiled in terms of fiscal year funding requirements.

It was necessary to make several assumptions in estimating the costs. Given these assumptions and several NASA-specified ground rules, and considering Hughes extensive experience in estimating costs for space programs, a high degree of credibility can be assigned to these estimates. However, since portions of the proposed designs remain to be defined and since many uncertainties remain concerning the assumptions, program schedule, and the interfaces between the thrust system and other parts of the Halley's comet spacecraft, these estimates should be considered only approximate 10 to 20% uncertainty seems reasonable

A. ASSUMPTIONS AND GROUND RULES

All costs are given in FY 1977 dollars (with no accounting for the potential effects of inflation). All costs are presented at the "G&A" level, (i.e., full contractor costs excluding fee). The total costs in each category therefore include

- Direct labor, including overhead, at $4,400 per man-month
- Other direct charges (e.g., purchased parts, computer services)
- 10% G&A surcharge applied to total direct charges.

Thrust system development and procurement costs, compiled in accordance with the WBS, include advanced development, parts procurement, design, fabrication, assembly, and testing of all thrust system components at all levels through system integration and testing and in all phases of the program (i.e , development, qualification, flight

hardware fabrication). The data are also broken down (approximately) so as to distinguish between the development phase and the flight-qualification and flight-hardware-procurement phases.

Support costs include the costs for all the ground equipment and services necessary from inception through delivery to the spacecraft; thrust system support during spacecraft integration, testing, and launch operations; all interface activities with the launch vehicles (IUS and shuttle); and the necessary support fixtures (e.g., shuttle forward cradle for the thrust system) Nominal support during the mission is also included.

Thermal vacuum facilities — two at Hughes and one at NASA LeRC, the Tank 6 facility — government-furnished equipment (GFE), were assumed to be available for the testing required without cost to the program, except that costs of any required modifications to these facilities are included, as are any costs for their operation (including liquid nitrogen). Rental of structural test facilities (structural qualification at the module and system levels, and acoustic vibration of flight modules and of the thrust system) is included in the estimates. The mission module and solar array simulators and mass models and the 900-series EMTs modified for performance verification development tests are other principal items assumed to be furnished by the government (and not priced).

The program plan is based on the assumption that advanced development will begin on 1 September 1977. For convenience, the FY 1978 cost includes the funds required for September of FY 1977.

Other ground rules and assumptions used in making the cost estimates are discussed (in Section 5.3) with the specific cost elements. The WBS used for compiling costs defined in the cost summary tables in 5.B.

B. COST SUMMARY

Table 43 shows the WBS used in compiling the cost summary, and presents the results of cost estimates for each WBS item. The first eight WBS items (through structure and harness) correspond to the development, fabrication, and testing of the principal subsystems Design integration

includes assembly of the thrust system and associated engineering support operations.

The major system engineering function, the next WBS item, includes system design and specifications, all system-level analysis work, and all interface activities, as differentiated from the engineering activities at the individual subsystem levels that are incorporated in the preceeding WBS items Similarly, the system test activity, the next WBS item, pertains to tests at the module-level and higher This includes the activities of a system test team of preparing test setups, writing procedures, and conducting test operations. Test activities at subsystem levels (before the subsystems are integrated into modules) are also covered within the pertinent subsystem WBS category.

AGE costs include electrical and mechanical tests, handling equipment, and the procurement of the shuttle cradle. Facilities costs, as discussed in the previous subsection, include facility modifications, operations, and rentals Spacecraft test and integration covers support to the spacecraft from the time the thrust system is delivered until it is shipped to the launch base. Pre-launch operations cover the nominal functions of shipment, pre-launch operations and testing, integration with the launch vehicle, final installation, and countdown—Mission operations cover support costs following launch (estimated at five men for the first six months and one man thereafter). Program management functions include all the required management, administration, and control operations, as well as data management, interface management, parts control, procurement, contract and subcontract management, product effectiveness, and reporting. A more detailed description of the principal items covered in each WBS category are given in Section 4.B.3

Table 44 presents cost estimates for each WBS item and for the total program by fiscal year funding requirements. A summary tabulation is presented in Table 45. The advanced development requirements, discussed in Section 4 A, are reflected in the $13 4 million funding required during fiscal year 1978, and, from 1 September 1977 through 30 September 1978.

Table 43. WBS Cost Breakdown for FY 1977 (Rough Estimate Excluding Fee)

WBS Category	Development			Qualification			Total Cost, 10^6
	Labor		Other Direct Charges 10^6	Labor		Other Direct Charges 10^6	
	Man Months	10^6		Man Months	10^6		
Thrusters and gimbals	225	1 0	0 4	840	3 7	0 7	5 8
PMaC – thrust module systems	2160	9 5	0 1	1140	5 0	0 4	15 0
PMaC – interface module system	1320	5 8	0 1	460	2 0	0 2	8 1
Thermal control	115	0.5	0 4	225	1 0	0.6	2.5
Propellant storage and distribution	20	0 1	0 3	115	0 5	--	0 9
Solar array drive	70	0 3	0 1	20	0 1	0 1	0 6
Structural mechanics	180	0 8	0 1	70	0 3	--	1 2
Structure and harness	180	0 8	1 3	70	0 3	0.1	2 5
Design integration	20	0 1	--	270	1 2	0 1	1 4
System engineering	500	2 2	--	455	2 0	--	4 2
System tests	115	0 5	--	340	1 5	0 1	2 1
AGE	45	0 2	0 2	180	0 8	0 5	1 7
Facilities	--	--	0 1	--	--	0 2	0 3
Spacecraft test and integration	--	--	--	90	0 4	--	0 4
Pre-launch operations	--	--	--	45	0 2	--	0 2
Mission operations	--	--	--	70	0 3	--	0 3
Program management	750	3 3	--	730	3 2	--	6 5
Total	5700	25.1	3 1	5120	22 5	3 0	53 7

[a] Fee excluded

[b] Expressed in FY 1977 dollars

Table 44. WBS/Fiscal Year Cost Breakdown (Rough Estimate, Excluding Fee)

WBS Category	FY 1978[a,b]	FY 1979	FY 1980	FY 1981	FY 1982	FY 1983	FY 1984	FY 1985	Total
Thrusters and gimbals	0 7	2 2	2 9	--	--	--	--	--	5 8
PMaC — Thrust module systems	5 2	6 0	3 8	--	--	--	--	--	15 0
PMaC — Interface module system	2 8	2 8	1 7	0 8	--	--	--	--	8 1
Thermal control	0 6	1 5	0 4	--	--	--	--	--	2 5
Propellant storage and distribution	0 2	0 6	0 1	--	--	--	--	--	0 9
Solar array drive	--	0 5	0 1	--	--	--	--	--	0 6
Structural mechanics	0 3	0 6	0 3	--	--	--	--	--	1 2
Structure and harness	0 5	1 5	0 5	--	--	--	--	--	2 5
Design integration	0 1	0 4	0 9	--	--	--	--	--	1 4
System engineering	1 1	1 1	1 0	0 8	0 2	--	--	--	4 2
System tests	--	0 3	1 2	0 6	--	--	--	--	2 1
AGE	0 1	0 7	0 5	0 4	--	--	--	--	1 7
Facilities	0 1	--	0 2	--	--	--	--	--	0.3
Spacecraft test and integration	--	--	--	0 2	0 2	--	--	--	0 4
Pre-launch operations	--	--	--	--	0 2	--	--	--	0 2
Mission operations	--	--	--	--	0 1	0 1	0 05	0 05	0 3
Program management	1 7	1 6	1 6	1 0	0 5	0 1	--	--	6 5
Total	13 4	19 8	15 2	3 8	1 2	0 2	0 05	0 05	53 7

[a]Fee excluded

[b]Includes September 1977

The totals in Table 44 show that the $53.7 million total cost of the thrust system is approximately equally divided between the development and qualification flight phases: $28.2 million and $25.5 million, respectively However, this division is somewhat artificial because it is dependent on the assumptions made, and no major significance should be attributed to it. It is estimated, however, that the cost of another thrust system flight phase for a post-Halley's comet mission would be about $18 million, since a significant portion of the $25 5 million flight/qualification costs would not recur.

C SUPPLEMENTARY DATA

The principal cost elements for each WBS category are listed below.

- Thruster and Gimbal
  - Unit design and development
  - Procurement and fabrication of all units (developmental, qualification, flight)
  - Unit tests through delivery to thrust system modules
  - Thruster life tests
  - Engineering support activities
- PMaC — Thrust modules and interface module
  - Unit design and development
  - Procurement and fabrication of all units (breadboards, developmental, qualification, flight)
  - Unit tests through delivery to thrust system modules
  - Design of test equipment
  - Engineering support activities
- Thermal Control
  - Heat pipes. development, procurement, life tests
  - Thermal analysis
  - Subsystem design and development, including thermal models and tests
  - Procurement and fabrication of all components (developmental, qualification, flight)
  - Engineering support until installation on the thrust system

- Propellant Storage and Distribution and Solar Array Drive
  - Subsystem design and development
  - Procurement and fabrication of all units (developmental, qualification, flight)
  - Subsystem tests through delivery to thrust system
  - Engineering support activities until system tests

- Structural Mechanics
  - Structural analysis: structural design requirements and definition
  - Coupled loads analyses (including models)
  - Analysis and design of solar-array and thrust-system (adapter) deployment
  - Definition, engineering, and performance of all structural tests
  - Design, procurement, and fabrication of test fixtures and instrumentation

- Structure and Harness
  - Design and development of the thrust modules, thrust system, adapter structure (including fittings), and harnesses
  - Procurement and fabrication of all components (developmental, qualification, flight)
  - Units tests through delivery to thrust system
  - Mass properties
  - Design and fabrication of all mass models
  - Materials engineering

- Design Integration
  - Design and development of assembly and integration procedures
  - Procurement and implementation of assembly and integration tooling
  - Balance and alignment tooling and operations
  - Manufacturing engineering and support

- System Engineering
  - System and mission analysis
  - System design
  - Specifications
  - Subsystem integration
  - System integration
  - Reliability analysis
  - Interfaces (all levels) — specifications, engineering, and management
  - System test engineering
  - Launch vehicle integration support and interfaces

- System Tests
  - Preparation
  - Procedures
  - Planning
  - Software
  - Setup
  - Conduct
  - Analysis
  - Reports

- AGE
  - Electrical AGE. development, fabrication, assembly, and checkout of system test consoles
    - Module tests – 1 set
    - System test – 1 set
  - Mechanical AGE:
    - Mechanical handling equipment (fixtures, slings, etc.)
    - Propulsion equipment (carts, Hg loading)
    - Alignment fixtures
    - Trailers
    - Shipping containers
    - Protective devices
  - Shuttle cradle (including thermal blankets)

- Facilities
  - Modification of vacuum chamber for module tests (thermal control)
  - Adapter for mounting thrust system in NASA LeRC facility ("Tank 6")
  - Rental of facility for thrust system acoustic flight acceptance test
  - Rental of facility for thrust system structural qualification test

- Spacecraft Test and Integration
  - Engineering, test, and operations support during spacecraft assembly, test, and integration operations
  - Thrust system and spacecraft system integration
  - Interface verification and tests
  - Thrust system tests on integrated configuration

- Pre-Launch Operations
  - Shipping
  - Handling at launch site
  - Propellant loading
  - Launch vehicle integration and shuttle integration
  - Pre-launch tests (including RFI)
  - Final installation and integration
  - Countdown and launch

- Mission Operations
  General support (telemetry analysis, anomaly resolution, operations planning and support)

- Program Management
  Program manager
  Technical management
  Administration
  Cost and schedule controls
  Procurement
  Subcontract management
  Parts control
  Product effectiveness and quality assurance
  Manufacturing management and support
  Data management and data bank
  Reports and presentations

Figure 88 shows the assumed manloading tables for system engineering and program management functions, respectively.

D. PROGRAM IMPLEMENTATION

An overall appraisal successfully developing, procuring, and testing the thrust system for the Halley's comet mission, in addition to the technical risks associated with the achievement of design goals, the resolution of interfaces (discussed in Section 3.C), must include the schedule risks in meeting the required milestones, and the economic risks of cost estimates.

The time available for accomplishing the Halley's comet mission is believed to be adequate provided that the initial phases of the program are implemented without delay. The key requirements are

- Immediate initiation of PMaC system design and of advanced development and procurement of breadboard units
- Immediate initiation of thruster performance verification tests
- Initiation of procurements for thruster components on or about 1 January 1978
- Initiation of heat pipe development and procurement in the spring of 1978

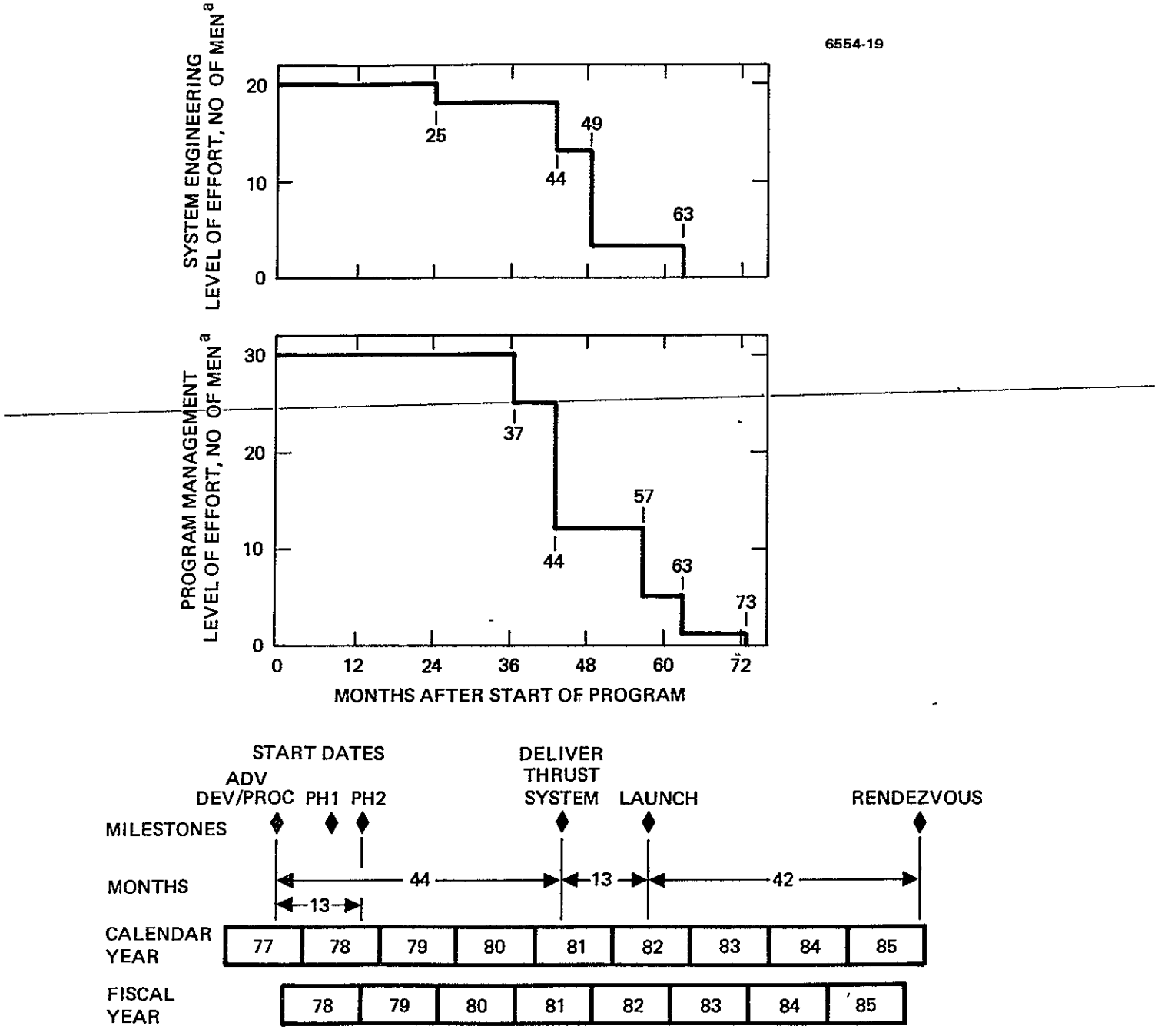

Figure 88. Proposed system engineering and program management manloading.

Postponing these advanced activities would probably result in non-recoverable schedule slippage The time spans for the other phases of the program, including system integration after thrust system system delivery and before launch, are believed to be tight but adequate, even allowing for a reasonable number of the development problems expected for this type of program.

Confidence in the overall success is based on identifying and scheduling for risks These risks are summarized in Table 45 in order of concern, with the most serious risks listed first

The entries in Table 45 necessarily include some of the technical and interface concerns of the preceding subsections to the extent that they affect schedule concerns. An important schedule concern involves PMaC electronics development Even with advanced development and procurement, and with the overlap provided in the program plan among the development, qualification, and flight procurement phases, the time available for these activities will require an intensive engineering effort. The overlap between these activities is itself a further concern (as indicated in Table 45) because of the possibility that significant design changes may be required. An equal concern is the potentially serious schedule slippage that could occur if the requirements for interface definition and management discussed in the preceding subsection are not met.

Specific potential concerns in the key areas of PMaC, structural design, and thermal control are discussed below. The potential technical problems implicit in some of the examples given are treated as schedule concerns. The risk appears to be not whether they can be resolved but whether they can be resolved within the time available These have therefore not been included in the explicit listing of technical risks in Section .

The schedule for the PMaC system is extremely tight, whether it can be met critically depends on the early definition of the interfaces with the solar array and with the mission module. Knowing the solar array output characteristics is fundamental to defining the power requirements of all PMaC units. Mission module characteristics (logic, power, EMI)

Table 45. Principal Schedule Risks

Tight PMaC development schedule (even with advance procurements)
Timely interface definition
Design characteristics of mission module and solar array
Interface requirements
Interface specifications
Prompt definition and early freeze of thrust subsystem design
Timely delivery of advance procurement critical parts
PMaC parts (hybrids)
Beryllium
Availability of heat pipes: development/delivery
Efficient management and control of interfaces
Spacecraft system interfaces
Shuttle interfaces
IUS interfaces
Overlap between development/qual/flight design and test
Impact of technical/design changes
Availability of personnel for parallel test operations
Unavailability of backup facilities for thrust module/thrust system tests
Special procurement risks (risk/cost trades)
Single shuttle cradle
Single adapter
Single beryllium vendor

have a direct effect on the design of the controller and of the inverter. Nine months have been allocated for breadboard circuit design, and all basic interfaces must be resolved early during that period. Furthermore, the schedule requires that the designing of the development units start 2 months after the start of breadboard design, and be completed within an 11-month period. These two activities must be completed on schedule to prevent significant schedule slippage downstream.

Several potential technical problems can be identified that could cause significant schedule slippage, although none of these is considered to pose a significant technical risk. Thruster/inverter operation at high power may uncover design compatibility or EMI problems. It may be necessary to significantly modify the proposed filtering and fault-protection circuits, particularly for conditions likely to occur during thruster operations in anomalous modes. The magnetic environment, because of the many high-power transformers and inductors present, may be quite severe.

Parts procurement presents an additional schedule risk. The time span allocated is based on the normal availability of commercial and high-reliability components. Some of these, however, may have deliveries longer than the 12 months allocated Of particular concern are the hybrid circuits, transistors, SCRs, and magnetics that may not be readily available.

The development schedule for the structure and thermal-control subsystems is not nearly as critical as for the PMaC units, but there are several potential problems in the areas of interface definition, procurement, and design that could lead to schedule slippage.

It is essential that interface loads and stiffness requirements be established early. Beryllium procurement cannot begin until tube diameters and the limits imposed on length and thickness variations are determined. Structural design integrity hinges on the validity of the dynamic load model used in the coupled analyses, and on the prompt initiation of the coupled analyses, which itself depends on the timely modeling of the other subsystems

Beryllium procurement poses some risks because, for the tube dimensions required, there is only one vendor source and because unique milling problems may be encountered. The proposed single adapter is not expected to be a schedule problem. Since the tubes will be designed for stability, they will operate at stress levels below their yield point Static development tests will demonstrate structural adequacy before qualification testing is begun. Having only a single shuttle forward cradle, which was assumed in the baseline program plan to save the approximately $0.5M that would be required for a backup cradle, may, however, imply some schedule risk.

The procurement of the heat pipes presents a potential schedule risk because of the requirement to provide a maximum heat transport capability in the range of 25 to 30 kW-cm (10 to 12 kW-in.). Although this requirement can probably be met with lead time provided in the development phase of the program, schedule delays (and an increase in mass) would result if a more conservative design that requires a lower transport capability is adopted later in the program (e.g., using more heat pipes). Similarly, schedule delays might occur if the heat pipes are damaged during the test program and require replacement. No procurement delays would be incurred, since the baseline plan incorporates sufficient spares for this contingency. The above problems could be alleviated or eliminated by incorporating more heat pipes in the baseline design, pending further tradeoff analyses of potential schedule risks versus weight and cost penalties.

The above discussion presents an example of the potential tradeoffs which exist among some of the technical and schedule concerns, system design parameters (notably mass allowance), and available funds. To properly weigh these tradeoffs with respect to system mass constraints, funding availability, and schedule implications and to assess the benefits that might be available, further analyses would be required

It is much more difficult to reliably assess economic risks. The cost estimates presented in Section 5.A, which are based on extensive experience in the design and procurement of space systems, are believed to be fairly accurate However, they are dependent on the assumptions

made regarding program scope and system interfaces, and, more importantly, on program contingencies arising from the technical, interface, and schedule risks. Furthermore, cost estimates depend on the procurement plan The estimates provided in Section 5.A should therefore be treated as, at best, a funding baseline, and plans for total program cost must take these additional factors into account

SECTION 6

CONCLUSIONS

The baseline thrust system design appears to be near optimal (in concept) for meeting the requirements of a Halley's comet rendezvous mission. We conclude that the ion thruster requirements could be satisfied by relatively minor modifications of the 900-series EMT, although postulated lifetime capabilities and reliability still need to be verified. The mass and projected performance capabilities of the thrust system meet the mission requirements.

A viable plan was prepared for developing, qualifying, and procuring the flight hardware to provide complete thrust system and spare parts within the schedule constraints dictated by Halley's comet. The costs required to perform this program were estimated to be about $54M (in FY 1977 dollars and excluding contractor fees), of which $13.5M is required in FY 1978 (prior to an official project approval decision).

We have attempted to identify and assess the technical and schedule risks, interfaces, and potential tradeoffs relevant to the thrust system. The schedule required appears to be feasible, but there is little, if any, margin for slippage. Technical risks exist, but they are considered resolvable through nominal engineering development. Interface considerations are critical, but are also considered resolvable by assigning a special management organization to monitor interfaces.

REFERENCES

1. Harold Kaufman, "Technology of Electron-Bombardment Ion Thrusters," Advances in Electronics and Electron Physics 36, 352-365 (1974)

2 T D. Masek, R.L. Poeschel, C R Collett, and D.E. Schnelker, "Evolution and Status of the 30 CM Engineering Model Ion Thruster," AIAA Paper No 76-1006, Key Biscayne, Fla , November 1976.

3 R.T. Bechtel and V K Rawlin, "Performance Documentation of the Engineering Model 30 CM Diameter Thruster," AIAA Paper No 76-1033, Key Biscayne, Fla., November 1976

4 G R. Sharp, J.E Cake, J C Oglebay, and F J Shaker, "Mass Study for Modular Approaches to a Solar Electric Propulsion Module," NASA TMX-3473, March 1977, NASA

5 H.J. King, et al., "Low Voltage 30-CM Ion Thruster Development," NASA CR-134731

6 M.J Mirtich, "The Effects of Exposure to LN_2 Temperatures and 2.5 Suns Solar Radiation on 30 CM Ion Thruster Performance," NASA TMX-71652 (1975).

7. J C. Oglebay, "Thermal Analytic Model of a 30 CM Engineering Model Mercury Ion Thruster," NASA TMX-71680 (1975)

8 M.J. Mirtich and W R. Kerslake, "Long Lifetime Hollow Cathodes for 30 CM Mercury Ion Thrusters," AIAA Paper No 76-985, Key Biscayne, Fla , November 1976

9. J L. Power, "Solutions for Discharge Chamber Sputtering and Anode Deposit Spalling in Small Ion Thrusters," AIAA Paper No. 75-399, New Orleans, La , 1975.

10. C. Collett, et al., "Thruster Endurance Test," NASA CR-135011, May 1976.

11. C. Collett, "Fabrication and Verification Testing of ETM 30 CM Diameter Ion Thrusters," NASA CR135193, April 1977

12 R L Poeschel and R.P. Vahrenkamp, "High Power Operation of a 30 CM Mercury Bombardment Ion Thruster," AIAA Paper No. 76-1007, Key Biscayne, Fla., November 1976.

248

PAGE INTENTIONALLY BLANK

13. Level II Program Definition and Requirements, Volume XIV Space Shuttle System Payload Accommodations, JSC-07700, Change No. 18

14. System Specification, "Performance and Design Requirements for the Department of Defense Space Transportation System," Volume 3 Interim Upper Stage System Segment, Basic Requirements, August 19, 1976

15. F D. Berkopec, J.C. Sturman, and R W Stanhouse, "Solar Array Drive System," Proc. 10th Aerospace Mechanisms Symposium, JPL-TM-33-777, Jet Propulsion Laboratory (1976)